



HAL
open science

Fluorene-based fluorescent markers: new insights in synthesis and applications into labeling of nucleic acids and imaging of cell membranes

Janah Shaya

► To cite this version:

Janah Shaya. Fluorene-based fluorescent markers: new insights in synthesis and applications into labeling of nucleic acids and imaging of cell membranes. Other. COMUE Université Côte d'Azur (2015 - 2019), 2016. English. NNT : 2016AZUR4066 . tel-02003596

HAL Id: tel-02003596

<https://theses.hal.science/tel-02003596>

Submitted on 1 Feb 2019

HAL is a multi-disciplinary open access archive for the deposit and dissemination of scientific research documents, whether they are published or not. The documents may come from teaching and research institutions in France or abroad, or from public or private research centers.

L'archive ouverte pluridisciplinaire **HAL**, est destinée au dépôt et à la diffusion de documents scientifiques de niveau recherche, publiés ou non, émanant des établissements d'enseignement et de recherche français ou étrangers, des laboratoires publics ou privés.

UNIVERSITE DE NICE-SOPHIA ANTIPOLIS – UFR Sciences
Ecole Doctorale de Sciences Fondamentales et Appliquées

THESE

Pour obtenir le titre de
Docteur en Sciences

de l'UNIVERSITE de Nice – Sophia Antipolis

Discipline : Chimie

Présentée et soutenue par
Janah Shaya

« Capteurs fluorescents à base de fluorène : nouvelles perspectives en synthèse et applications pour le marquage des acides nucléiques et en imagerie de la membrane cellulaire »

« Fluorene-based fluorescent markers; new insights in synthesis and applications into labeling of nucleic acids and imaging of cell membranes »

Thèse dirigée par le Prof. Alain BURGER et co-encadrée par le Dr. Benoît Y. MICHEL

Soutenue le 21 Septembre 2016

Jury:

Pr. Demchenko Alexander	Professeur, Académie Nationale des Sciences de l'Ukraine	Rapporteur
Pr. Smietana Michael	Professeur, Université de Montpellier	Rapporteur
Dr. Jazzar Rodolphe	Chercheur CNRS, Université de Californie	Rapporteur
Dr. Michel Y. Benoît	Maître de conférences, Université Nice Sophia Antipolis	Co-encadrant de thèse
Pr. Burger Alain	Professeur, Université Nice Sophia Antipolis	Directeur de thèse

إلى "البناني" لبنان جبران وخورى
وكل من يحميه....

**To my "*Lebanon*", the country of Gibran and Corey,
And everyone who keeps it safe....**

**A toi mon "*Liban*", Le pays de Gibran et Corey,
Et à tous ceux qui le protègent....**

Acknowledgements

First, I would like to express my sincere thankfulness to the “French ministry of education” and the “Doctoral school of Nice-Sophia Antipolis university (ED-SFA)” for offering me this Ph.D grant for three years. I am equally thankful to Pr. Alain Burger for the fruitful leadership of this thesis. In fact, Alain is present and evenly invested in all the work in his lab, especially the difficult starting of new projects like “my fluorenes”. His guidance, knowledge, resources, and ambition were indispensable. An in-line thank you might go here to Dr. Benoit Michel for his useful contributions. He is one of few chemists I’ve met with an inspiring talent in the art of “organic synthesis”. Dr. Rachid Benhida has the portion of the lion especially in the front lines of this project. I owe him for his support and the 3-year stay in the “molecules bioactives” group. I would also like to acknowledge all the permanent staff of our group and the ICN; in particular, the director of the école doctorale Dr. Elisabeth Taffin-de-Givenchy, Dr. Audrey Di Giorgio, Dr. Stephane Azouly and Dr. Sophie Poulain-Martini for the teaching experience, Dr. Maria Duca, Dr. Luc Demange, Dr. Cyril Ronco, Dr. Guilhem Godeau, Dr. Thierry Darmanin for setting the example of a researcher for me, Dr. Christophe Di Giorgio for all the synthesis advices, the director of the ICN Dr. Elisabet Duñach for the GCMS facilities, Dr. Lionel Massi for the mass spectrometry, Dr. Marc Gaysinski for the NMR spectroscopy, and Dr. Nadine Martinet for her tips and advices.

The list of acknowledgments will continue and I hope I do not forget anyone as research is a collaborative effort and many people play a direct or indirect role; Dr. Anthony Martin for sharing his knowledge on catalysis and for the pleasant talks, Dr. Sylvain Antoniotti for his precious remarks on sustainable chemistry, Dr. Fabien Fontaine-Vive for the pleasure of working with him on DFT calculations, and Prof. Nadia Patino for plenty of teachings and fun. Pr. Iyad Karamé, Dr. AbdelRehman Sidani, Pr. Peter Goekjian, and Dr. Rodolphe Jazzar deserve to be appreciated for being influential chemists that have planted the first eagerness for this domain in me. Iyad is a person to whom I am deeply indebted. A big thank you goes also to Dominique Bonhomme (Domi) and Frederic Benailli (Fredo) for the coffee and work time we spent. I hope that our work together will be validated in publications the soonest.

I have to warmly thank Pr. Alexander Demchenko, Pr. Michael Smietana, and Dr. Rodolphe Jazzar for revising this manuscript and being members of the thesis committee.

I would likewise address the great team in Strassbourg for the warm, helpful, and productive welcoming in their lab where we performed the cell imaging; Pr. Yves Mely, Dr. Andrey Klymchenko, Dr. Mayeul Collot, and the young researchers there; Dr. Yosuke-Niko, Bohdan, Dorian, Hassan, Iryna, Rajhan and others for the fun trips and nights we passed during my stay.

Nice lab has a list of young researchers that enriched this journey with good memories as well: Florian, Gabreilla, Hamza, Alexandra, Hellene, Coralie, Antoine, Sokaina, Loraine, Anne, Lauri, Sasha, Oleg, Malika, Nelli, Cecile. I wish you all the best in your future endeavors. Few words to some should be mentioned: Cate; Sursum Corda ou Janah va... we really missed you in the ICN, Niko; it was a pleasure to share the same lab with you, Anh; you will be truly missed my

dearest, Mauro; you lightened up fluorescence a bit more dude. Merci également à Marie le grand prof. de français pour les produits qu'elle a fait au cours de M1 stage.

I think I forgot Hella, not really! You will be remembered for long time. All the first translations, hang-outs, fun, and shouting have spiced "Nice" stay. Assia also did her share in translations and joy, merci! Altogether with Diaa, Ilheme, and Najiba, we had a great deal of time and food that I will definitely miss. Dr. Ilheme, despite your early departure from the ICN, the short time was enough to reveal a chemist and person of high standards and a friend for life.

Outside the lab, there are many people who had put up with me in all stages. They are a major highlight in my life. The Janwa; you witnessed it all and are still doing patiently, I will simply quote from your thesis: "Behind each work, there is a secret rider, you were always there", see you soon in Strass. George; an ever-lasting support and a melody for every occasion, laughing is the key of success as you say. Kawsar; the chief of chiefs, for god's sake we need to stop running and making rules; not everyone has your potential. Together, we made the perfect KG group of nice. Ramez; you left your space when you moved. Abed, Tharwat; travelling with you is beyond fun. Habeeb and Hawraa; you added a source of joy with our future chemist, Mariam. Finally Pascal; we will hopefully always meet or run away bro, I am so happy that I have met you.

Back home, the gratitude can go endless and I still have too many experiments to do, so I will cut it short. Thanks for everyone who supported me when I decided to change careers. I am very lucky to have a family that trusts my choices without questioning. You are too many, but I love you all. Mostafa and Iman; you are my residence and comfort. Jinan; you did all what I have to do for years. You, Naim, and your three ugly musketeers are blessings. Suzan and Samah, your craziness makes you so special and we are proud of your success with each day passing, Roy, Iyad, and Karam; you will be one of a kind (chemical) engineers, you know it. Jihan, Souaad, Makram, Fares, David, Osama, Wido.... Silvana; don't get lost in Cuba, I can't live without you all.

Distance did not make some any less of great friends: Rawad, a real brother; we will keep on roaming and reach, we shared all the crazy and wisdom times, all the fun, joy, plans, and determination-I hope you make it to my defense, Bilal, Bahaa; thanks for all and cheers, Naveen, Fadi, George, Anis, Samer, Dani, and the group leader in Dubai, Khodr; here it is man, our chemistry is finally in action, Lamece the royal; I will sum up the 10 pages of jokes you make of me into one line of don't stop because I will miss it, Jihan the one and only; from Lyon to Lebanon, and Marah; a real source of aspiration for many years, I will buy a house in Monaco and you will be invited. If anyone is forgotten, be sure it is for lack of time. I appreciate an equal list of people that I could not name.

Finally, there is nothing better than quoting from the French Nobel Prize winner Jacques Monod: "In science, self-satisfaction is death. Personal self-satisfaction is the death of the scientist. Collective self-satisfaction is the death of the research. It is restlessness, anxiety, dissatisfaction, agony of mind that nourish science." So here it is, a small plan of an unsatisfied scientist who lost his first grant in a war back in 2006, and kept the same target of research till July 2016.

Nice,
July, 2016

Table of Contents

• Dedication.....	2
• Acknowledgments.....	3
• Table of contents.....	5
• List of abbreviation.....	9
• Thesis statement and general presentation.....	11

Chapter One : Bibliographical Review

I. LUMINESCENCE	15
I.1 FLUORESCENCE	15
I.1.1 Stage 1: Absorption of light (excitation).....	15
I.1.2 Stage 2: Excited state and fluorescence lifetime.....	17
I.1.3 Stage 3-Fluorescence emission	18
II. FLUOROPHORES.....	20
II.1 INTRINSIC FLUOROPHORES	21
II.1.1 Fluorescent proteins.....	21
II.1.2 Chlorophyll.....	21
II.2 EXTRINSIC FLUOROPHORES	22
II.2.1 Genetically encoded proteins.....	22
II.2.2 Fluorescent nanocrystals.....	22
II.2.3 Small-molecule fluorophores.....	23
II.3 SOLVATOCHROMIC FLUOROPHORES.....	26
II.3.1 What is “solvatochromism” in fluorescence context (solvatofluorochromism)?	26
II.3.2 Negative solvatochromism:.....	26
II.3.3 Positive solvatochromism:	27
II.4 PUSH-PULL DYES.....	32
III. FLUORENE AND ITS DERIVATIVES.....	33
III.1 PARTICULAR FEATURES OF FLUORENE AND ITS DERIVATIVES.....	35
III.1.1 Two-photon absorption.....	35
III.1.2 Aggregation-Induced Emission Enhancement (AIEE)	36
III.1.3 Excimer formation	36
III.1.4 Twisted Intramolecular Charge Transfer (TICT).....	37
III.1.5 Profluorescence of fluorene derivatives for turn-on applications.....	37
III.1.6 Polyfluorenes (PF).....	37
III.2 ARRAY OF USES OF FLUORENE AND ITS DERIVATIVES.....	39
III.2.1 Fluorescence imaging and application related to biology.....	39
III.2.2 Optical data storage.....	39
III.2.3 Organic Light-Emitting Devices (OLEDs)	40
III.2.4 Dye-sensitized solar cells (DSSCs)	40
III.2.5 Non linear optical dyes in telecommunication.....	40
III.3 SYNTHESIS OF AMINOFLUORENES	40
▪ Conventional routes.....	40
▪ Buchwald-Hartwig amination	41
IV. FLUOROSENSING.....	43
IV.1 FLUORESCENCE LABELING AND DETECTION.....	44
IV.2 FLUORESCENCE SENSING.....	45
IV.2.1 FRET.....	46
IV.2.2 Anisotropy.....	47
V. MEMBRANE LIPIDS	47

V.1	CLASSIFICATIONS OF MEMBRANE LIPIDS.....	48
V.1.1	<i>Glycerophospholipids</i>	48
V.1.2	<i>Sphingolipids</i>	48
V.1.3	<i>Sterols</i>	48
V.2	HETEROGENEITY OF LIPID MEMBRANES AND RELATED FLUOROPHORES	49
V.2.1	<i>Level One: Lipid raft theory</i>	49
▪	<i>Fluorophores related to raft investigations and model membranes</i>	50
V.2.2	<i>Level two: Transmembrane lipid asymmetry</i>	50
▪	<i>Annexin V detection assays</i>	51
V.2.3	<i>Level three: heterogeneity among biological membranes</i>	52
V.3	FLUORESCENCE PROBING OF MEMBRANE LIPIDS.....	52
V.3.1	<i>Membrane probes</i>	52
VI.	NUCLEIC ACIDS	54
VI.1	STRUCTURE OF DNA.....	54
VI.2	DNA SYNTHESIS:	56
VI.3	THE CHEMISTRY BEHIND DNA SYNTHESIS	56
VI.3.1	<i>The phosphotriester approach</i>	57
VI.3.2	<i>The phosphite triester and H-phosphoramidite approach</i>	57
VI.3.3	<i>H-phosphonate approach</i>	58
VI.4	CHEMICAL SYNTHESIS OF DNA.....	59
VI.4.1	<i>Solution-phase synthesis</i>	59
VI.4.2	<i>Solid-phase DNA synthesis</i>	59
VI.5	FLUORESCENT LABELING OF NUCLEIC ACIDS	61
VI.5.1	<i>Non-covalent or non-specific labeling</i>	61
VI.5.2	<i>Covalent labeling</i>	63
VI.6	SYNTHETIC APPROACHES USED IN COVALENT LABELING OF ODNs.....	67
VI.6.1	<i>Pre-synthetic modification</i>	67
VI.6.2	<i>Post-synthetic modification</i>	67
VI.7	SELECTED SAMPLE APPLICATIONS OF FLUORESCENT NUCLEOSIDES.....	68
VI.7.1	<i>DNA sequencing</i>	68
VI.7.2	<i>Single nucleotide polymorphism (SNP)</i>	68
VI.8	FLUORENE DERIVATIVES IN THE CONTEXT OF DNA APPLICATIONS	68

Chapter Two : Air-stable palladium catalytic systems for sequential one-pot synthesis of unsymmetrical aminoaromatics

I.	OPTIMIZATION STUDIES.....	71
II.	SCOPE OF THE SELECTIVE MONOAMINATION REACTION	74
III.	DIAMINATION OF FLUORENES.....	75
IV.	SYNTHESIS OF UNSYMMETRICAL FLUORENES	75
V.	SCOPE OF THE SELECTIVE CONDITIONS ON DIBROMONAPHTHALENE, DIBROMOPYRIDINE, AND DIBROMOTHIPHENE.....	77
VI.	APPLICATION: A NEAR-IR PUSH-PULL SENSOR.....	78
VII.	CONCLUSION.....	79

Chapter three : Push-Pull fluorene dyes: synthesis and structure-photophysics relationship

I. SYNTHESIS	82
I.1 VARIATION OF THE ELECTRON-WITHDRAWING GROUP (EWG)	82
I.2 VARIATION OF THE ELECTRON-DONATING GROUP (EDG)	84
II. SPECTROSCOPIC STUDIES	84
II.1 - ACCEPTOR SERIES	84
II.2 - VARIED-AMINE SERIES	91
II.3 - HAMMETT CORRELATION	97
III. CONCLUSION	99

Chapter Four : Fluorene-based membrane probes and cell imaging

I. INTRODUCTION	101
II. SYNTHESIS	102
III. PHOTOPHYSICAL CHARACTERIZATION OF F1-F3	102
III.1 HYDRATION STUDY OF F1	105
III.2 PHOTOPHYSICAL CHARACTERIZATION IN LARGE UNILAMELLAR VESICLES OF DIFFERENT LIPID COMPOSITIONS.....	106
III.3 PHOTODEGRADATION STUDIES	109
IV. IMAGING	111
IV.1 IMAGING GIANT UNILAMELLAR VESICLES (GUV) WITH F3	111
IV.2 IMAGING CELLS WITH F1-F3.....	112
V. CONCLUSION:	114

Chapter Five : Fluorene-based DNA fluorescent markers; synthesis, DNA labeling, and applications

I. FLUORENE LABEL BY ANUCLEOSIDE APPROACH	116
II. FLUORENE LABEL CONNECTED TO DEOXYRIBOSE SUGAR	122
II.1 SYNTHESIS OF FM2-4	122
III. CHARACTERIZATION OF THE FREE FLUORESCENT MARKER (X) AND THE X-LABELED ODN SEQUENCES	126
III.1 SPECTROSCOPIC PROPERTIES OF THE NAKED FLUORESCENT NUCLEOSIDE (197).....	126
III.2 PKA DETERMINATION OF (197).....	128
III.3 PHOTOPHYSICAL CHARACTERIZATION OF THE X-LABELED ODNs	129
III.4 CD AND THERMAL DENATURATION STUDIES	132
III.5 FRET	134
IV. CONCLUSION	137

Conclusions and perspectives

I. GENERAL CONCLUSION	138
II. PERSPECTIVES	139

Résumé long

..... 141

Experimental part and SI

I. GENERAL METHODS 146

II. LIPID VESICLES..... 147

III. CELL LINES, CULTURE CONDITIONS, TREATMENT, AND IMAGING 148

IV. ODN SYNTHESIS AND PURIFICATION: 148

V. MALDI PROCEDURE 149

VI. PREPARATION OF SS AND DS LABELED DNA 149

VII. DENATURATION STUDIES AND MELTING TEMPERATURES 150

VIII. CIRCULAR DICHROISM 150

IX. CHAPTER 2 SYNTHETIC PROCEDURES..... 151

X. CHAPTER 3 SYNTHETIC PROCEDURES..... 164

XI. CHAPTER 4 SYNTHETIC PROCEDURES..... 174

XII. CHAPTER 5 SYNTHETIC PROCEDURES..... 179

XIII. SUPPLEMENTARY CHARACTERIZATION OF CHAPTER 3 195

 XIII.1 TRANSITION DIPOLE MOMENT OF PUSH-PULL DYES (IN DEBYE):..... 195

 XIII.2 DFT AND TDDFT CALCULATIONS. 195

XIV. SUPPLEMENTARY CHARACTERIZATION OF CHAPTER 4 199

 XIV.1 PHOTODEGRADATION DECAY CURVES OF F1-3 AS A FUNCTION OF TIME IN ETHANOL 199

 XIV.2 RATIO IMAGES FOR F2 PROBE IN CELLS 200

 XIV.3 COMPARISON OF THE INTENSITY OF DYES; F1, F2, AND F3 RESPECTIVELY..... 200

XV. SUPPLEMENTARY CHARACTERIZATION OF CHAPTER 5..... 202

 XV.1 PHOTOPHYSICAL CHARACTERIZATION OF DYE 190 202

 XV.2 HPLC PROFILES:..... 203

 XV.3 EXCITATION SPECTRA 203

 XV.4 MELTING TEMPERATURE CURVES..... 203

 XV.5 CD SPECTRA..... 204

 XV.6 ACCEPTOR DYES USED IN FRET 204

Referenes.....205

List of abbreviations

- $\bar{\nu}$ wavenumber
- **2-AP** 2-aminopurine
- **2PA** two-photon absorption
- **3-D** three dimensions
- **9-CHF** 9-cycloheptatrienyliidene fluorenes
- **A** absorbance
- **a** radius of the Onsager's cavity
- **a.u.** arbitrary unit
- **ACN** acetonitrile
- **ACQ** aggregation-caused quenching
- **Ac** acetone
- **AIEE** aggregation-induced emission enhancement
- **asap** as-soon-as-possible
- **BDF** base-discriminating fluorescence
- **BLA** bond length alternation
- **C** concentration
- **c** speed of light
- **CD** circular dichroism
- **CL** cholesterol
- **cm** centimeter
- **CuAAC** copper(I)-catalyzed alkyne-azide cycloaddition
- **D** Debye
- **DAPI** 6-diamidino-2-phenylindole
- **DBU** 1,8-diazabicycloundec-7-ene
- **DCE** dichloroethane
- **DCM** dichloromethane
- **DCPC** 2-cyanoethyl-N,N-diisopropylchlorophosphoramidite
- **DIEA** Hünig's base
- **DMF** dimethylformamide
- **DMSO** dimethylsulfoxide
- **DMTr** dimethoxytrityl group
- **DNA** deoxyribonucleic acid
- **DOPC** dioleoylphosphatidylcholine
- **DOS** diversity-oriented synthesis
- **DSSC** dye-sensitized solar cell
- **E** energy
- **EA** ethyl acetate
- **EDG/D** electron-donating group/donor
- **ESIPT** excited-state intramolecular proton transfer
- **EtOH** ethanol
- **eV** electronvolt
- **EWG/A** electron-withdrawing group/acceptor
- ϵ molar absorption coefficient
- **F** fluorene membrane probe
- **FC** flash chromatography
- **FLS** fluorescence lifetime spectroscopy
- **FM** fluorescent ODN marker
- **FRET** Förster Resonance Energy Transfer
- **G, A, T, C, U** guanine, adenine, thymine, cytosine, uracil respectively
- **GFP** green fluorescent protein
- **GUV** giant unilamellar vesicle
- **h** Planck's constant
- **H-bond** Hydrogen bonding
- **HGP** human genome project

-
- **HOMO** highest occupied molecular orbital
 - **I** inductive effect
 - **ICT** intramolecular charge transfer
 - **IR** infrared
 - **J** spectral overlap in FRET
 - **kDa** kilodalton
 - **k_{nr}** sum of non-radiative decay rates
 - **k_r** radiative decay rate
 - **L** ligand (tertiary phosphine)
 - **l** the light path length in a sample
 - **Ld** liquid-disordered phase
 - **Lo** liquid-ordered phase
 - **LUMO** lowest unoccupied molecular orbital
 - **LUV** large unilamellar vesicle
 - **M** mesomeric effect
 - **MeOH** methanol
 - **MO** molecular orbital
 - **MW** microwave
 - **N*** normal excited state
 - **NIR** near-infrared
 - **nm** nanometer
 - **nM** nanomolar
 - **ODN** oligonucleotide
 - **OLED** organic light-emitting device
 - **PC** phosphatidyl choline
 - **PCR** polymerase chain reaction
 - **PE** phosphatidyl ethanolamine
 - **PE solvent** Petroleum ether
 - **PF** polyfluorenes
 - **PP** push-pull dye
 - **PS** phosphatidyl serine
 - **Qdots** Quantum dots
 - **r** anisotropy
 - **R** donor-acceptor distance in FRET
 - **R_0** Förster distance where fluorescence transfer efficiency is 50 %
 - **RNA** ribonucleic acid
 - **RP HPLC** reversed-phase high-performance liquid chromatography
 - **rt** room temperature
 - **s** second
 - **S** singlet multiplicity
 - **SI** supplementary information
 - **SM** sphingomyelin
 - **SMS** single molecule spectroscopy
 - **SNP** single nucleotide polymorphism
 - **T** triplet multiplicity
 - **T*** ES IPT tautomer
 - **THF** tetrahydrofuran
 - **TICT** twisted internal charge transfer
 - **UV** ultraviolet
 - **vs.** versus
 - **X Y Z M** fluorene ODN labels (**FM**)
 - **Δf** Lippert's parameter
 - **$\Delta\lambda_{ss}$** Stokes shift
 - **λ** wavelength
 - **λ_{abs}** absorption maximum
 - **λ_{em}** emission maximum
 - **μ_E and μ_G** dipole moments of the excited and ground states
 - **π** aromatic core
 - **σ_P** Hammett value
 - **τ** fluorescence lifetime
 - **ϕ/QY** quantum yield

Thesis statement and presentation of the manuscript

The cutting-edge development of technology often takes place at interfaces of supposedly distinct disciplines of science. Research involving interdependent areas of synthetic chemistry, computations, photophysics, biophotonics, and imaging has evolved as a modern mean of analysis to unravel the scientific enigmas. “Fluorescence” is a domain that integrates virtually all the mentioned disciplines and extends to other frontiers of environmental detections, life, medicinal, and pharmaceutical sciences.

“Fluorescence” was observed first by Herschel in 1845 as a phenomenon from quinine solution under sunlight and was further described by Stokes in 1852. A century later, this novelty process was put in the service of science with the invention of “commercial fluorimeters” and “fluorescence microscopes”. The advances proceeded fast with “confocal microscopy” and more sophisticated Nobel-Prize instruments like the “Zewail’s femtosecond ($\times 10^{-15}$ s) spectroscopy”. Fluorescence instrumentations are nowadays advanced, not expensive, and easy-to-manipulate.

Eventually, fluorescence techniques have become crucial analytical toolbox for research and industry owing their success to many exquisite characteristics. These techniques are the most sensitive in the field of molecular sensing especially in probing intrinsic biological dynamics. Their sensitivity has attained the limit of *single* molecule detection with signal recordings that can be controlled at a distance. They demonstrate high degree of accuracy, non-invasive character in living cells, and ultrahigh spatial and temporal resolutions. Furthermore, fluorescence sensing is extremely versatile providing detections in solid, liquid, gas, and even at the interface of these phases. In addition to instrumentations, the growth in the “design and synthesis of fluorophores” undoubtedly remains the hallmark of progress in fluorescence applications.

An optimal fluorophore is essentially a molecular framework that compiles the required attributes from optical properties such as photostability, brightness, selective excitation and emission to chemical versatility such as tolerance to introduce substituents for bioconjugation and tuning solubility. Such rational design is a challenge by itself. From “organic chemistry” perspectives, this will at least involve a multi-step synthetic route to produce such a smart molecule; hence, adding more challenges of the known limitations of synthesis. Consequently, chemists are highly urged to bring forth new robust, step- and atom-economic routes to synthesize innovative probes and generate libraries of dyes that elucidate structure-property relationships.

In particular, our work has focused on metal-catalyzed reactions such as Buchwald-Hartwig aminations and copper(I)-catalyzed alkyne-azide cycloaddition (CuAAC) “click” reactions to create more viable alternatives to otherwise long employed routes. The developed *in-house* methodologies allowed accessing a fluorene-based library of push-pull dyes as a captivating class of environment-sensitive probes. A push-pull dye consists of a π -scaffold functionalized with an electron donor (D) and acceptor (A). The D- π -A system undergoes a photo-induced intramolecular charge transfer (ICT) state forming a low-energy molecular orbital (MO). Visible light provides sufficient energy to excite the electrons within this new MO, making these compounds generally colored. The ICT also generates dipole moments that augment the sensitivity of these fluorophores in response to polarity and changes of their environments.

The aromatic core (π) plays a key role in the design. Thus, came the choice of the fluorene family in this project. Fluorenes manifest desirable spectroscopic attributes, low cytotoxicity, and appreciable two-photon absorption cross-sections allowing cell imaging with reduced photodamage. Fluorene derivatives are extensively used in biomedical research and material sciences such as optoelectronics.

Two central investigations were explored using our fluorene probes, 1) labeling of oligonucleotides (ODNs), and 2) imaging of lipids in biomembranes.

In fact, despite the complete determination of the 3.5×10^9 base-pair DNA sequences in the human genome project (HGP) in 2001, this explosive acquisition of structural data has paraded very limited information about the complex biological function of DNA. To address these aspects, fluorescence spectroscopy offers an exquisite tool to characterize nucleic acids and to study their interactions, which are fundamentals to understand cellular events such as DNA repair, DNA methylation, and gene silencing. The search of suitable fluorescent markers that can monitor these interactions without affecting the structure and function of the labeled ODN sequences is still at its peak.

Likewise, the heterogeneous lipid distribution in cell membranes is a subject of intense investigations. Three levels of heterogeneity are distinguished. The lateral heterogeneity, described by the lipid raft hypothesis, is under debate till now. Rafts are believed to be behind many processes such as signal transduction and neurodegenerative diseases. Transmembrane lipid asymmetry is the second heterogeneity that is lost in programmed cell death (apoptosis). Defective apoptosis is the origin of detrimental diseases such as atrophy and cancer. Lastly, the differences between the plasma and intracellular membranes represent the third, least-explored heterogeneity. Thus, designing highly sensitive probes will help to understand the structure and

dynamics of biomembranes by sensing different parameters like hydration, viscosity, polarity, and order. This will in turn reflect in understanding the cellular processes and in finding solutions to futile medical problems such as cancer.

In conclusion, the purpose of this thesis was to advance a step in the areas of designing and synthesizing novel fluorescent probes that meet the rigorous and demanding conditions of the above-mentioned biological applications.

The body of the dissertation consists of 5 chapters and a conclusion stating the future perspectives.

- Chapter one is the introduction that states the background of this work.
- Chapter two describes a concise synthetic methodology to prepare a spectrum of aminoaromatics. The methodologies involve selective functionalization of dibromoaromatic scaffolds using air-stable palladium catalytic systems. In particular, rapid *mono*- and *di*-aminations were carried out in addition to sequential couplings of different moieties in one-pot. The synthesis was scaled up to prepare the essential probes used in the next chapters. The content of chapter 2 has recently been published online in *The Journal of Organic Chemistry*.
- Chapter three builds on the developed catalytic conditions of Buchwald-Hartwig amination to explore the effect of the donor part on push-pull molecules. Moreover, it describes various synthetic pathways to study the acceptor part including CuAAC, peptide couplings, and metal-halogen exchange reactions. In effect, we concluded the theoretical and experimental characterization and structure-photophysics relationships of 17 synthesized fluorophores including near-infrared (NIR) probes. The content of chapter 3 has recently been published in *Chemistry: A European Journal*.
- Chapter four takes the advantage of the rational design and the new “*ynone*” anchoring point of “chapter three” in bioconjugating the fluorene probes. This chapter describes the synthesis of three probes designed to image membrane lipids. The photophysical characterization of the dyes, their ability to probe large and giant unilamellar vesicles (LUV and GUV) of different lipid compositions, and the imaging of HeLa cells are reported. The optimized dye is the first plasma membrane-specific fluorene-based probe that can be a powerful tool for studying membranes surpassing the features of commonly used probes.
- Chapter five illustrates the synthesis of four emissive nucleobase analogues (phosphoramidites) exploring different linkers and sugars to rationalize the design of a fluorene-based DNA sensor. Then, it covers the journey of site-specific ODN

incorporations of the biosensors *via* solid-phase DNA synthesis, the difficulties encountered, the characterization and the hybridization studies of the labeled ODN sequences, and finally the preliminary application of the optimal biosensor as a mega-Stokes shift donor in a FRET pair. The recorded shift seems exceptional reaching up to 300 nm and very promising to validate the dye in future applications.

- A brief conclusion and future perspectives are stated at the end of the manuscript, followed by the experimental section.

Chapter 1:

Bibliographical Review

I. Luminescence

Luminescence is the process of emission of light quanta upon excitation by any source of external energy such as a chemical reaction (chemiluminescence), thermal energy (thermoluminescence), mechanical action on a solid (mechanoluminescence), light (photoluminescence), etc..

In particular, photoluminescence is defined as an optical property of a substance which absorbs photons and then releases the absorbed energy radiatively from its excited state.^[1,2] Chemical functionalities that absorb light in the ultraviolet or visible region are referred as chromophores. Absorption in the visible gives colored compounds.

Depending on the nature of the excited state, photoluminescence is classified into 2 forms, fluorescence and phosphorescence. A molecule or a molecular fragment that has the ability to fluoresce is called a *fluorophore*. A fluorophore is also commonly termed as a *dye* in reference to its color property.^[3,4]

I.1 Fluorescence

Fluorescence can be viewed as a three-stage process. Each stage and its corresponding optical measurements will be discussed in the following sections.

I.1.1 Stage 1: Absorption of light (excitation)

I.1.1.1 Light

Light is an electromagnetic radiation described in terms of a “wave-particle duality” concept. Precisely, light is characterized as a particle (*photon*) by its energy (E , eV) and as a wave by its wavelength (λ , nm) or wavenumber ($\bar{\nu}$, cm^{-1}) as shown in *eq. 1*,

$$E = h\nu = h\frac{c}{\lambda} \text{ and } \bar{\nu} = \frac{1}{\lambda}$$

Equation 1

where c and h are constant values signifying the speed of light and Planck’s constant

respectively.

The range of electromagnetic radiations suitable for optical studies and photochemistry is shown in *fig. 1* and is characterized by its E and λ .^[2,3]

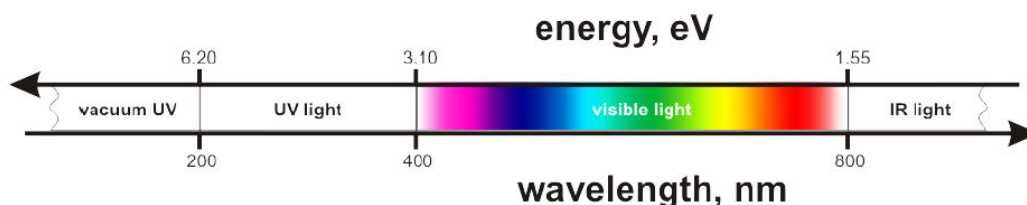


Figure 1. Range of electromagnetic radiation in optical studies and photochemistry^[5]

I.1.1.2 Absorption

An organic molecule resides in its ground state (S_0 , singlet by multiplicity) in the absence of external sources of perturbation. In the ground state, two electrons rest in the highest occupied molecular orbital (HOMO) while the lowest unoccupied molecular orbital (LUMO) is free. Exposing the molecule to a vacuum extreme-ultraviolet radiation ($\lambda < 200$ nm) can provide enough energy to ionize it by the expulsion of one of its electrons. However, exposition of the molecule to UV/visible radiation (200-800 nm) induces an electron transition from HOMO to LUMO causing an excited electronic state (S_1 , singlet by multiplicity). In the excited state, an *intersystem crossing* to a triplet multiplicity (T_1) can take place (*fig. 2*).^[2,4]

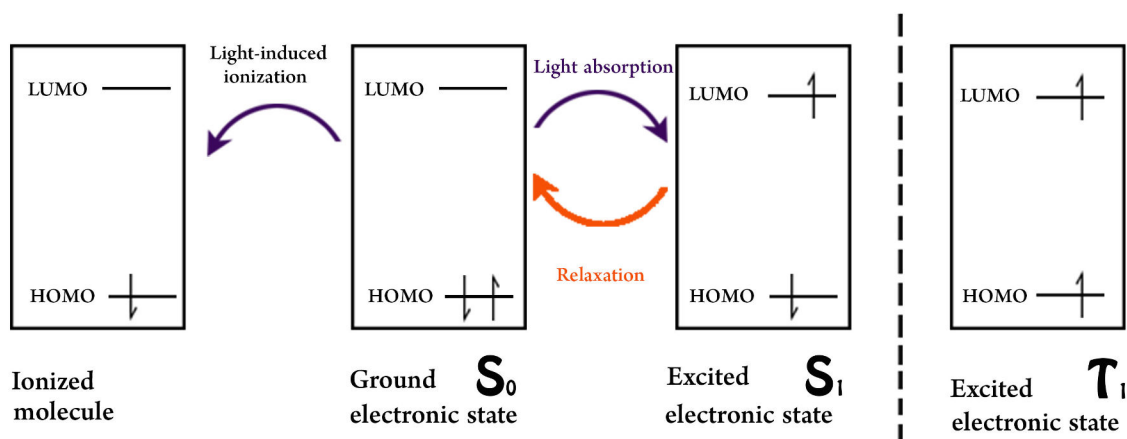


Figure 2. Light-induced phenomena

I.1.1.3 The Beer-Lambert law

The *absorbance* (A) measured at any wavelength on a spectrophotometer is proportional to

the dye concentration (C , mol/L) and the light path length in a sample (l , cm). The molar absorption coefficient (\mathcal{E}) is the proportionality coefficient in this relation (eq. 2).

$$A = \mathcal{E} \cdot C \cdot l$$

Equation 2

Many instrumentation and intrinsic factors can cause the fluorophore to absorb light non-linearly as a deviation from this law. Examples are: inner filter effect, broadband illumination, turbidity of biological samples, and molecular aggregation. The latter is the case of self-association that increases the particle size causing more light scattering or shift of its absorption maximum for instance. Aggregation is mainly observed if the fluorophore is concentrated or insoluble.^[3]

I.1.1.4 Molar absorptivity or absorption coefficient

Molar absorptivity or extinction coefficient (\mathcal{E}) signifies the probability of an electronic transition from the ground to excited state at a given wavelength.

- If $\mathcal{E} > 10^5 \text{ M}^{-1} \cdot \text{cm}^{-1}$, the transition is fully allowed.
- If $\mathcal{E} < 10^2 \text{ M}^{-1} \cdot \text{cm}^{-1}$, the transition is forbidden.
- If $10^2 < \mathcal{E} < 10^5 \text{ M}^{-1} \cdot \text{cm}^{-1}$, the transition is partially allowed.

In general, \mathcal{E} increases as the size of the fluorophore increases.^[6]

I.1.1.5 Franck – Condon principle

Since the electronic transitions (ex: S_0 - S_1) take place relatively faster (10^{-15} s) than the molecular vibrations (10^{-10} - 10^{-12} s), “*an electronic transition is most likely to occur without changes in the positions of the nuclei in the molecular entity and its environment*”.^[7] This principle can be applied to both absorption and fluorescence emission that will be further discussed using the *Jablonski* diagram (fig. 3).^[2]

I.1.2 Stage 2: Excited state and fluorescence lifetime

Fluorescence lifetime (τ) is the average “finite” time a fluorophore stays in the excited state prior to its return to the ground state. Generally, the fluorescence lifetime is in the range of 10^{-8} – 10^{-11} s. It depends on all decay forms of the fluorophore as shown in eq. 3,

$$\tau = \frac{1}{k_r + k_{nr}}$$

Equation 3

where k_r is the radiative decay rate and k_{nr} is the sum of non-radiative decay rates. Fluorescence lifetime spectroscopy (FLS) can provide insights into changes of the microenvironment of the fluorophore. These changes impose direct influence on the non-radiative decay rate by processes like collisional quenching, resonance energy transfer, and vibrational relaxation. This time-resolved measurement involves the irradiation of the sample with a short pulse of light and recording the decay of fluorescence intensity with time.^[3,8]

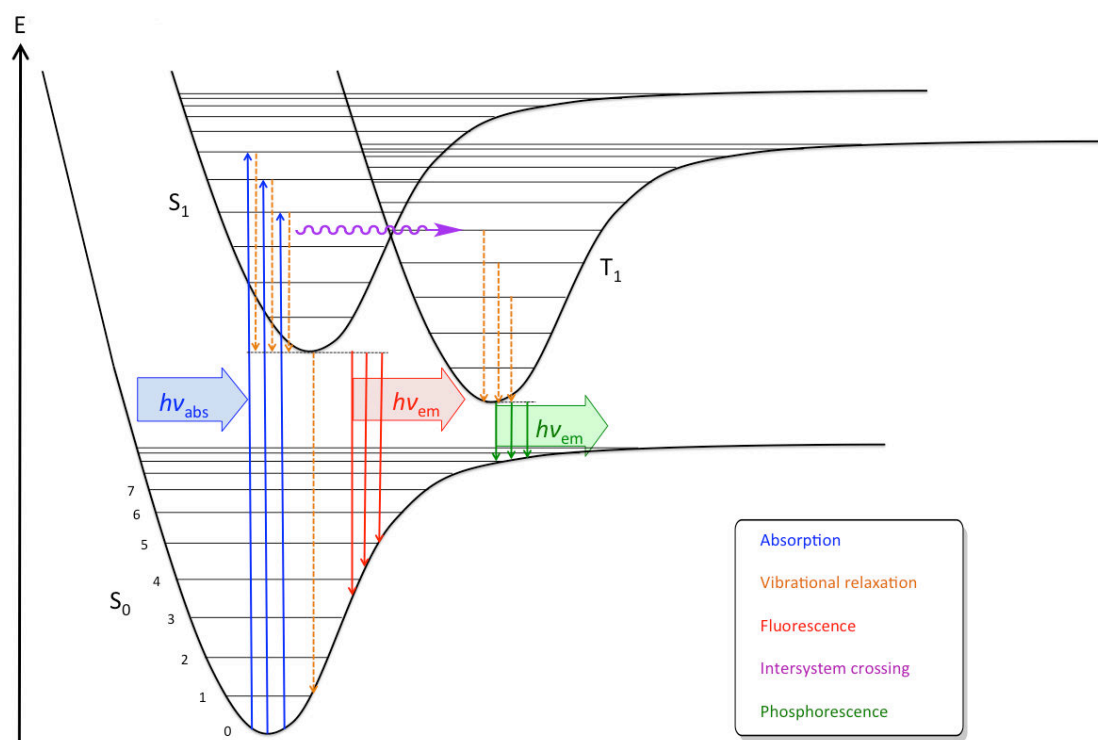


Figure 3. The Jablonski diagram^[9]

I.1.3 Stage 3-Fluorescence emission

The Jablonski diagram^[10] (fig. 3) shows the horizontal lines as the vibrational levels of the electronic states versus energy as the vertical axis. The electronic transition takes place from the lowest vibrational level of the ground state to different vibrational levels of the excited state. The arrows represent the different possible transition processes. An excited molecule undergoes vibrational relaxation (10^{-10} - 10^{-12} s) to the relaxed excited state. Fluorescence may occur if the system returns to S_0 emitting a photon (10^{-7} - 10^{-10} s). The molecule might also undergo an intersystem crossing changing its electron spin multiplicity from a singlet (S_1) to a triplet state (T_1); from which the transition to S_0 emits light as phosphorescence (10^{-1} - 10^{-4} s).^[4] According to *Kasha's rule*, luminescence emission occurs in an appreciable yield only from the lowest vibrational level of the excited state.^[11] As a matter of fact, the real archetype of energy

transition processes related to light absorption and return to the ground state is much more complex and can involve solvent relaxation, delayed fluorescence, and many non radiative processes and phenomena.^[3]

I.1.3.1 Steady-state measurement

Steady-state measurements as the major focus of this thesis, are carried out by exposing the sample to a continuous beam of light (fig. 4). The key optical properties that can be characterized are: the “Stokes shift” in homage to the British physicist Stokes and the fluorescence quantum yield.^[3]

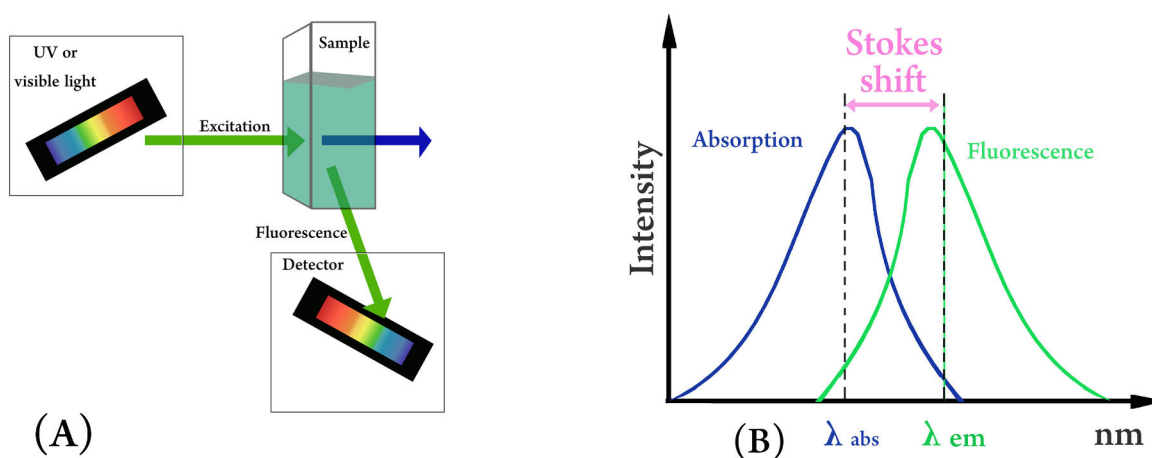


Figure 4. Steady-state measurement

I.1.3.1.1 “Stokes shift”

A fluorophore is mainly identified by its absorption maximum (λ_{abs}) and emission maximum (λ_{em}). Except for upconversion materials, fluorescence emission is generally shifted to the lower energy side compared to absorption ($\lambda_{em} > \lambda_{abs}$). This is mainly due to the dissipated part of absorbed energy in nonradiative relaxation. *Stokes shift* ($\Delta\lambda_{SS}$) is the difference between the band maxima positions of the absorption and emission spectra of the same electronic transition. $\Delta\lambda_{SS}$ can be calculated as shown in eq. 4 and is usually expressed in wavenumber $\bar{\nu}$ units. Wavelength l units are also used for convenience.^[3]

$$\Delta\lambda_{SS}(nm) = \lambda_{em} - \lambda_{abs} \quad \text{or} \quad \Delta\lambda_{SS}(cm^{-1}) = \bar{\nu}_{abs} - \bar{\nu}_{em}$$

Equation 4

1.1.3.1.2 Fluorescence quantum yield

The quantum yield (ϕ) is the ratio of the number of photons emitted to the number of photons absorbed (eq. 5). It identifies the efficiency of the fluorescence process versus the other decay pathways of the excited species.^[12]

$$\phi = \frac{\text{emitted photons}}{\text{absorbed photons}} = \frac{k_r}{k_r + k_{nr}}$$

Equation 5

1.1.3.1.3 Relative brightness

Relative brightness can be calculated as the product of \mathcal{E} and ϕ . Thus, it takes into account both the absorption and the fluorescence efficiency.

II. Fluorophores

Fluorophores constitute a platform of functional dyes and active molecules with marvelous applications in many fields from material to medicinal sciences.^[13,14] Some examples of the vast diversity of uses are enlisted in the “*section III.2*” related to fluorene molecules. However, since this work focuses on the design of fluorene push-pull dyes for labeling nucleic acids and imaging biomembrane lipids as target applications, the bibliographical review will be mostly guided towards these dimensions.

The design of novel fluorophores often aims to achieve the maximum number of the following features:^[1]

- **High extinction coefficient:** The higher \mathcal{E} implies a more efficient excitation. However, there should be a compromise in designing a dye that is relatively small in size but yet, possesses a high extinction coefficient.
- **High quantum yield**, and hence higher brightness: This detects the absolute sensitivity of fluorescence detection.
- **Optimal excitation wavelengths:** Excitation is optimized to obtain the highest brightness at wavelengths close to the absorption maximum. This feature should be chosen based on the application and the availability of the light source.
- **Large Stokes shift:** It allows to reduce the light-scattering effects and to collect more conveniently the emitted light.
- **Optimal emission wavelength:** The desired specificity is the narrow and red shifted

emission.

- **Optimal fluorescence lifetime,**
- **High photostability,**
- **Optimal solubility – penetration – reactivity in the used system.**

The plethora of dyes is extremely rich and diverse in structures, chemistries, and optical properties. Thousands of fluorophores are well described in literature. Due to this large variety, there is no ultimate universal criterion for classification. Here, we try to distinguish some classes, features, and applications in order to discuss few examples.

Fluorophores can be divided into two main classes based on their origins, namely intrinsic and extrinsic fluorophores.^[3]

II.1 Intrinsic fluorophores

Intrinsic fluorophores are those that occur naturally with an autofluorescence such as some amino acids (tryptophan and phenylalanine), nicotinamide, flavin, heme, chlorophyll, fluorescent protein (e.g. hemoglobin, green fluorescent protein (GFP)).^[3]

II.1.1 Fluorescent proteins

(GFP) isolated from jellyfish is one example (fig. 5). The folded structure of this fluorophore is encapsulated into a rigid hydrophobic cage increasing its fluorescence efficiency.^[15] The encoded GFP and variants were used as extrinsic fluorescent reporters for numerous biological processes (*vide infra*).

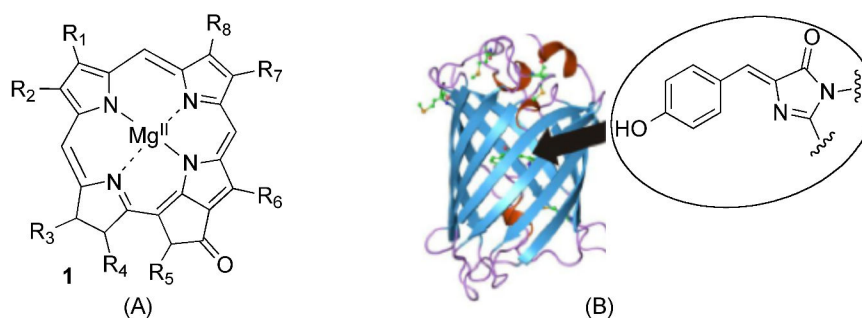


Figure 5. (A) Chlorin magnesium ligand, (B) X-ray structure of GFP and the chemical structure of the embedded fluorophore^[15]

II.1.2 Chlorophyll

Several types of chlorophyll exist. Their main component is the chlorin magnesium ligand (**1**, fig. 5). Light absorbed by chlorophyll is used to drive photosynthesis, dissipated as heat, or

emitted as fluorescence (1-2%). Despite this small proportion, fluorescence is easy to measure even in full sunlight. It is employed as an indicator of the photosynthetic energy conversion. This fact had resulted in devising special chlorophyll fluorimeters that revolutionized the plant and algae research.^[16]

II.2 Extrinsic fluorophores

Extrinsic fluorophores are synthetic molecules or modified biochemicals that can be added to a specimen to provide fluorescence or to change its spectral properties. Encoded fluorescent proteins, fluorescent nanocrystals and small-molecule fluorophores are three extrinsic classes.^[8,17]

II.2.1 Genetically encoded proteins

These fluorophores are often produced within cells.^[18,19] Advances in this field had led to achieve artificial, endogenous proteins with infrared emissions. The major limitation of these proteins is their relatively large sizes (30-50 kDa) compared to small-molecule fluorophores (0.2-2kDa). Their size restricts their applications as target-injectable probes and may perturb imaging of biological processes.^[8] (GFP) is a brilliant example that is used as a gene expression reporter and probe for previously invisible cellular processes (fig.5). GFP technology was the subject of the 2008 Nobel Prize in chemistry.

II.2.2 Fluorescent nanocrystals

The modern field of fluorescent nanocrystals is developing extremely fast for its prospective applications. Two examples are Quantum dots (*Qdots*) and upconversion nanocrystals (fig. 6).

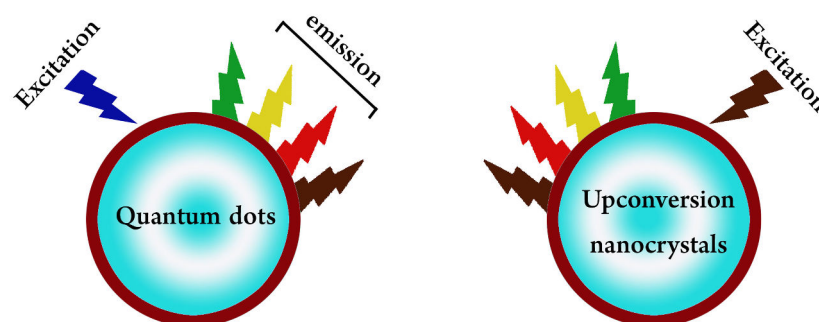


Figure 6. Fluorescent nanocrystals

Qdots are photostable nanoparticles with ultrahigh brightness, broad excitation ranges, and narrow emission peaks.^[20] To date, the relatively large size of Qdots and the toxicity of their

heavy metal constituents limit their applications.^[8]

Upconverting nanocrystals are unclassical fluorophores that produce anti-Stokes emission. They are excited at longer wavelength (NIR) and emit light at shorter wavelengths (NIR or visible). Endogenous fluorophores are not excited in this range. Hence, autofluorescence is reduced.^[8]

II.2.3 Small-molecule fluorophores

An array of small-molecule fluorophores is described spanning the emission spectrum from blue to NIR. These organic compounds typically contain extended conjugated π - bonds.^[8] There exists no benchmark to fairly classify this diverse class. We will categorize them generally into unsubstituted aromatic, classical, and environment-sensitive dyes. This classification mainly depends on their structure dictating their spectroscopic properties and hence, their applications.

II.2.3.1 Unsubstituted aromatic dyes

Nonpolar molecules, such as aromatic hydrocarbons, constitute one part of classical dyes. They are barely sensitive to polarity so they are rarely used in probing environmental interactions. Their low solubility in common organic solvents and the difficulties of their purifications are other limitations. Unsubstituted aromatics have been used in labeling nucleic acids (Section VI.5.2.2). Further, they are imminent scaffolds for single molecule spectroscopy (SMS) where the main objective is to detect the optical signal of *exactly one* molecule hidden deep within a condensed phase. In this dimension, the minimum number of functionalities in the design and the higher photostability of unsaturated aromatic dyes are prospective properties. The 3-D “pseudo-image” of single molecules of pentacene (**2**) in *p*-terphenyl (**3**) is shown as an example (fig. 7(A)).^[21,22]

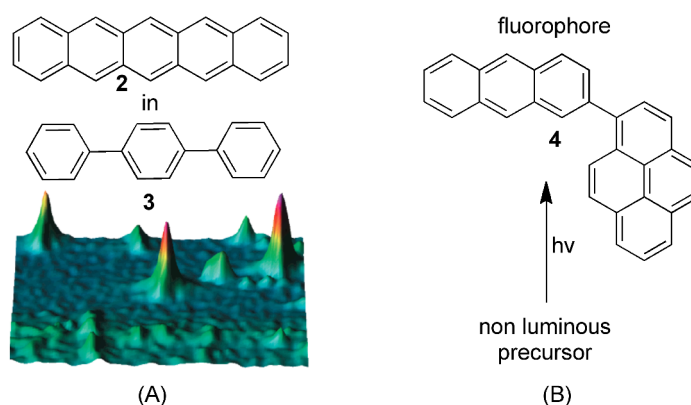


Figure 7. (A) SMS of pentacene in *p*-terphenyl,⁵⁵ (B) Pyrene-anthracene turn-on process

Another interesting pattern of this class, is the one-way (irreversible) conversion of a non-luminous precursor into highly fluorescent pyrene-anthracene (**4**) molecule by light or heat (fig. 7(B)).^[23] This kind of turn-on processes is very attractive to imaging and read-only memory devices. Moreover, naked pyrene, as well as its derivatives, has found many applications in biological detections since its spectroscopic properties exhibit a ratiometric response due to excimer formation.^[24,25] Excimers will be discussed in *section III.1.3* in context of fluorene dyes.

Finally, the luminescent polymers of these aromatic families (e.g. polyfluorenes, Section III.1.6) remain superb designs for many uses even in the absence of polar substituents.

The given examples highlight the importance of understanding the properties of aromatic molecules to architect innovative dyes. Fluorene as our major topic and a representative example of this category will be discussed in details in *section III*.

II.2.3.2 Classical dyes

A second category of classical fluorophores comprises some heteroaryl dyes such as xanthene-based dyes (fluoresceins (**5**), rhodamines (**6**)), cyanines (**7**), and BODIPY (**8**)) that have been employed as fluorescent labels for biomolecules (fig. 8).^[17,26] The spectral sensitivity of these dyes to environmental changes is small. The reason is that their electronic density is delocalized over the whole molecule as a typical feature of these resonant or mesomeric dyes. Two examples are briefly described here.^[17]

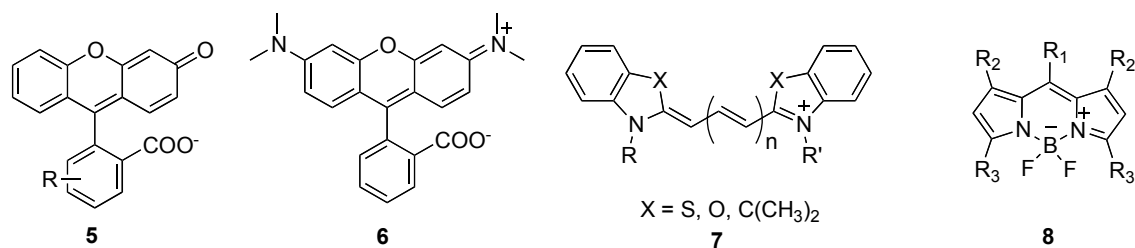


Figure 8. Examples of classical dyes

- **Fluoresceins**

Fluorescein (**5**) belongs to the xanthene family with absorption and emission maxima in the visible region (490 nm and 512 nm in water). Fluorescein is quite water-soluble and has appreciable extinction coefficient and high quantum yields. As a result, this family of dyes is one of the most used molecular probes in biolabeling. The drawbacks of these probes are the high rate of photobleaching and the self-quenching problems after bioconjugation.^[1,27]

- **Cyanines**

The group of cyanine dyes (**7**) is a representative family of long-wavelength fluorophores with high extinction coefficient ($> 100000 \text{ M}^{-1}\cdot\text{cm}^{-1}$) applied in bioconjugations.^[28] The basic structure of cyanines is made up of two aryl or heteroaryl groups linked by a polymethine chain with carbon-carbon double bonds. Classical cyanines have some disadvantages like low quantum yield and tendency to aggregate in aqueous media.^[26] Advanced derivatives of cyanine have been also reported with improved optical properties for more sophisticated applications.^[29]

II.2.3.3 Environment-sensitive dyes

Environment-sensitive dyes constitute a smart class of fluorophores that can sense biomolecular interactions. Unlike “classical” dyes, they possess the property of polarization of their electronic structures that changes upon optical excitation. This dynamic behavior imposes changes in their fluorescence properties (τ , λ_{em} , and ϕ) in response to molecular environment.^[1,17] Hence, they are suitable not only to label biological molecules but also to study their interactions (DNA/proteins, biophysical properties of membrane lipids).^[30-32] These dyes might also act as pH and ion chemosensors that respond by changes in their chemical structure by protonation/deprotonation or complexation reactions.^[33] We will focus on their basic sensitivity that is guided by excited state reactions (conformational change, charge, electron and proton transfer, etc.), non-covalent interactions with the surrounding (van der Waals, dipole-dipole, etc.), and hydrogen bonding.^[17] Clearly, many different interactions and dynamical processes govern the sensitivity of these dyes. It is hard to identify which factor is dominant in a particular environment. Other factors involve viscosity and rate of solvent relaxation, probe-probe interaction, changes in decay rates, etc. Nevertheless, this complexity rendered these dyes indispensable tools in understanding the dogma of vital biological processes.

Molecular rotors and solvatochromic fluorescent dyes are two classes of environment-sensitive dyes. Solvatochromism will be discussed in details in the next section. In essence, molecular rotors respond to changes in viscosity. The conjugated system of these dyes features high rotational flexibility in non-viscous environments (such as water) that quenches the fluorescence efficiency. On the other hand, viscous media (glycol solvents, biomembranes, biomacromolecules) restrict their rotation mobility increasing dramatically the intensity of their emission. Typical examples of molecular rotors are DCVJ probe (**9**) and the prodan analogue (**10**) depicted in *fig. 9(A)*.^[34,35]

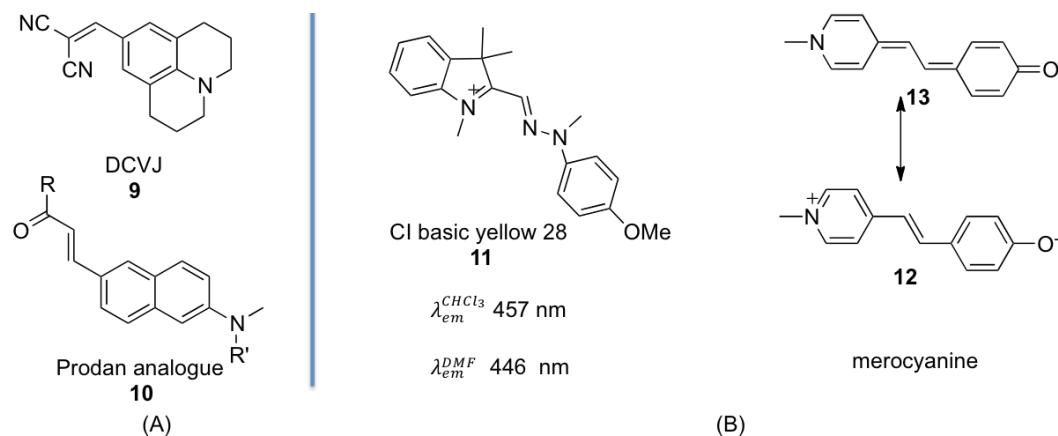


Figure 9. (A) Molecular rotors, (B) Examples of negative solvatochromism

II.3 Solvatochromic fluorophores.

These dyes detect polarity and hydration of their surrounding microenvironments. They have found tremendous applications.^[36]

II.3.1 What is “solvatochromism” in fluorescence context (solvatofluorochromism)?

Solvatofluorochromism can be simply defined as the effect of solvent upon the fluorescence emission of the dye and hence its color. Absorption is generally less sensitive to polarity compared to emission, with few exceptions like molecular rotors. This is because absorption of light is too fast (10^{-15} s) relative to the motions of the fluorophore or solvent (10^{-9} - 10^{-12} s) that have the key effect on emission.^[31,37] For simplicity, “solvatochromism” term will be used instead of “solvatofluorochromism” in the next sections.

II.3.2 Negative solvatochromism:

Relative to thousands of dyes that exhibit positive solvatochromism, this type is rare. Negative solvatochromism or hypsochromic shift signifies a displacement in emission band to a shorter wavelength (blue shift) with increasing solvent polarity. A hypsochromic shift is observed when the first excited state of the dye is less polar than the ground state. Some examples are shown in *fig. 9(B)* such as the CI Basic Yellow (**11**) with delocalized charge and certain merocyanine dyes (**12**) with polar ground state due to a large contribution from its canonical form.^[38]

II.3.3 Positive solvatochromism:

The great majority of dyes encounter a change in the emission band to a longer wavelength (red shift) with increasing solvent polarity. This is stated as “bathochromic shift”. In the sections that follow, discussions of solvatochromism will refer to this major category of dyes with bathochromic shifts.

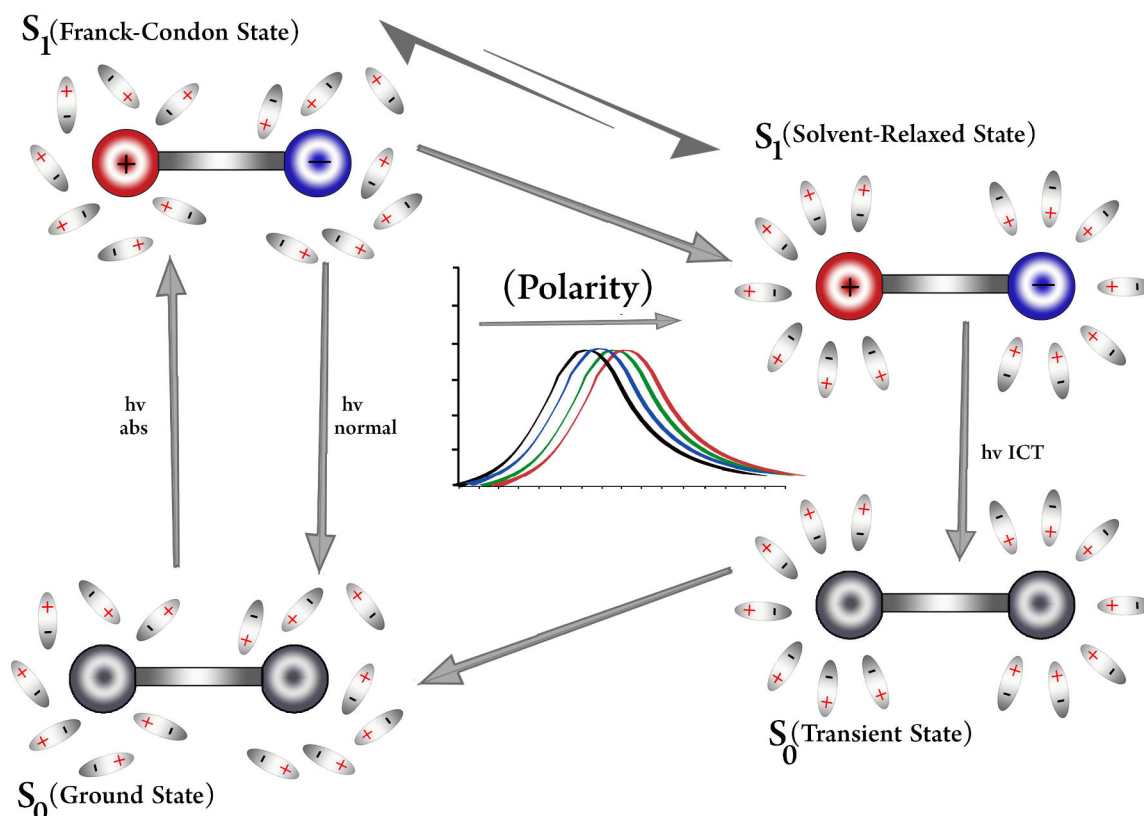


Figure 10. The Jablonski diagram illustrating the effect of solvent

To explain the general effect of solvent polarity, the Jablonski diagram (fig. 10) is considered. In its ground state (S_0), the fluorophore (in black) is surrounded by a sphere of solvent molecules (white). The system is promoted to an excited state (S_1) upon absorbing a photon of the appropriate energy. The dipole moment of the dye in its excited state (Franck–Condon state) increases dramatically due to an intramolecular charge transfer (ICT). The solvent molecules reorient (or relax) fast to accommodate the now larger dipole of the fluorophore. This solvent relaxation lowers the energy of the excited singlet state resulting in solvent-relaxed state (S_1). Simultaneously, the ground state is destabilized into a transient state (S_0) decreasing the gap of energy between the two states. Hence, the emitted photon will be of lower energy and the fluorescence band will be at a longer wavelength. As the polarity of the solvent increases, this

effect becomes larger and relaxation increases red-shifting the emission spectra. These effects are guided by the electronic polarizability of the solvent (described by its refractive index n) and the molecular polarizability (which results from reorientation of solvent dipoles as a function of the static dielectric constant, ϵ). In a similar manner to dipole-dipole interaction, protic solvents can interact with the fluorophore dipole through H-bonding decreasing the energetic band and red-shifting the emission. Water as an example causes a drastic red-shifted emission since it is a strong H-bond donor with a strong dipole.^[17,30] As described earlier, other interactions might also occur in the excited states as represented in *fig. 11* increasing the sensitivity of these dyes.^[3]

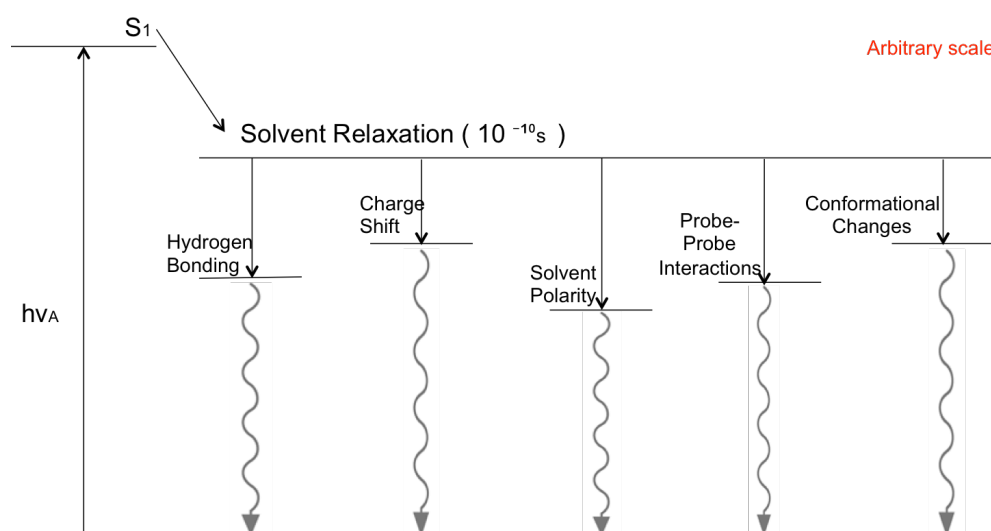


Figure 11. Possible interactions that can influence fluorescence emissions

Another important property of most environment-sensitive dyes is their poor fluorescence efficiency (quenching effect) in water and polar protic solvents. This is due to the sink of energy *via* H-bonds and formation of electron traps in bulk water in addition to the increased competition of the non-radiative decays since the energy gap becomes smaller. Manipulating this property has yielded predominant applications. Accordingly, when these dyes are incorporated into proteins or membrane lipids, they are shielded from the bulk water resulting in strong increase in fluorescence intensity (turn-on).^[17]

We will distinguish two types of solvatochromic dyes, two-band dyes based on excited-state intramolecular proton transfer ESIPT and single-band dyes based on excited-state charge transfer (CT or ICT). In addition, specific dyes show a special case of twisted internal charge transfer (TICT) that will be exemplified in the case of fluorenone (section III.1.4).

II.3.3.1 Two-band dyes

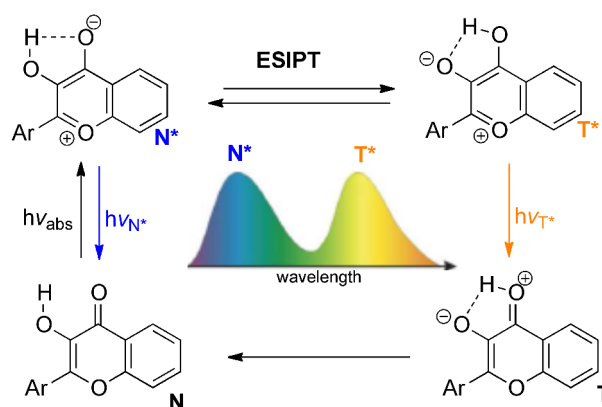


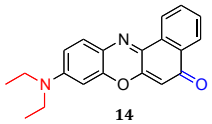

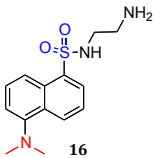
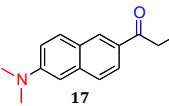
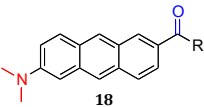
Figure 12. Dual emission by ES IPT mechanism

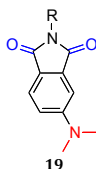
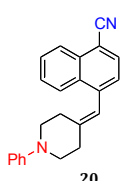
3-hydroxychromones are particularly interesting ES IPT dyes. The origin of their dual emission is the normal excited state (**N***) and the ES IPT tautomer (**T***) (fig. 12).^[39,40] The intramolecular H-bond occurs through a five-membered cycle much weaker than a six-membered one. As a result, the interactions are easily perturbed sensing any change in the environment (polarity, hydration, electric field, etc.). The response is translated as a change in the relative intensities of the two characteristic emission bands. Hence, these molecules are efficiently used to interrogate the biophysics of membranes, to probe the hydration of the major groove of DNA, and to discriminate the conformational changes of DNA/DNA and DNA/RNA duplexes; to name few investigations.^[41-43]

II.3.3.2 Single-band dyes

Examples of the most commonly used single-band dyes are depicted in *table 1*. Their characteristic emission is a single band that responds to changes in the environment polarity by its position and sometimes intensity.

Table 1. Environment-sensitive dyes

Fluorophore family	Representative dye	Example of properties in MeOH	Advantages	Drawbacks
Oxazines and phenoxazines (Ex: Nile Red) ^[44]		$\lambda_{abs} = 553 \text{ nm}$ $\lambda_{em} = 632 \text{ nm}$ $\phi = 38 \%$ $\epsilon = 45000 \text{ (Mcm)}^{-1}$	Red-shifted absorption, emission, high brightness	Moderate fluorescence solvatochromism, quenching in water
Nitrobenzoxadiazole (NBD) ^[45]		$\lambda_{abs} = 456 \text{ nm}$ $\lambda_{em} = 541 \text{ nm}$ $\phi = n. d.$ $\epsilon = 22000 \text{ (Mcm)}^{-1}$	Red-shifted absorption and emission, small size	Weak fluorescence solvatochromism, quenching in water
Naphthalene sulfonic acid derivatives (Ex: Dansyl EDA) ^[46]		$\lambda_{abs} = 335 \text{ nm}$ $\lambda_{em} = 526 \text{ nm}$ $\phi = 49 \%$ $\epsilon = 4600 \text{ (Mcm)}^{-1}$	High sensitivity to solvent polarity (red shift can reach to 200 nm)	UV absorption, very low extinction coefficient, quenching in water
Prodan ^[47]		$\lambda_{abs} = 361 \text{ nm}$ $\lambda_{em} = 498 \text{ nm}$ $\phi = 51 \%$ $\epsilon = 18400 \text{ (Mcm)}^{-1}$	Remarkable sensitivity to solvent polarity, high QY	UV absorption, low extinction coefficient, quenching in water
Prodan analogues (Ex: Anthradan) ^[48]		$\lambda_{abs} = 456 \text{ nm}$ $\lambda_{em} = 604 \text{ nm}$ $\phi = 41 \%$ $\epsilon = 12100 \text{ (Mcm)}^{-1}$	Red-shifted absorption and emission	Very low extinction coefficient, quenching in water

Phthalimide derivatives (Ex: 4DMP) ^[49]		$\lambda_{abs} = 396 \text{ nm}$ $\lambda_{em} = 534 \text{ nm}$ $\phi = 12 \%$ $\varepsilon = 6500 \text{ (Mcm)}^{-1}$	Strong sensitivity to polarity, small size and high rigidity	UV absorption of this family of dyes, low extinction coefficient, quenching in water,
Fluoroprobe ^[50]		$\lambda_{abs} = 308 \text{ nm}$ $\lambda_{em} = 695 \text{ nm}$ $\phi = 0.1 \%$ $\varepsilon = 12000 \text{ (Mcm)}^{-1}$	Strongest sensitivity to polarity, largest Stokes shifts	UV absorption, low extinction coefficient, quenching in water and other polar solvents

As general trends, these dyes are excited in the violet or UV region. They possess relatively low extinction coefficients compared to classical fluorophores. They show poor quantum yields in polar solvents, particularly in water, which is dramatically increased in apolar media. As a consequence, these dyes are employed for sensing polarity and hydration of the environments. They are well-established turn-on probes when they are shielded from the bulk water in investigations of proteins and lipid membranes. However, they pose problems in studying the biological processes in which all the steps are exposed to water such peptide-DNA interactions.^[17]

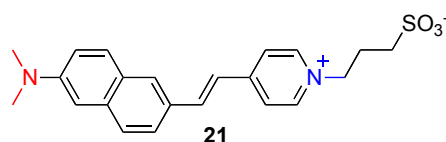


Figure 13. Styryl pyridinium electrochromic dye

Lastly, electrochromic dyes form a special case of environment-sensitive dyes that operate by the same photophysical (ICT) principle. An external electric field will induce the transition between the electronic states resulting in electrochromic shifts in absorption and emissions. Commonly, excitation spectra are used to detect the electrochromic effects since emission spectra can also be affected by polarity. Ideally, any solvatochromic dye may operate as an electrochromic one. The efficiency of the dye's response mainly depends on its structural geometry and transition dipole moment. The most commonly used ones are the rod-shaped molecules where the electron donor and acceptor moieties are installed on the two extreme opposite sides. Styryl pyridinium fluorophore (**21**) is an example of an efficient electrochromic

dye that is mainly used in membrane studies (fig. 13). It constitutes a turn-on probe to detect rigid domains of biomembranes.^[51] Two areas are still under research in this category of dyes; that is to synthesize new fluorophores with: a) strong electrochromic responses in emission and b) enhanced fluorescence efficiencies. Despite the diversity of the existing environment sensitive dyes, none of them combines the features of photostability, ultra brightness, red-shifted absorption, and high fluorescence solvatochromism. This critical overview (table 1) urges researchers to find new dyes with enhanced properties. So, comprehensive studies of how to design such fluorophores and the structure-photophysics relationships are still compelling.

II.4 Push-pull dyes

The (ICT) environment-sensitive dyes belong to a broader category of “push-pull” molecules (fig. 14). They consist of a conjugated (usually aromatic, π) system functionalized with an electron-donating and withdrawing group respectively abbreviated as donor (D) and acceptor (A).^[52]

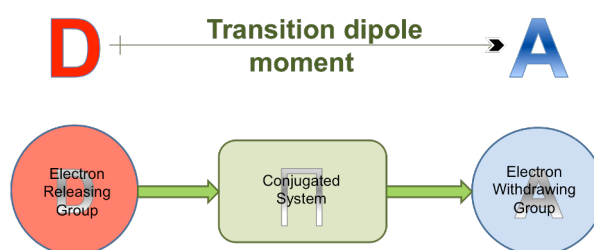


Figure 14. General architect of push-pull dyes

The D- π -A system undergoes a photo-induced intramolecular charge transfer (ICT) state forming a low-energy molecular orbital (MO). To briefly recall, visible light provides sufficient energy to excite the electrons within this new MO, making these compounds generally colored.^[52] The ICT also generates dipole moments that augment the sensitivity of these fluorophores in response to polarity.^[31,37] The extent of the ICT character has decisive effects on both the properties of the molecule. The two extreme forms of the ICT of a fluorene push-pull dye are illustrated in *fig. 15*.

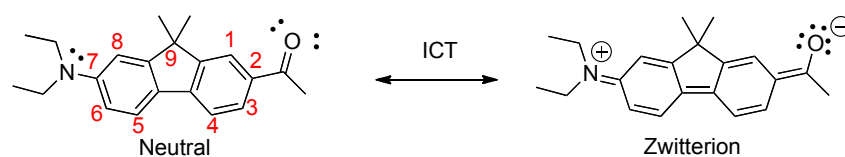


Figure 15. The neutral and ICT resonance forms of a fluorene push-pull dye

The π -conjugated framework in these compounds is typically made of multiple bonds (olefin or acetylene), aromatics (benzenoids), heteroaromatics (ex: thiophenes), or a combination of these spacers. D- π -A molecules adopt a linear arrangement. However, there are other arrangements of push-pull systems outside the scope of this thesis. Examples are quadrupolar (D- π -A- π -D) and octupolar ((D- π)₃-A) systems. In addition to their uses as fluorosensors, push-pull molecules have found fundamental applications in material sciences such as nonlinear optical (NLO) switches, electro-optic, piezochromic materials, and other science fields.^[52]

Typical electron donors are substituents with positive mesomeric (M) and inductive (I) effects such as OH, NH₂, OR and NR₂, heterocyclic moieties such as thiophene as well as some metallocenes. Typical electron acceptors featuring negative (M/I) effects involve NO₂, CN, CHO and electron deficient heterocyclic compounds such as benzothiazole and imidazole.^[52,53]

In principle, the ICT degree, the corresponding HOMO-LUMO gap, and hence; the optical properties and response can be tailored by:

- (i) The electronic nature of D and A groups,
- (ii) Efficient D-A interaction and planarization of the entire system,
- (iii) Extension, composition, and spatial arrangement of the π -linker,
- (iv) Reducing the bond-length alternation (BLA). The BLA can be defined as the difference between the average C-C single and multiple bond lengths of the π -system in its two limiting resonance forms (aromatic vs. zwitterionic).^[52]

III. Fluorene and its derivatives

As demonstrated, the aromatic core plays a key role in the architecture of efficient fluorophores. Thus, came the choice of the fluorene family as the (π) framework studied in this thesis.

Fluorene or 9H-fluorene is a rigid, planar polycyclic aromatic hydrocarbon with an extended π -electron delocalization (fig. 15). Fluorene forms white crystals that have violet fluorescence from which its name was derived.^[54] The benefits of the fluorene core are four-fold:

- First, the fluorene chromophore comprises a methylene group conjugated to two benzene rings (12 π electrons) in high electronic symmetry. This methylene bridge forces the two phenyl rings to be planar increasing their orbital overlap, the rigidity of

the system, and the degree of conjugation of electrons. The CH₂ bridge greatly compromises the lack of traditional auxochromic heteroatoms (N, O, S, etc.) in facilitating the charge transfer resulting in strong linear and nonlinear interactions upon excitation.^[54]

- Second, the absence of auxochromes in fluorenes constitutes an advantage over traditional heterocyclic chromophores. Endocyclic heteroatoms in other spacers prompt non-radiative deactivation of the excited states, thus decreasing the quantum yields.^[55] Auxochromes also facilitate the forbidden n- π transitions as powerful channels of photodegradation.^[2,3,56] Correspondingly, the chromophoric systems that include the fluorene nucleus demonstrated relatively high thermal and photochemical stability under both one and multi-photon excitation conditions.^[57,58]
- Third, the advantage of this family is its high fluorescence efficiency. Indeed, some fluorene derivatives fluoresce with quantum yields that approach “unity”.^[59-62]
- Fourth, the molecular backbone has two-fold versatile functionality. The acidity of the protons of the methylene group provides a potentially active site for condensation reactions. This position can be used to introduce side groups that can enhance the solubility in organic solvents or water and can tune the electronic properties at the same time. Further, the aromatic hydrogen atoms can be involved in substitution reactions. Positions 2, 7 and 4, 5 are the most reactive (fig. 15). The possibility of the selective functionalization of fluorenes on the CH₂ group or the aromatic rings opens up the gates to synthesis of unique soluble fluorophores with superb properties. This provides access to a broad range of physico-chemical, optical, electrical, and magnetic properties apt for various interesting applications by modulating the electronic abilities of the introduced groups. From structural perspectives, this allows the synthesis of practically important star-like or dendrimer dyes^[63,64] and the introduction of desired rigid linkers for covalent labeling of biological species such as DNA or amino acids.^[65-67]

This structural robustness and tunable behavior gave us a strong impetus to develop practical fluorene derivatives.

III.1 Particular features of fluorene and its derivatives

III.1.1 Two-photon absorption

- **Significance**

Several modern technologies exploit this process like two-photon fluorescence imaging and photodynamic cancer therapy.^[68,69]

The seminal work involving two light quanta in one elementary action by Maria Göppert-Mayer in her dissertation in 1931, has established the theoretical framework for two-photon absorption (2PA). 2PA is the near simultaneous absorption of two photons of identical or different frequencies in order to excite a molecule to a higher electronic state. The sum of the energies of the two photons is equal to the energy difference between the initial and final states of the transition. Recalling that energy is inversely proportional to wavelength, the two absorbed photons must have a wavelength about twice that needed for one-photon excitation (fig. 16). For instance, if a fluorophore absorbs UV light (350 nm), it can also be excited by 2PA of NIR (~ 700 nm).^[70]

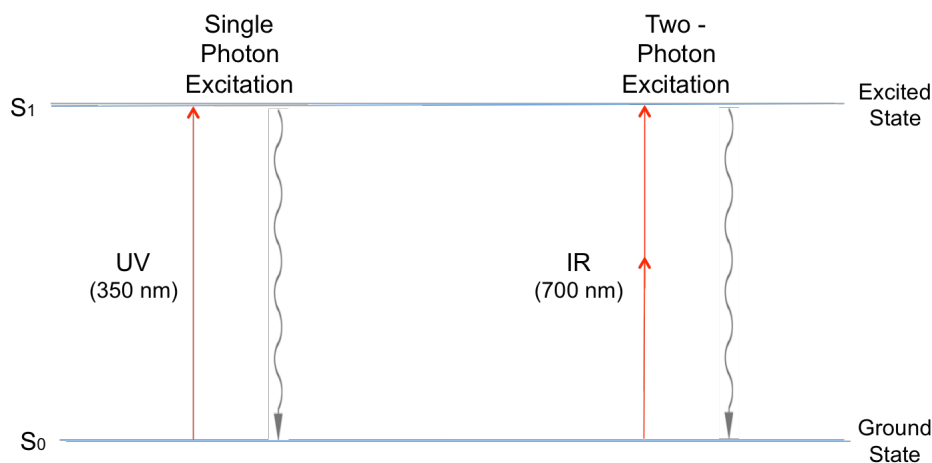


Figure 16. Single-photon versus two-photon absorption

A finite instant of time ($\sim 10^{-15}$ - 10^{-18} s) is afforded for a second photon to arrive and complete the excitation into the final electronic state. For this reason, practice of this pioneering work had to wait decades for the invention of the “laser” that provides high intensity radiations to effectuate such transitions.

Since this process depends on simultaneous absorptions, the resulting emission varies with the square of the excitation intensity (quadratic relationship). Thus, 2PA is a nonlinear optical process.

- **Two-photon fluorescence imaging**

The longer wavelength excitation minimizes the light scattering and autofluorescence caused by the ingredients of living tissues that normally absorb at shorter wavelength and fluoresce. Further, water absorbs minimally in the NIR regime; therefore, light can penetrate deeper into thick biological media. In two-photon fluorescence imaging, high spatial resolution is achieved and less phototoxicity is encountered by the biological samples.^[71-73] Fluorene derivatives have been extensively investigated and employed as dyes with appealing 2PA properties.^[59,60,74,75]

III.1.2 Aggregation-Induced Emission Enhancement (AIEE)

When a fluorophore is aggregated in the condensed phase, partial or total fluorescence quenching is often observed. This aggregation-caused quenching (ACQ) is a limitation in practical applications. As opposed to this effect, some distinguished fluorophores such as some fluorene derivatives possess the property of aggregation-induced emission (fig. 17).^[76] The AIE property has been applied in recent sensing technologies.^[77] Specifically, the aggregation of AIE molecules can be tuned by different parameters (electrostatic interaction, coordination interaction, hydrophobic interaction, steric hindrance, polarity, viscosity) to produce useful turn-on probes. In this context, the fluorene derivatives (**22**) and (**23**)^[78] are weakly emissive in solution. Upon aggregation, they show intense emission and change in fluorescence color.^[79]

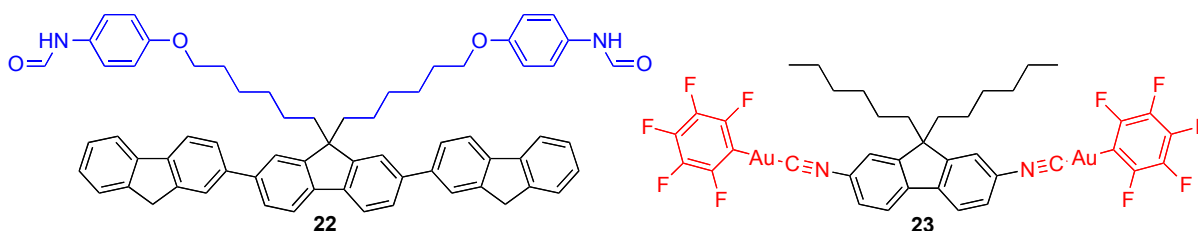


Figure 17. AIEE fluorene derivatives

III.1.3 Excimer formation

In fluorescence spectra, excimers are observed as strongly red-shifted bands in concentrated solutions. Excimers can be described as short-lived dimers that are unbound in their ground state but rather tightly bound in their excited state. Since 1970, excimers in fluorene were observed.^[80] Successive work has reported this behavior and its applications later, mainly in polyfluorenes,^[81] fluorenone (**24**), and its derivatives^[82-84] (fig. 18).

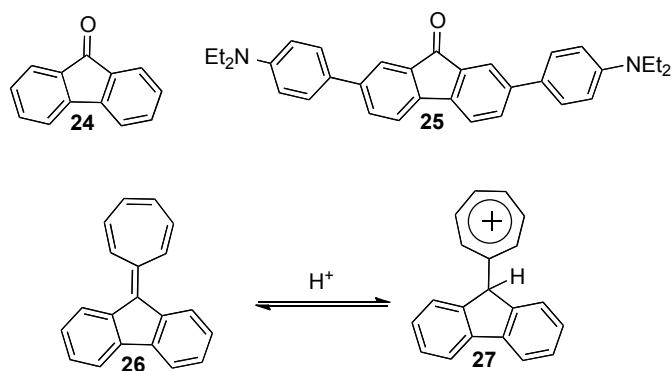


Figure 18. Some examples of distinct fluorene derivatives

III.1.4 Twisted Intramolecular Charge Transfer (TICT)

TICT is the special case of charge transfer that occurs due to conformational changes (distortion from planarity) in the excited state of the molecules. Literature shows that there is no clear agreement on the need of a real twisting in the molecule to achieve this process.^[3] TICT imposes more pronounced solvatochromism and can be controlled to have ratiometric response by switching fluorescence between two possible distinct states of the molecule (TICT vs. excimer emission) changing the solvent (e.g. fluorenone (**25**), fig. 18). Excimer emission of (**25**) appeared in apolar solvents. The emission gradually disappeared with increasing the solvent polarity where TICT emission started to appear. This paradigm can be seen as an interesting hypsochromic shift where red-shifted band of excimer is louder in apolar solvents such as toluene than a TICT band. Fluorenone derivatives are reported to participate in several donor-acceptor designs inducing TICT emission.^[77,83,85]

III.1.5 Profluorescence of fluorene derivatives for turn-on applications

The 9-cycloheptatrienylydene fluorenes (9-CHF, **26**) are “profluorescent” derivatives. They possess natural suppressed fluorescence, which is returned upon conversion to emissive species (**27**) under acidic conditions. 9CHFs can be used as chemosensors for the detection of pH and metal ions (fig. 18).^[86,87]

The 9-CHF scaffolds also demonstrate that aromatic hydrocarbons can be tailored for sensing techniques without the introduction of any auxochromic heteroatoms.

III.1.6 Polyfluorenes (PF)

PFs can be achieved by different polymerization reactions.^[88,89] For instance, fluorene monomers can be directly connected to each others *via* Pd- or Ni-mediated couplings at the 2 and 7 positions, producing a series of oligofluorenes or polyfluorenes (**28**) with increasing conjugation lengths (fig. 19).^[90,91] When the substituents at 9-position of PF (**28**) are butyl or

longer chains, the resulting polymers are highly soluble in non polar solvents.^[89] Alkyl chains marginally affect the optical properties of the polymers in dilute solutions since they are far from the conjugation system at positions 2 and 7. However, they induce an aggregation effect in solid states or once concentrated.^[92] In addition, the C-9 position is used to incorporate different charged functionalities as pendant groups to render PFs water-soluble and hence, suitable for biological detections.^[65,66] PF (**29**) is a typical example with fluorescence efficiency that ranges from 20 to 40 % in water (fig. 19).^[93] Bazan's group has extensively researched this kind of cationic polyfluorenes.^[94-97] These PFs have been employed in fluorescence studies and FRET experiments on DNA displaying appreciable variations in properties between single and double stranded DNAs (ssDNA and dsDNA).

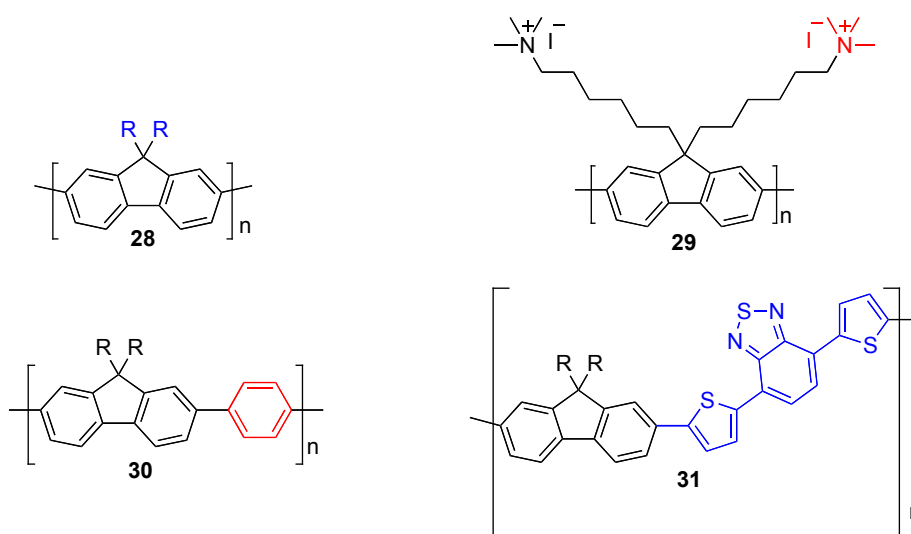


Figure 19. Polymers and copolymers of fluorenes

Regarding photophysics, polymerization can be viewed as an amplification mechanism to the properties of the parent fluorene family. Increasing the fluorene repeating units extends the π conjugation; thus, narrows the gap between the electronic bands. This, in turn, red shifts the absorption maximum up to 12 repeating units and the emission maxima up to 6 repeating units. The spectral properties of the polymer reach a constant level after this number of units. PFs generally absorb in the UV region and emit blue light. Their reported fluorescence yield exceeds 50 % both in solutions and solid states.^[98]

Moreover, color tuning of PFs can span the entire visible spectrum. This is easily achieved by copolymerization with appropriate comonomers such as benzene, naphthalene, thiophene, or benzothiadiazole. Polymers (**30**) and (**31**) are two examples (fig. 19). As a final note, polyfluorenes can show a desired ratiometric response (excimer vs. aggregate forms).^[81] All the mentioned virtues accompanied by the high thermal and chemical stability made PFs beneficial composites of all dimensions of fluorescence nanotechnology.^[99-101]

III.2 Array of uses of fluorene and its derivatives

Monomer and polymer derivatives of fluorenes found uses as functional dyes in many fields owing to the success in tailoring their desirable features.^[54]

III.2.1 Fluorescence imaging and application related to biology

Fluorenes manifest the needed spectroscopic virtues, low cytotoxicity, and appreciable 2PA cross-sections that allow cell imaging with reduced photodamage. They found important applications in biomedical research and phototherapy,^[102-104] as well as effective fluorosensors for ions,^[105,106] aggregations,^[84] proteins,^[101] and explosives.^[107] Fluorene derivatives are also active ingredients in different medicinal generics like antiviral drugs.^[108] Precisely, the applications related to apoptosis and nucleic acids will be discussed in their corresponding sections (V.2.2 and VI.8). With respect to the background of imaging plasma membranes, only a fluorene-quinolizinium cation membrane probe (**32**) is described in literature (fig. 20).^[109] Belfield group is pioneering in research related to novel fluorene derivatives, multiphoton imaging, and related applications.^[59,68,110-113] They have attributed the bright fluorescence of probe (**32**) to binding with cell membrane proteins. To the best of our knowledge, fluorene dyes have never reported as probes of plasma membrane lipids.

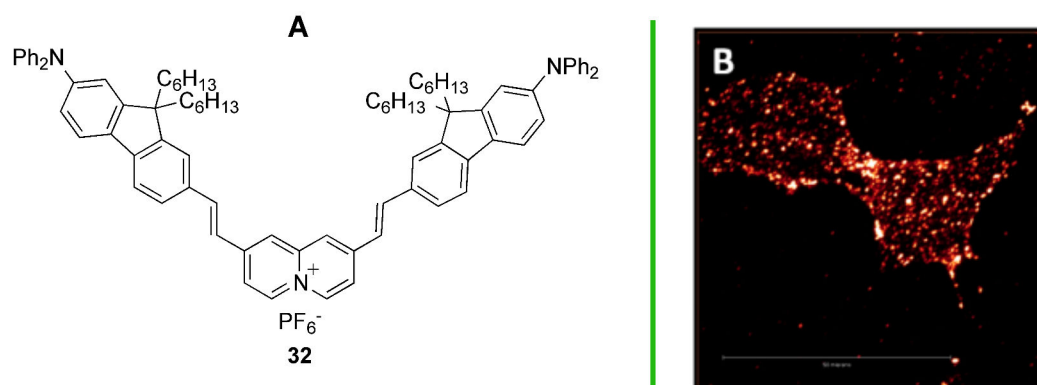


Figure 20. (A) The fluorene probe of cell membrane, (B) Fluorescent image of HeLa cells co-incubated with the probe

III.2.2 Optical data storage

Optical recording using dyes involves converting excitation energy into thermal energy by non-radiative decay. Essentially, fluorene dyes are coated as recording layers onto discs. ^[13,114]

III.2.3 Organic Light-Emitting Devices (OLEDs)

OLED is an available technology for emissive flat panel displays. PFs have favorable thermal and photostability as well as enhanced properties of packaging and solubility. They possess efficient emissions of UV or deep blue light making them perfect candidates to blue light emitting diodes.^[115,116]

III.2.4 Dye-sensitized solar cells (DSSCs)

DSSCs are designed of an efficient dye sensitizer (like fluorenes) anchored to a semiconductor. The light absorbed by the dye photo-induces an electron injection into the conduction band resulting in charge separation that is transported to a charge collector.^[117,118]

III.2.5 Non linear optical dyes in telecommunication

In telecommunications, data transmission is most efficient *via* IR laser radiation. Consequently, fluorene with high 2PA cross-section can effectively double the energy and convert the IR radiation to visible ones allowing easier detection of the signals.^[13]

III.3 Synthesis of aminofluorenes

▪ Conventional routes

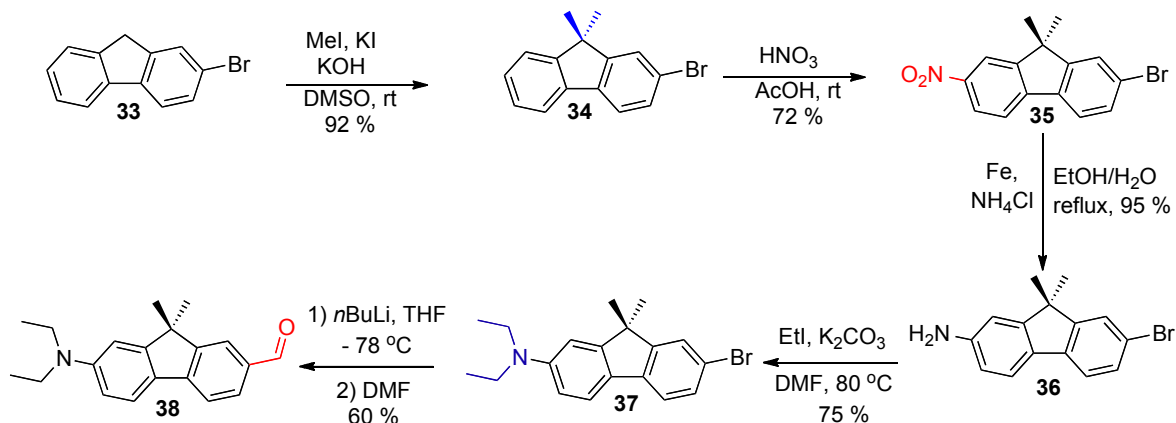


Figure 21. Synthesis of the fluorene analogue of prodan

To date, the introduction of the nitrogen nucleophile moiety into fluorene scaffolds is not easily accomplished. The described pathways to synthesize aminofluorenes involved long syntheses engaging harsh conditions as nitrations and Ullmann-type couplings.^[102,119] For instance, introducing aziridine^[120] and dimethyl amine^[85] was reported each in five steps. Even incorporating simpler amines such as benzyl amine requires three steps.^[121] The synthesis of the

most environment-sensitive analogue of prodan (**38**) is shown in *fig. 21*.^[60] Despite the advanced optical properties of this push-pull dye, catalytic routes could improve its synthetic access.

The synthesis was achieved by conventional methods, namely C9-dimethylation of (**33**), then regioselective mono-nitration followed by iron-mediated reduction to produce the amino intermediate (**36**). Nucleophilic substitution afforded the diethyl amine as the donor moiety of the design (**37**). The acceptor part was installed by a halogen-metal exchange with *n*-BuLi on adduct (**37**) followed by treatment with DMF to provide (**38**) as the push-pull dye.

This approach only permits installing some amine donors; cyclic amines cannot be introduced easily. This limitation prevents the tuning of optical properties; a necessary plan to rationalize the dye designs apt for the challenging applications.

Hence, finding new versatile methodologies to selectively introduce the amine moieties has evolved as a must. In that aspect, we envisioned the palladium-catalyzed C-N coupling reactions as a solution. A robust Buchwald-Hartwig amination can replace the aforementioned classical synthetic pathway by a shorter route.

▪ Buchwald-Hartwig amination

In 1995, Buchwald and Hartwig simultaneously introduced secondary amines to aryl Bromides (**39**) using different catalytic Pd systems (*fig. 22*).^[122,123] Several hundred publications have appeared ever since the early work reporting various efficient catalytic systems of varied palladium sources, ligands, bases, and other reaction conditions (inertness, temperature, solvent, and additives).^[124-127]

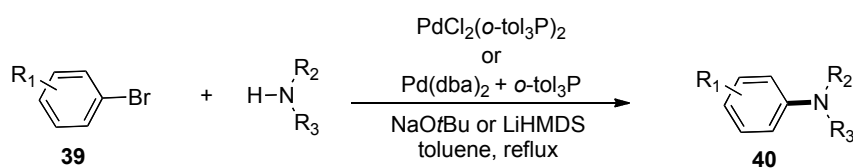


Figure 22. Primary developed Buchwald-Hartwig aminations

Many mechanisms have been beheld for the Pd catalytic cycle involved in this reaction. Since mechanistic studies is outside the scope of this thesis, a simplified cycle is illustrated in *fig. 23* to discuss the general considerations.^[128]

After the formation of the $L_n\text{Pd}(0)$ catalytic species (n commonly = 2, L = tertiary phosphines), oxidative addition of the aryl halide to $L_n\text{Pd}(0)$ forms a Pd(II) intermediate. Next, coordination of the amine followed by its deprotonation using a base takes place. The formed amide intermediate can produce the arylamine by reductive elimination regenerating the catalyst to

start a second cycle. However, a side reaction can occur in the final step wherein the amide undergoes a competing beta-hydride elimination yielding an undesired hydro-dehalogenated product and an imine.

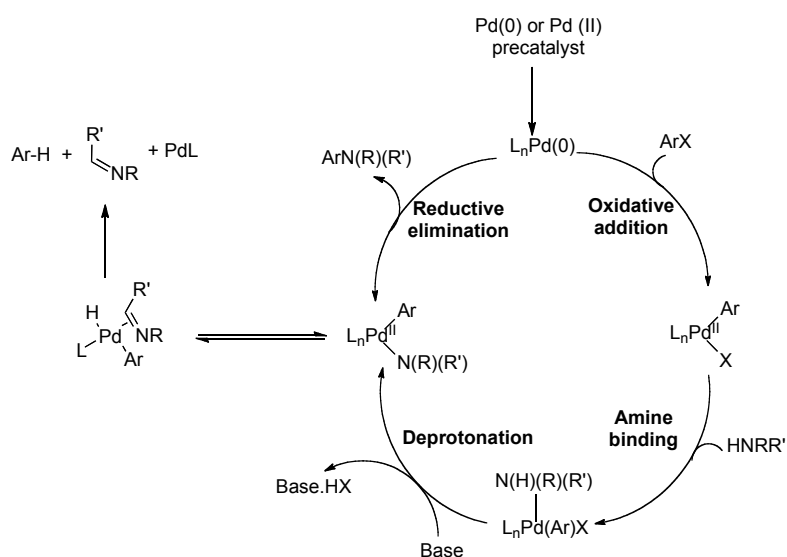


Figure 23. Simplified catalytic cycle for palladium-catalyzed amination

The electronic and steric properties of the catalyst and the substrate decide the rate of the oxidative addition step. Faster rates are achieved if the chosen catalyst is sterically unhindered and electron-rich. Considering the C-X bond that is broken in this step, the nature of the halide also affects the rate; which follows this general trend ($I > Br > Cl > F$).

The rate of the amine coordination step depends on both the amine substrate and the catalyst. The rate increases when the amine is more basic and/or sterically unhindered. Next, the acidity of the coordinated amine determines the rate of deprotonation step.

Reductive elimination depends on the metal/ligand properties. Generally, bulkier and electron poor ligands increase the rate of reductive elimination since this step in the cycle causes the Pd metal to return more electron-rich.

The final step has the biggest impact on the yield of this reaction. If the alkyl group attached to Pd has a β -hydrogen, this hydrogen might be transferred to the metal by forming a double bond on the alkyl group. This competition with the desired reductive elimination step can generate the Ar-H side product decreasing the yield.

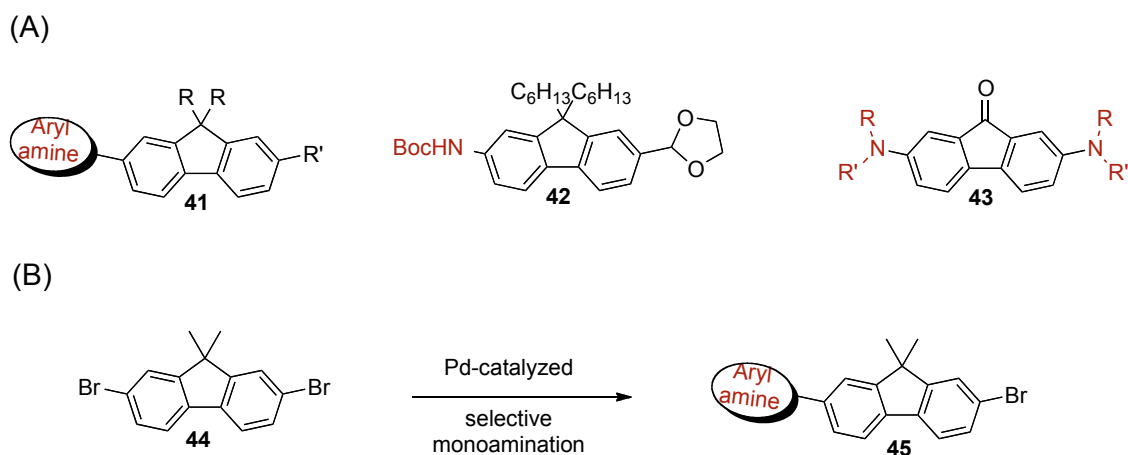


Figure 24. Pd-catalyzed synthesis of aminofluorenes

Considering fluorenes in particular, Pd-catalyzed aminations have been limited to aryl amines (**41**)^[61,83,103,129,130] and few other donors (**42**) and (**43**) in specific designs^[107,131,132] (fig. 24(A)). A general amination methodology has not been yet reported to diversify the amine donor onto fluorene dyes to the best of our knowledge.

▪ Selective C-N cross couplings

Pd-catalyzed coupling to one halogen in the presence of another competing halogen atom will be referred to as a “*controlled coupling*” in this work. In literature, such type of controlled couplings has been limited to a narrow array of substrates based on the halogen or pseudo halogen selectivities (Br/Cl, Br/Otf, or I/Br).^[83,133,134] Despite the easy access to simple dihalogenated aromatic scaffolds (e.g. dibromofluorene (**44**)), controlled couplings on these moieties have seldom been reported especially in the context of synthesizing beneficial materials (fig. 24).^[135-140] Conventional routes might still be preferred due to the overestimation of the role of glove box in Buchwald-Hartwig C-N couplings. The endless list of costly palladium sources, ligands, and bases also complicates the choice of a suitable system in synthetic chemistry. Hence, one of our main objectives was set to develop robust, air-stable catalytic conditions to diversify the library of dyes and to incorporate challenging amine donors otherwise inaccessible by classical aminations.

IV. Fluorosensing

Fluorescence is the most well-developed, successful, and sensitive technique in all biological sensing technologies (electrochemical, calorimetric, etc..) by virtue of its exquisite features such as:^[1]

- **Ultra-high sensitivity** detecting even trace amounts,
- **Absolute sensitivity** attaining the limit of detection of exactly a single molecule,^[21,22]
- **High temporal resolution** establishing precise and fast response,
- **Very high spatial resolution** allowing efficient cellular imaging,
- **Non-destructive and non-invasive character** allowing the remote control of interactions in living cells,
- **Boost in the domain of “synthetic fluorophores”** allowing low dosage and desired selectivity,
- **Good repetitiveness** of the measurements minimizing false recordings,
- **Versatility** providing detections in solid, liquid, gas, and even at the interface of these phases.^[1]

The illuminated cell (fig. 25) presented by *Thermo Fisher company* as a catalogue to choose a commercial fluorophore obviously demonstrates the strengths of fluorescence techniques. Nowadays, there exist relatively inexpensive dyes to precisely probe and image most of the important cell organelles, regions, and big part of cellular molecules including H_2O_2 , peroxyxynitrite, O_2 , Cu^+ , K^+ , cysteine, phosphatase, etc... ^{[141] [142]}

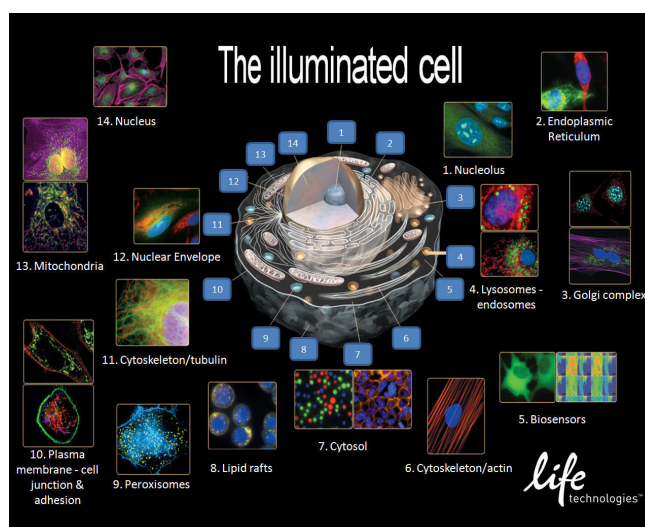


Figure 25. The illuminated cell

Fluorophores are used in two distinguished lines of fluorescence applications related to biological detections, labeling and sensing.^[1]

IV.1 Fluorescence labeling and detection

Fluorophores used in labeling often belong to the classical dyes that establish fluorescence

signals insensitive to environmental conditions. The response “signal” is only proportional to the concentration of the dye. The main role of these ‘labels’, ‘tracers’ or ‘tags’ is solely to detect a particular medium or site. These tools also provide good spatial resolutions for cell imaging. Fluorescent labels should be photostable with high brightness and should possess optimal conditions of excitation and emission.^[1]

IV.2 Fluorescence sensing

This domain comprises the environment-sensitive dyes. A *fluorosensor* or *reporter* is defined as a dye that undergoes structural or conformational change in response to specific factors or/and environmental conditions. These changes are reversible and independent of the concentration of the dye. They result in variation of the output signals, particularly the emission parameters. The photostability and brightness remain highly important, but a whole set of parameters could be controlled and optimized to unravel the molecular mechanisms and dynamics of complex biological machineries (nucleic acids, proteins, lipids, etc.). These parameters are summarized in *fig. 26* and have been discussed in the previous sections. Herein, FRET and anisotropy will be briefly defined.

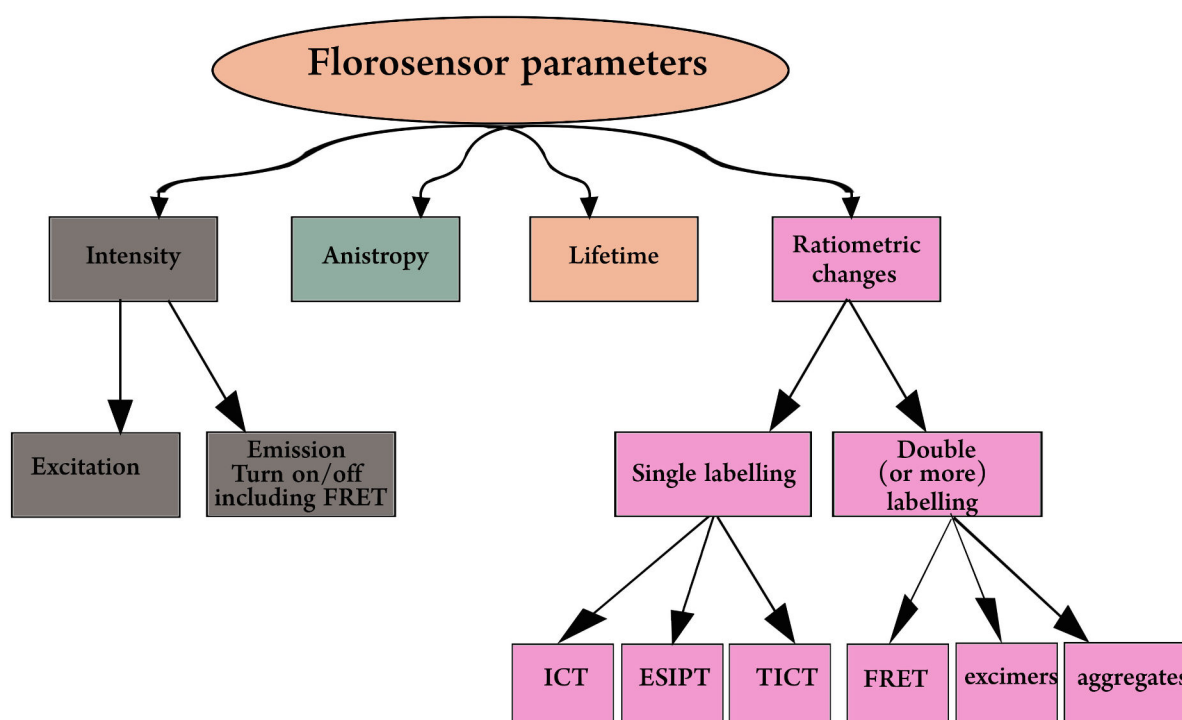


Figure 26. Parameters of fluorosensors

IV.2.1 FRET

Förster Resonance Energy Transfer (FRET)^[143] is a process occurring between compatible chromophores; namely a donor and an acceptor pair (fig. 27). The donor, initially in its excited state, transfers energy to the acceptor through a non-radiative dipole-dipole coupling resulting in quenching if the acceptor is a quencher, or a new fluorescence emission at wavelength typical for the acceptor if the latter is emissive.^[77] The criteria of a FRET platform include:

- Well-separated absorption spectra of the donor and acceptor to ensure independent excitations,
- Well-resolved emission spectra of the donor and acceptor for high accuracy in the measurement of fluorescence intensity ratios,
- Significant spectral overlap “**J**” between the emission of the donor and the absorption of the acceptor,
- Comparable brightness of the two dyes,
- Appropriate linkers to avoid fluorescence quenching in aqueous media,
- Energy transfer efficiency E inversely proportional to the sixth power of the distance between donor and acceptor as *defined in eq. 6*,

$$E = \frac{R_0^6}{R_0^6 + R^6}$$

Equation 6

where R signifies the distance between the donor and acceptor and R_0 is the Förster distance at which the fluorescence transfer efficiency is 50 %.

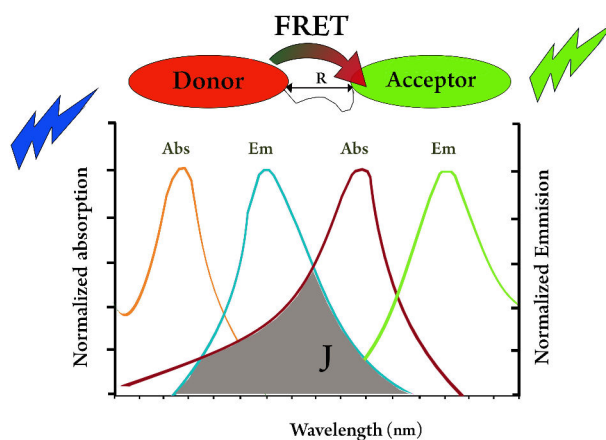


Figure 27. Schematic illustration of an efficient FRET

IV.2.2 Anisotropy

The extent of emission polarization of a fluorophore upon excitation is described in terms of the anisotropy (r). The origin of anisotropy is the transition moments that take specific directions within the fluorophore structure. When polarized light is applied to randomly oriented fluorophores, only a fraction of the molecules oriented in a particular way are excited. Fluorophores having their transition moments along the electric vector of the polarized light correspond to the best orientation for photoexcitation. Depolarized emission can commonly occur due to rotational diffusion that changes the orientation of the transition dipoles during the lifetime of the excited state. In turn, the rotational diffusion depends on the size and the structure of the rotating fluorophore and on the viscosity of the environment. Anisotropy measurements reveal the average angular displacement of the fluorophore that occurs between absorption and emission detecting changes in viscosity of the environment surrounding the fluorophore or its rotational mobility.

Since the time scale of rotational diffusion of biomolecules is in the same range of the decay time of many fluorophores, anisotropy measurement is a good fluorescence technique in biochemistry. For example, anisotropy measurements are used in quantifying proteins denaturation, studying their interactions with other macromolecules, and in probing the internal viscosities of biomembranes and their lipid compositions. This technique is particularly fruitful for studying the interaction and binding of small molecules bearing a fluorophore to larger target molecules (e.g. protein, DNA) since the interaction should result in a large reduction of the mobility of the probe detected by high anisotropy.^[1,3,144]

V. Membrane Lipids

Biological membranes are made up of composites of lipids with embedded proteins held by non-covalent interactions. Sugars are bonded to the lipids and proteins of the outer side of the membrane by covalent bonds. The most common arrangement of lipids is a bilayer acting as a barrier for the passage of polar materials. The physical nature of the bilayer membrane will vary depending on its lipid composition and surrounding environment. These physical properties along with the structural specificities of the lipids determine the function of the membrane. As a particular example, cell membranes separate and protect the interior of all cells from the exterior environment. They are also involved in various cellular processes such as transport, adhesions, and signaling.^[32]

V.1 Classifications of membrane lipids

The lipid structure is amphiphilic with a polar head and lipophilic alkyl chains. A biomembrane can contain up to thousands of lipid molecules that differ by their head groups, their hydrocarbon tails, and the degree of their unsaturation.

In mammalian membranes, lipids can be classified into three groups: glycerophospholipids, sphingolipids, and sterols (fig. 28).^[32]

V.1.1 Glycerophospholipids

The most common molecule of this series is phosphatidylcholine (**46**) forming > 50 % of biomembranes. It is composed of a diacylglycerol backbone (glycerol esterified with two fatty acids; most commonly one saturated and the other unsaturated) carrying a phosphate group (phosphatidic acid esterified by a choline). Other glycerophospholipids have variations in their structures like saturated instead of unsaturated fatty acids, ethanolamine instead of choline, ether instead of ester linkages.^[32]

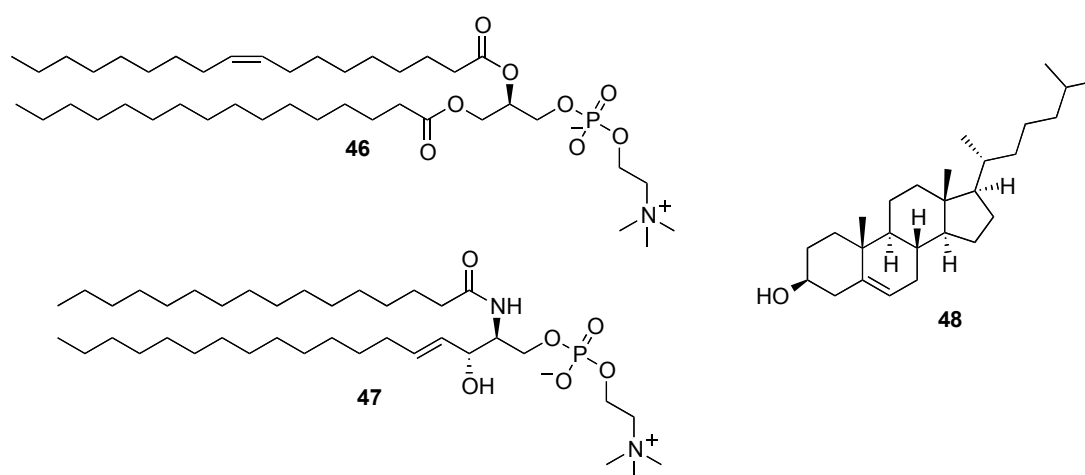


Figure 28. Lipids in mammalian membranes

V.1.2 Sphingolipids

Sphingomyelin (SM, **47**) is the most abundant molecule of this series. It is a zwitterionic lipid with a head group similar to that of the glycerophospholipids class. However, the other added groups are linked to sphingosine instead of glycerol. SM is interesting for its role in the formation of membrane microdomains “rafts”.^[32]

V.1.3 Sterols

They differ widely in structure from the other two groups. Cholesterol (**48**) is the most

abundant molecule. It is a four-ring steroid structure with a hydroxyl group and a short hydrocarbon chain.^[32]

V.2 Heterogeneity of lipid membranes and related fluorophores

Lipid molecules are not uniformly distributed in the membrane structure. There is an intrinsic asymmetry between the two monolayers at different levels.

V.2.1 Level One: Lipid raft theory

The lateral heterogeneity of biomembranes is still a controversial area of intense research. In literature, there is more than 4000 scientific papers debating this theory and attempting to track the membrane rafts by different sensing methodologies. To date, the exact nature and functioning of rafts are not entirely figured out.^[145] Fluorescence is an acute tool that should definitely help in probing this heterogeneity. This strongly depends on finding new appropriate fluorophores.

In 1997, Simons and Ikonen predicted the presence of lipid and proteins microdomains that are enriched in SM and cholesterol. They postulated that these microdomains play a fundamental role in many membrane and/or cellular processes such as signaling, formation of protein clusters, trafficking, and neurodegenerative diseases.^[146]

Lipid microdomains originate from the “phase transition” intriguing property of biomembranes. A biomembrane is often just above the melting temperature characteristic of its lipid constituents. At low temperature, the bilayer usually prevails as a highly ordered gel phase. When the temperature increases above the characteristic melting point of the lipid substituents, the transition into a liquid-crystalline phase takes place where lipid chains are disordered.^[147] Since the biomembrane is made up of different lipid molecules with different melting points, the phase transitions are smoothed and the two phases of liquid namely liquid-ordered (Lo) and liquid-disordered (Ld) can coexist.^[148]

Nowadays, rafts are defined as rigid yet dynamic heterogeneous microdomains that compartmentalize cellular processes and can be stabilized to form larger platforms.^[149] Biomembranes can be artificially assembled in model membranes. *Giant unilaminar vesicles* (GUVs) present the simplest model system of a lipid bilayer used to study the membrane rafts. GUVs are formed of lipids composing both Lo and Ld phases. Investigations on these model membranes can be summed up to show rafts as liquid-ordered phase Lo consisting of saturated lipids and cholesterol. Lo is surrounded by non-raft Ld domains consisting of unsaturated

lipids.^[150]

- **Fluorophores related to raft investigations and model membranes**

The most commonly used probes are lipophilic fluorophores that partition into Lo and Ld depending on their lipid composition. This complicates their use in cellular membranes, but they are still utilized in artificial models investigations.^[151]

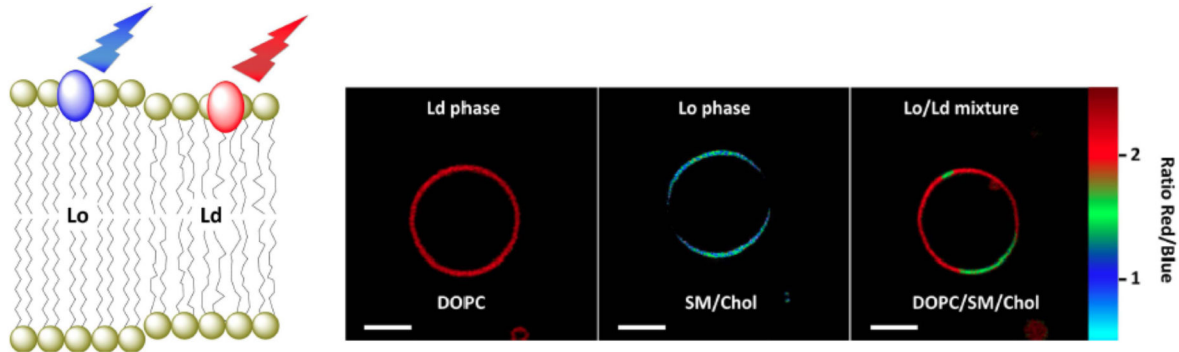


Figure 29. Imaging GUVs by a pyrene dye that stains Lo and Ld in different colours

Environment-sensitive dyes are prospective probes since they can stain by different colors, intensities, or fluorescence lifetimes upon partitioning into the different phases.^[151,152] An example of imaging model membranes using a pyrene dye is shown in *fig. 29*.^[153] Their use is still limited in cellular imaging. Hence, the challenge of developing new dyes that can help to elucidate the structure and biophysical properties of biological membranes is still ongoing.

V.2.2 Level two: Transmembrane lipid asymmetry

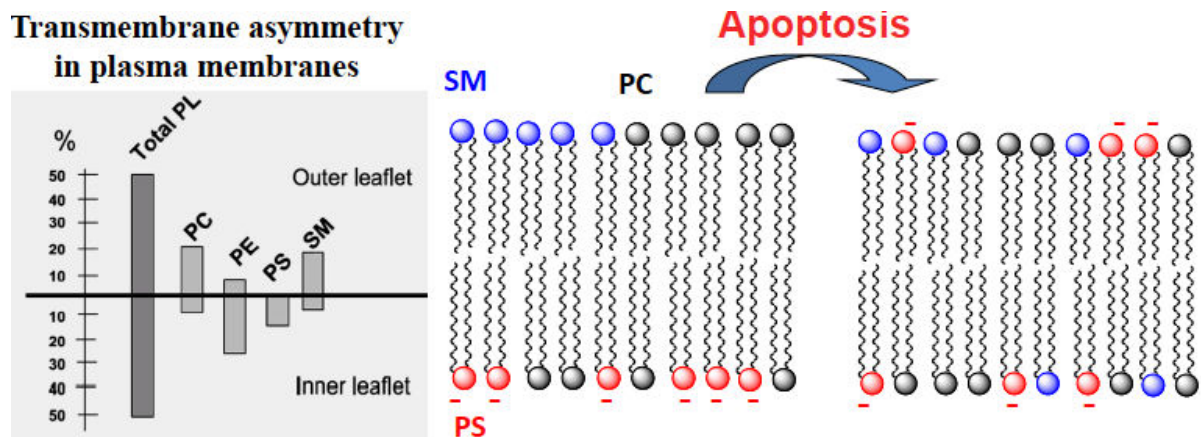


Figure 30. Lipid composition in plasma membrane and changes caused by apoptosis

The transmembrane lipid asymmetry constitutes the second heterogeneity. The outer leaflet

of the membrane is normally rich in SM and phosphatidyl choline (PC) whereas the inner leaflet contains phosphatidyl ethanolamine (PE) and phosphatidyl serine (PS). Apoptosis or programmed cell death cause this asymmetry to disappear (fig. 30).^[154,155] Defective apoptosis is the origin of detrimental diseases such as atrophy and cancer. Many methods based on all the biomachineries of the cell were developed to detect apoptosis. Among all, two fluorescence assays related to cell membranes will be briefly described here, Annexin V and F2N12S. Once more, the design of smart fluorophores will undoubtedly lead to overcoming the current limitations.

▪ Annexin V detection assays

In the presence of Ca^{2+} , the intrinsic Annexin V fluorescent protein binds specifically to PS. As a result, the membrane outer leaflet in apoptotic cell is *stained*. On the other hand, Annexin V is not able to penetrate the phospholipid bilayer in healthy cells, so it cannot detect any PS and the healthy cell stays *unstained*. In a dead cell, the integrity of the plasma membrane is lost, so the PS of the inner leaflet is also stained. If a membrane impermeable DNA label (e.g. propidium iodide) is added, only the dead cell will be *double stained*.^[156,157] This discriminative staining can be detected by fluorescence microscopy or flow cytometry. Developed versions of this assay were reported with high sensitivity able to detect *one* cell. One disadvantage of this detection is its high dependence on Ca^{2+} concentration.^[158]

▪ F2N12S detection assay

F2N12S is a synthetic 3-hydroxyflavone derivative that exhibits an ESIPT behavior. This results in a dual ratiometric fluorescence emission in response to variations in the lipid compositions of the membrane outer leaflet. The main disadvantage of this probe is the low photostability limiting a continuous fluorescence imaging.^[159] Some red-shifted and bright Nile red derivatives are used now to overcome these limitations.

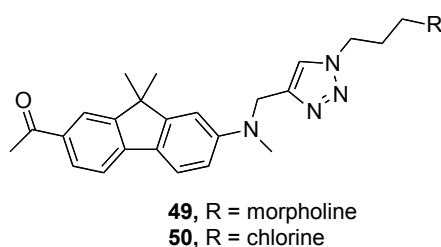


Figure 31. Fluorene probes employed in imaging lysosome and endoplasmic reticulum

From the broader scope of visualizing the changes of lysosomes and endoplasmic reticulum

during cancer cell apoptosis, two respective fluorene probes (**49** and **50**) developed by Belfield group, are depicted in *fig. 31*. Such probes exhibit low phototoxicity, high photostability, and excellent specificity and sensitivity.^[74,119]

V.2.3 Level three: heterogeneity among biological membranes

The least explored heterogeneity is the third one. It is represented by the differences in the composition and organization of lipids between the cell membrane and the intracellular membranes. For example, the concentration of cholesterol can reach up to 40 % in plasma membranes while it can be as low as 5% in some organelles like the membrane of the endoplasmic reticulum.^[160,161]

V.3 Fluorescence probing of membrane lipids

The physicochemical properties of biomembranes constitute the basic step to understand their functions. In that aspect, fluorescence microscopy (which provides visual information on the lateral organization) and spectroscopy (which affords data related to molecular interactions, microenvironment, and order) are powerful tools in such analysis. The design of an efficient fluorescent probe will guarantee the successful diagnosis of different parameters (viscosity, polarity, hydration, relaxation, potential measurement) as well as the molecular order and electrostatic potentials at the sites of the probe location. The dye should display strong affinity to the studied site distorting the structure of the membrane. It is usually smaller than the membrane width to detect the steep gradients of parameters across the membrane.^[2,32,151]

V.3.1 Membrane probes

Some parameters that should be addressed while designing a membrane probe are:

- What is the target of the study?
- Does it necessitate insensitive or sensitive dye? With potentiometric or ratiometric response?
- What structure is needed to best fit the biomembrane heterogeneity? Is it charged or not?

In particular, identifying the location and orientation of the probe is indispensable to avoid false conclusions. The simplest assumption is to use polar dyes to study the polar membrane interface, and nonpolar ones for its hydrophobic interior. However, this approach often fails because dyes show heterogeneous distribution in the bilayer. 3-hydroxyflavone and chromone families are neutral and relatively apolar molecules that can be functionalized with suitable

chemical moieties to determine their location as precisely as possible. For instance, the introduction of hydrophobic tails decides their affinities and orientation in the membranes, while attaching polar and charged substituents fixes their locations relative to the bilayer.^[151]

According to the most recent review in 2015, Demchenko classified membrane probes into three main categories (fig. 32).^[32]

V.3.1.1 Dyes partitioning into membranes

This category comprises the probes that do not have similarity in structure to lipids. They are efficient because of their high hydrophobicity that enables their partitioning into the lipid environment without being located in a particular site. Pyrene family is an example of probes that is used to monitor the biophysical dynamics by its excimer formation response.^[162] DPH (51) is another example used to inquire membrane fluidity by fluorescence anisotropy due to its polarization changes (fig. 32). It has no specific location in the membrane layer.^[163]

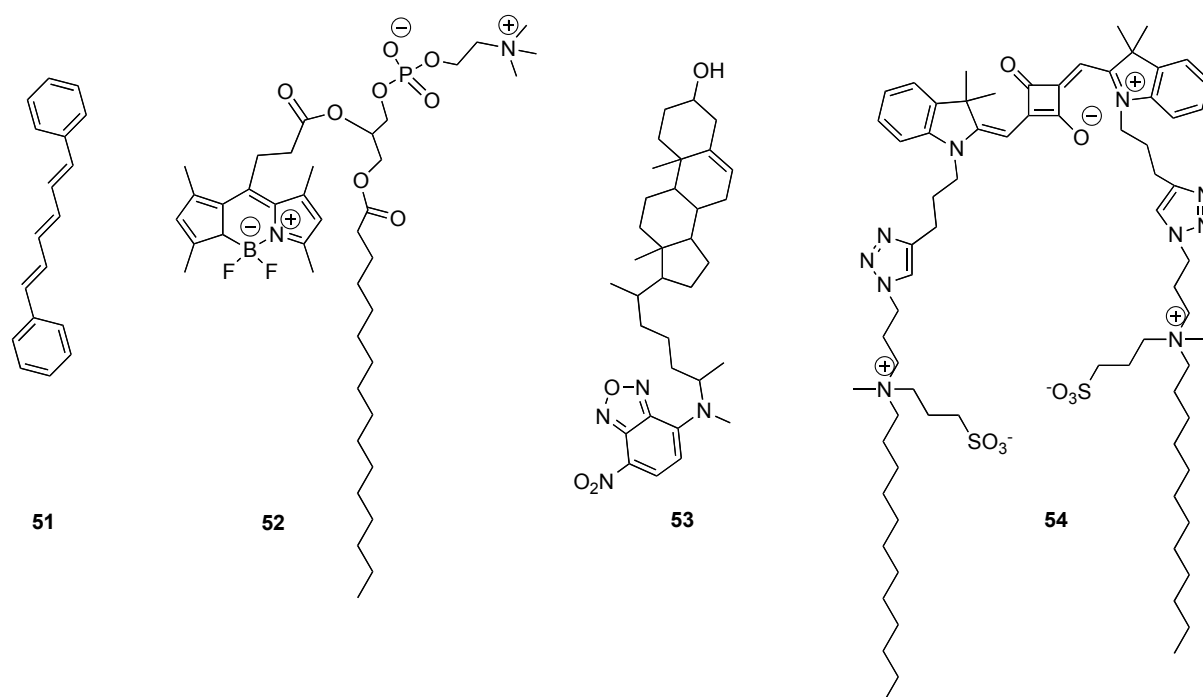


Figure 32. Selective examples of different biomembrane probes

V.3.1.2 Dyes as phospholipid derivatives

This class includes probes that are analogues to phospholipids or sterols. The fluorophore is usually installed on the polar head or the acyl chain of the phospholipid as in the 3-BODIPY-PC (52).^[164] Regarding sterols, it is installed on the oxygen atom or the side chain. The 25-NBD-cholesterol (53) is a typical example (fig. 32).^[165]

V.3.1.3 Dye derivatives of smart design

It consists of functionalized fluorophores with particular chemical moieties to introduce binding affinity to lipids, and hence to determine their particular location in the membranes. dSQ12S (**54**) is a very recent example of a squaraine dyes rational design with lipophilic and zwitterionic groups (fig. 32).^[166] This architecture was able to tune the cell entry allowing selective imaging of the plasma membrane versus the endoplasmic reticulum. The fluorescence enhancement achieved by this dye reached up to 110-fold in biomembranes declaring it as the brightest membrane probe to-date.

VI. Nucleic acids

Nucleic acids, mainly DNA (deoxyribonucleic acid) and RNA (ribonucleic acid), are linear biomacromolecules. DNA serves almost passively in storage and transmission of genetic information. The roles of RNA are quite more diverse in regulation of gene expression and protein synthesis. Small noncoding RNA molecules attract interest as potential targets for diagnostics and chemotherapy.^[167] This review will be related to DNA with few comments to compare with RNA.

VI.1 Structure of DNA

DNA and RNA are polymers made up of monomeric (deoxy)nucleotides (e.g. 10^3 - 10^6 monomeric deoxynucleotides for DNA). A (deoxy)nucleotide is a (deoxy)nucleoside connected to one or more phosphate groups. The (deoxy)nucleoside itself consists of one (deoxy)pentose sugar and one nucleobase. Nucleobases are majorly either purine (adenine (A) and guanine (G)) or pyrimidine bases (thymine (T), cytosine (C), and uracil (U)), (figure 33).^[168]

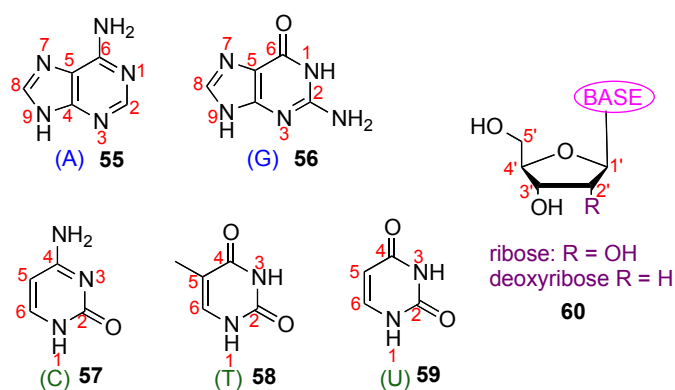


Figure 33. Building blocks of nucleic acids

In structure, DNA and RNA differ by the sugar and the nucleobases they contain. DNA majorly consists of 2-deoxyribose sugars and A, G, C, and T nucleobases (deoxynucleosides). On the other hand, RNA majorly contains ribose, A, G, C, and U instead of T (nucleosides).^[168]

The nucleobase is connected to the C-1' atom of the sugar through an N-glycoside bond in β -configuration; N1 for pyrimidines and N9 for purines. The nucleosides are, in turn, linked to each other through 3',5'-phosphodiester linkages.^[168] An example of the primary structure of an oligodeoxynucleotide (ODN) sequence is presented in *fig. 34(A)*. The sequence is denoted as d(ACT) in the 5'-3' direction.

- **Secondary structure**

Secondary structure is the set of interactions between the bases binding two strands (e.g. a double helix in DNA) or parts of the same strand together (e.g. a hairpin). The most common are the “Watson-Crick” base pairings where A is complementary to T or U by two hydrogen and G is complementary to C by three H-bonds (*fig. 34(B)*). These bases are termed canonical bases. The helix structure is formed by the coiling of the antiparallel strands around each other stacking the hydrophobic bases at the center of the helix with the negatively charged phosphate backbone on the outside. The stability of the duplex is determined by both the hydrogen bonding and the base stacking.^[168]

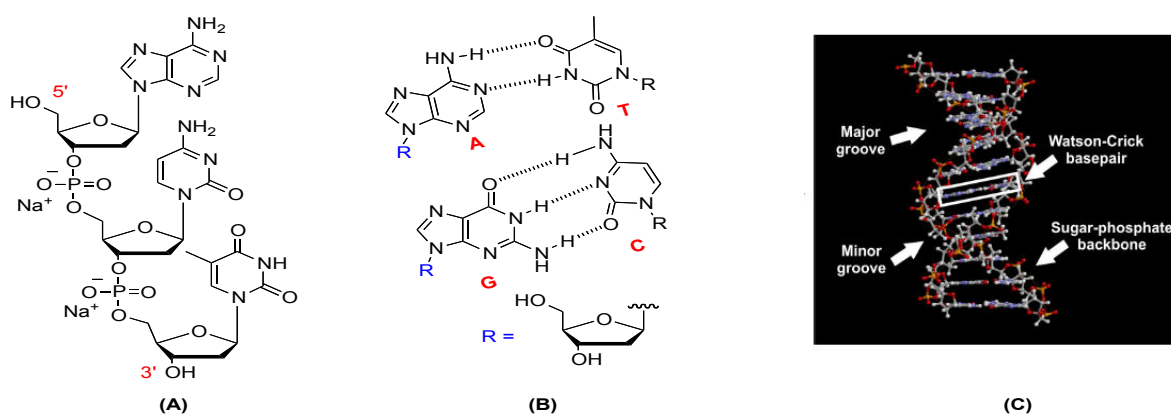


Figure 34. (A) DNA primary structure, (B) Watson-Crick base pairs, (C) Model of B-DNA

- **Tertiary structure**

The linear chain folds into a 3-D shape with two topological surfaces: the major and minor grooves. These grooves play essential roles in DNA-ligand and DNA-proteins recognitions. Three different forms of DNA duplexes exist. They can be distinguished by circular dichroism (CD) spectroscopy.^[169] They differ in all the structural parameters:

- Handedness - right or left
- Length of the helix turn
- Number of base pairs per turn
- Depth of the grooves

The most common form shown in *fig. 34(C)* is the anti-parallel, right-handed double helix termed “B-DNA”. Shorter and wider right-handed “A-DNA” form exists under dehydrating conditions whereas left-handed “Z-DNA” form prevails at high salt concentrations and in the presence of polyvalent metal ions.^[170]

- **Quaternary structure**

Basically, it is the high level organization of DNA into chromosomes.^[168]

VI.2 DNA synthesis:

Synthesis of DNA can be achieved by using an enzymatic approach, a chemical one, or a combination of both.

Enzymatic DNA synthesis involves the *in vitro* use of a DNA polymerase and nucleoside triphosphates. While this approach is outside the scope of this work, general comparison to the chemical DNA synthesis is presented in *table 2* to demonstrate its limitations precisely with respect to introducing modified nucleobases.^[171]

Table 2. chemical versus enzymatic synthesis of DNA

Chemical synthesis	Enzymatic synthesis
Synthesis of short DNA sequences (5-200 bases)	Synthesis of longer sequences
Allows the facile introduction of natural and modified nucleobases	Introduction of modified nucleobases depends on the tolerance of the DNA polymerase
Site-specific synthesis	Introduction of modified nucleobases is only predicted to some extent

VI.3 The chemistry behind DNA synthesis

Advances in *phosphorylation* chemistry enabled the facile synthetic access to millions of DNA assays. Chemical synthesis of DNA can produce sequences bearing both natural and chemically-

modified nucleobases.

There are four phosphorylation methods successfully engaged in the chemical synthesis of DNA sequences since the beginnings of this domain in 1950s. The *phosphodiester (61) approach* (fig. 35(A)) was more or less abandoned in the 1970s basically for modest yields, numerous possible side reactions, and complications of purification. Here, the other three approaches will be briefly addressed (fig. 35).^[172]

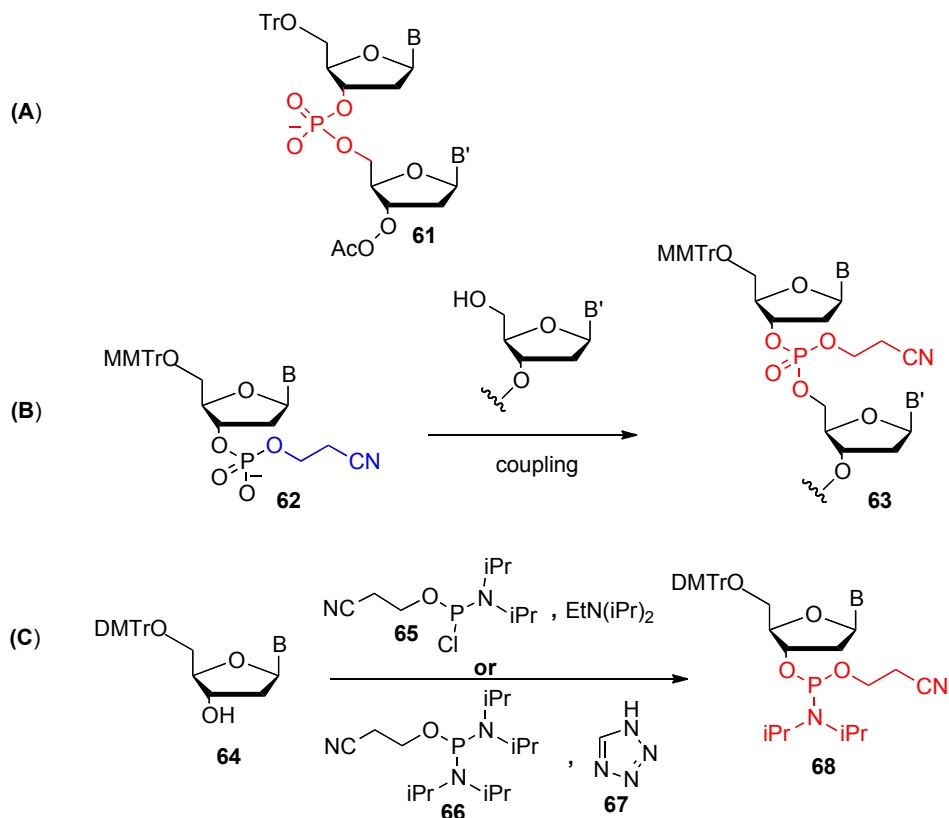


Figure 35. Phosphorylation methods employed in ODN synthesis

VI.3.1 The phosphotriester approach

The defining improvement of this approach compared to the phosphodiester one is the protection of the phosphate in the monomer with 2-cyanoethyl group excluding the side reactions on the free oxygen of the internucleosidic phosphate (**62**). As a result of the improved selectivity, more efficient coupling agents and catalysts were envisioned. The new chemistry was applied for the first time on solid-support initiating a research era that had led to the full automation of DNA chemical synthesis (fig. 35(B)).^[172]

VI.3.2 The phosphite triester and H-phosphoramidite approach

Compared to phosphate (V) reagents, phosphite (III) triesters are faster towards substitution

reactions speeding up the internucleosidic couplings into minutes. Yet, they are less stable.

Nowadays, the *N,N*-diisopropyl-*O*-cyanoethyl phosphoramidites (**68**) are the standards of the automated solid-support ODN synthesis.^[173] The common ways of synthesizing the phosphoramidite monomers are shown in *fig. 35(C)*. They involve:

- Direct nucleophilic substitution of the chlorophosphoramidite (**65**),
- Weak acid activation of the phosphordiamidite (**66**) by a weak acid such as 1H-tetrazole (**67**).

The full solid-support automated synthesis using this method will be discussed in section VI.4.2. The biggest disadvantage of the nucleoside phosphoramidites is their limited stability. These compounds are air-sensitive and acid-labile. Handling the phosphoramidite of the fluorescent nucleobase analogue remains one of the biggest challenges facing this field.^[172,174]

VI.3.3 H-phosphonate approach

The inherent instability of the nucleoside phosphoramidites had led to explore the H-phosphonates class. These compounds are highly stable, economic, and good candidates to achieve efficient couplings. Future advances in the H-phosphonate methods are envisaged to render this approach an optimal replacement to the current phosphoramidite chemistry used in synthesis.

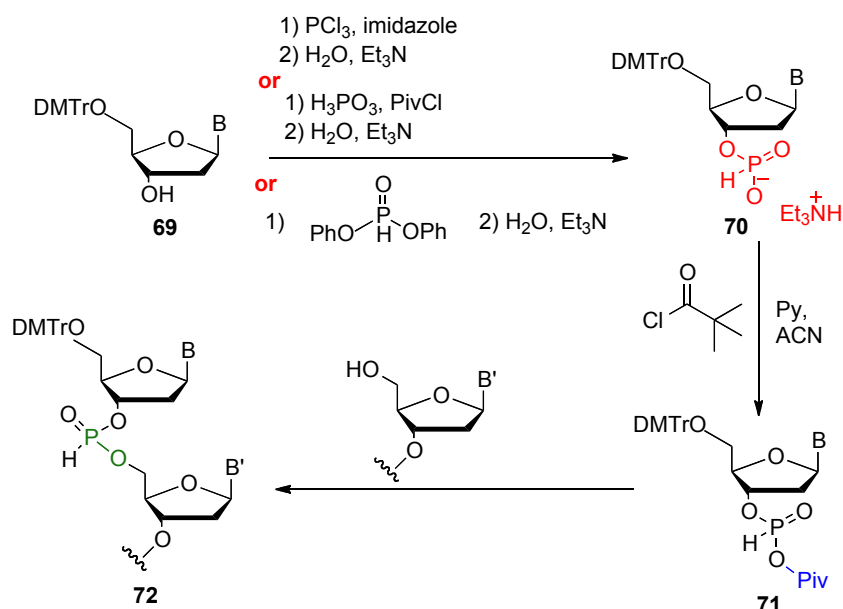


Figure 36. ODN synthesis *via* H-phosphonate chemistry

Three successful ways to synthesize the H-phosphonate monomers (**70**) are summarized in

fig. 36. Once obtained, they can be activated towards condensation by pivaloyl chloride furnishing a reactive anhydride (**71**), which in turn condenses with the 5' hydroxyl of the growing sequence. The excess of the activator acyl chloride reacts with the unphosphitylated hydroxyl; hence, saving the capping step used for this purpose in the automated phosphoramidites approach. Finally, the full length ODN is oxidized all at once by iodine establishing the phosphate (V) backbone of the sequence.^[172,174]

VI.4 Chemical synthesis of DNA

DNA chemical synthesis can be carried out in solution or on a solid support.^[175]

VI.4.1 Solution-phase synthesis

To date, phosphotriester chemistry is the only approach suitable for DNA synthesis in solution. Addition of one or more nucleotides at a time can be performed. Nonetheless, automation has not been yet developed for solution synthesis and laborious purifications are still required after each coupling step.^[175]

VI.4.2 Solid-phase DNA synthesis

This well-established methodology is typically achieved on a solid support using an automated instrument. One purification step of the final DNA is needed. The defining advantage of this method is the site-specific introduction of any natural base or nucleobase analogue. The DNA chain is grown stepwise assembling one nucleotide at a time. Therefore, the efficiency depends on every single coupling step. The maximum length of ODNs achieved by this method is around 200 bases. While ODN synthesizers can adapt to all the chemical approaches, phosphoramidite chemistry is the most common strategy because of its high coupling efficiencies although it necessitates the protection of the A (**73**), G (**74**), and C (**75**) nucleobases to avoid critical side reactions (*fig. 37*).^[174]

In details, the first nucleoside of the DNA strand is attached to the solid support. Its 5'-OH is protected with a (dimethoxytrityl) DMTr group (*fig. 37*).

- A) De-blocking (detritylation): The solid is treated with an acid, such as trichloroacetic acid, and washed out. DMTr group is cleaved resulting in a free 5'-OH on the first base.
- B) Base condensation (coupling): The introduced phosphoramidite nucleotide is activated by a weak acid (ex. tetrazole) to remove the *i*Pr₂N group and transform into a powerful phosphitylating agent that reacts with the 5'-OH of the first base joining the two bases *via* a phosphite linkage.

- C) Capping: Some 5'-OH groups remain unbound. Thus, acetic anhydride and 1-methylimidazole are added to block them via acetylation.
- D) Oxidation: The trivalent phosphite linkage is stabilized by oxidation into pentavalent phosphate group using iodine in aqueous basic media.

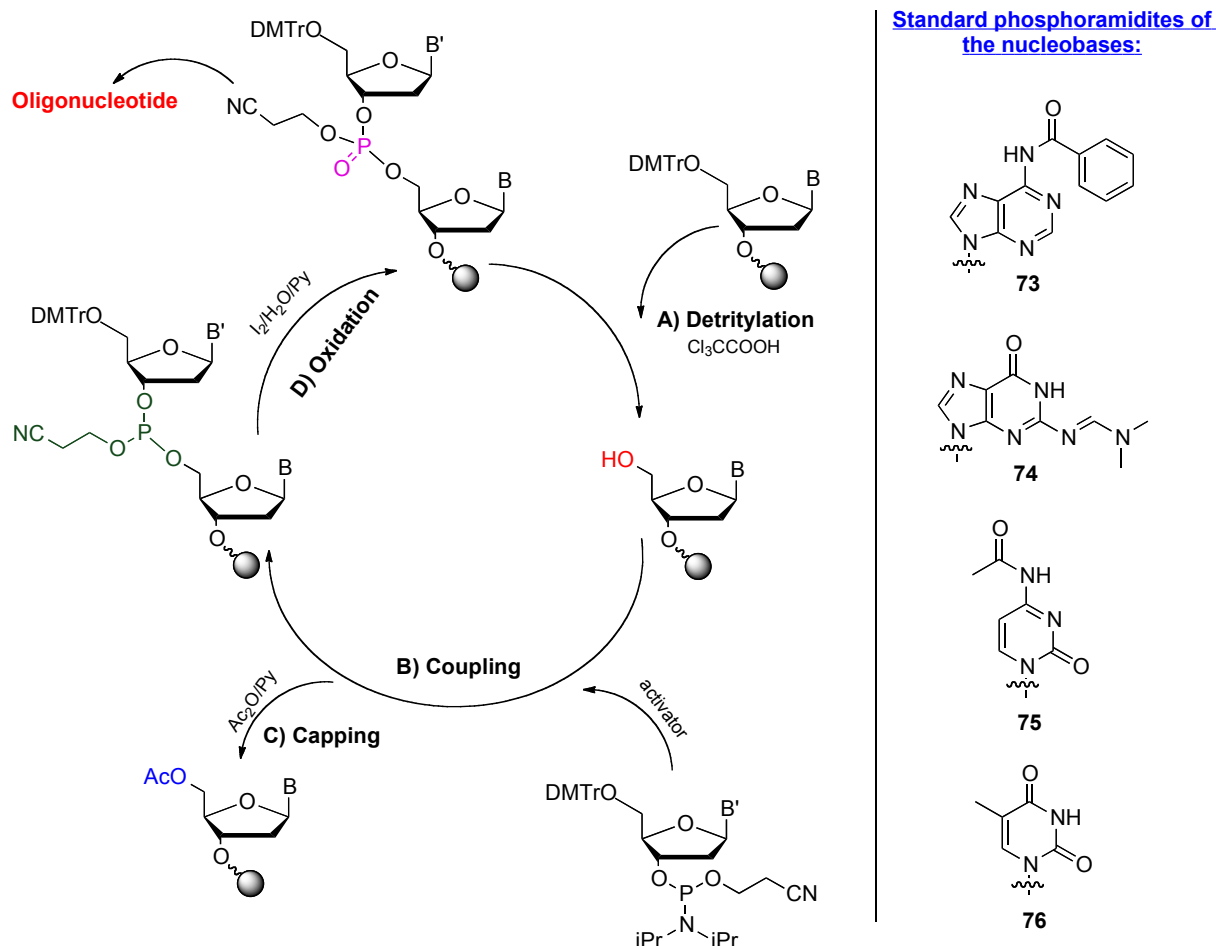


Figure 37. Solid phase oligonucleotide synthesis *via* phosphoramidite chemistry

As a result of the first cycle, one nucleotide residue is added to the ODN strand attached to the solid support. The strand is ready now to enter a second cycle till the programmed sequence is synthesized in full.^[174]

At the end, treatment with concentrated ammonia solution (rt or 55 °C for 8 h) will cleave the ODN from the solid support and liberate the phosphates from the cyanoethyl groups and the nucleobases from the protecting groups. Milder conditions can be utilized in this post-processing step if the ODN includes sensitive nucleotide analogues.

Lately, new shorter-step methods are emerging. For example, replacing the DMTr group with an aryloxycarbonyl (carbonate) will shorten the synthesis. That is, both the carbonate protecting

group and the oxidation of the phosphite internucleoside linkage can be achieved by treatment with an aqueous mixture of peroxy anions buffered at pH 9.6.^[176]

VI.5 Fluorescent labeling of nucleic acids

Fluorescence is the major detection technique in DNA diagnostics, sequencing, and genomics. This environmental-friendly detection technique with exquisite sensitivity has overwhelmed radiography detection. Fluorescence rituals are nowadays practiced in various dimensions such as visualizing nucleic acids within cells by microscopy,^[177] studying nucleic acid/protein interactions and conformational changes^[178,179], detecting polymerase chain reaction (PCR) products^[180], gel electrophoresis,^[181] single nucleotide polymorphism (SNP),^[182] etc..

Since nucleic acids lack adequate intrinsic emission (negligible quantum yields and very short decay times), the design of optimized fluorophores remains the momentum of a successful fluorescence investigation of DNA. A nucleic acid fluorescent probe should meet the spectroscopic demands (high brightness, photostability, selective excitation outside the range of absorption of biomolecules, etc..) and should have the versatility to be incorporated close to the site of the examination without perturbing the natural structure. This in turn, has enriched the library of fluorophores but without achieving the ultimate goal. The urge of finding new candidates increases with the compulsion of developing the DNA nanotechnology and grasping the depth of the fundamental cellular events such as gene silencing, DNA methylation, and DNA repair.

Here, the fluorescent labeling of DNA systems will be briefly discussed. In essence, the reporter fluorophore should be covalently or non-covalently introduced to DNA. It is worth noting that most of these labeling strategies can be also adapted to RNAs.

VI.5.1 Non-covalent or non-specific labeling

Such dyes are not sequence-specific. They are added to visualize DNA as reporters in experimental biology. Numerous dyes already exist.

VI.5.1.1 DNA intercalators

The DNA intercalators mostly share the same general features:

A. The classical structure of intercalating ligands is planar, aromatic that can fit into the DNA helix without disrupting the H-bonds. These ligands align such that the plane of the rings is parallel to that of the aromatic rings of the nucleobases.

B. The cationic structure of intercalators, where the rings bear cationic chains or protonated nitrogen atoms, favors electrostatic interactions with the negatively charged phosphate of the DNA structure.

When these dyes intercalate to DNA, their fluorescence efficiencies increase. Examples are ethidium bromide (**77**) that displays 20-fold increase in fluorescence once bounded and the dimer dyes YOYO (**78**) and TOTO (**79**) that are even more sensitive than ethidium bromide (fig. 38).^[3]

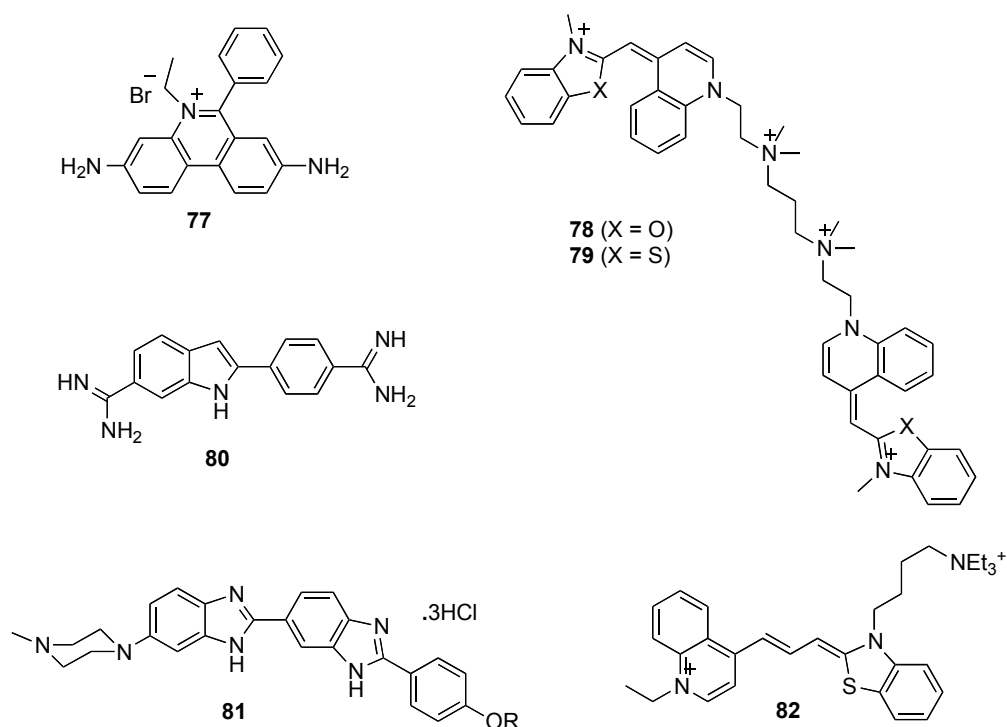


Figure 38. Fluorophores for non-covalent labeling

VI.5.1.2 DNA minor-groove binders

The fluorescent probe possesses several aromatic rings connected by single bonds and also contains H-bond donating groups. These features allow the probe to interact with nucleobases exposed into the minor groove. In the bonding state, fluorescence is turned on. The 6-diamidino-2-phenylindole (**80**, DAPI) dye binds to the minor groove mostly at A-T rich regions visualizing the DNA in intracellular imaging.^[183] Hoechst stains (**81**) are also used as binders that exhibit UV excitation and near-blue emission characteristics similar to those of DAPI.^[184] The DEAB-TO-3 dye (**82**) is a recent example that possesses most of the desired attributes for non-covalent labeling of ds-DNA (fig. 38).^[185]

VI.5.2 Covalent labeling

A number of covalent labeling strategies have been developed (fig. 39).^[186-189]

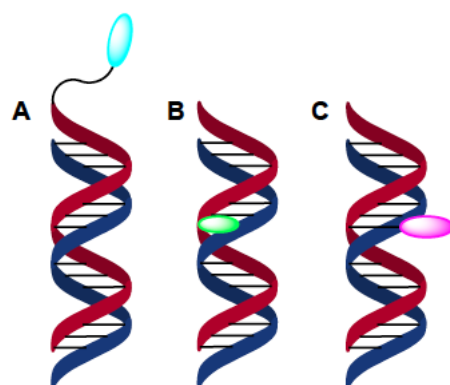


Figure 39. Covalent labeling strategies

VI.5.2.1 Strategy A: Fluorophore attached to the sugar-phosphate backbone

The fluorophore is chemically incorporated via a *flexible linker* (hydrocarbon, poly(ethylene glycol), etc.) to the phosphate group (e.g. 5'-position), to the ribose or to the nucleobase.^[171] Some of these markers are commercially available such as the fluorescein derivatives (**83**). Other examples are shown in *fig. 40* including thiophene (**84**), BODIPY (**85**), and pyrene (**86**) labels.^[190-192]

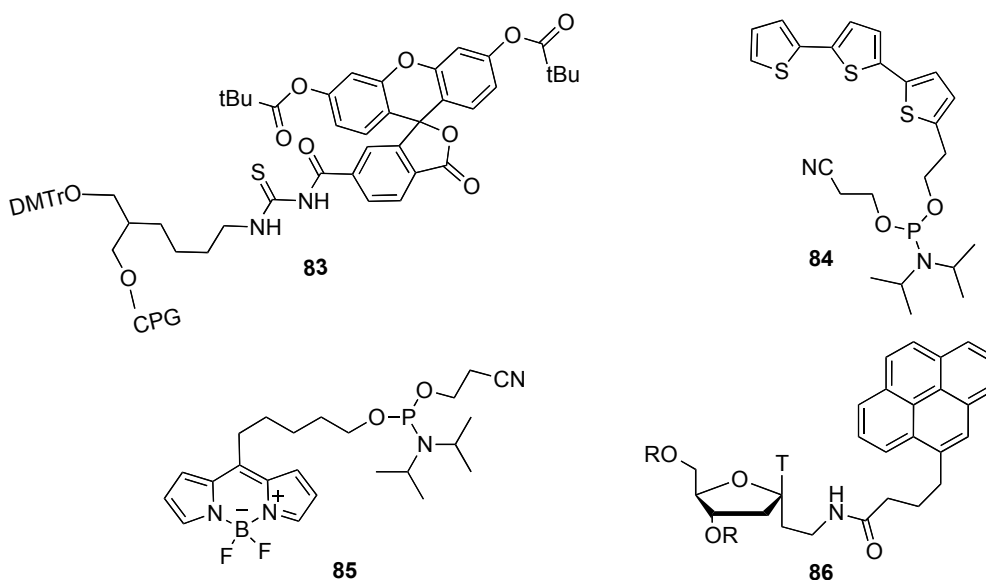


Figure 40. Fluorophores attached to the phosphate backbone

This type of labeling found huge applications in cellular imaging and DNA sequencing. However, it has some disadvantages. The flexible linear linker makes it hard to precisely identify

the position and the orientation of the fluorophore. In addition, the relatively large size of the fluorophores can disturb the DNA structure or react with the surrounding biomolecules such as proteins.

VI.5.2.2 Strategy B: Fluorophore replacing the natural base

This approach can be realized by connecting the fluorophore to the deoxyribose ring or to an nucleosidic moiety.

- **Fluorophore connected to deoxyribose (ribose)**

The fluorophore connected to deoxyribose can be an aromatic hydrocarbon, a heterocyclic compound, or a natural base mimic. This synthesis is usually demanding since it involves a diastereoselective method for the glycoside bond creation. The attached fluorophore should preferentially be in β -configuration.

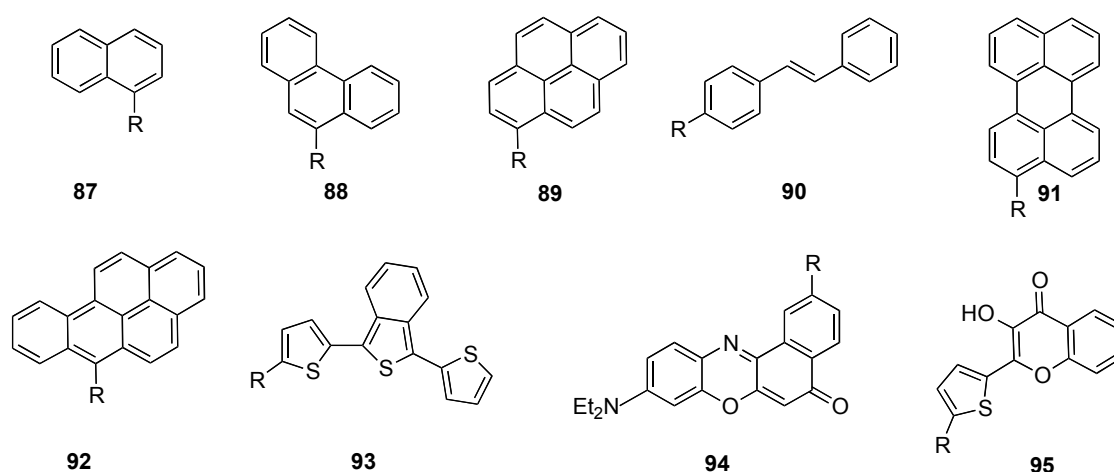


Figure 41. Fluorophores connected to deoxyribose (R)

The aromatic hydrocarbon nucleobase surrogates do not form Watson-Crick type hydrogen bonds. However, they participate in stacking interactions and can maintain the B-conformation and duplex stability. Many aromatic fluorophores were incorporated by this method. Naphthalene (87), phenanthrene (88) pyrene (89), and styrene (90) derivatives can be excited in the UV region (around 345 nm) outside the range of absorption of the natural nucleobases.^[193,194] They exhibit moderate fluorescence efficiencies, which even decrease once they are incorporated into DNA. More extended aromatic systems were also incorporated such as asperylene (91) and benzoperylene (92) nucleosides which showed red shifts in absorption and emission and higher quantum yields exceeding 90 % in some cases. Heterocyclic nucleobase substitutes were also successfully introduced to deoxyribose sugar.^[186] Some examples are poly-

thiophene (**93**),^[194] Nile Red (**94**)^[195] and thienylchromone (**95**) nucleosides. The latter was incorporated into ODNs in our group and was successfully used to study the DNA/protein interactions (fig. 41).^[41,43]

- **Nucleobase fluorescent analogues**

Nowadays, it is well established that minor chemical modification in the structure of natural nucleobases can change them into highly emissive nucleoside analogues. These fluorophores have the advantage of being comparable in sizes to the natural bases. This helps in maintaining the same type of bonding (Watson-Crick) and hence, not perturbing the DNA conformation.

Pteridines as an example is a frequently used family of fluorescent base analogues in DNA studies. Their QYs can reach up to 30 %. Among this family, DMAP (**96**) as an adenine analogue and 3-MI (**97**) as a guanine analogue are two interesting examples.^[196] These probes are very sensitive to the environmental and conformational changes (fig. 42).

2-Aminopurine (**98**, 2-AP) was one of first examples of fluorescent base analogues. 2-AP became commercially available now. This adenine analogue is red-shifted in absorption to 305 nm. Thus, it can be selectively excited in the presence of natural nucleobases and amino acids. 2AP is widely used since it is highly sensitive to microenvironment.^[196]

Another method of improving the fluorescence of natural bases is by expanding their conjugated π -systems by adding a vinyl (**99**) or aromatic group (**100**) or by fusing an additional aromatic ring (**101**).^[197-199] These analogues exhibits high sensitivity to changes in their microenvironments, red-shifted absorptions and emissions, as well as fluorescence efficiency that can reach up to 75 % in aqueous media.

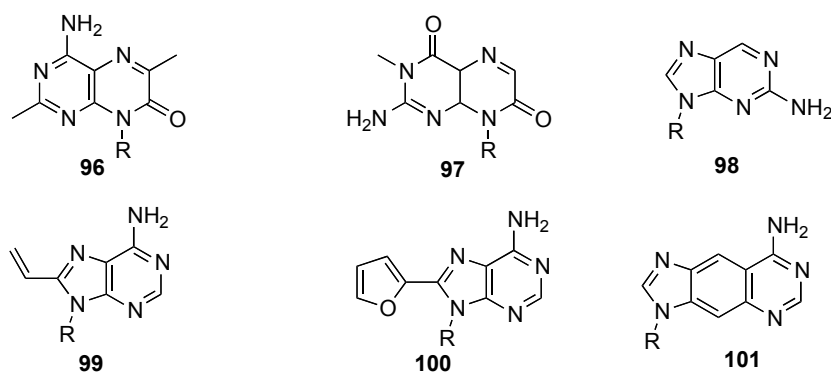


Figure 42. Nucleobase fluorescent analogues

- **Fluorophore connected to an nucleosidic moiety**

In this approach, an nucleosidic mimic replaces the deoxyribose sugar. The main advantage is the low synthetic complexity since typical mimics are acyclic. Two fluorophore-nucleoside structures the 1,3-diol (**102**) and the "Antopolsky" sugar (**103**) derivatives shown in *fig. 43*.^[26,200,201]

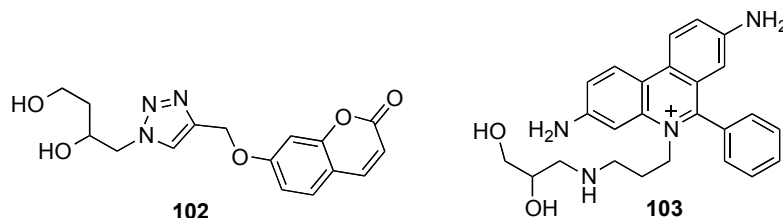


Figure 43. Fluorophores connected to nucleosides

VI.5.2.3 Strategy C: Chromophore (mainly fluorophore) modifying the natural base

Typically, the fluorophore is linked to the nucleobase through a short *spacer*. This approach is kind of combination of the previous two methods. The reporter dye will be located outside the DNA helix. The rigidity of the spacer allows controlling the position and orientation of the dye relative to the DNA major or minor grooves. The other advantage is the capacity of preserving the Watson-Crick pairings of bases and hence, the stability and conformation of the DNA helix. Acetylene moiety is commonly used as a short spacer that preserves the electronic communication between the nucleobase and the chromophore (*fig. 44*).

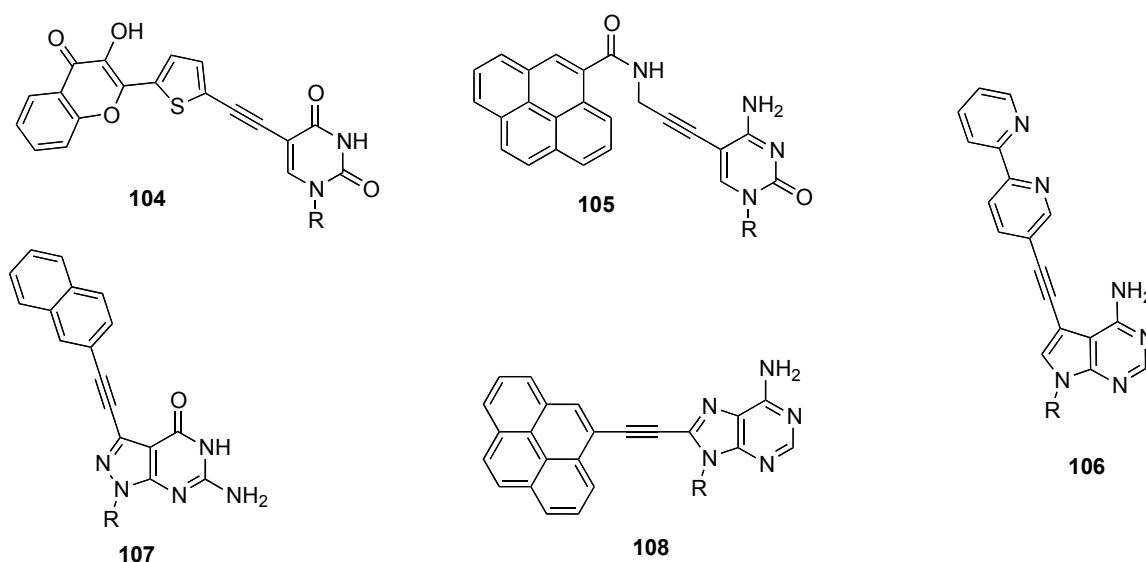


Figure 44. Chromophores modifying the natural bases

The spacer is commonly introduced at the C-5 of the pyrimidines (e.g. **104** and **105**) and C-

7 of the purines.^[42,202] Indeed, 7-deazapurine analogue containing carbon atom instead of nitrogen at position 7 is employed to introduce the spacer at C-7 (e.g. **106** and **107**).^[203] Position C-8 of purines as in analogue (**108**) is less preferred since it is directly exposed to the phosphate-sugar backbone, so a substituent at this position might lead to destabilize the duplex.^[204,205] This approach of labeling was reported in the introduction of fluorenes into ODNs (Section VI.7).

VI.6 Synthetic approaches used in covalent labeling of ODNs

Covalent labeling can be carried out by pre-synthetic or post-synthetic modification of oligonucleotides.

VI.6.1 Pre-synthetic modification

The most common approach is the addition of the fluorophore during solid-phase ODN synthesis using phosphoramidites chemistry. Hence, it requires the synthesis monomers in which the fluorophore is incorporated into a nucleobase, sugar, or an artificial backbone beforehand. The fluorophore should be stable to the conditions of solid-phase synthesis particularly the basic conditions of the deprotection steps. Generally, this method is highly selective and good yielding. It is appropriate to all the three strategies of covalent labeling. The synthesis of the monomer and its stability remain the major burdens.

VI.6.2 Post-synthetic modification

In this case, covalent labeling is performed by attaching a small reactive group into the phosphoramidite building block before the solid-phase synthesis. Afterwards, *post-synthetic modification* reactions of the active group on the ODN strand with the fluorophore or its precursor are carried out on the solid support or in solution. This approach is suitable to sensitive dyes that do not support the conditions of the DNA synthesizer and to diversity-oriented labeling where different fluorophores can be attempted on a single strand. Modification in solution is also appropriate to visualize DNA within cells using developed bioorthogonal ligations. The major limitation is the efficiency of the post-synthetic reaction. It has to be selective, fast, high-yielding, and to tolerate aqueous media and functional moieties of the DNA backbones.^[206] Another limitation is the steric hindrance that faces labeling the DNA by the strategy B (that is fluorophore replacing the nucleobase).

Classical post-synthetic ligations involve amine or thiol groups reacting with different moieties such as activated esters, haloacetyls, maleinimides, or disulfides. Modern techniques

involve Cu-catalyzed oxidative acetylenic coupling^[207] and Pd-catalyzed Sonogashira reactions.^[171,208] Regarding bioorthogonal modifications, click chemistry (Cu-catalyzed and Cu-free azide-alkyne cycloadditions),^[209-212] Staudinger ligations, and Diels-Alder cycloadditions have been reported.

VI.7 Selected sample applications of fluorescent nucleosides

VI.7.1 DNA sequencing

DNA sequencing is the process of identifying the specific order of nucleotides in a DNA molecule. It is an indispensable tool in all disciplines of biology, diagnostics, medicine and forensic sciences. Fluorescence improved the historical methods using radioactively-labeled ODNs particularly in terms of speed and safety of sequencing. Further, Fluorescent labeling enabled all four bases to be identified in a single lane instead of 4 different lanes. Over the time, this has led to synthesize competitive machines that produced draft sequence of the human genome.^[213,214]

VI.7.2 Single nucleotide polymorphism (SNP)

SNP is a variation in a single nucleotide at a particular position in the genome that shows an appreciable degree of variation within a population (e.g. >1%). It underlies the biological diversity like the difference in susceptibility to diseases among humans.^[215]

Hence, SNP detection has been the subject of particular attention for its impact on human health. Two main approaches exist. The first is an enzymatic approach involving DNA ligases, DNA polymerases (e.g TaqMan) or nuclease. The second, involves a complementary synthetic ODN bearing a fluorescent reporter targeting the SNP site (Molecular Beacons, Base-Discriminating Fluorescence - BDF).^[202,216] The fluorophore expresses a fluorescence pattern depending on the nucleotides of the SNP site.^[182]

VI.8 Fluorene derivatives in the context of DNA applications

To conclude, *fig. 45* displays the fluorene derivatives that were described in different investigations of DNA.

Fluorene (**109**) was found to be a cell-permeable DNA sensitive dye. The combinatorial synthesis reported testing the permeability of 805 different dyes and their sensitivity to DNA. Fluorene was one out of 8 dyes to show fluorescence sensitivity.^[217]

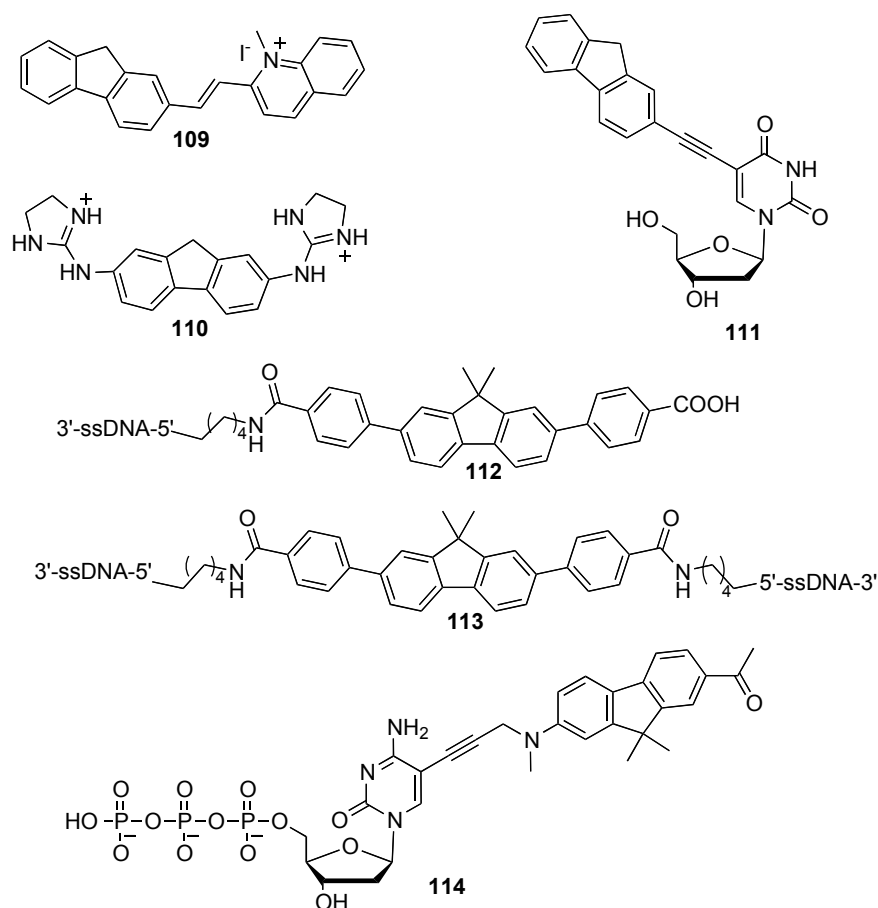


Figure 45. Fluorene derivatives employed in DNA investigations

The fluorene cationic derivative (**110**) showed a strong affinity to DNA with high sequence selectivity. The investigation was performed by plasmon resonance and thermal denaturation experiments as well as circular dichroism and UV studies. Fluorene cation demonstrated the ability of selective binding to some sequences and intercalation to others contrary to other cationic species of anthracene.^[218]

The fluorene molecule was incorporated to a uracil moiety at the C-5 position via an ethynyl linker. Afterwards, the labeled ODNs were prepared *via* solid-phase synthesis using phosphoramidite chemistry of nucleoside (**111**). The investigation was extended to incorporate fluorenone moieties into ODNs realizing excimer emissions. Successive publications reported different ODN applications such as hybridization studies, molecular beacons, and SNP detections.^[184,219,220]

Fluorenes (**112**) and (**113**) have been used as small molecule/DNA probes to design FRET pairs validating the efficiency of fluorene family in biosensing.^[221-223]

The push-pull fluorene triphosphate (**114**) has been introduced into DNA by an enzymatic

synthesis and employed in DNA/lipid and DNA/protein interactions yielding valuable information on the hydration and dynamics. The color change portrayed in the DNA/lipid interaction is visible even by naked eye.^[224]

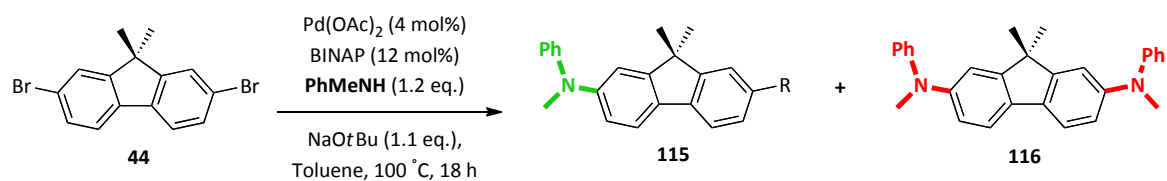
Chapter Two

Air-stable palladium catalytic systems for sequential one-pot synthesis of unsymmetrical aminoaromatics

This chapter discusses the methodology we have examined to invest the advances of the palladium catalysis platform in the search of new fluorescent tools. Palladium-catalyzed methodologies have emerged as reliable avenues to generate benign aromatic products. Here, our focus was directed towards five objectives that have not been completely explored in literature: 1) the limitations of introducing aliphatic amines onto fluorene scaffolds to achieve diversity-oriented synthesis (DOS),^[225,226] 2) the absence of elaborated reports on selective functionalization of cheap and easily accessible dibromoaromatic scaffolds as starting materials of fluorophores, 3) the increasing demand of finding air-stable catalytic systems that can benefit synthetic chemists and researchers working on the interfaces of science disciplines, 4) the importance of finding new accesses to install different groups (acceptor and donor for example) in one-pot, and 5) the lack of extensive studies related to microwave (MW) enhancement effects on controlled couplings. The screening of various air-stable palladium catalytic systems for selective functionalization of dibromofluorenes is presented in the first part. The scope and the limitations of the proposed methodology (monoamination, diamination, and sequential one-pot couplings) will be discussed in the second part exploring different classes of amines and dibromoaromatics. The described content will appear in *The Journal of Organic Chemistry* asap.

I. Optimization studies

Our aim was to improvise the Buchwald-Hartwig couplings of aryl amines to bromofluorenes;^[61,83,103,129,130] yet to find versatile coupling conditions that work as efficiently upon introducing more challenging aliphatic amines (aziridine and diethyl amine for example). For that purpose, a stoichiometric mixture of dibromofluorene and *N*-methylaniline as an acyclic aliphatic-aromatic substrate was chosen. Then, we set out to screen different palladium catalytic conditions. The most successful screening experiments are summarized in the table of *fig. 46* displaying the changed parameter of each entry. Their corresponding results are depicted as bar graphs showing the GCMS conversion and the selectivity of *mono/di* aminated products (**115/116**) in *fig. 47*.



Entry	Deviation from standard conditions	Screened Ligands
1	PPh ₃	<div style="display: flex; justify-content: space-around;"> <div style="text-align: center;"> <p>PPh₃ L1</p> <p>PCy₃ L3</p> <p>DavePhos L5</p> <p>RuPhos L7</p> <p>XantPhos L9</p> </div> <div style="text-align: center;"> <p>P(o-Tol)₃ L2</p> <p>PtBu₃ L4</p> <p>BrettPhos L6</p> <p>JohnPhos L8</p> <p>BINAP L10</p> </div> </div>
2	P(o-Tol) ₃	
3	PCy ₃	
4	P(t-Bu) ₃	
5	DavePhos	
6	BrettPhos	
7	RuPhos	
8	JohnPhos	
9	XantPhos	
10	-	
11	Cs ₂ CO ₃	Base
12	KOtBu	Base
13	Pd(dba) ₂	Catalyst
14	Dioxane	Solvent
15	rt	Temp
16	MW (45 min)	Activation
17	8 mol%	Ligand
18	Doubled	Loading

Figure 46. Optimization of the reaction conditions

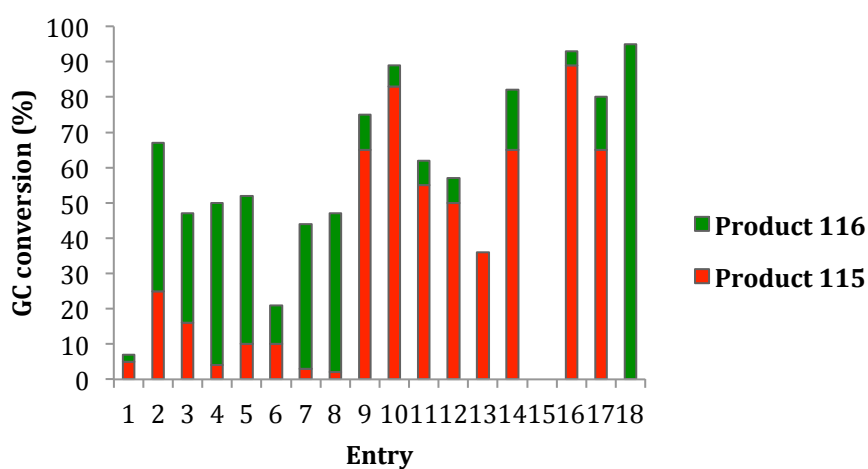


Figure 47. Results of the optimization study

Monodentate triarylphosphines, such as PPh₃ and P(*o*-Tol)₃ were tested with low success (entries 1-2). PPh₃ exhibited a poor conversion (5%) whereas P(*o*-Tol)₃ favored diamination (25 %) with dehalogenation side reactions. Reductive dehalogenation was also observed with first generation ligand PCy₃ (entry 3). Almost all the other ligands afforded the aminated products (**115** and **116**) in complete mass balance relative to the amine starting materials (entries 3-10). The monodentate ligands (**L4-8**) mainly led to the diaminofluorene (**116**) (entries 3-8). The chelating bidentate ligands (XantPhos and BINAP) resulted in the *mono*-aminated fluorene (**115**) as the major product (entries 9-10).

The absence of the undesired reduced products with most ligands can be rationalized since dialkylbiaryl Buchwald ligands (**L5-8**) display some bidentate character like BINAP forming 4-coordinate complexes that suppresses the competing β -hydride elimination.^[227] The favored *di*-amination with these Buchwald-type ligands could have resulted from their electron-rich density that facilitates the oxidative addition and their bulkiness that accelerates the reductive elimination.^[128] Accordingly, the produced *mono*-aminated fluorene of a catalytic cycle might enter a subsequent catalytic cycle *via* oxidative addition of its second C-Br bond with relatively fast kinetics preventing its isolation as final product.

On the other hand, the distinct *mono*-amination using BINAP ligand is remarkable. Although computational studies could provide a mechanistic insight, calculations with BINAP are highly demanding. Many intermediates comprising a very bulky ligand with four flexible phenyl groups in different conformations would be involved. A recent study reported different mechanistic possibilities in the catalytic cycle of BINAP.^[228] Among all of them, it has been hypothesized that the hemilability of this bisphosphine may switch to a monodentate ligand as a possible route. Our experimental data suggest that bidentate ligands impose a definite influence on the selectivity of *mono*-amination contrary to monodentate ones. Other parameters related to BINAP are the steric bulkiness and the turnover-limiting step in the catalytic cycle. It is known that the turn-over limiting step of the arylbromide coupling with amines using bisphosphines is the conversion of the Pd(0) complex to an arylpalladium (II) halide complex.^[229,230] This rate-determining step could have played a role as well in dictating the selectivity. One perspective of this work is to carry out some DFT calculations with our collaborators to probe the mechanism of this reaction in depth.

Cs₂CO₃ as a representative of carbonate base demonstrated a moderate conversion (entry 11). *t*-BuOK and *t*-BuONa almost gave the same efficient results (Entries 10 vs 12). Pd(*dba*)₂ was *mono*-selective; however, the reaction did not reach to completion after 18 h (entry 13). The observed slower kinetics is consistent with the more sterically-hindered Pd(*dba*)L₂ species.^[231]

The cross-coupling did not work at room temperature (entry 15). Dioxane (entry 14) mostly afforded the *mono*-product, nonetheless the reaction was cleaner in toluene. MW activation gave the shortest reaction time (entries 10 vs 16). The best molar ratio of the [Pd]:ligand was optimized as 1:3 with a loading of 4 mol% (entries 10 vs 17). A lowering to 1 mol% inevitably slowed down the reaction rate. Premixing the catalytic system significantly accelerated the kinetics presuming an efficient activation of Pd(0) complex. It is noteworthy that premixing becomes a prerequisite in the case of BINAP.^[232] The *mono*-amination conditions were established as follows: Pd(OAc)₂ (4 mol%), BINAP (12 mol%), NaOtBu (1.1 eq), amine (1.2 eq), toluene MW irradiations for 45 min (entry 16). Doubling the catalytic loading along with excess of amine (entry 18) led to complete diamination.

II. Scope of the selective monoamination reaction

Next, the scope and limitations of the selective mono-amination were examined. The chosen *mono*-amination conditions were applied to introduce a variety of amines (fig. 48).

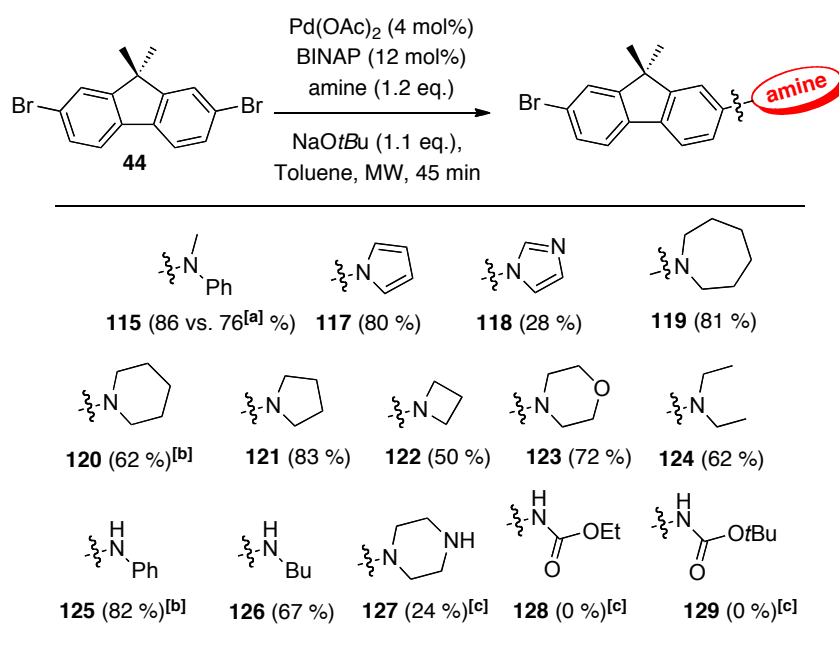


Figure 48. Scope and limitation pattern of the selective *mono*-amination of **44**; yields in parenthesis. ^[a] Under thermal heating conditions; ^[b] Reaction performed at 1-gram scale; ^[c] GCMS conversion to the product.

The selective *mono* cross-coupling was efficient on pyrrole (**117**, 80 %), cyclic secondary amines (**119-123**, 50-81 %), and primary amines (**125-126**, 67-82 %). To our delight, the diethylamine was also coupled efficiently (**124**, 62 %).

Most reactions proceeded to completion in 45 mins under MW irradiation. Piperidine (**120**) and azetidine (**122**) were irradiated twice for 45 mins, their isolated yields remained moderate (50-62 %). The reaction was efficiently scaled-up to one gram (**124-125**). Considering the unprotected piperazine (**127**), low conversion of starting material was obtained. Surprisingly, no dimerization was observed. This might open up new prospects for conjugation avoiding the additional steps of protection-deprotection of piperazine. The reaction conditions were limited on imidazole (**118**). Regarding carbamate coupling (**128-129**), it required higher palladium catalytic loadings, which yielded the debrominated *mono*-coupled derivative as the major product. Since carbamates present a different reactivity: *t*-BuOH, NMP, and THF were likewise screened without success.^[233,234]

III. Diamination of fluorenes

As discussed previously, minor modification of the catalytic system allows for the preparation of diaminofluorenes (fig. 49).^[235] A control reaction by using a large excess of amine (5 eq.) evidenced no inhibition of the process. This does not support the hypothesis that amines might bind as ligands to Pd in this case.^[236] A range of diaminofluorenes (**116** and **130-133**) was prepared in good to excellent yields (61-89 %). The employed conditions revealed to be effective and tolerant towards various model aliphatic and aromatic amines.

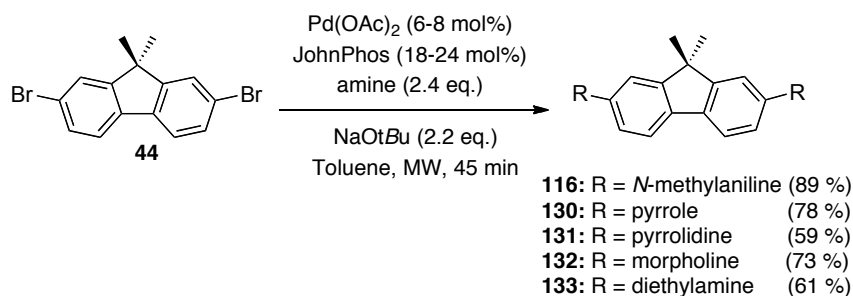


Figure 49. diamination reaction of **44**

IV. Synthesis of unsymmetrical fluorenes

Next, we examined the synthesis of unsymmetrical fluorenes using a one-pot 2-step protocol. In this case, MW conditions were too harsh and generated inseparable mixtures. On the other side, thermal heating proved to be promising. We targeted two sequential pathways; C-N/Stille and C-N/C-N couplings. Stille coupling can install a direct electron withdrawing group (such as Bromo-2,1,3-benzothiadiazole) on the fluorene molecule establishing a push-pull dye in one

step. Likewise, it can deliver a vinylaminofluorene as an intermediate of numerous target materials such as push-pull carbaldehydes via oxidative cleavage, polyfluorenes and copolymers via metathesis or Mizoroki-Heck cross-coupling.^[237-239]

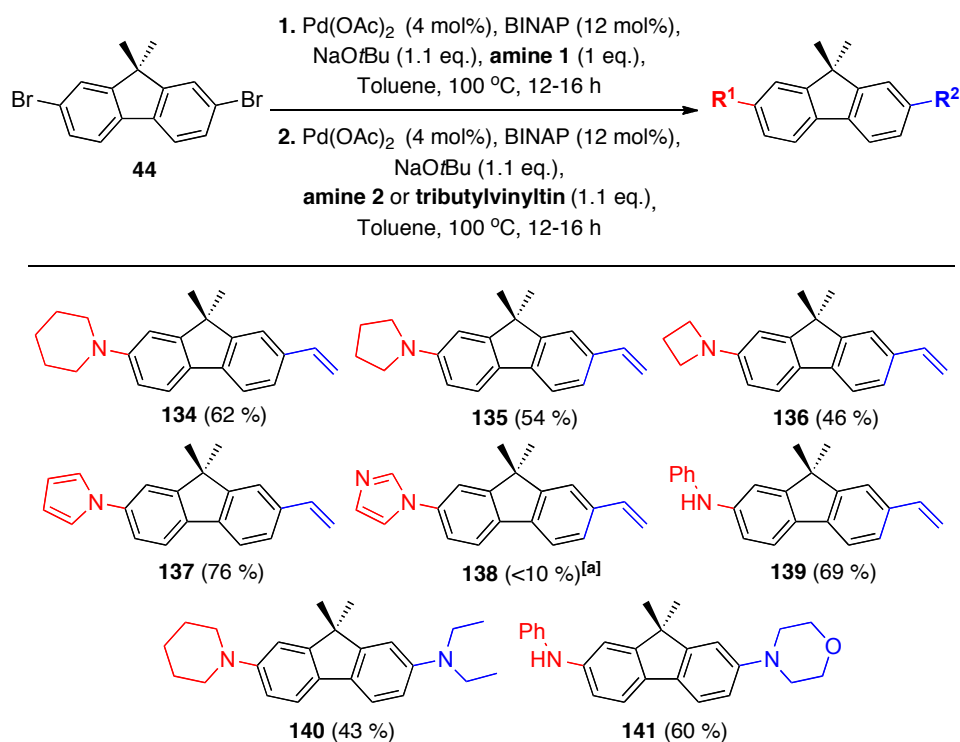


Figure 50. Sequential couplings of **44**; yields in parantheses, ^[a] GCMS conversion.

The limitations of this type of desymmetrization (fig. 50) are reflective of those of selective *mono*-amination (e.g. compare products **138** and **118**). The choice of amines^[240] that worked efficiently for monoamination (fig. 48) would lead to an efficient sequential one-pot C-N/C-N and C-N/Stille couplings. Transmetalation seems easier than incorporation of amine into the Pd complex in the catalytic cycle of the second step. This makes the vinyl moiety more facile to introduce without isolating the intermediate of the first-step. The purification of vinylaminofluorene revealed to be also easier than separation of a mixture of different possible aminofluorenes. This has led to the vinylpyrrol product (**137**) isolated as the highest yield of this series (76 %).

As a result, the sequential C-N/Stille couplings realized products (**134-139**, 46-76 %) using the optimized conditions of entry **8** (fig. 50). Specifically, once the *mono*-aminated product was formed (12-16 h), tributylvinyltin and a subsequent catalytic loading were concomitantly added. On the other hand, the sequential couplings of two distinct amines had yielded products (**140-141**, 43-60 %) by sequential one-pot C-N/C-N couplings. Regarding the second catalytic loading,

the reaction showed poor yields when it was not followed by a subsequent addition of the catalytic system. The addition of a second stoichiometric amount of the base is mandatory. We chose to concentrate on the double addition to obtain good yields, as many factors can directly deactivate the palladium catalyst outside the glove box and this challenging reaction aims to synthesize useful materials.

Fig. 51 compares the one-pot approach (69 %) to the classical two-step synthesis (75 %) of compound (**139**). The good yield demonstrates that the developed procedure is cost- and time-efficient in synthesizing interesting products.

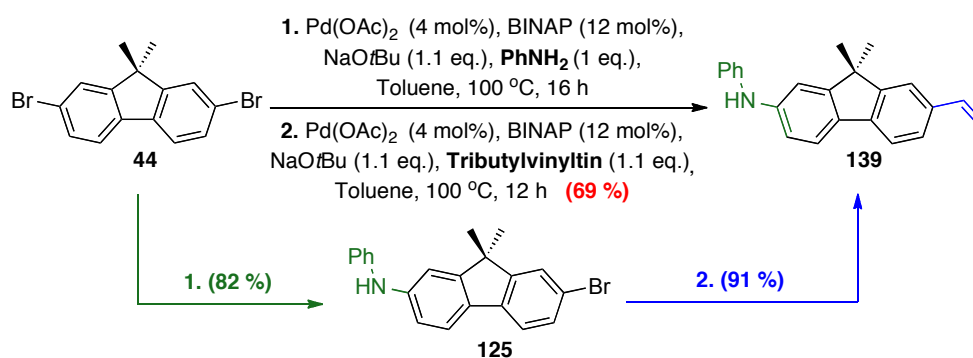


Figure 51. Sequential one-pot *versus* classical two-step synthesis of **139**

V. Scope of the selective conditions on dibromonaphthalene, dibromopyridine, and dibromothiophene

To explore the limits of our methodology on other aromatic families, the optimized conditions of monoamination, diamination, and the sequential cross-couplings of two variant groups were applied to unactivated 2,7-dibromonaphthalenes, 2,5-dibromopyridine, and 2,4-dibromothiophenes as models of electron-neutral, electron-deficient, and electron-rich dihalogenated aromatic scaffolds respectively.

The results are illustrated in *fig. 52*. Regarding the electron-neutral naphthalene moiety, all the optimized catalytic systems worked as adequately as on fluorenes. Aromatic and aliphatic amines were introduced with *mono*- or *di*-selectivity as desired furnishing (**142-145**, 65-83 %). The sequential synthesis of naphthalenes bearing varied combinations of amines was fruitful and generated compounds (**146-147**) in appreciable yields (53-64%).

The electron-deficient pyridine reacted in higher yields (**148-153**, 57-94%). (**152**) was prepared as an example of the sequential addition in significant yield (71 %). It is worth noting that 2,5-dibromopyridine underwent monoamination with 0,5 mol% Pd(OAc)₂ catalytic system or even with excess amine (5 eq.) in the absence of palladium catalyst. Nevertheless, *di-* or sequential amination of this heteroaryl compound required the developed catalytic conditions. The electron-rich 2,4-dibromothiophene appeared as a scope limitation.

Arylaminothiophenes were obtained successfully and were stable to isolate (**154-155**, 42-54 %). Amination was still selective on such electron-rich aromatic scaffold. Considering saturated cyclic amines (**156-158**), the *mono/di* conditions were selective with acceptable conversions (47-72 %). However, these electron-rich products proved to be unstable upon isolation.

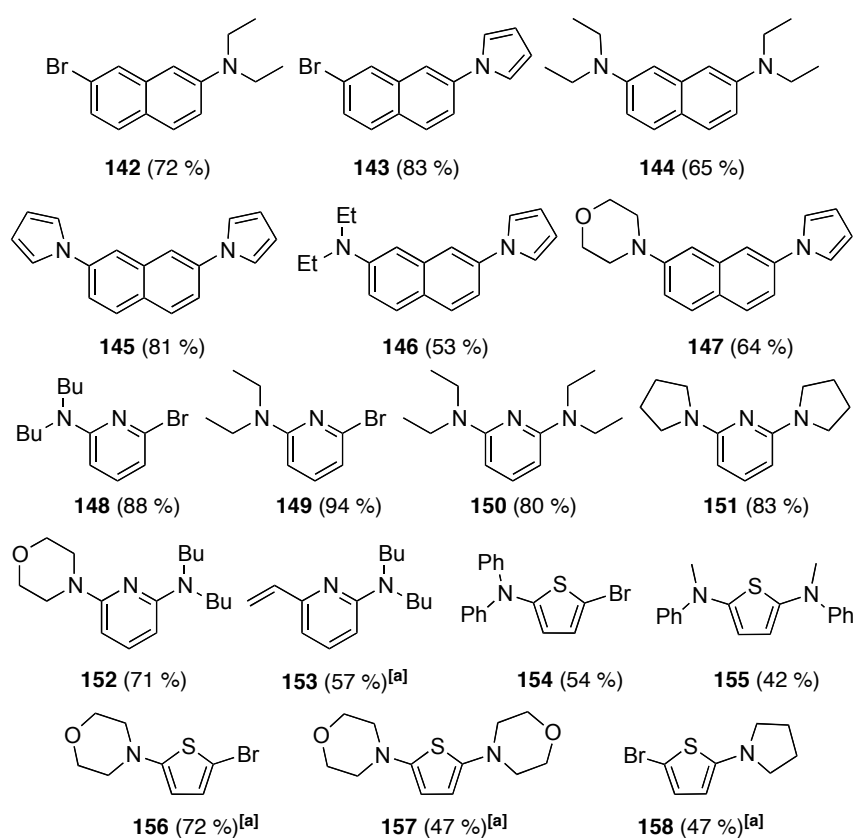


Figure 52. Scope and limitations of different dibromoaromatic scaffolds, [a] GCMS conversion to the product.

VI. Application: a near-IR push-pull sensor

The strength of this method permitted to access in a 3-step simple protocol (fig. 53) the NIR probe (**159**; $\lambda_{abs} = 395$ nm and $\lambda_{em} = 640$ nm in chloroform, fig. 54). This multi-component reaction clearly asserts the versatility of our synthetic approach. The synthesis was concise and

good yielding. It resulted in synthesis of an advanced dye without the tedious isolation of two intermediates.

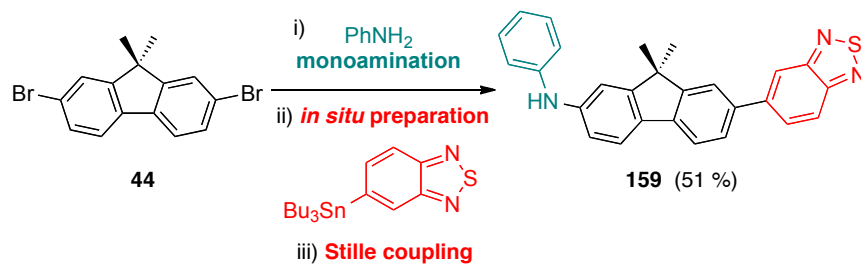


Figure 53. Construction of push-pull sensor **159**

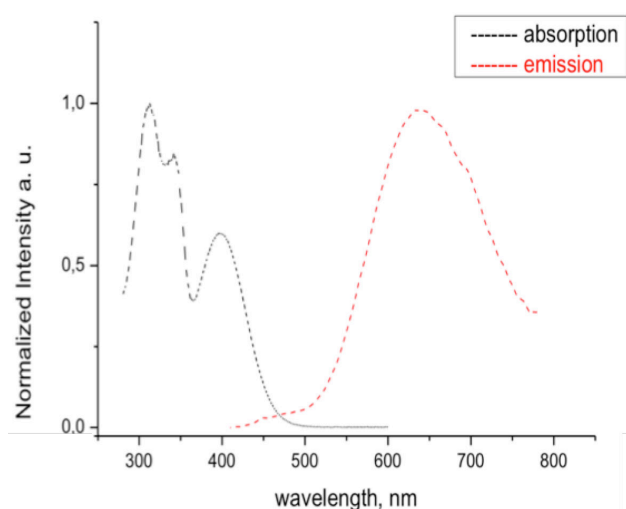


Figure 54. Absorption and emission spectra of **159** in chloroform

VII. Conclusion

To conclude this chapter, the new methodology is summarized in *fig. 55*. The selective functionalization of dibromoaromatic scaffolds using air-stable palladium catalytic systems was carried out. This methodology involved rapid *mono*- and *di*-selective Buchwald-Hartwig aminations *via* microwave irradiation. The conditions were optimized to couple sequentially different moieties in one pot. Couplings with a wide scope of amines allowed accessing a new library of symmetrical and unsymmetrical derivatives (37 examples). Using this versatile method, a near-IR push-pull sensor was prepared installing the electron-donating and withdrawing groups through a multi-component reaction. These conditions revealed to be gram-scalable, and adaptable to various groups; hence, promoting facile use in synthetic chemistry. The optimized conditions will be explored more in the DOS-synthesis of a library of

push-pull fluorene dyes in chapter 3 for photophysical characterization and in the synthesis of DNA probes with NIR emission in chapter 5.

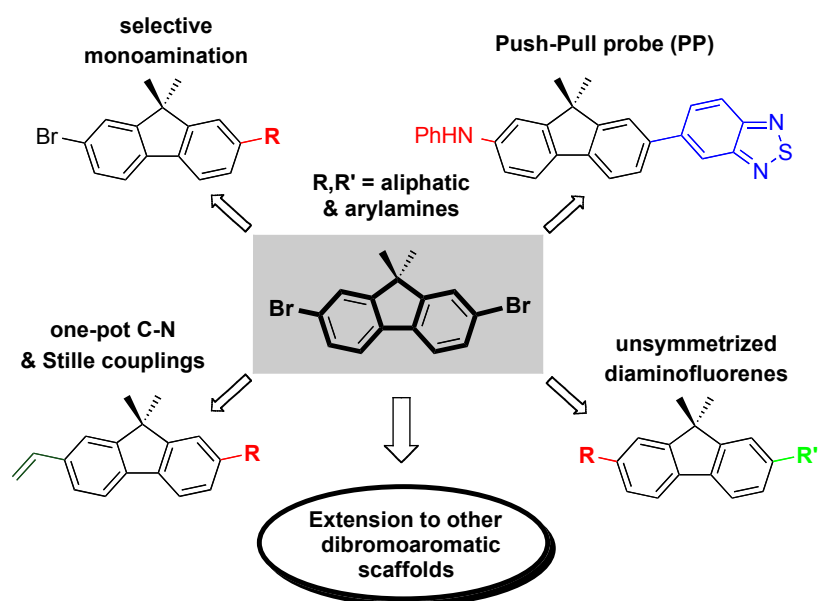


Figure 55. Selective functionalization of dibromoaromatics

Chapter Three

Push-Pull fluorene dyes: synthesis and structure- photophysics relationship

Few studies in literature have rationalized the structure-photophysics relationships in the field of chromophores to a certain extent.^[113,241-244] In the case of 2,7-disubstituted fluorenes, such investigations are still needed. The diverse multi-step syntheses could be a reason. In this chapter, we set to optimize the synthetic routes to diversify the electron-withdrawing group from an aldehyde, ketotriazole or succinyl to methylenemalonitrile, or benzothiadiazole. Then, we have built on our developed Pd-catalyzed methodology to vary the donor from aliphatic or aromatic amines to saturated cyclic amines ranging from aziridine to azepane (fig. 56). First, the synthesis of a library of 16 push-pull fluorene dyes will be described. Among them, several derivatives bear conjugation anchors to follow the effect of further couplings on their spectroscopic properties for biolabeling applications. In the second part of the chapter, we will present the photophysical characterization, the theoretical TD-DFT calculations, and different correlations enclosing structure-property relationships. The main two objectives of this part of the thesis are: 1) to find the optimal D- π -A combination in terms of visible absorption, laser excitation accessibility, brightness, Stokes shift, and prospects for bioconjugation, and 2) to accomplish concise and scalable synthetic accesses to the dyes that will be used in the next chapters.

N.B: The order of the chemical structures still follows the systematic numbering of the thesis, but the discussion will refer to abbreviating the target **push-pull** dyes as (**PP1-16**) and the intermediate (**161**) as (**I-6**) since this material has already been published. Additional TD-DFT

calculations, data, and correlations are provided as supplementary information (SI-XIII) in the experimental part.

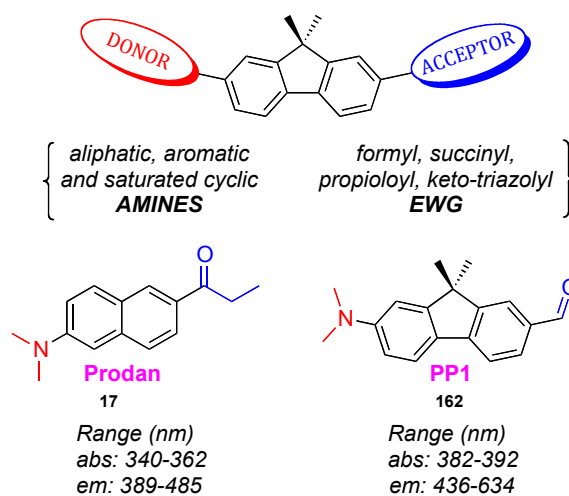


Figure 56. Structure of Prodan and the design of the D- π -A fluorenes in this study.

I. Synthesis

I.1 Variation of the electron-withdrawing group (EWG)

Different EWG with negative mesomeric or/and inductive effects were screened. Dimethylamine was chosen as the donor. Considering **PP1** and other fluorenes in the literature, we noticed that upon converting the formyl EWG into an acetyl moiety, the absorption coefficient decreased and the maximum was blue-shifted from the visible into the UV range.^[60,85] These drawbacks limit the utility of such dyes in bioconjugation. Therefore, our major objective was to introduce an EWG bearing an attachment point that retains the vital photophysical properties of the dye once bound as a biosensor. We envisaged the succinyl and propioloyl linkers as being compatible for peptide and click 1,3-dipolar couplings, respectively. Next, we incorporated benzothiadiazole and methylenemalonitrile known to display forceful EW abilities.^[62,115]

The robust synthesis developed to access the fluorene derivatives **PP1-6** is outlined in *fig. 57*. The synthesis was achieved by conventional methods,^[60,85] namely C9-dimethylation, then regioselective mono-nitration followed by iron-mediated reduction to afford the aminofluorene (**36**) in 49% yield over three-steps. Reductive amination using NaCNBH₃ and paraformaldehyde provided the key adduct (**160**) with the dimethylamino (D) group in 87% yield. (**160**) was used to disclose a variety of acceptors in addition to the interesting intermediate **I-6** with a vinyl group to describe the effect of this group on the design. Primarily, halogen-metal exchange with

n-BuLi on adduct (**160**) followed by treatment with DMF gave **PP1** in 70% yield. Grignard addition of the ethynyl group to **PP1** followed by oxidation using MnO₂ at 0 °C generated the ethynyl ketone **PP2** in an excellent yield (98%). Noticeably, dimerization was observed when this reaction was allowed to proceed at room temperature for longer times. To test the effect of conjugation, **PP2** was converted to the keto-triazolyl derivative **PP3** in 70% yield with *n*-hexyl azide under copper-assisted azide-alkyne Huisgen cycloaddition (CuAAC).

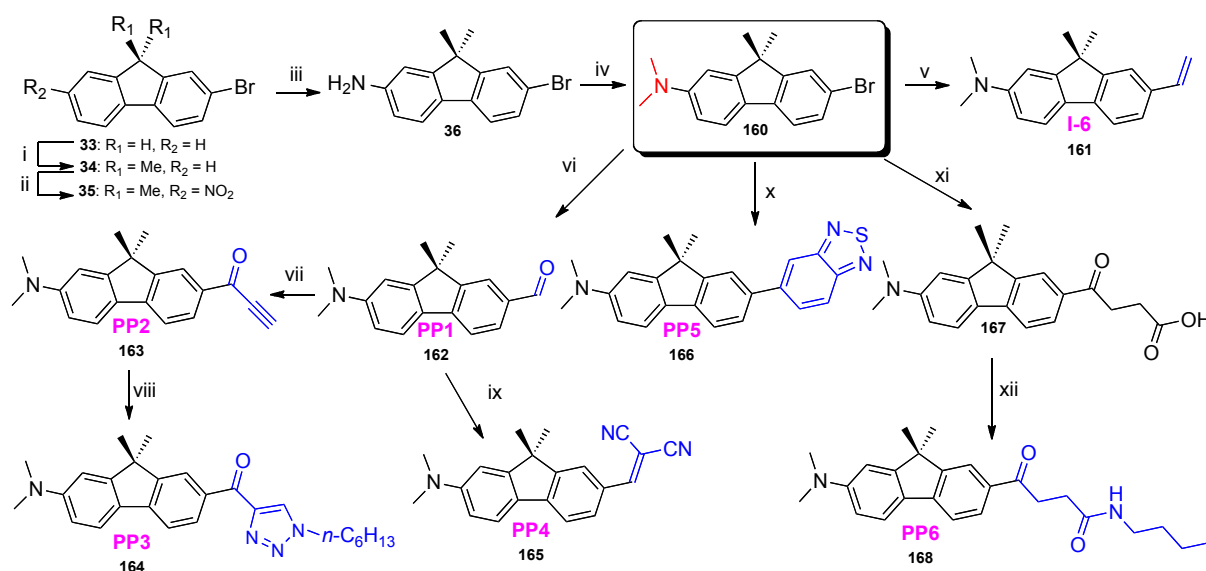


Figure 57. Synthetic pathways leading to **PP1-6**. Reaction conditions: i) KOH (4 eq.), KI (0.1 eq.), MeI (2.3 eq.), DMSO, rt, overnight, 93%; ii) HNO₃, AcOH, rt, 2 h, 73%; iii) Fe (3 eq.), NH₄Cl (2 eq.), EtOH_(aq), 80 °C, 4 h, 72%; iv) (CH₂O)_n (5 eq.), NaCNBH₃ (3 eq.), AcOH, rt, overnight, 87%; v) Pd(PPh₃)₄ (5 mol%), tributylvinyltin (1 eq.), toluene, 80 °C, overnight, 80%; vi) *n*-BuLi (1.2 eq.), DMF (2 eq.), THF, -78 °C, 3 h, 70%; vii) a. Ethynylmagnesium bromide (1.4 eq.), THF, 0 °C, 2 h, b. MnO₂ (15 eq.), DCE, 0 °C, 1 h, 98% (2-steps); viii) *n*-HexN₃ (1.1 eq.), CuI (2 eq.), DIEA (5 eq.), AcOH (1 eq.), DCE, 3 h, 70%; ix) malonitrile (2 eq.), Al₂O₃ (4 eq.), toluene, overnight, 70 °C, 85%; x) a. Pd(PPh₃)₄ (10 mol%), Bu₃SnSnBu₃ (1.3 eq.), toluene, 100 °C, 3 h, b. Pd(PPh₃)₄ (10 mol%), 5-Bromo-2,1,3-benzothiadiazole (2 eq.), 100 °C, overnight, 82%; xi) Mg (2 eq.), BrCH₂CH₂Br, succinic anhydride (2 eq.), THF, 60%; xii) DIC (1.1 eq.), HOBT (1.1 eq.), Et₃N (1.1 eq.), *n*-BuNH₂ (1.5 eq.), THF, rt, overnight, 72%.

Next, the methylenemalonitrile was introduced by Knoevenagel condensation on the formyl of **PP1** in the presence of Al₂O₃ to yield **PP4** (85%).^[62] Stille coupling of intermediate (**160**) and tributylvinyltin gave **I-6** in very good yield (80%). The target **PP5** was obtained by coupling 5-bromo-2,1,3-benzothiadiazole to stannyl fluorene generated *in situ* (82%). Lastly, the succinic linker was obtained by the formation of the Grignard of fluorene (**160**) at 60 °C and the subsequent addition of succinic anhydride in THF at 0 °C to give compound (**167**) in 60% yield. As a preliminary example of peptide functionalization,^[245] *n*-butyl amine was ligated to this compound using DIC and HOBT as activators to form **PP6** in 72% yield.

I.2 Variation of the electron-donating group (EDG)

To evaluate the effect of the donor, a concise 2-step route was planned based on our developed Pd-catalyzed C-N cross-coupling protocol (chapter 2). In a first step, formylation of fluorene (**34**) at the C-7 position was optimized to obtain the key intermediate (**169**) with a fixed aldehyde acceptor (fig. 58). Different formylating reagents, Lewis acids (AlCl₃, TiCl₄, ZrCl₄), solvents (THF, CH₃CN, CH₂Cl₂), temperatures, and durations were assessed. Isolation of the different aldehyde regioisomers proved to be a troublesome task. Nevertheless, the desired fluorene-2-carbaldehyde derivative (**169**) was the exclusive product of the Friedel-Crafts reaction performed with ZrCl₄ and Cl₂CHOCH₃ in CH₂Cl₂ at 0 °C for 1 h. Diformylation is an inescapable side product if the reaction conditions are not strictly controlled.

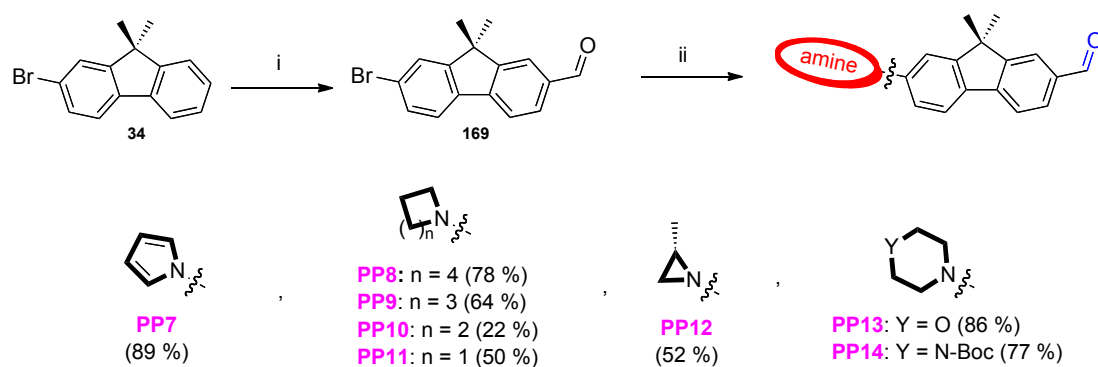


Figure 58. Synthetic pathway leading to **PP7-14**. i) Cl₂CHOCH₃ (1.5 eq.), ZrCl₄ (1.5 eq.), CH₂Cl₂, 1 h, 0 °C, 77%; ii) Amine (1.2 eq.), *t*-BuONa (1.2 eq.), Pd(OAc)₂ (5 mol%), BINAP (10 mol%), Toluene, MW (300 W/ 180 °C), 30 min. **PP7-14** are systematically numbered (**170-177**) respectively.

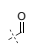
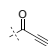
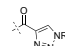
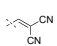
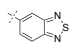
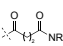
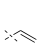
Subsequently, Buchwald-Hartwig aminations of (**169**) were carried out using Pd(OAc)₂, BINAP, and NaOtBu in toluene, under MW radiation (300 W / 180 °C) for 30 mins; synthesizing **PP7-14** in 22-86% range of yields (fig. 58). Generally, the defined route was rapid, efficient, and gram-scalable.

II. Spectroscopic studies

II.1 - Acceptor series

Unsymmetrical D- π -A fluorenes differing by their EWGs were characterized by UV and fluorescence in a wide range of solvents.^[31] The photophysical properties in selected solvents are summarized in *table 3*.

Table 3. Spectroscopic properties of selected fluorophores with various-EWG and the same dimethylamino donor.

Solvent $E_T(30)^{[b]}$	$\lambda, \Delta\lambda_{SS}^{[c]}$ (nm)	<i>Fixed Donor (NMe₂) / Varied-Acceptor</i> ^[a]						
		PP1 	PP2 	PP3 	PP4 	PP5 	PP6 	I-6 
	ϵ ($10^3 \cdot M^{-1} \cdot cm^{-1}$) ^[d]	35.5	17	38	30.5	27	16.5	30.5
H ₂ O (63.1)	λ_{abs}	386	421	nd ^[f]	501	446	373	353
	λ_{em}	624	615	nd	682	648	620	473
	$\Delta\lambda_{SS}$	238	194	nd	181	202	247	120
	Φ ^[e]	0.04	0.005	nd	0.01	0.01	0.07	0.13
EtOH (51.9)	λ_{abs}	388	413	396	476	407	370	349
	λ_{em}	562	596	622	680	539	563	428
	$\Delta\lambda_{SS}$	174	183	226	204	132	193	79
	Φ	0.48	0.11	0.06	0.12	0.01	0.71	0.5
CH ₃ CN (45.6)	λ_{abs}	384	409	389	474	404	368	350
	λ_{em}	521	620	578	679	498	523	432
	$\Delta\lambda_{SS}$	137	211	189	205	94	155	82
	Φ	0.6	0.12	0.77	0.18	0.01	0.55	0.55
DMSO (45.1)	λ_{abs}	392	419	402	488	420	373	354
	λ_{em}	534	628	582	710	516	521	445
	$\Delta\lambda_{SS}$	142	209	180	222	96	148	91
	Φ	0.9	0.18	0.85	0.19	0.02	0.72	0.75
CHCl ₃ (39.1)	λ_{abs}	391	414	399	486	414	381	350
	λ_{em}	492	570	532	608	672	492	411
	$\Delta\lambda_{SS}$	101	156	133	122	258	111	61
	Φ	0.62	0.34	0.72	0.45	0.04	0.54	0.02
Dioxane (36)	λ_{abs}	382	405	391	467	409	364	350
	λ_{em}	453	509	488	583	593	456	395
	$\Delta\lambda_{SS}$	71	104	97	116	184	92	45
	Φ	0.8	0.48	0.52	0.3	0.34	0.73	0.34
Toluene (33.9)	λ_{abs}	387	407	394	474	413	374	346
	λ_{em}	436	490	473	566	548	450	388
	$\Delta\lambda_{SS}$	49	83	79	92	135	76	42
	Φ	0.56	0.5	0.86	0.26	0.5	0.6	0.62

[a] Reported values are the averages of two or more independent and reproducible measurements, ± 1 nm for wavelengths. [b] Reichardt's parameter was employed to scale the polarity of the solvents.^[31] [c] For convenience, Stokes shifts ($\Delta\lambda = \lambda_{em} - \lambda_{abs}$) were expressed in nm rather than in cm^{-1} . Excitation wavelength used was the absorption maximum. [d] Molar extinction coefficients (ϵ) in dioxane, relative standard deviations are equal to or less than 5%. [e] Quantum yields (Φ) were determined using quinine sulfate in 0.1 M HCl solution ($\lambda_{ex} = 350$ nm, $\Phi = 0.54$)^[246] or 4'-(dimethylamino)-3-hydroxyflavone in ethanol ($\Phi = 0.27$)^[247] as references, relative standard deviations are equal to or less than 15%. [f] Not determined, the compound was insufficiently soluble in water.

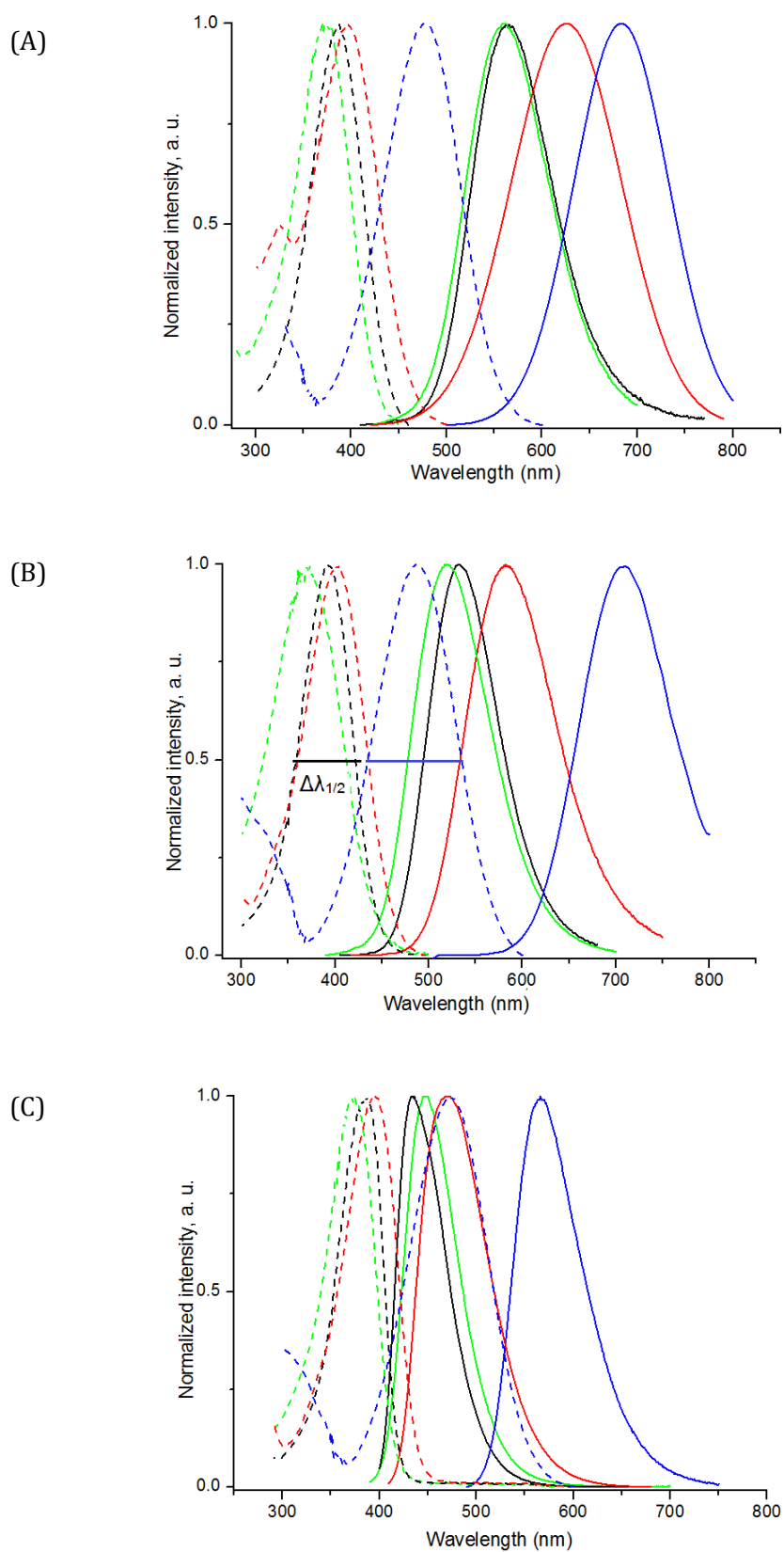


Figure 59. Absorbance (dotted line) and emission (solid line) spectra for **PP1** (black), **PP3** (red), **PP4** (blue), **PP6** (green) in EtOH (A), DMSO (B), and toluene (C) as representatives of protic, aprotic polar, and aprotic apolar solvents respectively. Excitation wavelength used was the corresponding absorption maximum.

PP1^[60,85] with dimethylamino (D) and formyl (A) substituents was set as the reference. The difference in wavelength ($\Delta\lambda_{SS} = \lambda_{em} - \lambda_{abs}$) was employed to simplify the comparisons as an indication of Stokes shift. In the carbonyl acceptors, the triazolyl **PP3** absorbed as strongly as **PP1** ($38 \cdot 10^3 \text{ M}^{-1}\text{cm}^{-1}$ in dioxane), whereas **PP2** and **PP6** showed a two-fold hypochromicity (decrease in absorptivity to around $17 \cdot 10^3 \text{ M}^{-1}\text{cm}^{-1}$). The three carbonyl dyes absorbed in the visible range (370-413 nm in ethanol and displayed particular large Stokes shifts in polar solvents (e.g. 183-226 nm in ethanol). They showed gradually an increased bathochromic shift in their emission maxima when going from the most apolar aprotic solvent to the most polar solvent (table 3, fig. 59). Compared to **PP1** reference, **PP3** presented a similar absorption, whereas the emission maximum was red shifted in polar solvents. By contrast, the absorption of **PP6** was blue shifted, while the emission showed little change (fig. 59). The quantum yields of **PP3** and **PP6** were in the range of 52 to 86% in all of the tested solvents except in ethanol and water where they were considerably reduced. Altogether, **PP3** demonstrated superior absorption and emission properties to those of **PP6**.

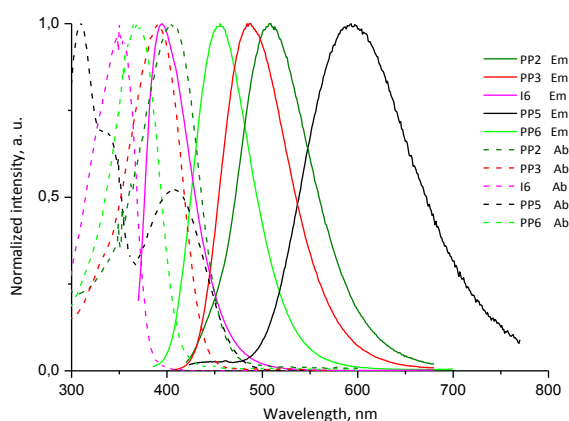


Figure 60. Absorption and emission spectra of the selected EWG-varied dyes in dioxane. Excitation wavelength used was the corresponding absorption maximum.

Presenting benzothiadiazole acceptor, **PP5** revealed two distinct absorption maxima around 320 and 450 nm (fig. 60). This dye was only emissive in aprotic and non-polar solvents with mega-Stokes shifts (130-258 nm). This character is quite uncommon for solvatofluorochromic dyes in apolar media;^[2,3] hence, it might open new perspectives in applications in the future.

Among all the considered acceptors, the methylenemalonitrile moiety **PP4** presented the most accentuated EW abilities translated in the largest red-shift of both maxima (Figure 59).^[248,249] The absorption was located in the blue spectral window (467-501 nm, table 3) perfectly matching excitations with the argon laser line. The full width at half-maximum height

of **PP4** is relatively narrow ($\Delta\lambda_{1/2} \sim 64$ and 82 nm, respectively) illustrating a useful asset for selective excitation.

The intermediate **I-6** was emissive even in water (13%). Its fluorescence was quenched only in chloroform or upon adding 1% (v/v) of trifluoroacetic acid to 1,2-dichloroethane. The weak EW nature of the vinyl group accounts for the observed blue-shifted absorption and emission. (table 1, fig. 60). Reichardt's $E_T(30)$ scale was used to evaluate the sensitivity of the dyes to polarity, which followed the order: **PP4** > **PP3** > **PP1** \approx **PP6** (slope comparison in fig. 61).

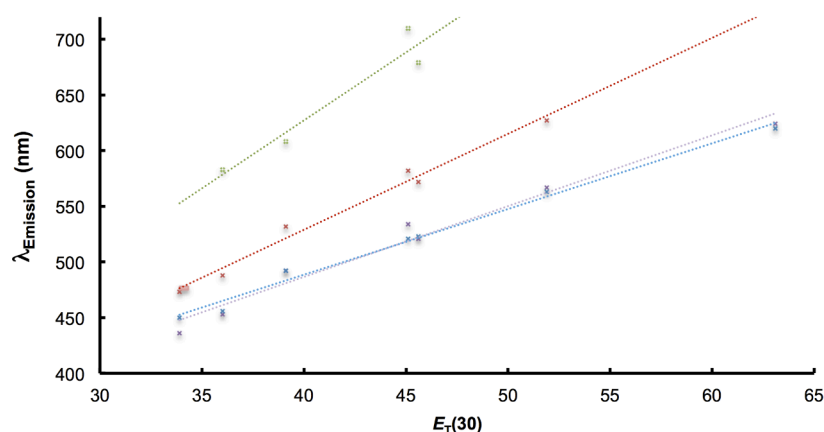


Figure 61. Dependence of the emission on the empirical polarity parameter $E_T(30)$ for selected acceptor-varied fluorenes **PP1** (violet), **PP3** (red), **PP6** (blue), and **PP4** (green). Correlation factors R^2 are respectively 0.97, 0.98, 0.99 and 0.93. The linear plots shown were obtained with all the tested solvents except for **PP4**, for which deviation from linearity was observed when protic solvents were included.

The emission maximum was proportionally red-shifted along the range of polarity. This quantitative parameter largely accounts for the dielectric constant of the solvent and its H-bond donor ability.^[31] The strong positive solvatochromism in the dyes' emission emphasizes the large ICT character of their excited states.

Lippert-Mataga model and Transition dipole moment calculations

The positive solvatochromism was further substantiated using the Lippert-Mataga model.^[250,251] The Stokes shifts were plotted as a function of the orientation polarizability in aprotic solvents since this model only takes into account the dipole-dipole interactions.

The linear plots shown were obtained with aprotic solvents according to the Lippert's eq. 7,

$$v_A - v_F = \frac{2}{hc} \Delta f \frac{(\mu_E - \mu_G)^2}{a^3}$$

Equation 7

Where h ($= 6.6256 \times 10^{-27}$ ergs) is the Planck's constant, c ($= 2.9979 \times 10^{10}$ cm/s) is the speed of light, and a is the radius of the Onsager's cavity. ν_A and ν_F are the wavenumbers (cm^{-1}) of the absorption and emission, respectively, $\Delta\nu$ is the Stokes shift (cm^{-1}), Δf is the Lippert's parameter, and μ_E and μ_G are the dipole moments of the excited and ground states, respectively.

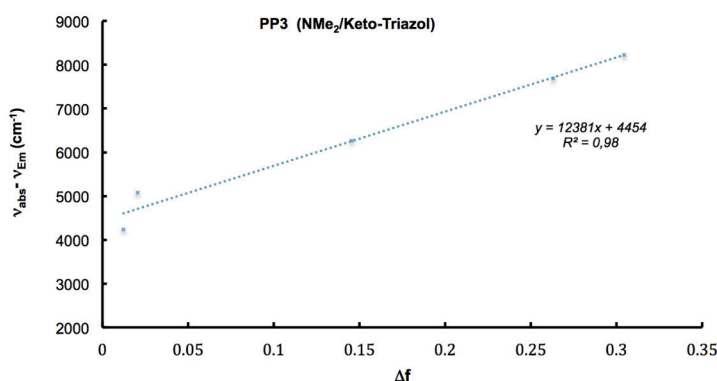


Figure 62. Lippert-Mataga function plot of **PP3**. Correlation factors R^2 is 0.93.

The plots demonstrated linear relationships. A representative trend is shown for **PP3** in fig. 62. The differences between the dipole moments of the ground and excited states ($\mu_E - \mu_G$) were 12.9, 12.6, 13.5, and 14.1 D for **PP2**, **PP6**, **PP3**, and **PP4** respectively (SI-XIII). These results confirm the increase of the dipole moments in the excited states.

PP1, **PP4**, and **PP6** were then investigated as representative examples in acetonitrile, chloroform, and toluene by DFT and TDDFT calculations.^[252] The DFT optimization essentially gave the geometry close to planar (fig. 63). Simulations satisfactorily reproduced the entire absorption spectra with slight red shift compared to the experimental values. Calculations showed that the electronic transitions arose from an electron promotion between the HOMO and the LUMO. In the frontier molecular orbitals, the HOMOs were localised at the fluorene and partially on the donor and the LUMOs at the acceptor and the benzene ring attached to it. Thus, the main contribution of the transition (ICT) dipole is in the plane of the molecule along the D-A axis.

To sum up, these fluorophores exhibited important λ -shifts to the red in both their absorptions and emissions relative to *prodan*. The absorption of the dyes was negligibly affected by polarity (<10 nm) except for the moderate bathochromic shift of **PP4** (35 nm). By contrast, all considered dyes showed forceful variations in their colors of emission. The positive solvatofluorochromism confirms the presence of a strong ICT character only at the excited state of these dyes. The modeling and calculations also support this conclusion. By contrast to the

peptide-coupled product **PP6**, the conservation of the desired optical properties for **PP3** upon conjugation *via* CuAAC makes the ynone **PP2** a more attractive anchoring point for biolabeling.

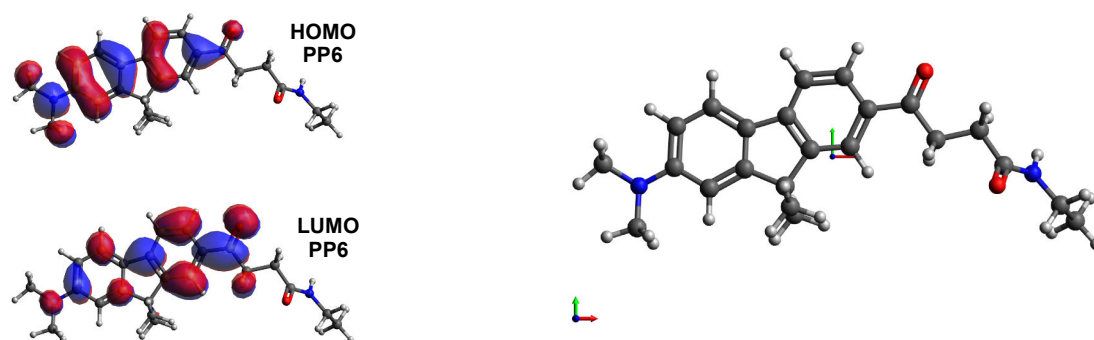
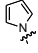
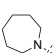
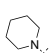
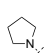
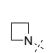
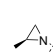
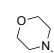
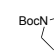


Figure 63. DFT-TDDFT simulations of **PP6**. *Peptide side chain was shortened to 2 carbons to reduce the calculation time.* Representation of the HOMO and LUMO frontier molecular orbitals (*Left*). Ground state optimized coplanar structure (*Right*).

II.2 - Varied-amine series

Different cyclic amines were characterized using the carbaldehyde as a fixed acceptor. The main data are listed in *table 4*.

Table 4. Spectroscopic properties of fluorophores with various amines and the same formyl acceptor

Solvent $E_T(30)^{[a]}$	λ , $\Delta\lambda_{SS}$ (nm)	<i>Varied-Amines / Fixed Acceptor (-CHO)</i> ^[a]							
		PP7 	PP8 	PP9 	PP10 	PP11 	PP12 	PP13 	PP14 
ϵ ($10^3 \cdot M^{-1} \text{cm}^{-1}$)			31.5	27.5	25	36	24	25	33
H ₂ O (63.1)	λ_{abs}	349	411	376	407	377	345	353	377
	λ_{em}	520	630	630	622	621	555	614	606
	$\Delta\lambda_{SS}$	171	219	254	215	244	210	261	229
	Φ	<1	0.02	0.02	0.03	0.05	0.16	0.05	0.03
EtOH (51.9)	λ_{abs}	338	398	373	395	380	342	365	362
	λ_{em}	430	572	565	570	572	522	566	561
	$\Delta\lambda_{SS}$	92	174	192	175	192	180	201	199
	Φ	<1	0.45	0.38	0.45	0.44	0.33	0.41	0.44
CH ₃ CN (45.6)	λ_{abs}	336	397	376	391	377	351	365	362
	λ_{em}	435	528	530	532	532	483	518	518
	$\Delta\lambda_{SS}$	99	131	154	141	155	132	153	156
	Φ	<1	0.52	0.64	0.54	0.61	0.49	0.61	0.6
DMSO (45.1)	λ_{abs}	345	405	385	400	386	355	375	375
	λ_{em}	448	532	540	538	538	486	530	527
	$\Delta\lambda_{SS}$	103	127	155	138	152	131	155	152
	Φ	<1	0.84	0.93	0.77	0.84	0.64	0.78	0.84
CHCl ₃ (39.1)	λ_{abs}	340	402	380	396	384	352	368	366
	λ_{em}	419	500	505	501	500	460	485	484
	$\Delta\lambda_{SS}$	79	98	125	105	116	108	117	118
	Φ	<1	0.62	0.65	0.62	0.48	0.46	0.68	0.58
Dioxane (36)	λ_{abs}	338	394	375	391	375	350	365	363
	λ_{em}	448	454	456	454	462	450	450	449
	$\Delta\lambda_{SS}$	110	60	81	63	87	100	85	86
	Φ	<1	0.71	0.87	0.6	0.66	0.11	0.65	0.62
Toluene (33.9)	λ_{abs}	340	397	371	394	378	352	365	365
	λ_{em}	375	440	447	439	442	428	429	449
	$\Delta\lambda_{SS}$	35	43	76	45	64	76	64	84
	Φ	<1	0.6	0.64	0.68	0.7	0.07	0.46	0.65

[a] As in Table 3.

PP7 was established as the negative control given its blue-shifted absorption and emission and its extremely low quantum yield (< 1%). Such characteristics were expected due to the weak

electron donation of the nitrogen's lone pair as part of the aromatic sextet of pyrrole. The DFT twisted geometry of the pyrrole and fluorene rings could also contribute to this poor donating ability (fig. 64).

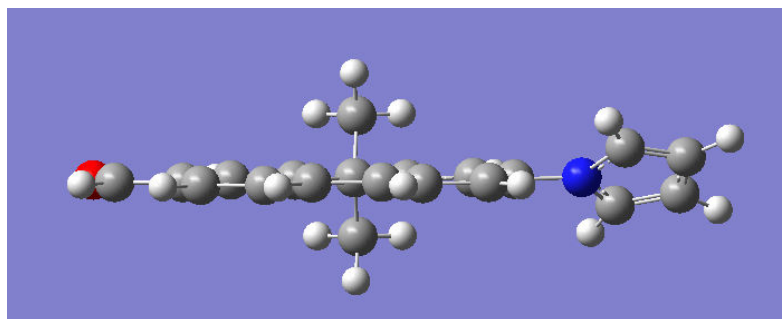


Figure 64. Optimized DFT structure of **PP7**

Compared to **PP1**, the 4- to 7-membered amine rings of **PP8** and **PP10** bathochromically shifted the absorption (10-15 nm, and 20-25 nm in water). The substitution of the methyl group by a longer alkyl chain red-shifted the absorption maxima, in agreement with an increased inductive effect. By contrast the 4- and 6-membered amine rings of **PP9** and **PP11** resulted in an unexpected hypsochromic shift (5-15 nm) as shown in *table 4* and *fig. 65-66*.

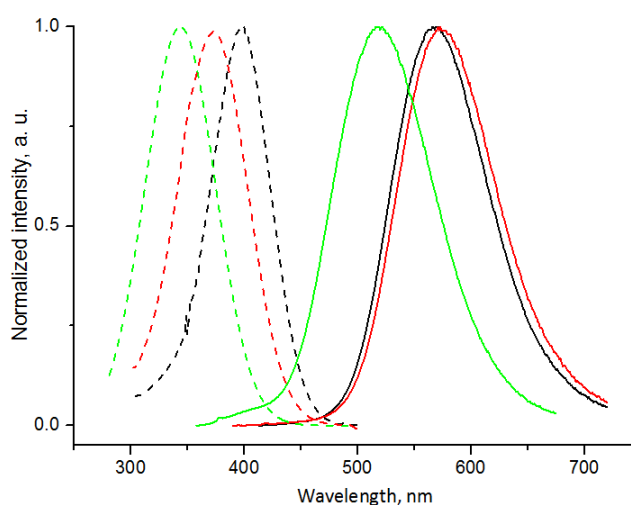


Figure 65. Absorbance (dotted line) and emission (solid line) for **PP8** (black), **PP9** (red), **PP12** (green) in EtOH. Excitation wavelength used was the absorption maximum.

PP8-11 were strongly emissive except in water and gave almost similar fluorescence spectra along the solvent polarity (fig. 66). *Fig. 67* depicts the dramatic Stokes shift and solvatofluorochromism of **PP9** as an example of this series.

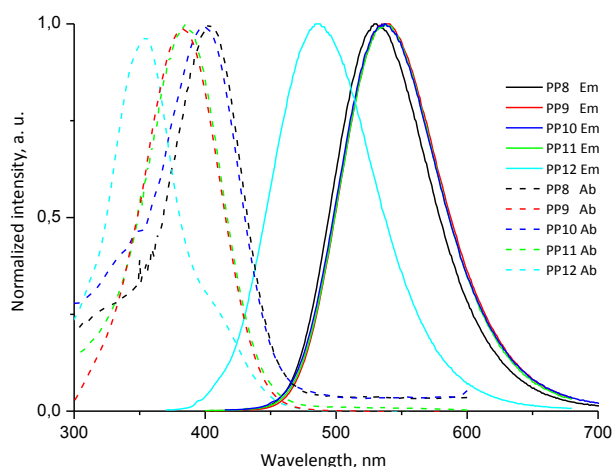


Figure 66. Absorption and emission spectra of **PP8-12** in DMSO. Excitation wavelength used was the absorption maximum.

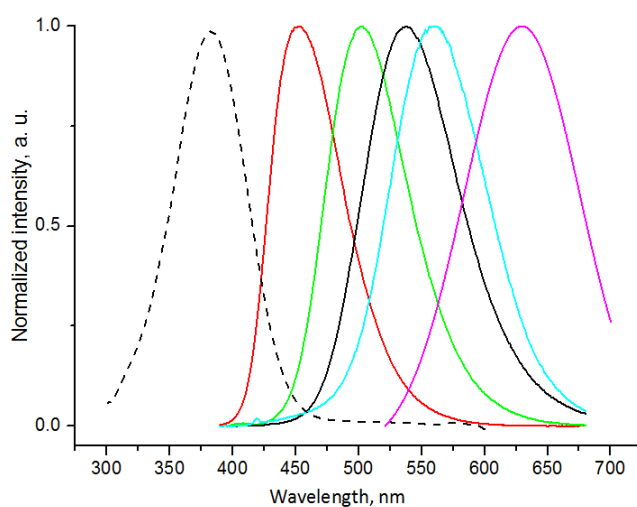


Figure 67 Absorbance (dotted line) and emission (solid line) for PP9 in toluene (red), chloroform (green), DMSO (black), EtOH (cyan) and H₂O (magenta). Since absorption is weakly solvatochromic, one representative spectrum was shown.

A common property of solvatochromic dyes with strong ICT character is their low quantum yields in water. The azetidine donor was reported to overcome this limitation and to prevent the quenching of the sensors in aqueous media.^[253,254] It was proposed that this donor can disfavor the formation of the poorly emissive, twisted internal charge transfer (TICT) states in water. Unfortunately, applying this strategy on fluorene family was not successful. **PP11** bearing the azetidine donor was not emissive in aqueous media. This quenching can not be resulting from

the formation of H-aggregates since the absorption maxima of the fluorene derivatives were not blue-shifted in H₂O vs. other solvents.^[92] An explanation could be that water molecules are acting as an electron-trap for the excited species.^[255]

PP12 was noticeably emissive contrary to the reported aziridine derivatives of other families like rhodamine.^[253] Compared to the other members of the series, **PP12** was characterized by reduced quantum yields in nonpolar solvents and considerable hypsochromic shifts in absorption and emission (table 4 and fig. 66). It was proposed that the electron-donating ability of this three-membered heterocycle was diminished^[256] due to the increased *s* character of the orbital of nitrogen atom's lone pair and the structurally- and electronically-enforced pyramidalised nitrogen.^[257] This proposal was ascertained with the bent DFT structure of **PP12** compared to the coplanar fluorene-piperidine **PP9** (fig. 68). The sum of the three C-N-C bond angles (304° versus 333° for trimethylamine) confirms the pyramidalized geometry of the aziridine nitrogen and the planar geometry (348° versus 360° for trigonal geometry) of the piperidine nitrogen. Control analysis of aziridine *versus* 2-methylaziridine derivative proves that the added methyl has no effect on the geometric parameters (SI).^[258,259] The $\mu_E - \mu_G$ of **PP12**, determined by the Lippert-Mataga model, was the lowest in this series (11.4-13.7 D); thus, attesting its weaker donating ability.

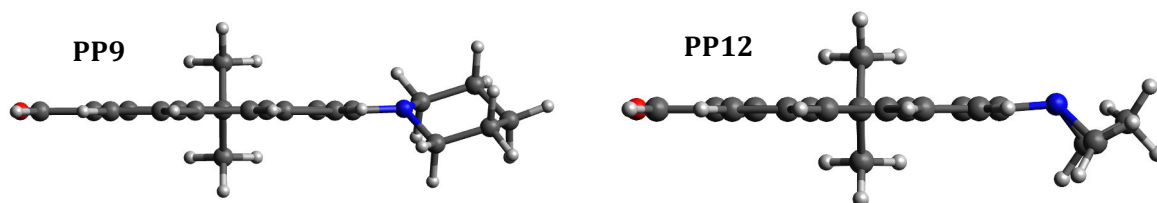


Figure 68. Ground-state optimised structures of **PP9** and **PP12**

Regarding the series of cyclic amines, **PP8-11** showed perfect overlap of the emission dependence on $E_T(30)$ inferring marginal effect of the ring size (between 4 and 7 members) on fluorescence properties (fig. 69).

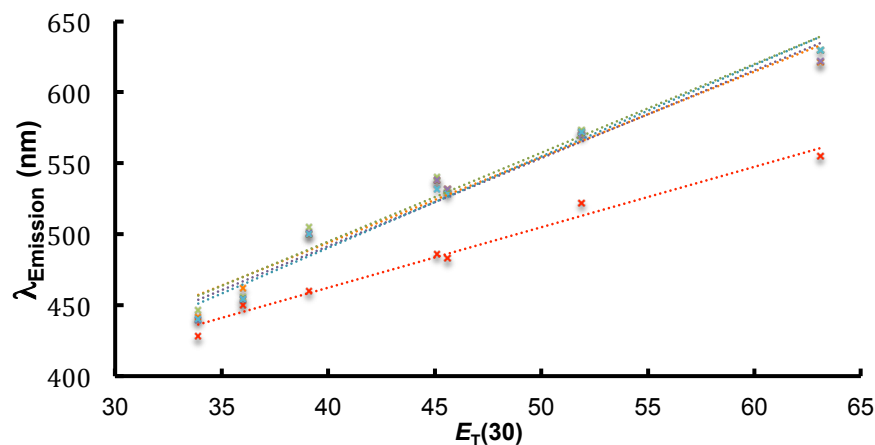


Figure 69. Dependence of the emission maxima for cyclic amine-varied fluorenes **PP8-11** (overlapping) and **PP12** (red linear trend below the overlap) on the empirical polarity parameter $E_T(30)$ of all the set of solvents

Interestingly, the strong quenching in water and the important brightness of these dyes in environments of distinct polarities provide the opportunities to develop turn-on sensors upon shielding from water. Aziridine **PP12** appeared as the weakest donor among all the considered aliphatic amines. On a side note, aziridine is a popular functional group for cycloadditions in the area of fullerene-fluorophore organic devices.^[130,258-260] The straightforward access to **PP12** is highly valuable in replacing the long employed classical routes. A conjugation of aziridine should convert this dye into a 5-membered ring adduct that can be detected by a red shift in spectroscopic properties.

The presence of another heteroatom in the donor group was studied with morpholine **PP13** and its piperazinyl analogue **PP14** comprising a second amine for subsequent peptide coupling. Compared to **PP9** with a similar 6-membered amine ring, the introduction of a nitrogen or oxygen atom blue-shifted the absorption maxima indicating that the negative inductive effect of the second heteroatom had imposed tangible charge redistribution (table 4). The emissions of **PP13-14** showed bathochromic shifts with little deviations relative to the maxima of **PP9**. Accordingly, with blue-shifted absorptions but yet relatively comparable emission maxima, **PP13-14** demonstrated larger Stokes shifts. The molar absorptivities in dioxane were 25.10^3 and $33.10^3 \text{ M}^{-1}\text{cm}^{-1}$ respectively. The quantum yields of these two dyes followed the same trends as the reference compounds **PP9** and **PP1** and fell nearly in the same range depending on the solvent used.

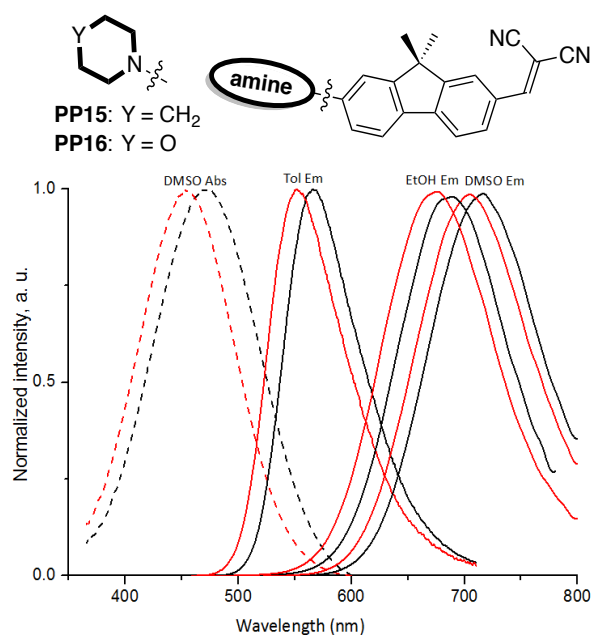


Figure 70. Absorbance (dotted line) and emission (solid line) for the optimized push-pull dyes **PP15** (black) and **PP16** (red) in representative solvents. **PP15-16** are systematically numbered 178-179. Excitation wavelength used was the corresponding absorption maximum.

Finally, the methylenemalonitrile **PP15-16** with piperidine and morpholine groups were respectively synthesized by Knoevenagel condensation on the formyl group of **PP9** and **PP13** (85 % and 72 % yields respectively) to verify the potential synergic effect of the A and D on the photophysics. *Fig. 70* shows their absorption and emissions in selected solvents. The absorptions of **PP15-16** appeared in the visible range (440-475 nm, $34\text{-}36 \cdot 10^3 \text{ M}^{-1}\cdot\text{cm}^{-1}$) allowing a selective excitation with the blue diode (445 nm) or the argon ion laser line (488 nm). The fluorescence remained in the NIR region (705-713 nm) in polar solvents yielding spectacular mega-Stokes shifts (DMSO and H₂O: 240-260 nm, toluene: 105 nm).

The differences in the dipole moments ($\mu_E\text{-}\mu_G$) of **PP15-16** (14.4 and 14.9 D) were comparable to that of **PP4** (14.1 D) as the highest among all of the studied dyes. The large dipole differences assert the strongest electron-withdrawing ability of the methylenemalonitrile in agreement with DFT calculations. The quantum yields of **PP4**, **PP15**, and **PP16** strongly correlate with the $E_T(30)$ scale confirming the close relationship between the quantum yield and the sensitivity of the CT-type excited states to polarity (figure 71). The decrease of the emission intensity in polar solvents is typical for solvatochromic dyes with strong ICT character. It was advanced that the reduced energy gap between the excited and ground states in polar solvents favored internal conversion and thus non radiative energy release.^[261] This linear trend can help to anticipate the emissive behaviour of the dyes with the strongest transition dipole moment in a medium of known polarity.

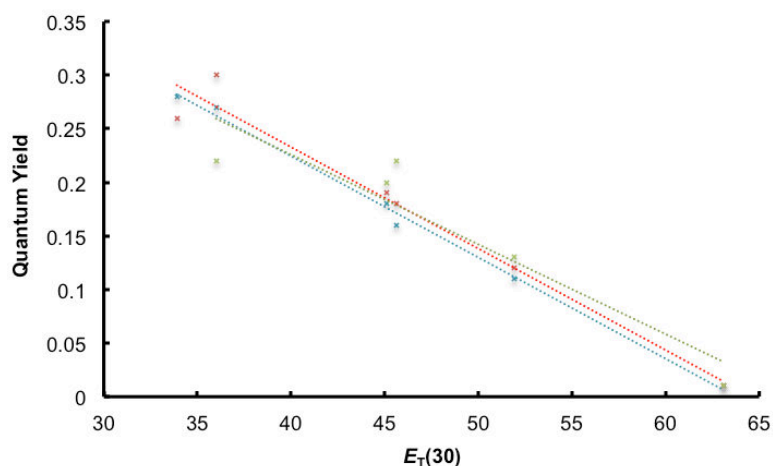


Figure 71. Dependence of the quantum yield for **PP4** (red), **PP15** (blue) and **PP16** (green) on the empirical polarity parameter $E_T(30)$. The linear trends were obtained with all the representative solvents, except chloroform (correlation factors R^2 are respectively 0.965, 0.996, 0.87).

II.3 Hammett correlation

The correlations of the absorption and emission maxima to the σ_p Hammett substituent constants were assessed.^[262] This approach could complement the challenging predictions of emission of fluorophores with CT in the excited state by TD-DFT.^[263] Thus, four representative molecules were selected: **PP1** as a reference, **PP4** as the strongest acceptor, **PP12** as the weakest donor, and **I-6** as a control.

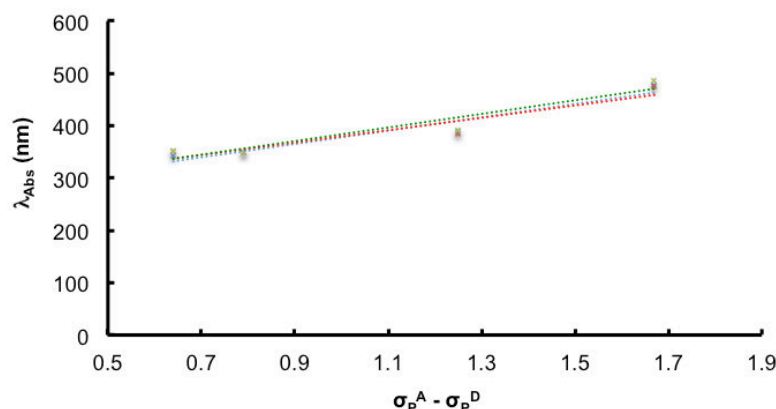


Figure 72. Dependence of the respective absorption maxima of **PP12**, **I-6**, **PP1**, and **PP4** (in EtOH (blue), acetonitrile (red) and chloroform (green)) on the donor/acceptor Hammett σ_p value ($\sigma_p^A - \sigma_p^D$). Correlation factors R^2 are 0.94, 0.89, and 0.91 respectively.

Since the D and A substituents in the fluorene derivatives present a mesomeric relationship like in *para*-disubstituted aromatic derivatives, photophysics of the selected examples were

depicted as a function of the σ_p values ($\sigma_p^A - \sigma_p^D$). The absorption maxima of the whole set correlated strongly with the σ_p parameter reflecting the difference between the ED and EW properties of the substituents in the wide range of polarity (fig. 72).

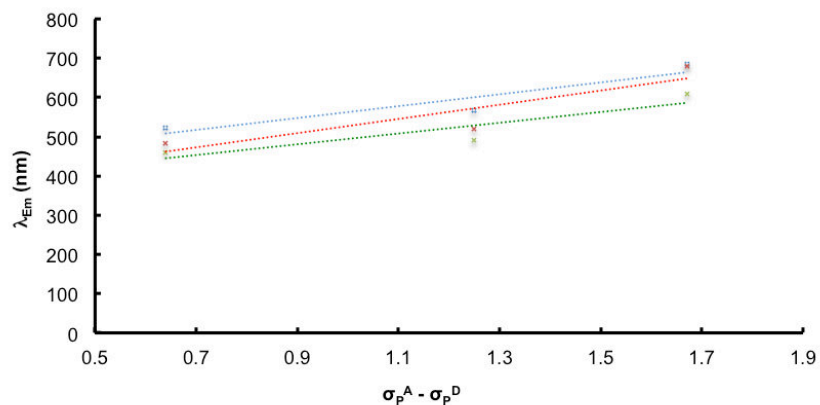


Figure 73. Dependence of the respective emission maxima of **PP12**, **PP1**, and **PP4** (in EtOH (blue), acetonitrile (red) and chloroform (green)) on the donor/acceptor Hammett σ_p value ($\sigma_p^A - \sigma_p^D$). Correlation factors R^2 are 0.88, 0.81, and 0.83 respectively.

In parallel, the linear trend between emission maxima and σ_p values was noticed exclusively with the dyes presenting large solvatofluorochromism (**PP1**, **PP12**, and **PP4**, fig. 73). Indeed, since the emission occurs through charge-transfer mechanism, this correlation is consistent with the observation that stabilization of the excited states was highly sensitive to polarity. To verify these predictions, the absorption and emission maxima of a reported fluorene dye (diethylamino D and formyl A) were calculated in three solvents (ethanol, acetonitrile, and chloroform).^[60,85] The anticipated absorption maxima were in agreement with those recorded experimentally (table 5). The emission maxima were slightly red-shifted (10-20 nm) compared to the experimental values. The error was within the acceptable margin. Hence, this paradigm is an interesting tool to predict spectroscopic properties in the prerequisite design of advanced probes.

Table 5. Prediction study with a Hammett constant-based model

Solvent	Prediction $\lambda_{abs} / \lambda_{em}$ (nm)	Experimentally $\lambda_{abs} / \lambda_{em}$ (nm)
CHCl ₃	401 / 507	399 / 497
Acetonitrile	395-396 / 541	394 / 518
EtOH	395 / 576	395 / 554

III. Conclusion

In summary, we rationally designed, synthesized, and characterized a library of fluorescent push-pull dyes based on a 2,7-disubstituted fluorene scaffold. These emissive D- π -A derivatives were prepared by straightforward and gram-scalable synthetic pathways. The various electron-withdrawing groups were efficiently introduced on a common and easily accessible synthon *via* different methodologies including amongst others: Stille coupling, CuAAC, and peptide coupling. The screening of electron-donating groups was chemoselectively carried out *via* a versatile Buchwald-Hartwig amination on a fluorenyl carbaldehyde intermediate obtained by an optimized formylation reaction. Photophysical studies highlighted the most promising compounds in terms of brightness, mega-Stokes shift, excitation accessibility, and versatility for subsequent conjugation. The propioloyl linker was introduced for conjugation and converted into the ketotriazolyl derivative whilst maintaining the desired optical properties. Such characteristics make the ynone a prospective anchoring point for biolabeling that we build on in the next two chapters. By combining the attractive ED (morpholine, piperidine) and EW (methylenemalonitrile) groups, the synergic effect was tested. These studies led to new push-pull fluorenes with red-shifted absorption and emission. Due to an enhanced intramolecular charge transfer, the dyes were highly solvatochromic over the entire polarity scale and even NIR emissions were observed in protic solvents. DFT calculations confirmed these experimental observations. Correlation of a selected set of D- π -A emitters with Hammett σ_p values of the considered donor/acceptor pairs provides a complementary tool to anticipate the spectroscopic features desired for specific applications.

Chapter Four

Fluorene-based membrane probes and cell imaging

Fluorescence imaging has revolutionized the way to observe cellular structures and to understand their functions.^[264] In that aspect, small molecule dyes have attracted major attention in advanced applications since their size might be less perturbative than fluorescent proteins and nanoparticles. Further, the chemistry and photophysics of an organic label can be finely tuned. Among organic labels, the turn-on fluorescent probes are extremely attractive for imaging since they ensure simple and convenient use without the need to wash the excess of reagent. In addition, their signal-to-noise ratios are expected to be high. The fluorescent probe should also display high brightness, photostability, and selectivity to the target in order to maximize the imaging resolution. As a matter of fact, the access to organic probes that fulfill all these meticulous requirements is highly challenging from both perspectives of tuning the design and its synthesis. Considering the structure-property relationships and the optimized synthetic routes of chapter 3, we decided on the most prominent properties in terms of visible absorption, laser excitation, accessibility, brightness, Stokes shifts, and positive solvatochromism to access membrane probes. This chapter will present the synthesis of 3 new advanced analogues of **PP3** comprising a) a polar deoxyribosyl head (**F1**), b) a lipophilic long alkyl chain (**F2**), and c) an amphiphilic anchoring group to fix the dye at the membrane interface and prevent its internalization. Then, we will discuss the spectroscopic characterization of the three dyes, their ability to probe large and giant unilamellar vesicles (LUV and GUV) of different lipid compositions, and the imaging of HeLa cells.

I. Introduction

Considering the characteristics of **PP3** dye in particular from chapter 3 (fig. 74), this probe absorbs in the violet (400 nm) and demonstrates an ICT character amongst the highest. Moreover, **PP3** exhibits bright and red-shifted emission ($\Delta\lambda_{ss} > 100$ nm) in aprotic solvents. The largest displacement of its emission is shown in polar solvents where the dye turns almost non-emissive in water. Additionally, the click 1,3-dipolar conjugation of the propioloyl linker adopted in **PP3** synthesis confirmed the conservation of the desired optical properties upon conjugation. This promising ynone group for biolabeling and the turn-on property upon shielding the dye from water render this design of a fluorene dye a good candidate for sensing biomembranes and probing their lipid domains. Regarding this application, there is a strong demand to realize new probes that overcome the drawbacks of the existing environment-sensitive ones such laurdan (**180**), a lipophilic analogue of prodan (**17**), and Nile Red (**14**) derivatives (fig. 74).^[265-267]

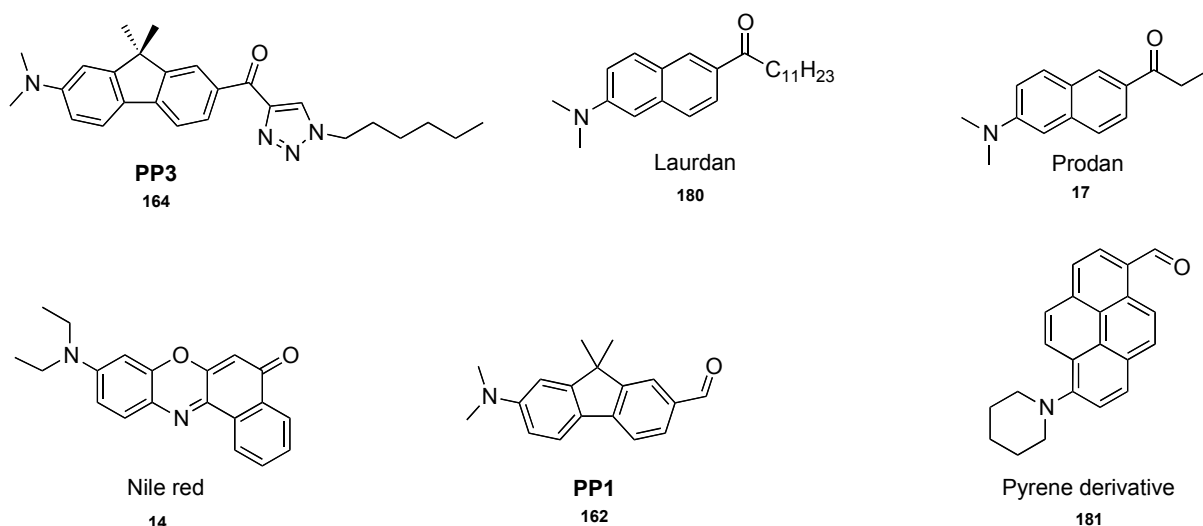


Figure 74. Common dyes for comparisons

An effective membrane probe should present the following rigorous properties; it should be excitable in the visible, stain exclusively the plasma membrane with high contrast, distinguish the liquid domains of the membrane by changing its fluorescence color, intensity, or lifetime, show minimal internalization and interference from cell auto-fluorescence, and operate in the visible and NIR spectral window (above 700 nm) open for multi-colour imaging. Searching for probes with the particular attribute of responding specifically to lipid domains can inevitably help in deciphering the lateral heterogeneity of the cell membranes described by the lipid raft hypothesis.^[151,268] Lipid rafts are hitherto under debate and are believed to be the origin of fundamental biological processes and diseases.

II. Synthesis

The clickable hydrophobic fluorene core (**163**) was prepared as described in chapter 3. The synthesis of the azido derivatives (**182-184**) was carried out by methods reported in literature (detailed in SI-XI).^[166,269,270] Next, the clickable ynone (**163**) was converted to the keto-triazolyl derivatives (**F1**, 80 % yield) with β -azidodeoxyribose, (**F2**, 75 %) with *n*-dodecyl azide, and (**F3**, 61 %) with the azido amphiphilic chain *via* CuAAC reactions (fig. 75). The optimized click conditions involved $\text{CuSO}_4 \cdot 5\text{H}_2\text{O}$ (0.5 eq.), sodium ascorbate (0.7 eq.), DMF/water (3/1), at room temperature for 1-3 h.

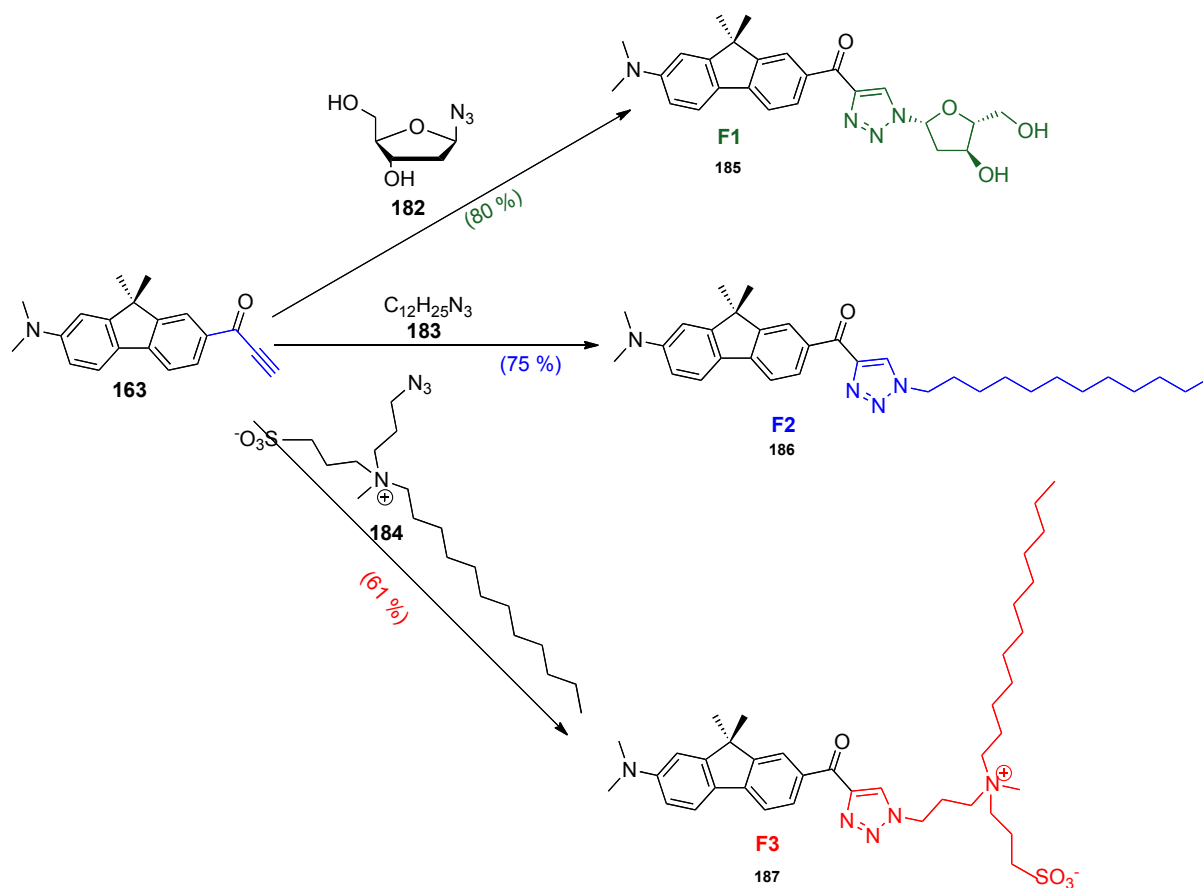


Figure 75. Synthesis of the membrane probes **F1-3** *via* CuAAC; $\text{CuSO}_4 \cdot 5\text{H}_2\text{O}$ (0.5 eq.), sodium ascorbate (0.7 eq.), DMF/water (3/1), rt, 1-3 h

III. Photophysical characterization of F1-F3

We first investigated the impact of the triazole substituent on the UV/visible and fluorescence properties in a set of aprotic and protic solvents with large range of $E_T(30)$ parameter (table 6). The absorption and emission spectra are shown in *fig. 76*.

Table 6. Spectroscopic properties of **F1-3** and the parent dye **PP3** for comparison^[a]

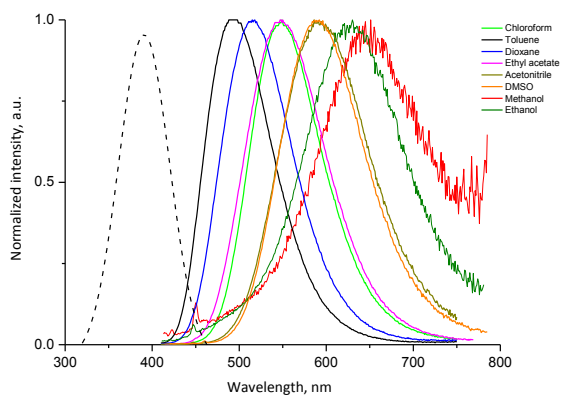
Solvent $E_T(30)$	ϵ_{\max} ($10^3 \cdot M^{-1} \cdot cm^{-1}$)	PP3	F1	F2	F3
		37.6	38.0	37.1	35.0
Phosphate Buffer ^[b] (63.1)	λ_{abs} (nm)	n.d.	390	401	409
	λ_{em} (nm)	n.d.	n.d.	n.d.	n.d.
	$\Delta\lambda_{\text{SS}}$ (nm)	n.d.	n.d.	n.d.	n.d.
	Φ (%)	n.d.	n.d.	n.d.	n.d.
MeOH (55.4)	λ_{abs} (nm)	n.d.	395	400	399
	λ_{em} (nm)	n.d.	651	647	676
	$\Delta\lambda_{\text{SS}}$ (nm)	n.d.	256	247	277
	Φ (%)	n.d.	1,5	3	2
EtOH (51.9)	λ_{abs} (nm)	396	403	400	397
	λ_{em} (nm)	622	630	629	636
	$\Delta\lambda_{\text{SS}}$ (nm)	226	227	229	239
	Φ (%)	6	6	8	8
ACN (45.6)	λ_{abs} (nm)	389	395	391	390
	λ_{em} (nm)	578	586	578	587
	$\Delta\lambda_{\text{SS}}$ (nm)	189	191	187	197
	Φ (%)	77	42	51	61
DMSO (45.1)	λ_{abs} (nm)	402	405	402	401
	λ_{em} (nm)	582	592	584	592
	$\Delta\lambda_{\text{SS}}$ (nm)	180	187	182	191
	Φ (%)	85	53	75	93
Chloroform (39.1)	λ_{abs} (nm)	399	403	404	402
	λ_{em} (nm)	532	549	539	559
	$\Delta\lambda_{\text{SS}}$ (nm)	133	146	135	157
	Φ (%)	72	74	56	66
Ethyl acetate (38.1)	λ_{abs} (nm)	n.d.	393	390	392
	λ_{em} (nm)	n.d.	550	527	547
	$\Delta\lambda_{\text{SS}}$ (nm)	n.d.	157	137	155
	Φ (%)	n.d.	72	61	69
Dioxane (36)	λ_{abs} (nm)	391	394	393	397
	λ_{em} (nm)	488	515	502	517
	$\Delta\lambda_{\text{SS}}$ (nm)	97	121	109	120
	Φ (%)	0.52	82	96	72
Toluene (33.9)	λ_{abs} (nm)	394	391	399	402
	λ_{em} (nm)	473	498	472	518
	$\Delta\lambda_{\text{SS}}$ (nm)	79	107	73	116
	Φ (%)	0.86	60	85	54

[a] as table 3, [b] 20 mM buffer, pH 7.4.

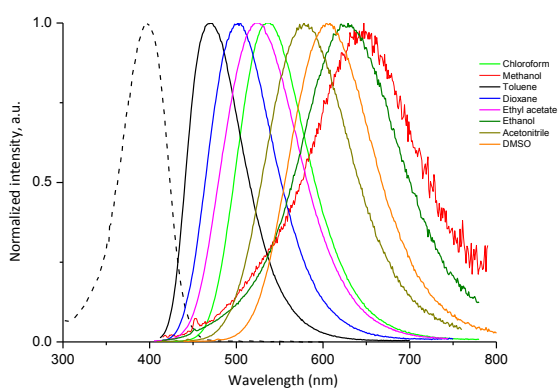
The 3 dyes absorbed strongly in the violet around 400 nm (35.10^3 - $38.10^3 M^{-1} \cdot cm^{-1}$ in dioxane). Their absorption maxima demonstrated little dependence on the polarity change ($\Delta\lambda_{\text{abs}} < 20$ nm) displaying almost no solvatochromism. This is an evidence of the absence of ICT character in their ground states contrary to dyes presenting solvent-dependence of their absorption spectra. An important example of this class of dyes with ICT character in their ground states is the Nile Red (**14**). However, their emission maxima were red-shifted with large Stokes shifts (e.g. **F1**:

from 107 nm in toluene to 256 nm in MeOH for $\Delta\lambda_{ss}$). In sharp contrast to absorption, their emission exhibited high sensitivity to solvent changes. The marked red shift upon the increase in the solvent polarity is in line with the data of the parent compound **PP3** (Table 6).

A)



B)



C)

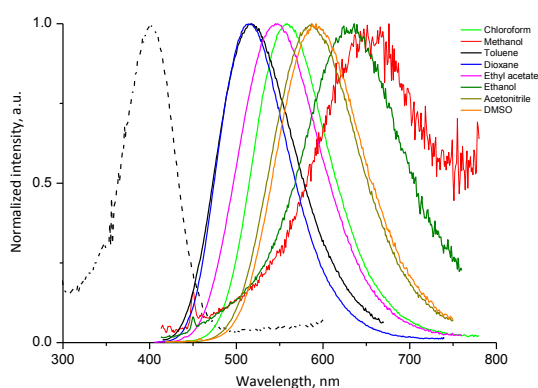


Figure 76. . Normalized absorption in toluene as a representative solvent (dotted line) and emission (full line) spectra in different solvents: A) **F1**, B) **F2**, and C) **F3**. Excitation wavelength used was the corresponding absorption maximum.

III.1 Hydration study of **F1**

We next explored the influence of hydration on the emission of dye **F1** in mixtures of dioxane and water.

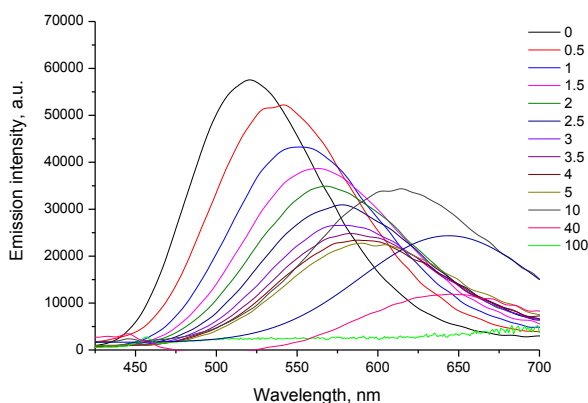


Figure 77. Dioxane-water titration of **F1**, the numbers signify the increasing percentage of water in dioxane

As evidenced in *fig. 77*, hydration shifts the position of the emission band to the red and results in increased quenching of the fluorescence, which is common in dyes with strong ICT character. In particular, three concentration regions might be distinguished; low polarity medium disturbed by relaxing sole water molecules characterized by blue-shifted emission and brightness, second region with collective effect of water but when it was still not a bulk solvent translated in a collective red shift and decrease in the quantum yield and the third region characterized by quenched emission where the water became a bulk solvent. Hence, The shift from polar aqueous environment to apolar aprotic dioxane results in a turn-on (>25 fold) of the

fluorescence intensity. These significant differences confirm the prominent efficiency of the push-pull dyes for sensing membrane lipids (aprotic media).

III.2 Photophysical characterization in large unilamellar vesicles of different lipid compositions

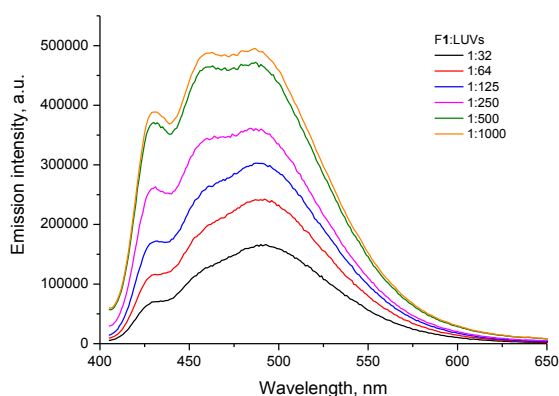


Figure 78. Fluorescence of **F1** at different concentration ratios of SM/CL LUVs (phosphate buffer 20 mM, pH 7.4). Excitation wavelength used was 390 nm.

LUVs are the simplest models to study biomembranes. Spingomyelin (SM) and cholesterol (CL) were used to produce liquid ordered membrane phase (Lo); while, liquid disordered membrane phase (Ld) was obtained with the unsaturated phospholipid, dioleoylphosphatidylcholine (DOPC).^[151] First, the optimal probe:lipid ratio was determined with **F1** by varying the concentration of SM/CL LUVs.

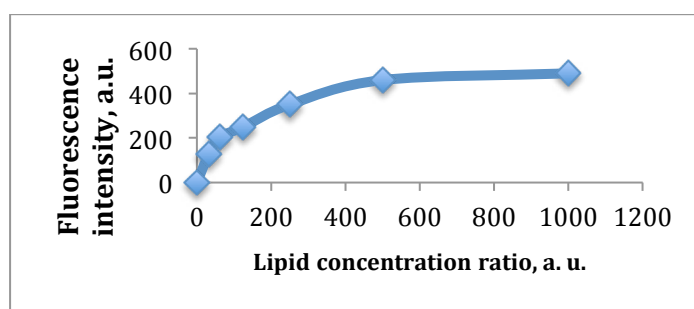


Figure 79. Variation of fluorescence intensity of **F1** as a function of SM/CL LUVs concentration ratio (in phosphate buffer 20 mM, pH 7.4); the unit concentration of **F1** was 0.4 μ M.

As shown in *fig. 78-79*, the fluorescence intensity of **F1** increases upon addition of LUVs and saturates at lipid:probe ratio about 500:1. This infers that nearly all the dye molecules were bound to lipids above this ratio. These data also verify the efficient binding of the probe to the lipid membrane, which is about 3 times more favorable than that of the Nile Red derivative probe.^[265] It is worth noting that the binding effect on fluorescence was instantaneous; the same

spectra were reproduced after the samples were left for 5, 10, 15 min at rt or at 60 °C.

Table 7. Investigations in LUVs^[a]

Solvent		F₁	F₂	F₃
LUVs DOPC	λ_{abs} (nm)	390	410	399
	λ_{em} (nm)	510	545	514
	$\Delta\lambda_{\text{SS}}$ (nm)	120	135	115
	Φ (%)	57	24	59
LUVs DOPC/CL (1/0,9) ^[a]	λ_{abs} (nm)	390	406	397
	λ_{em} (nm)	500	539	508
	$\Delta\lambda_{\text{SS}}$ (nm)	110	133	111
	Φ (%)	64	28	67
LUVs SM/CL (1/0,9) ^[a]	λ_{abs} (nm)	384	408	403
	λ_{em} (nm)	427-454-487	487	493
	$\Delta\lambda_{\text{SS}}$ (nm)	n.d.	79	90
	Φ (%)	51	63	99

[a]Same as table 3; Excitation wavelength used was 390 nm.

Next, the ability of dyes **F1-F3** for probing LUVs of different compositions was tested. The emission spectra were recorded (fig. 80). The main spectroscopic properties are given in *table 7*.

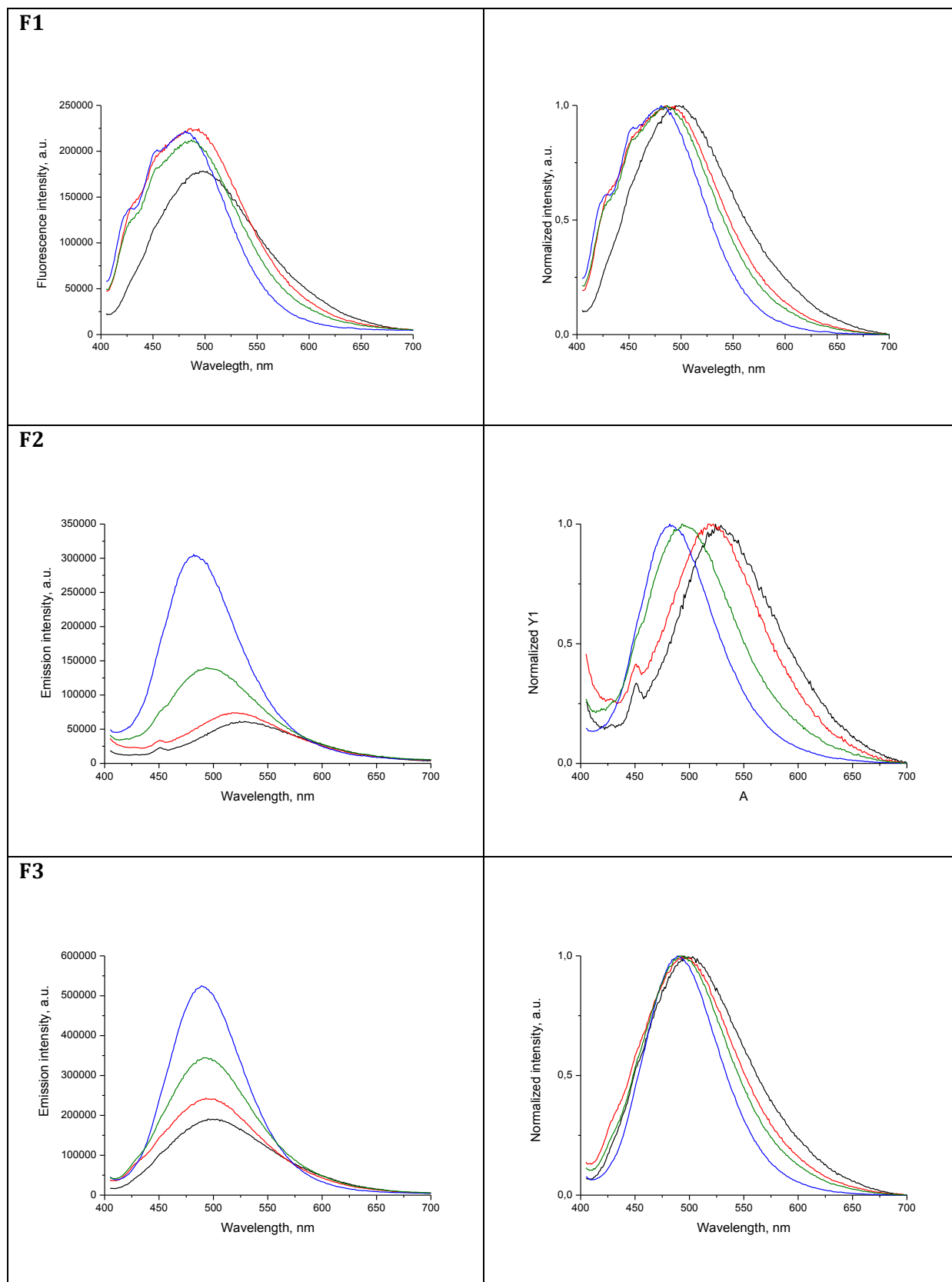


Figure 80. Emission spectra of **F1-F3** (150 nM) in different LUVs (100 μ M) in phosphate buffer (20 mM pH 7.4); black (DOPC), red (DOPC/CL), blue (SM/CL), green (DOPC/SM/CL). Excitation wavelength used was 390 nm.

The absorption maxima of **F1-F3** in different lipid vesicles were around 400 nm. By contrast, their emissions disclosed apparent dependence on the lipid composition and liquid phases of the LUVs. Binding of **F1-F3** to lipid vesicles resulted in considerable increase of the fluorescence intensities. Depending on the lipid composition, the quantum yields varied from 57-68, 24-63 and 59-99% for **F1**, **F2**, and **F3** respectively (table 7). Remarkably, **F2** and **F3** attested an increase in quantum yields up to three folds in liquid ordered phases (SM/CL and SM/DOPC/CL). In addition, **F1-F3** showed a significant shift of their emission to the blue (e.g. from 545 to 487 nm) when lipid phase changed from Lo (SM/CL) to Ld (DOPC). This is consistent with the fact that the Lo phase is less hydrated as a consequence of the higher level of lipid packing as compared to the Ld phase.^[151] The differences in the emission ($\Delta\lambda_{em}$) between the two extreme states were 23, 68, and 21 nm for **F1-F3** respectively. Thus, **F2** demonstrates the highest sensitivity that compares favorably to laurdan and Nile red probes with $\Delta\lambda_{em}$ of 48 and 36 nm, respectively.^[153,265] On the other hand, lower sensitivity to phase changes for **F1** and **F3** are related to the presence of groups that anchor the dye at the interface. The response of the environment-sensitive probes to phase variation is frequently associated with changes in the location and orientation of the fluorophore in membranes.^[152] Therefore, the anchor groups in **F1** and **F3** may limit the freedom of the dye, thus decreasing its sensitivity. Nevertheless, the sensitivity of **F1** and **F3** to the different phases could be sufficient for imaging applications.

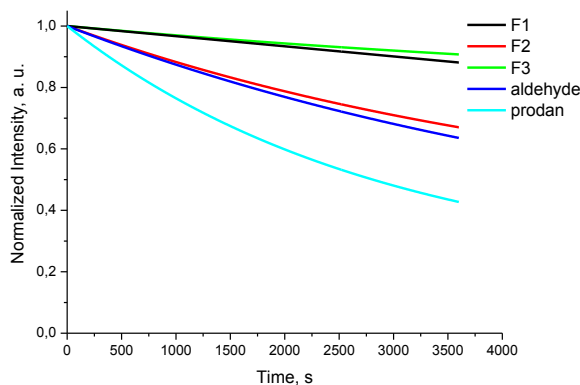
III.3 Photodegradation studies

Afterwards, we investigated the time-dependence photodegradation of **F1-F3** in their free forms in (fig. 81A), bound to lipid vesicles (DOPC) (fig81B), and in ethanol (SI-XIV) under continuous illumination of the samples. Xylene was chosen as a representative high boiling point apolar solvent mimicking hydrophobic environment. Indeed, photostability of fluorosolvatochromic dyes in apolar media is a major concern since it represents a severe limitation in imaging applications. This is particularly critical in lipid membranes since the commonly used dyes (prodan, laurdan, and Nile red) photobleach rapidly in this apolar environment.^[60,153] Prodan (**17**) and the fluorene-carbaldehyde derivative (**162**) were used as references (dyes shown in fig. 74).

F1-F3 portrayed different behaviors in xylene and DOPC vesicles (fig. 81). In xylene, the emission intensities were more than 90% for **F1** and **F3**, about 70% for **F2** and the aldehyde, and 50% for prodan after 1 h illumination. Once bound to DOPC vesicles, the intensities were more than 90 % for **F1**, **F3**, and the aldehyde, but 45% for **F2** and prodan after 1 h. First, these results confirm the superior photostability of the fluorene dyes compared to prodan. Noticeably,

F1 and **F3** demonstrate the highest photostability in both tested conditions. This higher photostability without oxygen depletion indicates that generation of reactive oxygen species, which often accounts for photobleaching of small organic dyes, is limited for fluorene dyes.^[264,271] **F1** and **F3** were more photostable compared to **F2** probably because they bear polar groups that could increase the local polarity of the environment in solvent and in lipid bilayer.

A) Xylene



B) DOPC LUV

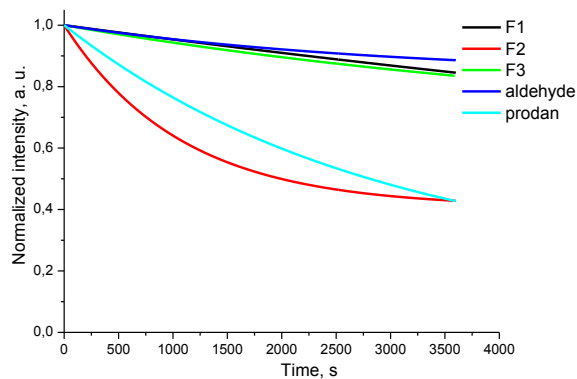


Figure 81. Photodegradation decay curves of **F1-3** as a function of time in A) xylene, and B) LUVs (DOPC). Photodegradation was performed at 400 nm with the xenon lamp in the spectrofluorometer (Emission and excitation slits = 8).

The lower photostability of **F2** parallels its shown higher sensitivity to detect lipid order. In polar media like ethanol, the dyes demonstrated the highest photostability in accordance with the typical increase in the singlet-triplet energy gap which render intersystem crossing less

favorable and leads to less free oxygen radical species.^[60,153] Their emission intensity remained above 95 % after 1 h.

IV. Imaging

IV.1 Imaging giant unilamellar vesicles (GUV) with F3

The significant shifts in emission of the new probes in Lo and Ld phases open the possibility for ratiometric imaging of lipid order in membranes by recording the emission intensities at two different wavelengths. **F3** was used to image GUVs made of DOPC and DOPC/SM/CL since in imaging cells and model membranes, it showed better features compared to the other two dyes (SI-XIV) most probably due to its orientation. The ternary mixture of lipid molecules is a simplified system to model co-existence of lipid domains. **F3** was then added to adherent GUVs at concentration of 100 nM and studied without washing by confocal microscopy to evaluate its capability to visualize Ld and Lo phases. The images were processed by collecting the emission of the blue and green regions separated at 500 nm (fig. 82A-B). The ratiometric image was obtained by dividing the image of the green channel by the one of the blue channel (fig. 82C). **F3** distinguishes well the Lo and Ld phases through variations in the green/blue ratio signal (fig. 82C). Thus, separated Lo (magenta) and Ld (yellow-green) domains were clearly observed.

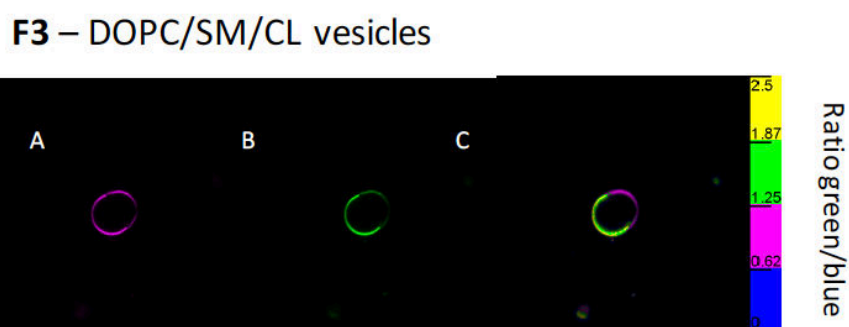


Figure 82. Confocal fluorescence image of DOPC/SM/CL GUVs stained with **F3**. Images were obtained by collecting emission of the A) blue channel; B) green channel. C) Ratiometric green/blue imaging of GUVs, the ratios of intensities are displayed by using the color code given on the right scale.

F3 - DOPC vesicles

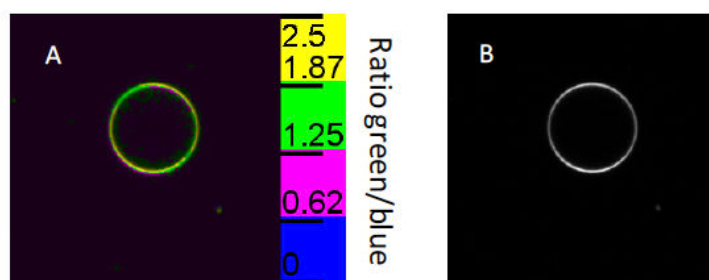


Figure 83. Confocal fluorescence image of DOPC GUVs stained with **F3**. A) Ratiometric green/blue imaging of GUVs, the ratios of intensities are displayed by using the color code given on the right scale. B) Image were obtained by collecting fluorescence intensity recorded for both channels.

Control experiment conducted with the DOPC vesicles confirms this interpretation (fig. 83) as the membranes appear in green pseudo-color corresponding to one of the phases observed in the ternary mixture (fig. 82C). **F3** stains only the membrane giving bright images with low background fluorescence (fig. 83B). **F3** performs comparably to the Nile Red derivative (NR12S) probe to stain membranes and distinguish lipid domains in model LUVs.^[265]

IV.2 Imaging cells with F1-F3

Fluorescence microscopy was next used to examine the staining of cells with the probes **F1-F3**. Adherent HeLa cells were incubated with **F1-F3** probes at a concentration of 100 nM and imaged after 5-10 min of incubation. **F1-F3** presented noticeable differences in their internalization and distribution within cells as evidenced in *fig. 84*. **F3** displayed bright fluorescence exclusively in plasma membranes (colored in magenta, *fig. 84E*) without internalization of the dye. The ratiometric fluorescence image gave a uniform distribution evidence of the domination of the Lo phase in the cell plasma membranes as it was previously observed with laurdan and NR12S probes.^[265,272] By contrast, **F1** and **F2** dyes were distributed differently (*fig. 84A-D*). The fluorescence intensity image indicates that **F1** and **F2** penetrate into the cells and mainly stain the cytoplasm (*fig. 84B* and *84D*). It should be noted that the fluorescence intensity of **F2** in cells was relatively low, which is probably related to very low solubility of this dye in water. Unlike **F1** and **F3**, it probably precipitates before staining the cell membranes.

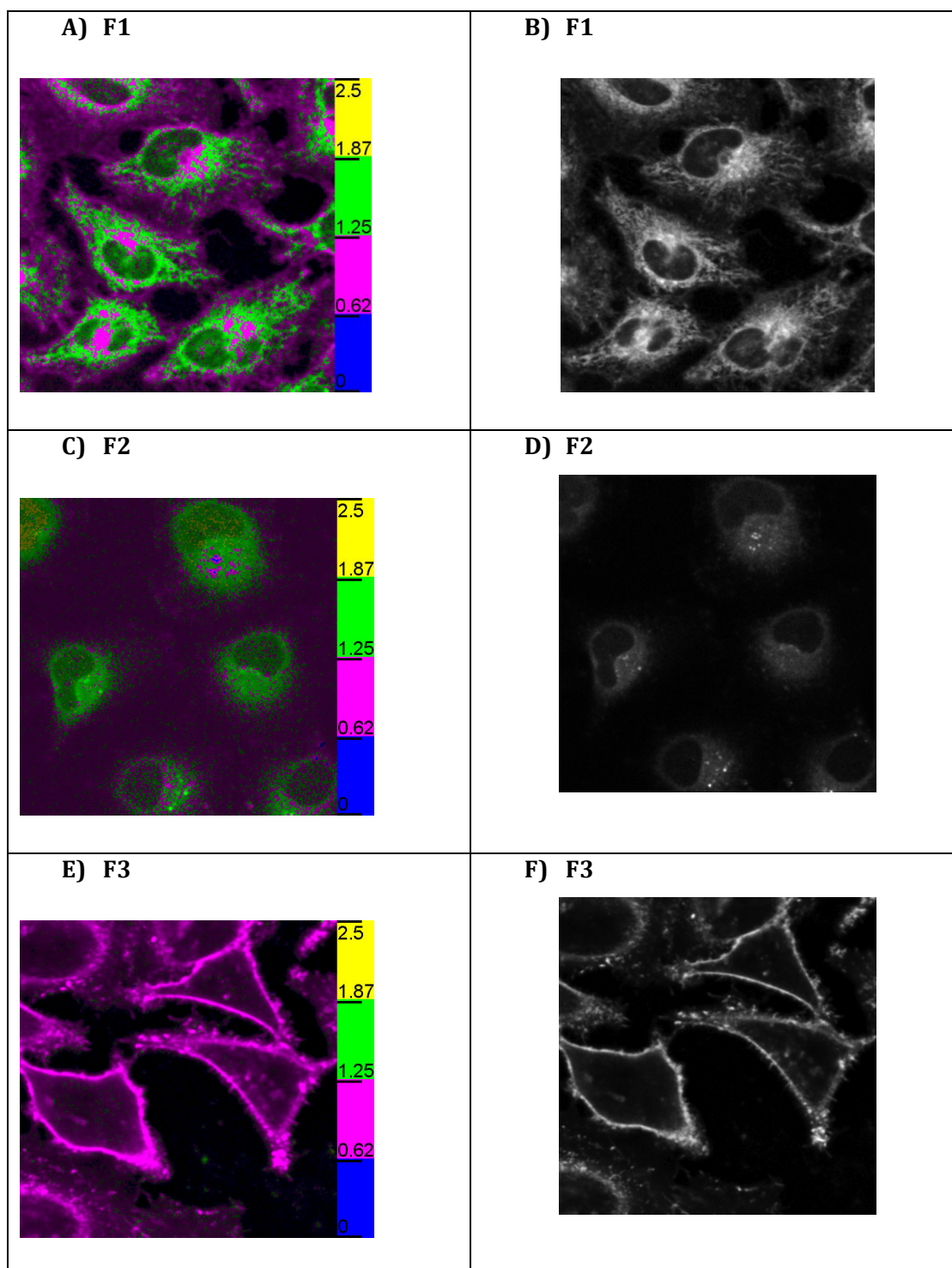


Figure 84. Confocal fluorescence image of HeLa cells stained with **F1**: A) and B); **F2**: C) and D); **F3**: E) and F). Concentration of **F1-F3** of 100 nM. Left column: ratiometric green/blue imaging, The ratios of intensities are displayed by using the color code given on the right scale. Right column: imaging obtained by collecting fluorescence intensity recorded for both channels.

The ratio images further suggest that the intracellular compartments stained in green represent membrane close to the liquid disordered phase as found in endoplasmic reticulum and other membrane-containing organelles (fig. 84A and 84C). The magenta color observed well for **F1** probe, which matches the liquid ordered phase, corresponds well to the cell plasma

membrane staining. The results are in line with those obtained recently with internalizing solvatochromic laurdan and pyrene probes.^[153,272,273] Altogether our results support the original design of **F3** to obtain the desired probe for staining the plasma membrane without internalization. On the other hand, **F1** can stain both cell plasma membranes and cytoplasm showing a clear contrast in their lipid organization.

V. Conclusion:

In conclusion, we have demonstrated the ability of the fluorene family to be a cornerstone of highly sensitive probes that can help in understanding the biophysical behavior of cell membranes by synthesizing three novel probes based on a new design. This work validated the versatility of the introduced ynone linker in biolabeling without compromising the appreciable spectroscopic properties of the core dye. In effect, **F3** dye surpasses the features of commonly used laurdan probe for instance. Some of the established improvements compared to laurdan are: red-shifted absorption that matches the 405 nm diode laser, higher brightness, decreasing the used concentration for such staining by ~10-15 folds, high photostability, comparably strong sensitivity to different liquid domains of cell membrane. Moreover, fluorene derivatives present high 2PA cross-section at common wavelengths around 800 nm, which makes them attractive in two-photon excitation microscopy. **F3** is the first plasma membrane-specific fluorene-based probe that can be a powerful tool for studying membranes.

Chapter Five

Fluorene-based DNA fluorescent markers; synthesis, DNA labeling, and applications

This chapter outlines the syntheses of four DNA fluorescent markers (**FM1-4**) comprising push-pull fluorene dyes and their site-specific incorporation into oligonucleotides (ODNs). Indeed, this work is a summary of different study designs that have been carried out in parallel to the previous chapters. Both classical and Pd catalytic routes have been used in establishing the four phosphoramidites that were employed in successive campaigns of solid-phase synthesis

of DNAs. Emphasis on synthetic details and degradation studies will be presented to explain the encountered difficulties and argue the compatibility of the alkyl chain of the amino group in DNA labeling by fluorene dyes. In conclusion, the efficient introduction of a stable fluorene amidite into 15-mer ODN sequences has been performed. Spectroscopic characterization (UV, fluorescence, thermal denaturation, CD) of the final labeled ODNs in different contexts of flanking and opposite natural bases will be discussed. The performance of the fluorene dye as a donor in radiative FRET pair application will be also enclosed as a preliminary application. Using Dy681 as the acceptor, the FRET has demonstrated a ratiometric turn-on in NIR region with one of the widest shift to-date ($\Delta\lambda = 300$ nm). This study will be completed in due-time.

I. Fluorene label by anucleoside approach

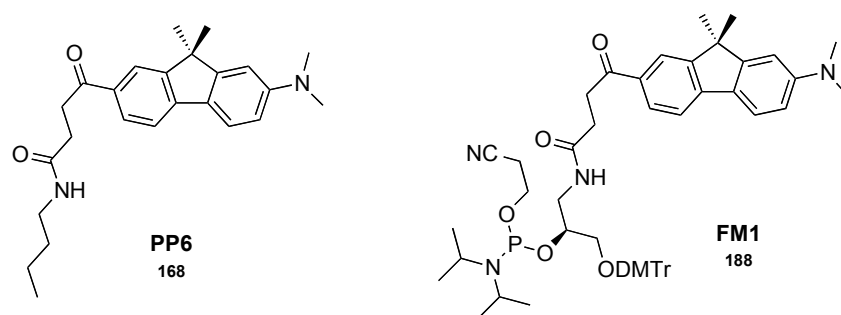


Figure 85. The first phosphoramidite **FM1** and its analogue **PP6**

Building on the aldehyde (A) extension into a succinyl linker and the optimized peptide coupling (**PP6**) discussed in chapter 3, our first approach to covalently-label oligonucleotides was to ligate the succinyl moiety of (**167**) to an anucleosidic moiety “(S)-3-aminopropane-1,2-diol” (**189**, fig. 85-86). This anucleoside linker was developed by the group of Antopolsky^[201] in 2001 but pervasively used by Wagenknecht group to synthesize artificial DNAs labeled with various fluorophores ever since.^[200,274-277] Their reports show insignificant effect of the “anucleoside” group on the duplex stability. Indeed, they have published a list of universal base analogues that supports the hypothesis of the loss of duplex stability mainly originating from removal of the base rather than sugar replacement by anucleosidic units.^[278] The “Antopolsky” linker is basically a 1,2-diol fragment with one primary hydroxyl for selective protection with 4,4'-dimethoxytrityl (DMTrCl) reagent and one secondary hydroxyl for phosphitylation. It comprises as well an amine to introduce the dye *via* a peptide coupling. Thus, this first choice was envisioned to evaluate the preliminary integrity of the push-pull fluorene in ODNs avoiding

the synthetic complexity of deoxyribose chemistry. Phosphoramidite **FM1** was our first target as **PP6** analogue (fig. 85).

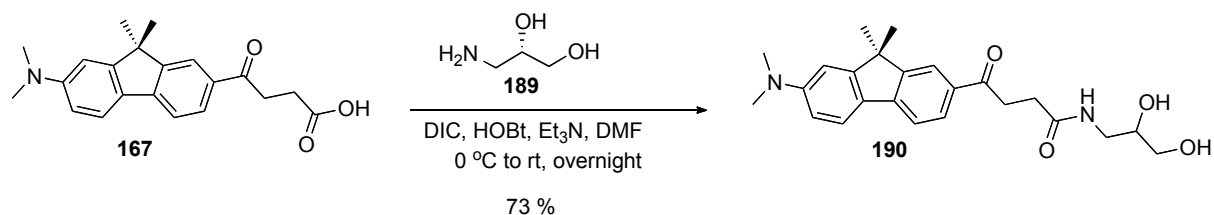


Figure 86. Synthesis of **190**

To study the photophysical properties of the fluorene-nucleoside derivative (**190**), we performed the peptide coupling of (**167**) and (**189**) using DIC and HOBT as activators (73 %, fig. 86). The emission solvatochromism of this adduct literally spanned the full range of 450-630 nm with increasing the polarity (fig. 87, SI-XV). The quantum yields were 10 % in water, 36 % and 42 % in methanol and ethanol respectively, and 51-82 % in all the tested aprotic solvents displayed.

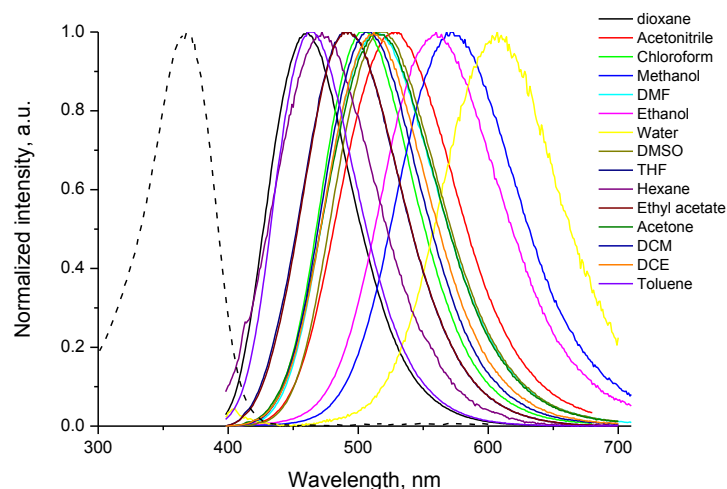


Figure 87. Solvatofluorochromism of **190**. Normalized representative absorbance (dotted line) and emission (solid line) spectra in different solvents

Its absorption showed the regular little solvatochromism and was in the UV-region (around 370 nm). These results are very close to that obtained for **PP6**. They indicate that substituting butylamine chain by aminopropane-1,2-diol linker has a marginal effect on the photophysical properties of the fluorene dye. As **PP6**, compound (**190**) shows appreciable quantum yield in water in line with the observation that fluorene dyes with lowest ICT character in excited states

demonstrate largest fluorescence efficiencies in water (chapter 3).

The large solvatofluorochromism of (**190**) and its emissive character in aqueous media were promising and overcoming the drawback of its UV absorption. So, we proceeded further into synthesizing its phosphoramidite **FM1**.

Protection of (**190**) with DMTr group proved to be very difficult. Different reaction conditions were tried (DMF, pyridine, ACN, DBU, Et₃N, rt, 60 °C, 130 °C) and none of them was successful. Therefore, we protected the primary OH of aminopropanediol (**189**) before the amide bond formation. The optimized synthesis of **FM1** is summarized in *fig. 88*.

The NH₂ group of (**189**) was protected using CF₃COOCH₃ (98 %). Next, the DMTr group was selectively introduced to the primary OH group after treatment with DMTrCl in anhydrous pyridine generating (**192**) in 78 % yield. The amino group was deprotected by methanolic ammonia solution (98 %).^[201] The product (**193**) was coupled afterwards to the succinyl linker of fluorene (**167**) giving the fluorene anucleosidic mimic (**194**) in 71 % yield. HBTU was more efficient in this peptide ligation than DIC-HOBT.^[245]

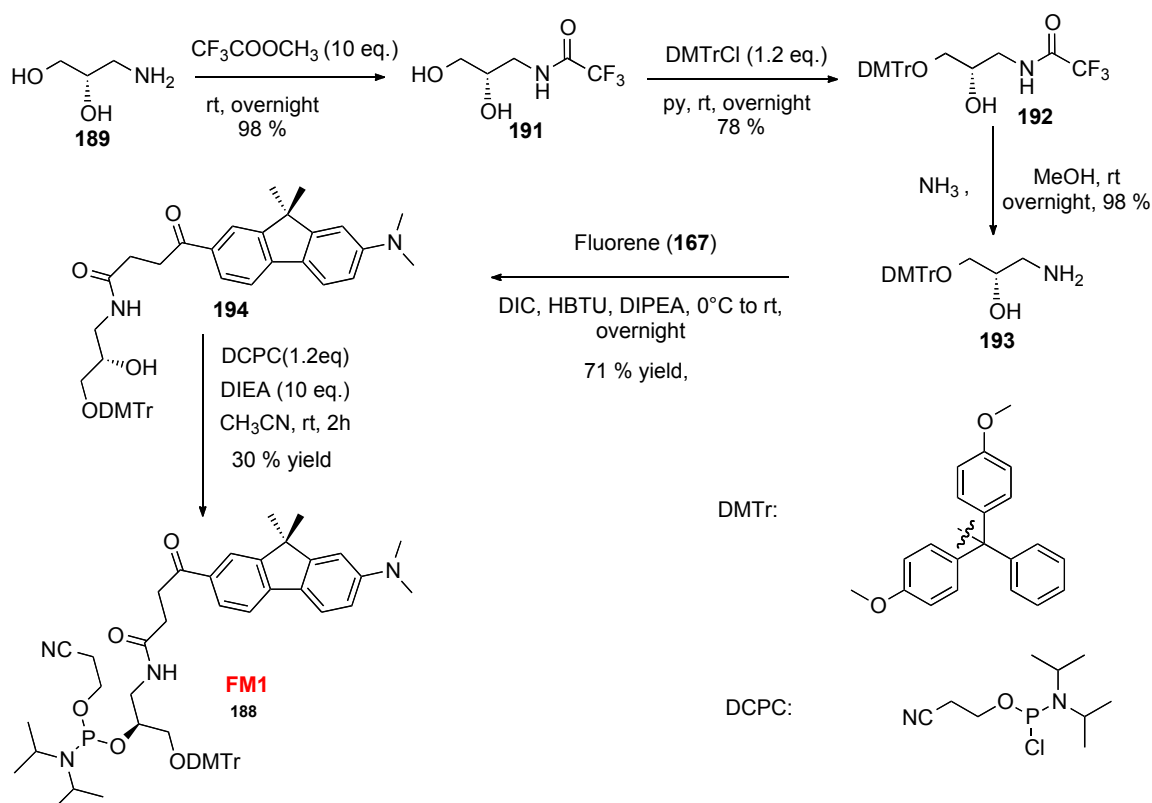


Figure 88. Synthesis of **FM1**

Product (**194**) was dried by coevaporation with benzene and subjected to nucleophilic substitution with 2-cyanoethyl-N,N-diisopropyl-chlorophosphoramidite (DCPC) in anhydrous

acetonitrile in the presence of Hünig's base (DIEA).^[173] Despite the cautions in handling this product, the conversion remained modest and the final product (**FM1**), which is quite sensitive to oxidation and to hydrolysis,^[172] was isolated in 30 % yield after very quick FC purification. **FM1** was obtained as a mixture of two diastereoisomers due to the introduction of a chiral phosphorus atom. The structure of the phosphoramidite was confirmed by ¹H and ³¹P NMR spectroscopy, and LCMS.

FM1 was freeze-dried from dry benzene solution and was processed into automated solid-phase DNA synthesis using standard protocol with minor modifications (SI-IV). To evaluate the stability of the dye under deprotection conditions, four 15-mer ODNs incorporated by this label (abbreviated as **M**) in the middle of each sequence were synthesized (table 8): **AMA** and **TMT** with “DMTr-on” mode, **GMG** and **CMC** with “DMTr-off” mode. The “on” mode signifies that the ODN contains the 5'-DMTr group after ODN synthesis completion on solid phase. The “off” mode means that DMTr is cleaved using the synthesizer by cycling Cl₃CCOOH on the solid support for few minutes. The coupling efficiency was monitored by the trityl profile and revealed to be low (30-60 %). This can be attributed to the chosen lengthy linker that might have interfered in the coupling step of the fluorophore to other natural nucleotides during the synthesis.

The ODNs were cleaved from the solid support using concentrated aqueous ammonia solution at rt for 2 h. The ammonia solution was left to stand overnight to deprotect the sequences. The volatiles were removed by lyophilization under vacuum. The **AMA** and **TMT** sequences were treated with 50% aqueous acetic acid for 1 hour. Then, the lipophilic DMTr component was extracted with ether. The four crude ODNs were purified by RP-HPLC controlled by UV absorbance monitoring on a photodiode array detector at two wavelengths: 255 and 370 nm, which approximately correspond to the absorption of the DNA natural nucleobases and fluorene, respectively (fig. 89).

The purified ODNs were characterized by Maldi TOF/TOF, UV-absorption, and fluorescence. Unfortunately, the mass of the ODNs showed either truncated sequences or a difference of 15 a.m.u. from the expected one (table 8). The 15 mass difference is compatible with the loss of a methyl group either from the amino substituent or fluorene at C-9 position.

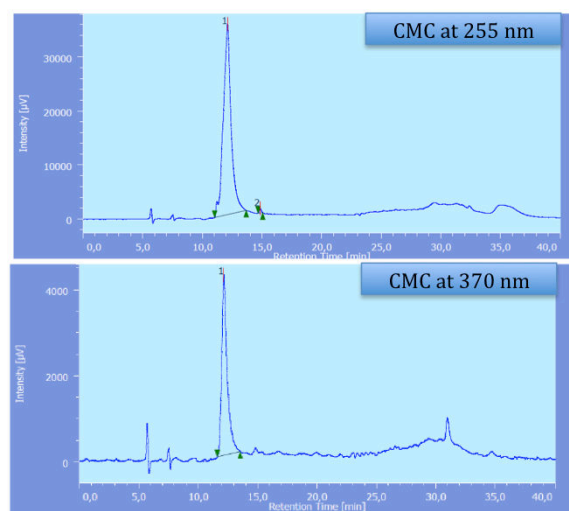


Figure 89. HPLC profile of CMC single strand ODN

Table 8. Theoretical and found masses of the synthesized ODNs

Abbreviation	Labeled sequence	Theoretical mass	Mass found
TMT	CGT TTT TMT TTT TGC	4689	4675
AMA	CGT TTT AMA TTT TGC	4707	2086.5 truncated sequence (CGTTTTA)
CMC	CGT TTT CMC TTT TGC	4659	4644
GMG	CGT TTT GMG TTT TGC	4739	4725

Despite the mass defect, we will discuss the spectroscopic data of the first batch of ODN labeling for the significant differences from the other labeling strategies that we used later (*vide infra*).

Table 9. Spectroscopic data of the **M**-labeled ODNs

Samples ^[a]	λ_{abs} (nm)	λ_{em} (nm)	$\Delta\lambda_{\text{ss}}$ (nm)	Φ (%) ^[b]	pH
TMT	350	512	162	10	7
CMC	350	519	169	12	7
AMA	350	509	159	16	7
GMG	350	497	147	28	7

[a] 1 μM of ODN in buffer pH 7.0 (10 mM cacodylate, 150 mM NaCl); [b] Quantum yields determined using quinine sulfate in 0.1 M HCl solution ($\lambda_{\text{ex}} = 350$ nm, $\Phi = 0.54$)^[246] and 7-(dimethylamino)-9,9-dimethyl-9H-fluorene-2-carbaldehyde ($\lambda_{\text{ex}} = 390$ nm, $\Phi = 0.46$)^[85] as references, $\pm 2\%$ mean standard deviation.

The absorption and emission spectra of the ODNs (table 9, fig. 90) are consistent with the incorporation of the fluorene label into them. The absorption maximum was about 20 nm blue shifted in ODNs in comparison to the value of the free dye **190** (350 vs. 370 nm). This further suggests the donating ability of the amine was decreased supporting the hypothesis that the mass defect is originating from the loss of the methyl from the amine moiety and not from the C-9 position. The alkyl substituents at C-9 position are demonstrated to have minor effect on spectroscopic properties as compared to that of donor groups in push-pull molecules.^[52]

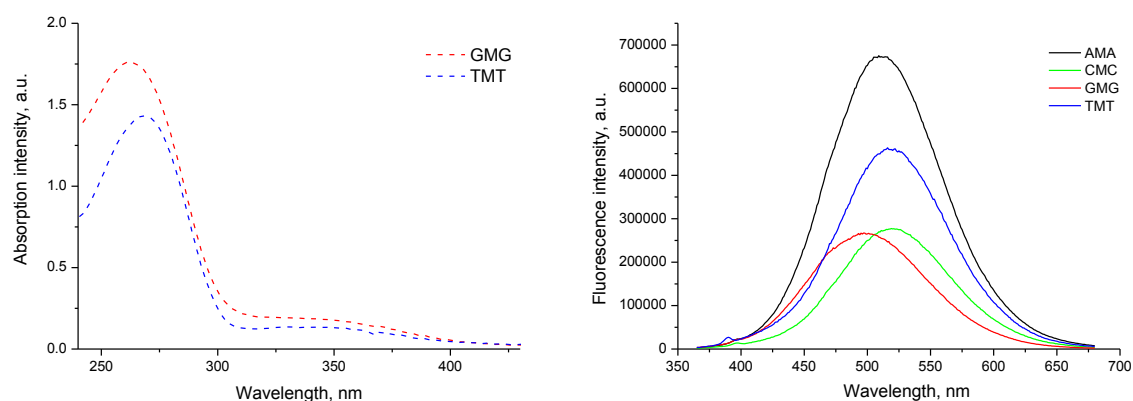


Figure 90. Absorption and emission spectra of the labeled ODNs. Excitation wavelength used was the corresponding absorption maximum.

Given the unexpected mass, the low efficiency of the fluorophore incorporation into ODNs, and the difficulties in the convergent 10-step synthesis of the **FM1**, we have decided to change the strategy of the labeling to track the chemical group that is not compatible with solid-phase synthesis and that is fragmenting in the process.

II. Fluorene label connected to deoxyribose sugar

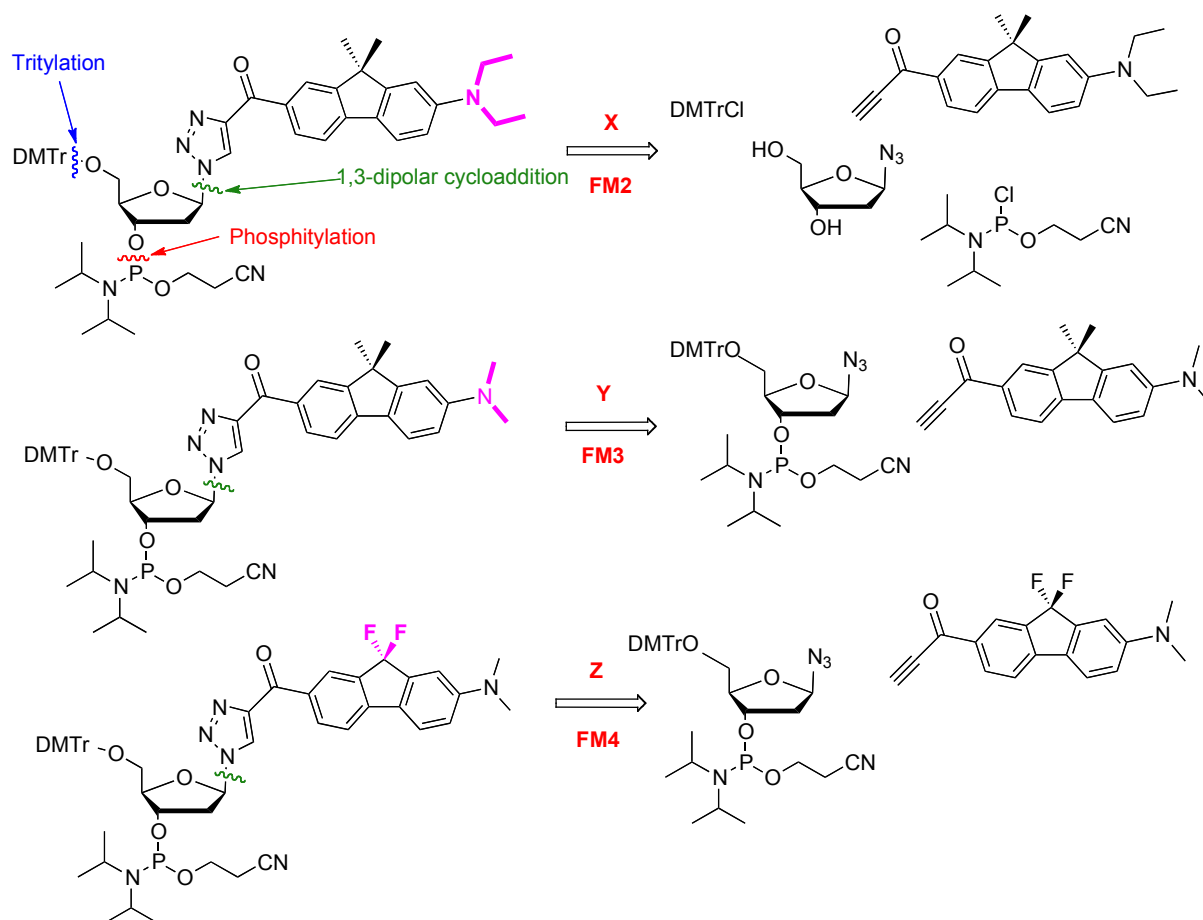


Figure 91. Retrosynthetic plan of **FM2-4**

Accordingly, the fluorene dye still replaces the natural base but is connected to a deoxyribose moiety instead of the nucleoside linker. The retrosynthesis was based on “click-chemistry” similar to that of the membrane probes (chapter 4). Three fluorene-labeled phosphoramidites (**FM2-4**) were planned with controlled variation of the fluorene precursor changing the diethyl amine of **FM2** to dimethyl amine in **FM3** and the dimethyl substituents of the C-9 position into difluoro atoms in **FM4** (fig. 91).

II.1 Synthesis of **FM2-4**

FM2 was prepared by 7-step convergent synthesis starting from 2,7-dibromo-9,9-dimethylfluorene (**44**), (fig. 92). Selective C-N coupling on (**44**) installed the diethyl amine as the donor (57 %), after which metal-halogen exchange reaction with *n*-BuLi in DMF introduced the formyl (A) group resulting in the push-pull dye (**195**, 60 %). Grignard addition followed by oxidation gave the clickable synthon (**196**, 55 %). The optimized CuAAC conditions (chapter 3) with the 3,5-*p*-ditoyl-2-deoxyribosyl azide established the clicked fluorene-sugar product,

which was deprotected by treatment with methanolic potassium carbonate solution yielding the artificial fluorene nucleoside (**197**) in good 61 % two-step yield. The primary OH of the deoxyribose was protected by DMTr and its secondary OH was phosphitylated achieving the second phosphoramidite **FM2** (57 % yield in two steps). The synthesis was shorter and more facile than the synthetic route of **FM1**. It should be mentioned that the same precautions of air and humidity should be strictly abided by and that the DMTr protection step suffered from reproducibility in my work.

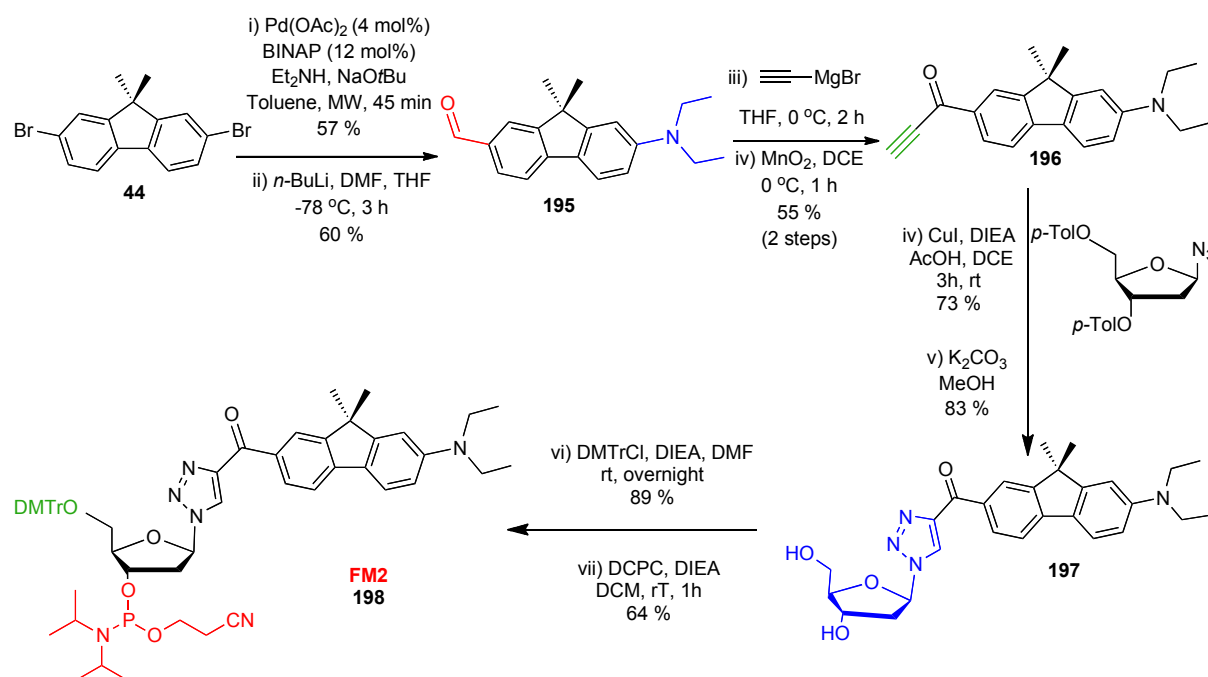


Figure 92. Synthesis of **FM2**

FM3 was prepared from the clickable adduct (**163**, chapter 3) and following the same consecutive steps (iv-viii, 24 % yield over 4 steps) used in the synthesis of phosphoramidite (**FM2**), (fig. 93). The full synthetic route is described in the experimental part (SI-XII).

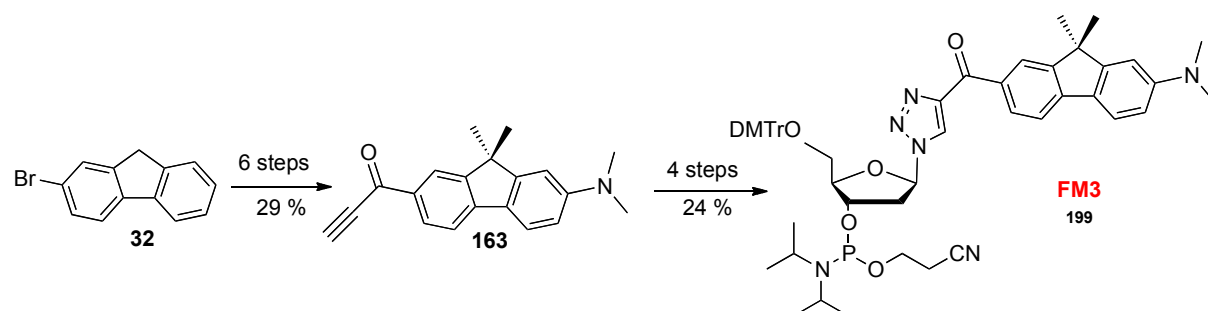


Figure 93. Synthesis of **FM3**

Next, the synthesis of **FM4** was carried out. The electrophilic and nucleophilic fluorinating reagents used for the optimization are shown in the *SI-XII section*.^[279] Briefly, electrophilic fluorination on the benzylic position of (**32**) did not work in our hands. (**32**) was transformed into fluorenone (**200**) by oxidation, Nucleophilic fluorination procedures were attempted producing inseparable mixture of mono and difluorinated fluorene in low yields. Fluorenone (**200**) was protected and fluorination using Olah's reagent (pyridinium poly(hydrogen fluoride)) was the best condition achieving nucleophilic substitutions by two fluoride ions and resulting in the desired 2-bromo-9,9-difluorofluorene (**202**) in 87 % yield over three steps without the need of any purification (fig. 94). The conversion of (**202**) into its corresponding phosphoramidite **FM4** was done by the same used protocols (SI-XII) in the convergent synthesis of **FM2-3** (5 % yield over 10 steps).

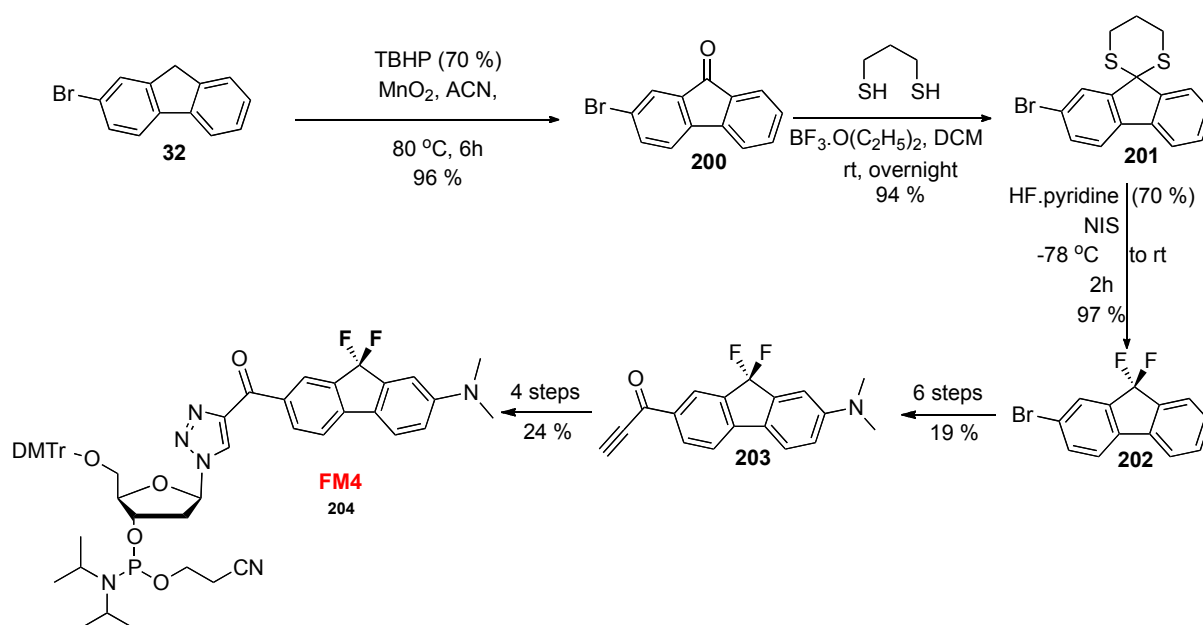


Figure 94. Synthesis of **FM4**

NMR and HRMS were employed to characterize the diastereomers of each phosphoramidite before administering the ODN synthesis (SI). The results were indisputable; degradation was not taking place under the conventional inert and anhydrous conditions before the solid-phase synthesis. Different DNA oligomers labeled with the **X**, **Y**, and **Z** fluorene dyes were synthesized using respectively **FM2**, **FM3** and **FM4** and the “DMTr-off” mode. The coupling profiles on the synthesizer were generally better than those of the nucleosidic moiety **FM1**. In some cases, the coupling of the artificial base attained 90 % value. Selected sequences were treated and purified (fig. 95 and SI) with the same procedures described before and characterized by Maldi TOF/TOF (table 10).

Table 10. Theoretical and found masses of selected ODN sequences

Abbreviation	Labeled sequence	Theoretical mass	Mass found
TXT	CGTTTTT X TTTTTGC	4755	4756 [M+H] ⁺
CXC	CGTTTT CX CTTTTGC	4722.9	4755.5 [M+Na] ⁺
GXG	GCAAAAG X GAAAACG	4878	4880 [M+H] ⁺
AYA	GCAAAA AY AAAAACG	4823	4806
TYT	CGTTTTT Y TTTTTGC	4735	4715-4718
TZT	CGTTTTT Z TTTTTGC	4727.2	4713

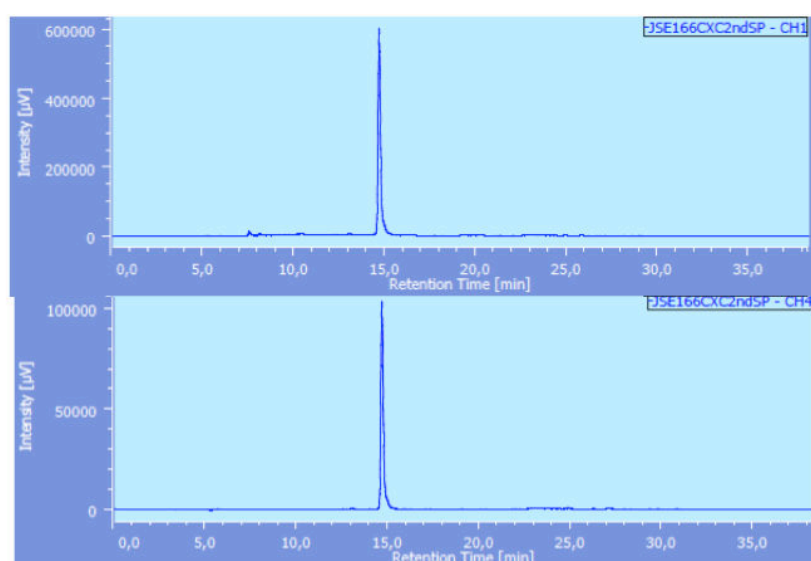


Figure 95. HPLC profile of CXC single strand ODN (255 nm up – 390 nm down) as an example of purity

FM2 bearing diethyl amine and dimethyl C-9 substituents was the only compatible phosphoramidite to solid-phase ODN synthesis. **CXC**, **TXT**, and **GXG** sequences solely had the correct mass without loss of fragments (table 10). They were subsequently used in steady-state fluorescence measurements in the rest of our work.

The other two phosphoramidites (**Y** and **Z**) gave labeled ODNs with mass lower than anticipated. Demethylation of the amine can possibly explain the cleavage of a fragment that corresponds to 14-18 a.m.u., since demethylation of the C-9 substituent can now be excluded by the stability of **FM2** holding the same chemical groups. Tertiary amine oxidation is well documented.^[280] In line with the proposed mechanism, the cleavage starts through a radical process that involves the departure of a proton from the alkyl substituent followed by single electron transfer (SET). It is known, in particular, that the departure of a methyl proton, which is

more acidic, is kinetically favored compared to the one of an ethyl chain. The cleavage could be favored by the oxidation step of the solid-phase synthesis. To get further insight on the sensitivity of fluorenes **Y** and **Z** to oxidation and conditions of ODN synthesis, the integrity of the naked nucleosides (not incorporated in ODN) was verified under the same conditions of the synthesizer (iodine, acids, etc..) using HPLC, LCMS, NMR, and MALDI. The nucleosides were relatively stable and none of the experiments showed a degradation pattern. Thus, the preferential cleavage of the amine methyl group may be facilitated when attached to the ODN.

III. Characterization of the free fluorescent marker (**X**) and the **X**-labeled ODN sequences

III.1 Spectroscopic properties of the naked fluorescent nucleoside (**197**)

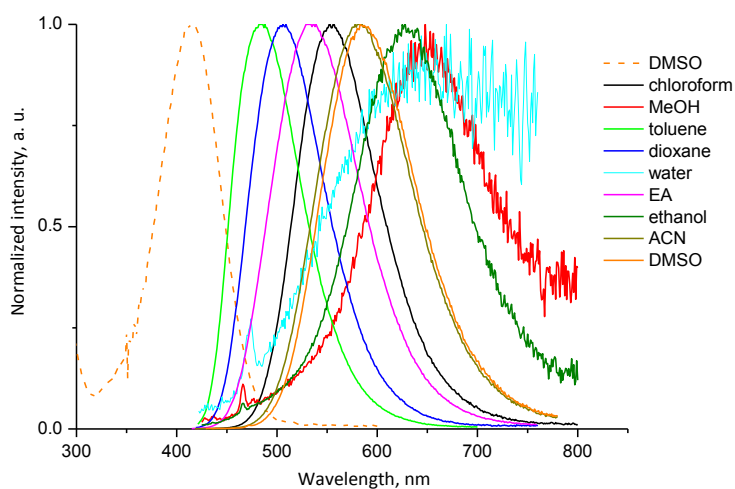


Figure 96. Solvatofluorochromism of **197**. Normalized representative absorbance (dotted line) and emission (solid line) spectra in different solvents. Excitation wavelength used was the corresponding absorption maximum.

The absorption and fluorescence spectra of the diethylamino fluorene nucleoside (**197**) were recorded in a set of solvents to be compared to compound (**190**) and to the dimethylamine donor in (**F1**), (discussed in chapter 4). Dye (**197**) has similar spectroscopic features to those of (**F1**). The major difference imposed by the diethyl amine was the slight red-shift in absorption by 6-20 nm to the visible region (>400 nm) in different solvents in line with an increased

inductive effect. The emissions of the two dyes appeared comparable in their maxima with a marginal enhancement in fluorescence efficiency by diethyl amine (table 11, fig. 96).

Table 11. Spectroscopic properties of **197**

Solvent	ϵ_{\max} [a]	$32.10^3 \text{ M}^{-1}.\text{cm}^{-1}$			
Water	λ_{Abs} (nm)	415	DMSO	λ_{Abs} (nm)	412
	λ_{Em} (nm)	-		λ_{Em} (nm)	583
	$\Delta\lambda_{\text{SS}}^{\text{[b]}}$ (nm)	-		$\Delta\lambda_{\text{SS}}$ (nm)	171
	Φ (%)	-		Φ (%)	83
Methanol	λ_{Abs} (nm)	413	Ethyl acetate	λ_{Abs} (nm)	400
	λ_{Em} (nm)	648		λ_{Em} (nm)	539
	$\Delta\lambda_{\text{SS}}$ (nm)	235		$\Delta\lambda_{\text{SS}}$ (nm)	139
	$\Phi^{\text{[c]}}$ (%)	2		Φ (%)	82
Ethanol	λ_{Abs} (nm)	409	Dioxane	λ_{Abs} (nm)	405
	λ_{Em} (nm)	628		λ_{Em} (nm)	506
	$\Delta\lambda_{\text{SS}}$ (nm)	219		$\Delta\lambda_{\text{SS}}$ (nm)	101
	Φ (%)	8		Φ (%)	64
Acetonitrile	λ_{Abs} (nm)	404	Toluene	λ_{Abs} (nm)	408
	λ_{Em} (nm)	585		λ_{Em} (nm)	488
	$\Delta\lambda_{\text{SS}}$ (nm)	181		$\Delta\lambda_{\text{SS}}$ (nm)	80
	Φ (%)	75		Φ (%)	90
Chloroform	λ_{Abs} (nm)	415			
	λ_{Em} (nm)	557			
	$\Delta\lambda_{\text{SS}}$ (nm)	142			
	Φ (%)	79			

[a] Same as table 3.

Polar protic solvents quenched fluorescence like in **F1** case. The quantum yields of (**197**) were 2 % in methanol and 8 % in ethanol. In these polar protic solvents, the dye exhibited dramatic red shifts to the NIR region.

Increasing the percentage of methanol to dye (**197**) dissolved in dioxane solvent shifted the position of the emission band to the red and resulted in increased quenching of the fluorescence (fig. 97).

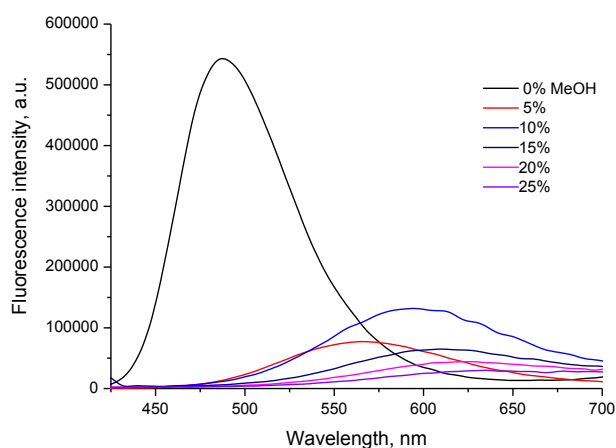


Figure 97. Fluorescence of **191** in dioxane-methanol mixtures

Comparing (**197**) to the nucleosidic dye used in **FM1** marker (section I), this labeled nucleoside was red-shifted in both its absorption and emission (fig. 87 vs. 96). This dye demonstrated high solvatofluorochromism in wide range (488-648 nm) with mega-Stokes shifts (from 80 nm in toluene to 235 nm in methanol).

III.2 pKa determination of (**197**)

The pH dependence of absorption was studied for the naked dye (**197**) to calculate its pKa (fig. 98A). Under acidic conditions (pH = 2), the amine is protonated resulting in absorption maximum of 320 nm. As pH increases, the percentage of the neutral form of (**197**) increases translated in the appearance of a second band at 415 nm. The absorption maximum related to the protonated form completely disappears after pH = 7.

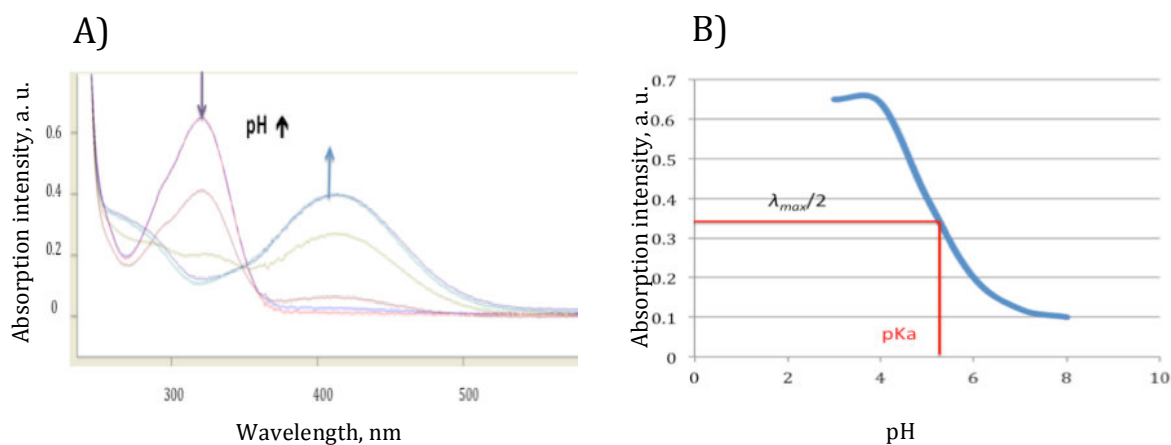


Figure 98. pH dependence of absorption of dye **197**

pKa of the dye can be extracted at $\lambda_{\max}/2$ of the plot of absorption intensity as a function of pH. The experimental pKa of the naked nucleoside was around 5.4 (fig. 98B).

III.3 Photophysical characterization of the X-labeled ODNs

The UV and fluorescence of the synthesized ODNs in their single- and double-stranded forms were recorded in cacodylate buffers. The spectroscopic properties in addition to the melting temperatures of the duplexes are summarized in *table 12*.

Considering the ss-ODNs, **TXT** and **CXC** revealed to be completely non emissive in buffer of pH 7 contrary to **GXG** sequences (fig. 99). When T or C but not G flanked **X**, their absorption maxima were blue-shifted (~ 330 nm) inferring that the flanking bases and the poly-anionic charge DNA had an additional effect on the pKa of the fluorene nucleoside. Each sequence has supposedly a distinct pKa different from the naked nucleoside and from the fluorene in other sequences. Indeed, calculations and experimental studies suggest the presence of regions of increased proton density around DNA that can reach 2 orders of magnitude greater than that of bulk solvent.^[281] Accordingly, rising the pH should return the label to its emissive non-protonated form that absorbs at ~ 425 nm (fig. 99). We have determined the pH at which each sequence fluoresced the maximum. **CXC** and **TXT** were characterized in cacodylate buffer of pH = 8.4, whereas **GXG** was not protonated and still emissive at pH = 7 suitable for studies at physiological pH.

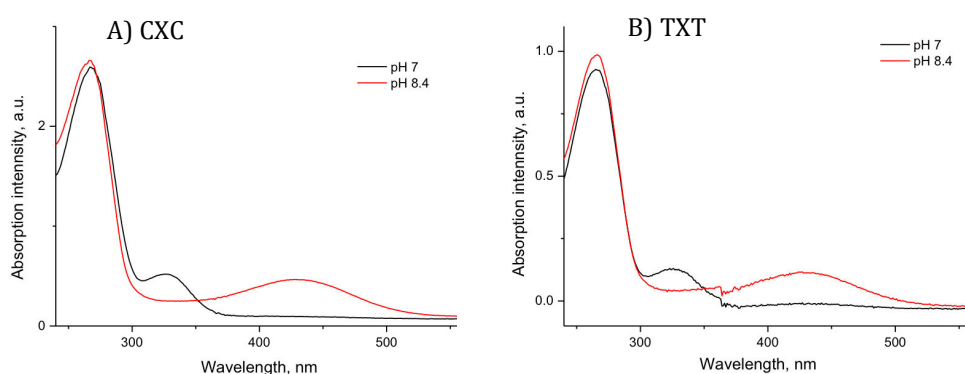


Figure 99. pH dependence of **CXC** and **TXT** in buffer (10 mM cacodylate, 150 mM NaCl)

The three labeled sequences were poorly emissive (2-6 %) with absorption in the visible range of 435-445 nm and emission in the red region of 660-675 nm (table 12). Compared to the free dye **191**, the **X** label exhibits red shifted absorption (20-35 nm). Such shifts are classically

observed for intercalated dyes.^[200,282] The emission spectra fit those observed for the free dye in 20-25% methanol in dioxane.

Table 12. Spectroscopic data of the **X**-labeled ODNs

Samples ^[a]	T _m (°C) ^[b]	ΔT _m (°C) ^[c]	λ _{abs} (nm) ^[d]	λ _{em} (nm)	Δλ _{SS} (nm)	Φ (%) ^[e]	pH
TXT	0	-	435	660	225	5	8.4
TXT·AAA	37	-10	440	655	215	4	8.4
TXT·ATA	39	-8	445	650	205	3	8.4
TXT·AAbA	41	-6	445	665	220	5	8.4
CXC	-	-	440	650	210	6	8.4
CXC·GAG	42	-11	445	660	215	4	8.4
CXC·GTG	41	-12	445	650	205	5	8.4
CXC·GAbG	45	-8	445	650	205	5	8.4
GXG	-	-	445	675	230	2	7
GXG·CAC	42	-11	440	675	235	2	7
GXG·CCC	48	-5	450	640	190	11	7
GXG·CGC	46	-7	440	650	210	4	7
GXG·CTC	46	-7	450	640	190	6	7
GXG·CXC	46	-7	445	650	205	2	7
GXG·CAbC	45	-8	440	675	235	2	7

[a] 1 μM of ODN in buffer pH 7.0 for **GXG** and 8.4 for **TXT** and **CXC** (10 mM cacodylate, 150 mM NaCl); [b] Melting temperature; ±0.5°C; [c] ΔT_m corresponds to the difference in T_m with the wild type duplexes **TAT·ATA**, **CAC·GTG** and **GAG·CTC**; [d] Absorption wavelength reflects the ones recorded by excitation spectra (for higher sensitivity at 1 μM) [e] Quantum yields determined using quinine sulfate in 0.1 M HCl solution (λ_{ex} = 350 nm, F = 0.54)^[246] and 7-(dimethylamino)-9,9-dimethyl-9H-fluorene-2-carbaldehyde (λ_{ex} = 390 nm, Φ = 0.46)^[85] as references, ±2 % mean standard deviation.

It is also important to compare these **X** properties to the anucleosidic **M**-labeled sequences of the first approach despite their mass defects (table 9 vs. 12). The **M**-labeled sequences absorbed in the UV range (350 nm) and fluoresced in the green region (530-550 nm). Their fluorescence intensities were much higher (10-28 % for **M** labeled ODNs). This suggests that the flanking bases were able to impose a more significant hydrophobic environment around the fluorene anucleosidic label. This might be favored due to the more flexible nature of anucleosidic linkers.

We then studied the hybridization effects. The **GXG** 15-mer sequence was hybridized with 6 complementary strands comprising in the position opposite to fluorene dye **X**: one of the canonical bases at a time, another **X** dye, or an abasic site (table 12). The **CXC** and **TXT** 15-mers were hybridized with three complementary strands including opposite to the fluorene: A or T bases as representatives of purines and pyrimidines, or an abasic site.

When complementary strands were added to **TXT** and **CXC**, the emissions were little changed (fig. 100, table 12). The quantum yields of the **TXT** and **CXC** ds-DNAs were nearly the same as

the ss-DNA regardless of the base opposite to the fluorene (purine, pyrimidine, or abasic site). The wavelenghtes of the emission were marginally varied (+/- 10 nm).

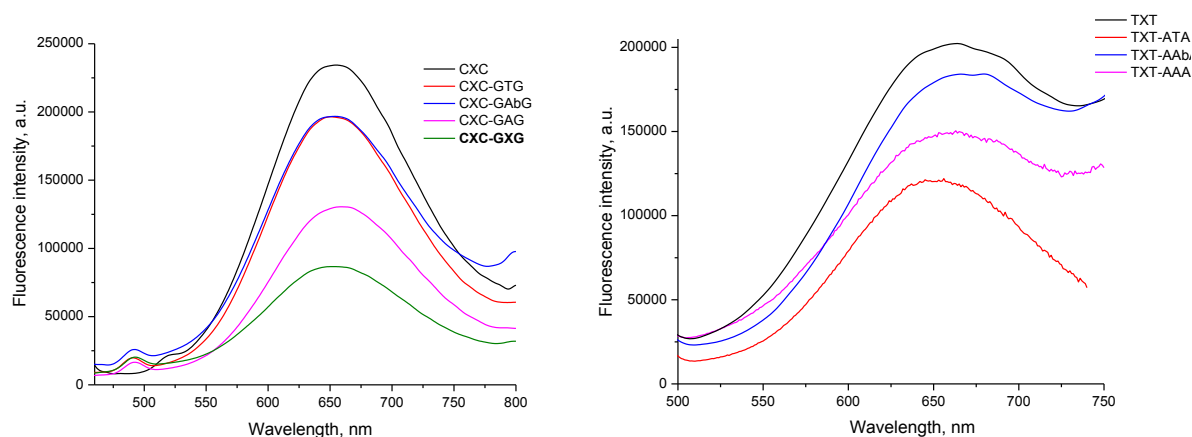


Figure 100. Fluorescence of ss and ds **CXC** and **TXT** sequences. Excitation wavelength used was 440 nm.

The characterization of the single-strand and hybridized **GXG** oligomer at pH=7 was different. First the ss-**GXG** was barely emissive (2 %) with more significant red shifts by 10 nm in absorption and 25 nm in emission compared to **TXT** and **CXC** (fig. 101 and table 12). To my supreme delight, the dye **GXG** composition was efficient in base-discriminating the opposite thymidine and cytidine in the duplexes. The fluorescence intensity of the duplex DNA was increased by 6 folds ($\Phi = 11\%$) with a pronounced blue shift in emission from 675 nm in ss-GXG to 640 nm when complemented with **CCC** sequence. The **CTC** hybridization resulted in the same shift in emission and 3-fold enhancement in quantum yield (6 %). These characteristics validate that the fluorene design can be useful in detection of target genes and single nucleotide polymorphism (SNP) typing.^[182]

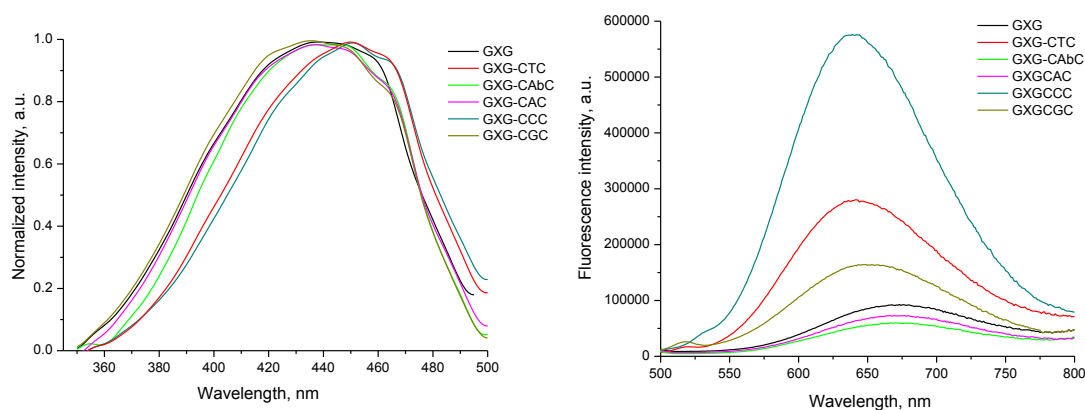


Figure 101. Excitation and emission spectra of **GXG** investigations. Excitation wavelength used was 440 nm.

To conclude, the red emission and the modest fluorescence efficiencies entail that neither the flanking bases in ss DNA nor the different types of hybridization in dsDNA were able to impose a significant hydrophobic environment and that the fluorene nucleoside is likely exposed to hydrophilic media in all cases. However, the change in the fluorescence wavelength and intensity demonstrated a valuable sensitivity of our fluorene dye with high ICT character in particular environment of DNA (e.g. **GXG**). ICT dyes are usually limited on this detection in hydrophilic media. Therefore, the brightness of this fluorene dye is satisfactory relative to its small size and high ICT character. Furthermore, the **GXG** sequence offered an easy-detectable change in its emission maximum (> 30 nm) in response to structural changes in DNA. Detection using probe **X** depends on a change of the fluorescence signal rather than on the thermal stability of duplexes. In this sense, probe **X** can be compared to the few BDF probes developed by Saito and co-workers for genotyping of SNP.^[179,203]

III.4 CD and thermal denaturation studies

The driving forces of double helix formation between complementary strands are the hydrophobicity of the nucleobases, the base-stacking and the complementary hydrogen bonding.^[170] Hence, it is important to study the stability of the duplex once an artificial derivative is introduced as a nucleobase surrogate. For that reason, the fluorene conjugate was located in the middle of the sequences to avoid any structural perturbation of the duplex due to end effects. We assessed the influence of the fluorene label on the secondary structure of the duplexes by monitoring the temperature-induced absorbance changes at 260 nm and recording the circular dichroism (CD) spectra (SI-XV).

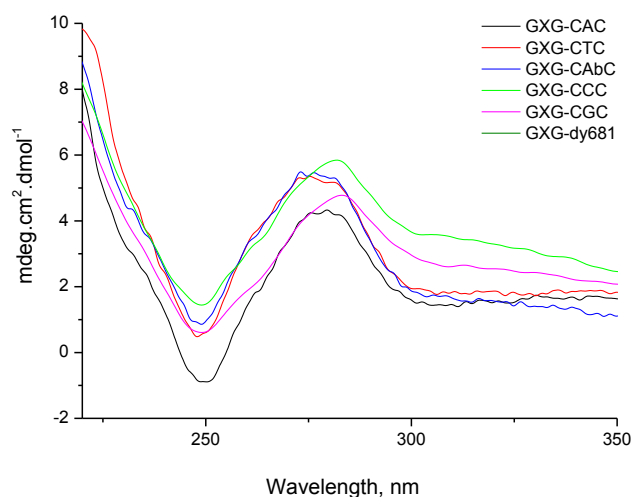


Figure 102. CD results of **GXG** investigations

As a representative example, the CD experiments of **GXG** hybridization are shown in *fig. 102*. All the tested hybridized DNAs demonstrated the same conformational signature with negative and positive peaks at around 250 and 280 nm respectively, consistent with a B-type helix.

The thermodynamic stability of the ds-DNA was evaluated using the DNA melting temperature (T_m). T_m is defined as *the temperature at which half of the DNA strands are in the double-helical state and half are in the random coil states*. A larger T_m value infers a higher thermodynamic stability of the duplex.^[283] Absorbance of the ds-DNA sample at 260 nm was recorded as a function of temperature. The melting curves were converted into a plot of α versus temperature, where α represents the fraction of single-strands in the duplex state (SI-XV). The melting temperatures were extracted from these curves using the mathematical analysis described in literature.^[283] The representative curves of **GXG** duplexes are depicted in *fig. 103*. Thermal denaturation studies showed that the hydrophobic fluorene impose some destabilization to the duplexes compare to the corresponding wild type duplex (table 1, $\Delta T_m = -12$ to -5°C), but they duplexes were stable below 30°C (*fig. 103*).

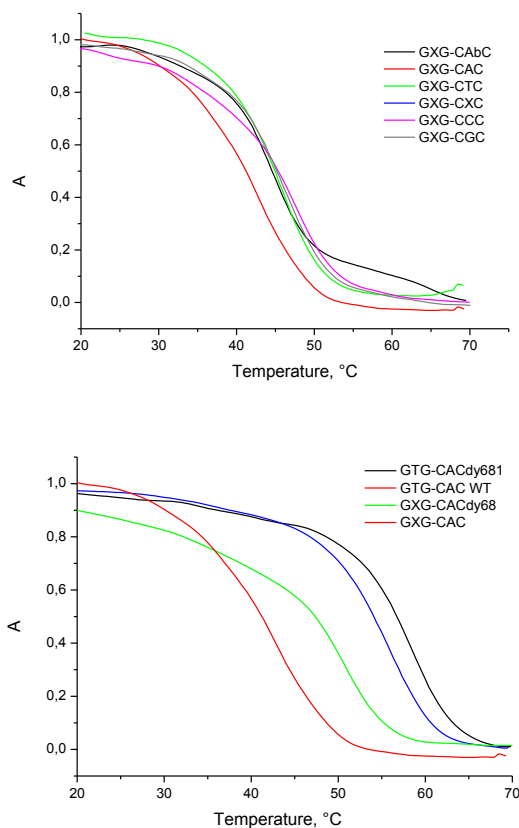


Figure 103. Melting temperature curves of **GXG** duplexes (up), **GXG-FRET** duplexes and control experiments (down)

Taken together, CD and thermal denaturation experiments show that the fluorene nucleoside can substitute a natural base opposite in DNA opposite a natural base or an abasic site giving duplexes of B-conformation that are stable to conduct all the spectroscopic studies at 25°C.

III.5 FRET

Many features predict that the push-pull fluorene can meet the requirements of an emissive donor in a radiative Förster Resonance Energy Transfer (FRET) pair with an acceptor dye; compatible absorption with readily available violet laser (405 nm), important extinction coefficient ($3.2 \times 10^4 \text{ M}^{-1}\cdot\text{cm}^{-1}$) relative to its small size, most probable rigid conformation allowing the possibility to control the orientation of the emissive dipole and its distance from the acceptor.^[1]

In that aspect, the obtained B-conformation of the DNA helix offers an exclusive architecture for this application. The mega-Stokes shifts can be employed to excite acceptors in the red or near-IR such as Dy681 and Dy781 (structures and main properties in the SI). We hypothesize that using the label **X** as the donor might build a turn on FRET pair where it can act as the light collector and interact with an acceptor as the emitter. FRET should operate at the condition the

FRET rate (k_T) is superior to the non-radiative rate (k_{nr}) of the donor (fig. 104). Important to note, the FRET rate is dependent to the distance separating the donor and the acceptor and thus should be controlled and tuned using the DNA architecture.

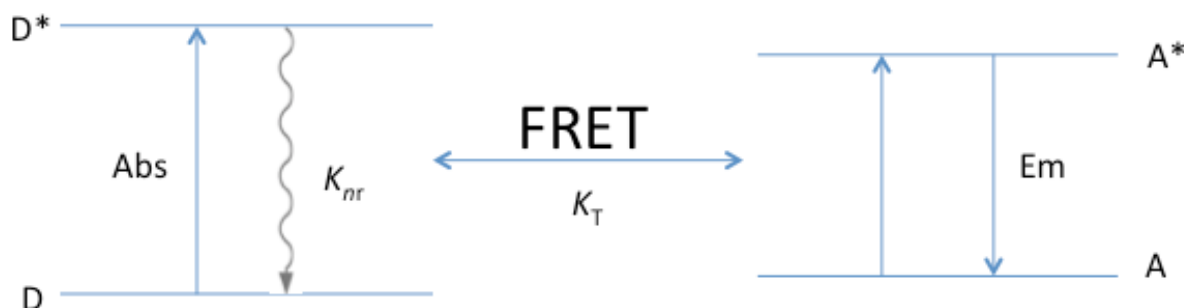


Figure 104. Simplified energy diagram explaining the turn on FRET between the donor **X** and the acceptor *Dy681*. Turn off: in the absence of the acceptor, the k_{nr} of the donor rate is dominating the deactivation process. Turn on: In the presence of the acceptor FRET is dominating ($k_T > k_{nr}$).

Such a preliminary design of FRET pair is to the best of our knowledge original. It should greatly improve the signal-to-noise ratio in fluorescence detection and imaging, obviates the self-quenching and light scattering, and overcome the drawback of single labeling with mega-Stokes shift dyes that is usually accompanied by poor quantum yields in aqueous media.

Upon formation of the duplex between **GXG** and the complementary sequence labeled by *Dy681*, an efficient energy transfer was realized with emission maximum at 725 nm. The achieved shift of 300 nm is not reported to-date in literature. We are conducting more studies in the lab to confirm this principle.

As the *Dy681* concentration was gradually increased, an increase of the emission band was displayed resulting from the inherent duplex formation (fig. 105). Saturation was reached upon adding more than 1eq. (100 % fig. 104) of *Dy681*. Comparing the addition of 1 eq. *Dy681* to **GTG** and **GXG** clearly demonstrate the efficiency of the FRET. In the absence of the donor, the reduced emission of *Dy681* in the single and double stranded forms is due to the fact that *Dy681* also absorbs at excitation wavelength (about 400nm) albeit less efficiently than the donor **X** (fig. 106).

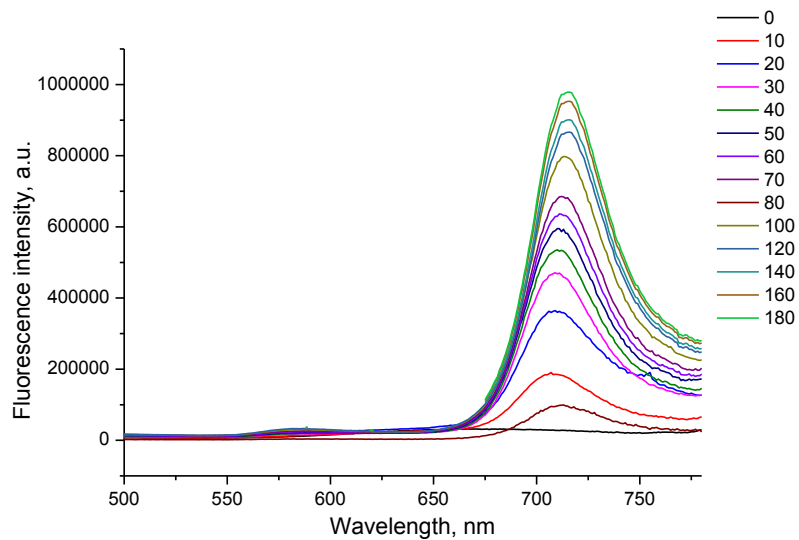


Figure 105. Fluorescence titration of **GXG** with Dy681 ($\lambda_{exc} = 420$ nm)

Comparing the addition of 1 eq. Dy681 to **GTG** and **GXG** clearly demonstrates the efficiency of the FRET. In the absence of the donor, the reduced emission of Dy681 in the single and double stranded forms is due to the fact that Dy681 also absorbs at excitation wavelength (about 425 nm) albeit less efficiently than the donor **X** (fig. 106).

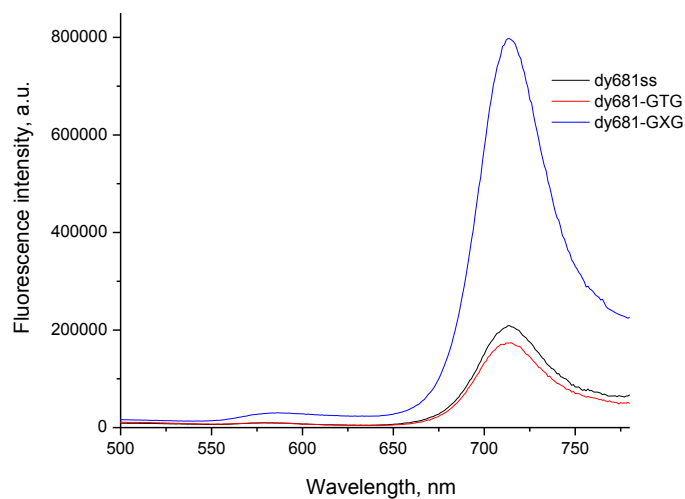


Figure 106. Control experiments for energy transfer ($\lambda_{exc} = 420$ nm)

IV. Conclusion

We established the framework of preparation of fluorescent nucleoside analogue **FM4** incorporating a 2,7-push-pull fluorene as a nucleobase surrogate. Detailed spectroscopic studies evidenced a high sensitivity to protic media through a dramatic Stokes shift. That observation augured interesting prospects for nucleic acid labeling. The nature of the alkyl chain on the amino group revealed to be crucial for the integrity of the fluorophore once incorporated in ODNs. Labeled sequences exhibited a far-red emission but modest quantum yields considering their large charge transfer. In duplexes of different compositions, the dye revealed to efficiently base-discriminate opposite cytidine and thymidine. Once incorporated in DNA, the full separation of the absorption and emission led us to analyze this dye as a mega-Stokes shift donor in an emissive FRET pair combination with the NIR emitting Dy681. The resulting biosensors display switch-on emission that opens new opportunities for DNA-DNA and DNA-protein interactions.

Conclusion and perspectives

I. General Conclusion

The goal of this work was to find new fluorene-based push-pull dyes as powerful biosensors. The rational designing of novel probes that meet the rigorous demands of biological applications urged us to develop efficient synthetic access to conclude a diversity-oriented synthesis of fluorene dyes. The optimized routes allowed us to synthesize fluorophores inaccessible by classical routes or otherwise too demanding to achieve. Structure-photophysics relationships of the library of 2,7-push-pull fluorenes had led in turn to produce biosensors that were successfully employed in respective contexts of imaging cell membranes, labeling ODN sequences, hybridization studies in DNA duplexes, base-discrimination fluorescence, and FRET applications.

First, selective functionalization of readily accessible dibromoaromatic scaffolds *via* air-stable palladium catalytic systems was optimized. The methodologies involved rapid *mono*- and *di*-selective Buchwald-Hartwig aminations *via* MW irradiation, and sequential one-pot C-N/Stille or C-N/C-N couplings. The scope of this work comprised synthesis of 37 symmetrical and unsymmetrical aminoaromatic derivatives based on fluorene, naphthalene, pyridine, and thiophene families in addition to a NIR sensor prepared through three-component one-pot reaction.

Next, we used the Pd-catalyzed methodology to study the effect of varying the electron donating ability on the spectroscopic behavior of the fluorene push-pull design. Introduced donors comprised aliphatic, aromatic, and saturated cyclic amines ranging from aziridine to azepane. To screen the electron withdrawing abilities of the acceptor, various reactions were performed including amongst others: Stille coupling, CuAAC, and peptide coupling that afforded to install the aldehyde, ketotriazole, succinyl, methylenemalonitrile, and benzothiadiazole groups. Among the synthesized dyes, conjugation attachment points were fixed to follow the effect of further couplings on the optical properties for biolabeling purposes. Photophysical characterization, Hammett and Lippert-Mataga correlations, in addition to theoretical TD-DFT calculations enclosed the structure-property relationships and rationalized the ICT character of the push-pull dyes. The most promising compounds in terms of brightness, mega-Stokes shift, excitation accessibility, and versatility for subsequent conjugation were used to design the biosensors used afterwards. Particularly, the propioloyl linker was converted into ketotriazolyl derivatives maintaining the desired optical properties upon bioconjugation.

Later, 3 new advanced fluorene dyes were synthesized for membrane studies. The three probes comprised respectively: a) a polar deoxyribosyl head b) a lipophilic long alkyl chain, and c) an amphiphilic anchoring group to fix the dye at the membrane interface and prevent its internalization. Spectroscopic characterization of these fluorophores, their tendency to probe large and giant unilamellar vesicles of different lipid compositions, and imaging of HeLa cells were investigated. This study demonstrated the ability of push-pull fluorenes to be a cornerstone of highly sensitive probes that can help in understanding the biophysical behavior of cell membranes. In effect, the optimal dye surpasses the features of commonly used Laurdan probe. Some of the established improvements are: red-shifted absorption that matches the 405 nm diode laser, higher brightness, decreasing the used concentration for such staining by ~10-15 folds, high photostability, comparably strong sensitivity to different liquid domains of cell membrane.

Lastly, we synthesized four fluorene phosphoramidites and incorporated them into oligonucleotides *via* automated solid-phase synthesis. Detailed spectroscopic studies evidenced a high sensitivity to protic media through a dramatic Stokes shift and to acidity. That observation augured interesting prospects for nucleic acid labeling. The nature of the alkyl chain on the amino group revealed to be crucial for the integrity of the fluorophore once incorporated in ODNs. Labeled sequences exhibited a far-red emission but modest quantum yields considering their large ICT character. In duplexes of different compositions, the dye revealed to efficiently base-discriminate opposite cytidine and thymidine. Once incorporated in DNA, the full separation of the absorption and emission led us to study this dye as a mega-Stokes shift donor ($\Delta\lambda = 235$ nm) in an emissive FRET pair combination with the NIR emitting Dy681. The resulting biosensors display switch-on emission that opens new opportunities for DNA-DNA and DNA-protein interactions.

II. Perspectives

Considering the Pd-catalyzed methodology, a complete one-pot synthesis seems promising. First, the exact role of the second catalytic addition should be understood by screening separately different ligands, bases, and catalytic combinations. Next, the introduction of different coupling moieties with one palladium loading could be attempted to evaluate the results. A Suzuki coupling partner is interesting to advance as well. An asymmetric version of the reaction testing *S*, *R*, and *rac*-BINAP is likewise possible.

Regarding the distinct behavior of BINAP on the monoselectivity of aminations, DFT calculations will provide an insight to comprehend the mechanism. As mentioned, computational studies with BINAP are highly challenging.

With respect to the fluorene library, electrochemical characterization involving cyclic voltametry is now in process on the sideway of the thesis. This is extremely interesting in fluorene case knowing that they are widely used in solar cells and OLEDs.

The synthesized membrane probes can be used in two-photon investigations and fluorescence microscopy. Indeed, fluorenes have large 2P absorption cross-sections at common wavelengths around 800 nm and high photostabilities. The probes can be further taken to biology interfaces with cytotoxicity and *in vivo* applications

The fluorene DNA label is currently studied in FRET applications with dy681 and dy781 leading to 300 and 390 nm shift between the excitation and emission maxima respectively. The related experiments are not finished at the time being for technical limitations of our fluorometer in emission range after 800 nm. Nonetheless, this will be certainly one of the records in FRET applications.

The DNA labeling at this stage should combine the nucleosidic linker (for the higher hydrophobic environment it imposed) with diethyl amine donor (for its compatibility with solid-phase synthesis) to test the outcome of a new marker, which is highly prospective.

Postsynthetic labeling by fluorene dyes was already started successfully by CuAAC reaction of **PP2** with commercial sequences bearing azido moieties. Three labeled sequences were achieved efficiently in 24 h compared to presynthetic labeling route that spanned a whole thesis. This is simply a marvelous alternative. It avoids the tedious work of DNA synthesis and allows for screening different fluorene dyes in limited time, which in turn will lead to enhanced fluorene biosensors and applications

As side prospective projects, **PP2** was also bioconjugated to spermine and amino acids to study their intercalations and DNA/protein interactions. Completing this story is still ongoing. Last, Fluorenone derivatives were prepared with interesting excimer properties that are currently in the stage of photophysical characterization.

Résumé long

Le développement pointu de la technologie implique souvent les interfaces de disciplines scientifiques prétendues distinctes. La recherche portant sur les domaines interdépendants de la chimie de synthèse, calculs théoriques, photophysique, biophotonique et imagerie a évolué comme un moyen moderne d'analyse pour comprendre les énigmes scientifiques. La "Fluorescence" est un domaine qui intègre pratiquement toutes les disciplines mentionnées et étend à d'autres frontières de détections environnementales, de la médecine et des sciences de la vie et pharmaceutiques.

La " Fluorescence " a été observée par Herschel en 1845 comme un phénomène de la solution de quinine sous la lumière du soleil et a été décrite plus en détail par Stokes en 1852. Un siècle plus tard, ce processus de nouveauté a été mis en service de la science avec l'invention des «fluorimètres commerciaux» et les "microscopes à fluorescence". Les progrès ont procédé rapidement avec la «microscopie confocale» et des instruments plus sophistiqués ayant obtenus le prix Nobel comme le " spectroscopie de femtoseconde de Zewail ($\times 10^{-15}$ s)". Les instrumentations de fluorescence sont aujourd'hui avancées, pas chers et faciles à manipuler.

Les techniques de fluorescence sont devenues des outils analytiques cruciaux pour la recherche et l'industrie grâce à des nombreuses caractéristiques exquises. Ces techniques sont les plus sensibles dans le domaine de la détection moléculaire, en particulier pour l'étude d'interaction dynamique en biologie. Leur sensibilité a atteint la limite de détection d'*une seule molécule* avec des enregistrements de signaux contrôlés à distance. Ils montrent une précision élevée, un caractère non-invasif dans les cellules vivantes et des résolutions spatiales et temporelles ultra-hautes. En outre, la détection de Fluorescence est extrêmement polyvalente, elle est possible à l'état solide, liquide, gaz et même à l'interface de ces phases. En plus d'instrumentations, l'avancement dans "la conception et la synthèse de fluorochromes" reste sans aucun doute la marque de progrès dans les applications de fluorescence.

Un *fluorophore* optimal est essentiellement un cadre moléculaire qui compile les attributs nécessaires à partir des propriétés optiques telles que la photostabilité, la luminosité, l'excitation sélective et l'émission à la polyvalence chimique telles que la tolérance à introduire des substituants pour la bioconjugaison et le réglage de la solubilité. Une telle conception rationnelle est un défi en soi. De la perspective " de la chimie organique ", cela implique au moins une voie de synthèse multi-étapes pour produire une telle molécule intelligente; par conséquent, ajoutant plus de défis des limites connues de la synthèse. Par conséquent, les chimistes sont

fortement invités à présenter des nouvelles routes, robustes et présentant une économie d'atomes pour synthétiser des sondes innovantes et générer des bibliothèques de colorants qui élucident les relations structure- propriété.

En particulier, notre travail a porté sur les réactions catalysées par des métaux tels que les aminations Buchwald - Hartwig et les réactions de cycloaddition alcyne - azoture catalysée par le cuivre (I) (CuAAC), la chimie "click" pour créer des alternatives plus viables pour des routes d'emploi plus longues. Les méthodologies développées ont permis l'accès à une bibliothèque de colorants push-pull à base de fluorène comme une classe captivante de sondes sensibles à l'environnement. Un colorant push-pull est constitué d'un squelette- π fonctionnalisé avec un donneur d'électrons (D) et un accepteur (A). Le système D- π -A subit un transfert intramoléculaire de charge (TIC) photo-induit formant une orbitale moléculaire (OM) à faible niveau énergétique. La lumière visible fournit suffisamment d'énergie pour exciter les électrons dans cette nouvelle OM, ce qui rend ces composés généralement colorés. Le TIC génère également des moments dipolaires qui augmentent la sensibilité de ces fluorophores en réponse à la polarité et les changements de leur environnement.

Le noyau aromatique (π) joue un rôle clé dans la conception. Ainsi, le choix de la famille fluorène est venu dans ce projet. Les Fluorènes manifestent des attributs spectroscopiques souhaitables, de faible cytotoxicité et une absorption à deux photons très appréciable des sections transversales permettant l'imagerie cellulaire avec un photo vieillissement réduit. Les dérivés de fluorène sont largement utilisés dans la recherche biomédicale et les sciences de matériaux tels que l'optoélectronique.

Deux applications centrales ont été explorées en utilisant nos sondes fluorène, 1) l'étiquetage des oligonucléotides (ODN), et 2) l'imagerie des lipides dans les membranes biologiques.

En fait, malgré la détermination complète des séquences d'ADN de 3.5×10^9 paires de base dans le projet du génome humain (HGP) en 2001, cette acquisition explosive des données structurales a défilé des informations très limitées sur la fonction biologique complexe de l'ADN. Pour répondre à ces aspects, la spectroscopie de fluorescence offre un outil exquis pour caractériser les acides nucléiques et d'étudier leurs interactions, qui sont fondamentales pour comprendre les événements cellulaires tels que la réparation et la méthylation de l'ADN, et le silençage génique. La recherche de marqueurs fluorescents appropriés qui peuvent surveiller ces interactions sans affecter la structure et la fonction des séquences ODN marqués est encore urgente.

De même, la distribution hétérogène des lipides dans les membranes cellulaires est un sujet d'investigations intenses. Trois niveaux d'hétérogénéité existent. L'hétérogénéité latérale, décrite par l'hypothèse de *radeaux lipidiques* est en débat jusqu'à maintenant. *Les radeaux* sont soupçonnés d'être derrière de nombreux processus tels que la transduction du signal et les maladies neurodégénératives. L'asymétrie des lipides transmembranaires est la deuxième hétérogénéité qui est perdue dans la mort cellulaire programmée (apoptose). L'apoptose défectueuse est à l'origine de maladies nuisibles tels que l'atrophie et le cancer. Enfin, les différences entre le plasma et les membranes intracellulaires représentent la troisième hétérogénéité moins explorée. Ainsi, la conception de sondes très sensibles aidera à comprendre la structure et la dynamique des membranes biologiques par la détection de différents paramètres tels que l'hydratation, la viscosité, la polarité et l'ordre. Cela va aider à son tour dans la compréhension des processus cellulaires et à trouver des solutions à des problèmes médicaux fustes comme le cancer.

En conclusion, le but de cette thèse était de progresser une étape dans les domaines de la conception et la synthèse de nouvelles sondes fluorescentes qui répondent aux conditions rigoureuses et exigeantes des applications biologiques mentionnées ci-dessus.

Le corps de la thèse se compose de 5 chapitres et une conclusion indiquant les perspectives d'avenir.

- Le premier chapitre est l'introduction qui indique l'arrière-plan de ce travail.
- Le contenu du deuxième chapitre a été publié récemment dans "*The Journal of Organic Chemistry*". Ce travail décrit la fonctionnalisation sélective des squelettes dibromoaromatiques en utilisant des systèmes catalytiques de palladium stable à l'air. Les méthodologies ont impliqué des mono- et di-aminations sélectives de Buchwald-Hartwig par irradiation aux micro-ondes. Les conditions ont été optimisées pour coupler séquentiellement différents réactifs en « One Pot ». Le couplage avec un large éventail d'amines a permis l'accès à une nouvelle bibliothèque de dérivés symétriques et asymétriques (37 exemples). En utilisant cette méthode polyvalente, un capteur push-pull proche de l'infrarouge a été préparé en installant des groupements donneurs d'électrons et en retirant d'autres par une réaction à plusieurs composants. Ces conditions ont révélé d'être faisable à grande échelle et adaptés à plusieurs groupes; par conséquent, facilitant l'utilisation en chimie de synthèse. Les conditions optimisées seront plus explorées dans la DOS-synthèse d'une bibliothèque de colorants push-pull de fluorène dans le chapitre 3 pour la caractérisation photophysique et dans la synthèse de sondes d'ADN avec émission proche infrarouge (NIR) dans le chapitre 5.
- Le contenu du chapitre trois a été publié récemment dans "*Chemistry: A European Journal*". Ce projet a rationnellement conçu, synthétisé et caractérisé une bibliothèque de colorants

fluorescents push-pull à base d'un squelette de fluorène 2,7-disubstitué. Ces dérivés émissives D- π -A ont été préparés par des voies de synthèse directes et à grandes échelles. Les différents groupements accepteurs d'électrons ont été efficacement introduits sur un synthon commun et facilement accessible par des méthodologies différentes, y compris, entre autres: couplage Stille, CuAAC et couplage peptidique. Le criblage des groupements donneurs d'électrons a été effectué chimiosélectivement via une amination polyvalente de Buchwald-Hartwig sur une carbaldéhyde fluorényle intermédiaire obtenu par une réaction de formylation optimisée. Les études photophysiques ont mis en évidence les composés les plus prometteurs en termes de luminosité, des déplacements de Stokes, d'accessibilité, d'excitation et la polyvalence pour la conjugaison ultérieure. L'agent de liaison de propiolyle a été introduit pour la conjugaison et converti en dérivé cétotriazolyl tout en conservant les propriétés optiques souhaitées. Ces caractéristiques font de l'ynone un point d'ancrage prospectif pour l'étiquetage biologique sur lequel on se base dans les deux chapitres suivants. En combinant les groupes accepteurs ED (morpholine, pipéridine) et donneurs EW (méthylenemalonitrile), l'effet synergique a été testé. Ces études ont conduit à de nouvelles fluorènes push-pull avec absorption et émission décalée vers le rouge. En raison d'un transfert de charge intramoléculaire amélioré, les colorants étaient très solvatochromiques sur l'échelle de la polarité entière et même les émissions proches infrarouges ont été observées dans des solvants protiques. Les Calculs DFT ont confirmé ces observations expérimentales. La corrélation d'un ensemble de D- π -A émetteurs dont les valeurs Hammett σ_p des paires donneur/accepteur considéré fournit un outil complémentaire pour anticiper les caractéristiques spectroscopiques souhaitées pour des applications spécifiques.

- Dans le quatrième chapitre, nous avons démontré la capacité de la famille fluorène d'être une pierre de base pour des sondes très sensibles qui peuvent aider à comprendre le comportement biophysique des membranes cellulaires en synthétisant trois nouvelles sondes fluorescentes avec une nouvelle conception. Ce travail a validé la polyvalence d'agent de liaison ynone introduit en étiquetage biologique sans compromettre les propriétés spectroscopiques appréciables du noyau du colorant. En effet, la sonde F3 dépasse les caractéristiques de "Laurdan" couramment utilisé par exemple. Certaines des améliorations établies par rapport à Laurdan sont: une absorption décalée vers le rouge qui correspond au laser diode de 405 nm, une luminosité plus élevée, ce qui diminue la concentration utilisée pour ces marquages de ~ 10-15 fois, une photostabilité élevée, une sensibilité comparativement élevée aux différents domaines liquides de membrane cellulaire. En outre, les dérivés fluorine présente une haute cross-section 2PA aux longueurs d'onde communes autour de 800 nm, ce qui les rend attrayants en microscopie d'excitation à deux photons. F3 est la première sonde à base de fluorène

spécifique pour la membrane plasmique qui peut être un outil puissant pour étudier ces membranes.

- Le chapitre cinq présente les synthèses de quatre marqueurs d'ADN fluorescents (FM1-4) comprenant les colorants push-pull de fluorène et leur incorporation spécifique aux oligonucléotides (ODNs). En effet, ce travail est un résumé des différents plans d'études qui ont été menés en parallèle aux projets précédents. Les deux voies, Palladocatalytisée et classique, ont été utilisées pour établir les quatre phosphoramidites employées dans les campagnes successives de synthèse d'ADN en phase solide. L'accent sur les détails de synthèse et les études de dégradation sera présentée pour expliquer les difficultés rencontrées et argumenter la compatibilité de la chaîne alkyle du groupe amine dans l'étiquetage de l'ADN par des colorants fluorènes. En conclusion, nous avons établi le cadre de la préparation d'analogue nucléotidique fluorescent FM4 comme un substituant de base nucléique. Les études spectroscopiques détaillées ont témoigné une sensibilité élevée aux milieux protiques par un décalage dramatique de Stokes. Cette observation augurait des perspectives intéressantes pour l'étiquetage de l'acide nucléique. Les séquences marquées ont présenté une émission rouge lointain, mais des rendements quantiques modestes compte tenu de leur grand transfert de charge. En duplex de compositions différentes, le colorant a montré son efficacité à discriminer les bases opposées cytidine et thymidine. Une fois incorporé à l'ADN, la séparation complète de l'absorption et l'émission nous a conduits à analyser ce colorant comme un donneur donnant un déplacement de Stokes important vers les proches infrarouges dans une combinaison FRET émissive avec le colorant Dy681. Les biocapteurs résultants affichent un enclenchement d'émission qui ouvre de nouvelles possibilités pour les interactions ADN-ADN et ADN-protéines.

Experimental section

I. General methods

All reactions involving water- or air-sensitive material were performed in oven-dried glassware under an argon or nitrogen atmosphere by using Schlenk techniques employing double-line argon-vacuum lines and dry solvents. The synthetic intermediates were co-evaporated twice with toluene and dried in *vacuo* before use in reactions that need anhydrous conditions. All chemical reagents were obtained from commercial sources (Aldrich, Acros, Alfa Aesar) and were used as supplied. Anhydrous solvents and amine reagents were obtained by distillation followed by three cycles of degassing (or recrystallization in case of solid nucleophiles) according to standard procedures.^[284] The reactions were monitored simultaneously by gas chromatography (GC/MS) and by thin-layer chromatography and visualized both by UV radiation (254 & 365 nm) and by spraying with relevant staining agent (KMnO₄ or Ninhydrin) followed by a subsequent warming with a heat gun. Column chromatography^[285] was performed with flash silica gel (40–63 μm) with the indicated solvent system, using gradients of increasing polarity in most cases. ¹H NMR (200 and 500 MHz), ¹³C NMR (50 and 125 MHz, recorded with complete proton decoupling) spectra were obtained with samples dissolved in CDCl₃, CD₂Cl₂, CD₃OD, DMSO-*d*₆, acetone-*d*₆, CD₃CN, or TFA-*d*₁, with the residual solvent signals as internal references: 7.26 ppm for CHCl₃, 5.32 ppm for CDHCl₂, 3.31 ppm for CD₂HOD, 2.50 ppm for (CD₃)(CD₂H)S(O), 2.05 ppm for (CD₃)(CD₂H)C(O), 1.94 ppm for CD₂H₂CN, 11.50 ppm for CF₃COOH for ¹H NMR experiments, and 77.0 ppm for CDCl₃, 53.8 ppm for CD₂Cl₂, 49.0 ppm for CD₃OD, 39.4 ppm for (CD₃)₂S(O), 30.8 ppm for (CD₃)₂C(O), 164.2 ppm CF₃COOD for ¹³C NMR experiments.^[286] Chemical shifts (δ) are given in ppm to the nearest 0.01 (¹H) or 0.1 ppm (¹³C). The coupling constants (*J*) are given in Hertz (Hz). The signals are reported as follows: (s=singlet, d=doublet, t=triplet, quint=quintet, sext=sextet, m=multiplet, br=broad). Assignments of ¹H and ¹³C NMR signals were achieved with the help of D/H exchange, COSY, DEPT, HMQC, HSQC, HMBC experiments. Regular mass spectra (LCMS) were recorded on an Esquire 3000 Plus apparatus (ion trap mass spectrometer) with ESI in both positive and negative modes. Analytical GC/MS analyses were performed with a Shimadzu QP2010S-MS (ion trap mass spectrometer) chromatograph (EI 70 eV). High-resolution mass spectrometry (HRMS) was conducted with a FINIGAN MAT 95 (hybrid ion trap–Orbitrap mass) spectrometer with EI or ESI techniques. Systematic nomenclatures were used for the assignments of each spectrum. For fluorene, the assignments followed the systematic

nomenclatures for the six-membered rings and alphabetical letters for the central 5-membered ring.

All solvents for absorption and fluorescence experiments were of spectroscopic grade. Absorption spectra were recorded on a Cary 4 spectrophotometer (Varian) using 1 cm quartz cells. The samples used for spectroscopic measurements contained $\approx 0.1\%$ v/v of the stock solvent. Fluorescence spectra were recorded on FluoroMax 4.0 spectrofluorometer (Jobin Yvon, Horiba). Excitation wavelength was used as mentioned in the corresponding experiments. Stock solutions of the push-pull dyes were prepared using dioxane ($< 10\%$ v/v of DMF was added in case of insoluble dyes). The samples used for spectroscopic measurements contained $\approx 0.1\%$ v/v of the stock solvent.

II. Lipid vesicles

Dioleoylphosphatidylcholine (DOPC) and cholesterol (CL) were purchased from Sigma-Aldrich. Bovine brain sphingomyelin (SM) was from Avanti Polar Lipids (Alabaster, AL). Large unilamellar vesicles (LUVs) were obtained by the extrusion method as previously described.^[287] Briefly, a suspension of multilamellar vesicles was extruded by using a Lipex Biomembranes extruder (Vancouver, Canada). The size of the filters was first $0.2\ \mu\text{m}$ (7 passages) and thereafter $0.1\ \mu\text{m}$ (10 passages). This generates monodisperse LUVs with a mean diameter of $0.11\ \mu\text{m}$ as measured with a Malvern Zetamaster 300 (Malvern, U.K.). LUVs were labeled by adding aliquots (generally $2\ \mu\text{L}$) of probe stock solutions in dimethyl sulfoxide to 1-mL solutions of vesicles. Since the probe binding kinetics is very rapid, the fluorescence experiments were performed a few minutes after addition of the aliquot. A 20 mM phosphate buffer, pH 7.4, was used in these experiments. Concentrations of the probes and lipids were generally 0.3 or 0.4 and $100\ \mu\text{M}$, respectively.

Giant unilamellar vesicles (GUVs) were generated by electroformation in a home-built liquid cell (University of Odense, Denmark), using previously described procedures.^[265] A $0.1\ \text{mM}$ solution of lipids in chloroform was deposited on the platinum wires of the chamber, and the solvent was evaporated under vacuum for 30 min. The chamber, thermostatted at $55\ ^\circ\text{C}$, was filled with a 300 mM sucrose solution, and a 2-V, 10-Hz alternating electric current was applied to this capacitor-like configuration for ca. 2 h. Then, a $50\ \mu\text{L}$ aliquot of the obtained stock solution of GUVs in sucrose (cooled down to room temperature) was added to $200\ \mu\text{L}$ of 300 mM glucose solution to give the final suspension of GUVs used in microscopy experiments. The staining of GUVs was performed by addition of an aliquot of the probe stock solution in DMSO to obtain a $0.1\ \mu\text{M}$ final probe concentration (final DMSO volume $< 0.25\%$).

III. Cell lines, culture conditions, treatment, and imaging

HeLa cells were cultured in Dulbecco's modified Eagle medium (D-MEM, Low glucose, +GlutaMAX, Gibco-Invitrogen) supplemented with 10% (v/v) fetal bovine serum (FBS, Lonza), and 1% antibiotic solution (penicillin-streptomycin, Gibco-Invitrogen) in a humidified incubator with 5% CO₂/95% air atmosphere at 37 °C. CEM-SS lymphocytes (ATCC) were cultured in PRMI 1640 (Gibco-Invitrogen) supplemented with 10% (v/v) fetal bovine serum (FBS, Lonza), and 1% antibiotic solution (penicillin-streptomycin, Gibco-Invitrogen) in a humidified incubator with 5% CO₂ atmosphere at 37°C. The cell concentration of 5–10*10⁴ cells ml⁻¹ was maintained by removal of a portion of the culture and replacement with fresh medium 3 times per week. In fluorescence spectroscopy experiments, CEM-SS cells were also washed twice with HBSS using centrifugation before addition of the probes. To stain the cell suspension with **F1-3** probes, an appropriate aliquot of its stock solution in DMSO was added to the lymphocytes (10⁶ per mL) in HBSS buffer to obtain a final probe concentration of 100 nM. Spectroscopic measurements were performed under stirring. For the microscopy studies, attached HeLa cells were washed two times by gentle rinsing with HBSS. A freshly prepared solution of **F1-3** in HBSS was then added to the cells to a final concentration of 100 nM. Imaging was performed directly without washing step after 5-10 min.

Confocal microscopy images were taken on a Leica TSC SPE-II confocal microscope with HXC PL APO 63x/1.40 OIL CS objective. The excitation light was provided by a 405 nm laser while the fluorescence was detected at two spectral ranges: blue and green separated at 500 nm). The ratiometric images were generated by using special macros under Image J that divides the image of the green channel by the one of the blue channel. For each pixel, a pseudo-color scale is used for coding the ratio, while the intensity is defined by the integral intensity recorded for both channels at the corresponding pixel.

IV. ODN synthesis and purification:

The ODN synthesis was performed on an Expedite 8900 DNA synthesizer (Applied Biosystem) using the "trityl on or off" modes and ultra-mild Pac phosphoramidite chemistry on a 0.2 μmol scale. Reagents and solvents, as well as dT, Ac-dC, Pac-dA, and dmf-dG or iPr-Pac-dG phosphoramidites were purchased from Link Technologies and Chemgenes. The standard DNA assembly protocol "DMT on or off" was used except for the following modifications: 5-Ethylthio-1H-tetrazole (ETT) was used as activating agent; Pac- anhydride was used for capping; a longer coupling time (1200 s) was applied to the fluorene and the next coming phosphoramidites.

Non-labeled ODNs were purchased from Microsynth AG. The ODNs were cleaved from the solid support and deprotected with concentrated aqueous ammonia at room temperature for 12 h. The ODNs were analyzed (0.5 mL/min) and purified (2.5 mL/min) by RP HPLC (HPLC apparatus: Waters™ 600 Controller with Waters™ 996 Photodiode Array Detector and Jasco LC-Net II / ADC apparatus. Columns: analytical, 300 × 4.60 mm, 5 μm particle size, Clarity® 100Å, Phenomenex®; semi-preparative, Clarity® 5u Oligo-RP column 250 x 10 mm Phenomenex®). The following gradient system was used: 100 % A –(30 min)→ 60 % A / 40 % B –(5 min)→ 100 % B –(5 min)→ 100 % A with A=Buffer pH 7.0 (1.9 L of MilliQ® water, 160 mL acetonitrile, 28 mL triethylamine, 12 mL of acetic acid) and B=0.2 CH₃CN:0.8 Buffer.

V. MALDI procedure

Dibasic Ammonium Citrate (DAC) (98% capillary GC) was obtained from Sigma. Acetonitrile of HPLC grade was purchased from VWR chemical. Ultrapure 3-Hydroxypicolinic Acid (3-HPA) MALDI matrix was purchased from Protea Biosciences. C4 pipette tips (Zip-Tip) were from Millipore.

The samples (500 pmol) were diluted to 10 μL of water and were desalted with a C4 pipette Tips (Zip-tip). The Zip-tip was activated before use with 2 x 5 μL of water: CH₃CN (50:50) and 2 x 5 μL of DAC (50 mg/ml diluted in water). The 10 μL of the ODN solution was loaded on Zip-tip by drawing and expelling ten times. Next the zip-tip was washed with 3 x 5 μL of DAC (50 mg/mL) and 3 x 5 μL of water. Elution was performed with 1.5 μL of 3-HPA matrix (80 mg/mL, 50:50 CH₃CN:DAC) directly on MALDI plate. The ODN profile obtained in a ABSciex MALDI-TOF/TOF mass spectrometer in reflector mode with external calibration mixture (cal Mix 1+2 distributed by ABSciex). MALDI-TOF/TOF-MS analysis: MS spectra were recorded manually in a mass range of 500-6000 Da resulting from 400 laser shots of constant intensity fixed at 6200. Data were collected using 4000 series Explorer (AB SCIEX) experiments.

VI. Preparation of ss and ds labeled DNA

The ODNs were analyzed in cacodylate buffer pH 7.0: 10 mM cacodylate, 150 mM NaCl.

Preparation of the single strand solution: the solution of the sample was prepared by mixing 400 μL of a stock solution of 20 mM cacodylate buffer solution pH 7.0 for GXG and pH 8.4 for CXC and TXT, 80 μL of 1.5 M NaCl solution, 12.5 μL of 64 μM ssODN and 285 μL of MilliQ® water.

Preparation of the double strand solution: 400 μL of a stock solution of 20 mM cacodylate respective buffer solution 80 μL of 1.5 M NaCl solution, 12.5 μL of 64 μM **ODN1**, 12.5 μL of 64 μM **ODN2** and 260 μL of MilliQ® water.

VII. Denaturation studies and melting temperatures

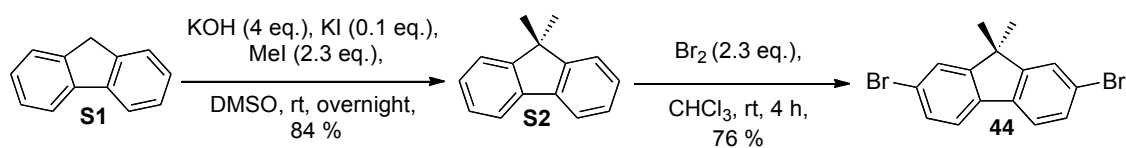
Melting curves were recorded by following the temperature-dependence of the absorbance changes of the sample (1 μM concentration of each strand). Absorption spectra were recorded in a Peltier thermostated cell holder on a Cary 4 spectrophotometer (Varian). Wavelength for detection was 260 nm. The pathlength of cell was 1 cm. The temperature range for denaturation measurement was 5 – 80 °C. Speed of heating was 0.3 °C/min. Cacodylate buffer pH 7.0 was used (10 mM cacodylate buffer, 150 mM NaCl). The melting curves were converted into a plot of α versus temperature, where α represents the fraction of single-strands in the duplex state. The melting temperatures were extracted from these curves after differentiation as described elsewhere.^[283]

VIII. Circular dichroism

Circular dichroism spectra were recorded with 1 μM solution of the canonical dsDNA and labeled dsDNA (fluorene label with variation of its opposite) in the respective cacodylate buffer at 25 °C on a Jasco J-810 spectropolarimeter.

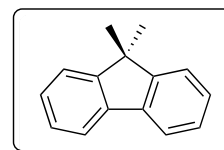
The products will appear in the SI according to the respective order of discussions in chapters 2-5 and not in ascending order of numbers.

IX. Chapter 2 synthetic procedures

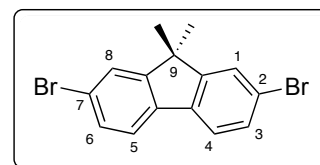


Scheme 1. Synthesis of 2,7-dibrominated fluorene starting material (**44**)

9,9-dimethyl-9H-fluorene (S2): To a stirred solution of 9H-fluorene S1 (3.00 g, 18.1 mmol, 1 eq.) in DMSO (35 mL) at 60 °C, were sequentially added potassium iodide (300 mg, 1.8 mmol, 0.1 eq.), iodomethane (5.76 g, 40.6 mmol, 2.25 eq.), and very cautiously powdered potassium hydroxide (8.30 g, 146.8 mmol, 4 eq.). The resulting reaction mixture was stirred at room temperature overnight before being poured into 200 mL of water. A light yellow precipitate was formed, then filtered out, washed with cold water, and dried under vacuum. The light yellow solid was purified by crystallization from methanol to provide the title compound S2 (2.94 g, 84 %) as white crystals. ¹H-NMR (200 MHz, CDCl₃, δ): 7.77-7.73 (m, 2H), 7.48-7.42 (m, 2H), 7.41-7.33 (m, 4H), 1.51 (s, 6H). ¹³C-NMR (50 MHz, CDCl₃, δ): 153.7 (2C), 139.3 (2C), 127.4 (2C), 126.9 (2C), 122.7 (2C), 120.1 (2C), 47.4, 27.3 (2C). GC-MS (*m/z*): 194.2 [M]⁺.



2,7-dibromo-9,9-dimethyl-9H-fluorene (44): To a solution of S2 (2.18 g, 11.2 mmol, 1 eq.) in CHCl₃ (25 mL) in a reaction vessel suspended in ice bath, liquid bromine (1.40 mL, 25.8 mmol, 2.3 eq.) was carefully added dropwise. The reaction mixture was stirred for 4 h, quenched with sat. aq. Na₂S₂O₃ (15 mL), and extracted with CHCl₃ (3*15 mL). The separated organic layer was washed with brine, dried over anhydrous MgSO₄, and concentrated *in vacuo*. The crude product was purified by crystallization from DCM/MeOH to give **44** (2.85 g, 76 %) as white crystals. ¹H-NMR (200 MHz, CDCl₃, δ): 7.55 (d, ³J=8.0 Hz, 2H, H4,5), 7.54 (d, ⁴J=1.5 Hz, 2H, H1,8), 7.45 (dd, ⁴J=1.5 Hz, ³J=8.0 Hz, 2H, H3,6), 1.46 (s, 6H). ¹³C-NMR (50 MHz, CDCl₃, δ): 155.4 (2C), 137.3 (2C), 130.5 (2C), 126.3 (2C), 121.6 (4C), 47.5, 27.0 (2C). MS (*m/z*): 352.0 [M]⁺.



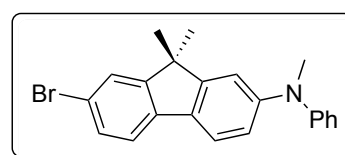
General Procedure (GP-A): Pd(OAc)₂ (4 mol%), *t*-BuONa (1.1 eq.), and BINAP (12 mol%) were added to a previously-dried reaction tube containing a magnetic bar. The tube was purged with argon for 3 cycles using Schlenk technique. The mixture was dissolved in toluene (0.1 M) and stirred for 15 min under argon at rt. Then, the dibromo aryl reagent (1 eq.) was added, followed by 15 min of further stirring (at rt or 100 °C for better). Finally, the amine (liquid or dissolved in

toluene) (1.1 eq.) was added, and the reaction mixture was irradiated in the microwave oven at 300 W/ 180 °C for 45 minutes (or classically heated at 100 °C in an oil bath overnight for thermal activation). The reaction was concomitantly monitored by TLC and GCMS until complete conversion. The resulting mixture was cooled down to room temperature, diluted by CH₂Cl₂, and filtered over a pad of Celite®. The volatiles were removed under reduced pressure, and the residue was purified by silica gel column chromatography using a slow gradient to give the desired product.

Following GP-A, 115 and 117- 126 series of products were prepared on 100 mg scale (0.28 mmol) except when otherwise indicated.

7-bromo-*N*,9,9-trimethyl-*N*-phenyl-9*H*-fluoren-2-amine

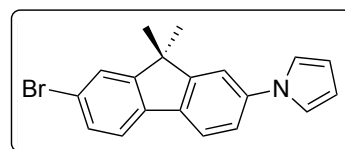
(115): Eluent for flash chromatography (PE/Et₂O = gradient up to 98:2, *R_f* = 0.45) providing **115** as a yellow solid (89 mg, 0.24 mmol, 86 %). ¹H-NMR (200 MHz, CDCl₃, δ): 7.49-7.16 (m, 6H), 7.02-6.86 (m, 5H), 3.29 (s, 3H), 1.34 (s, 6H). ¹³C-NMR (50 MHz, CDCl₃, δ): 155.5, 154.9, 149.1 (2C), 138.4, 131.5, 130.1, 129.4 (2C), 126.1, 121.6, 120.8 (3C), 120.6, 119.8, 119.4, 114.4, 47.2, 40.7, 27.7 (2C). HRMS (ESI⁺): *m/z* calcd for C₂₂H₂₁NBr: 378.0852 [M+H]⁺; found 378.0855.



Thermal heating: (80 mg, 0.21 mmol, 76 %).

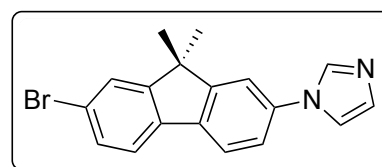
1-(7-bromo-9,9-dimethyl-9*H*-fluoren-2-yl)-1*H*-pyrrole

(117): Eluent for flash chromatography (PE/Et₂O = gradient up to 98:2, *R_f* = 0.45) providing **117** as a yellow solid (74 mg, 0.22 mmol, 80 %). ¹H-NMR (200 MHz, CDCl₃, δ): 7.72 (d, ³*J*=8.0 Hz, 1H), 7.60-7.36 (m, 5H), 7.16 (t, *J*=2.0 Hz, 2H), 6.40 (t, *J*=2.0 Hz, 2H), 1.52 (s, 6H). ¹³C-NMR (50 MHz, CDCl₃, δ): 155.7, 155.0, 140.6, 137.6, 135.9, 130.4, 126.3, 121.4, 121.1, 121.1, 120.0, 119.7 (2C), 115.4, 110.6 (2C), 47.7, 27.1 (2C). HRMS (ESI⁺): *m/z* calcd for C₁₉H₁₇NBr: 338.0539 [M+H]⁺; found 338.0540.



1-(7-bromo-9,9-dimethyl-9*H*-fluoren-2-yl)-1*H*-imidazole

(118): Eluent for flash chromatography (PE/Et₂O = gradient up to 98:2) providing **2c** as a yellow solid (24 mg, 0.07 mmol, 28 %) ¹H-NMR (200 MHz, CDCl₃, δ): 7.90 (s, 1H), 7.75 (d, ³*J*=8.0 Hz, 1H), 7.59 (d, ³*J*=8.0 Hz, 1H), 7.57 (s, 1H), 7.47 (dd, ³*J*=8.0 Hz, ⁴*J*=2.0 Hz, 1H), 7.40-7.32 (m, 3H), 7.23 (s, 1H), 1.51 (s, 6H). ¹³C-NMR (50 MHz, CDCl₃, δ): 155.7, 155.3, 137.7, 137.0, 136.9,

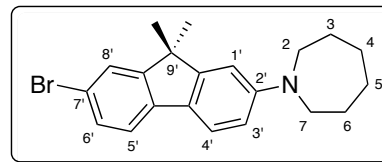


135.8, 130.6 (2C), 126.4, 121.8, 121.7, 121.3, 121.0, 118.6, 116.4, 47.5, 27.1 (2C). HRMS (ESI⁺): m/z calcd for C₁₈H₁₆N₂Br: 339.0491 [M+H]⁺; found 339.0494.

1-(7-bromo-9,9-dimethyl-9H-fluoren-2-yl)azepane

(119): Eluent for flash chromatography (PE/Et₂O = gradient up to 98:2, R_f = 0.5) providing **119** as a yellow solid (83 mg, 0.23 mmol, 81 %).

¹H-NMR (200 MHz, CDCl₃, δ): 7.51 (br d, ³ J =8.0 Hz, 1H, H4'), 7.46 (br s, 1H, H8'), 7.43-7.34 (m, 2H, H5',6'), 6.70 (br s, 1H, H1'), 6.68 (br d, ³ J =8.0 Hz, 1H, H3'), 3.53 (t, ³ J =6.0 Hz, 4H, CH₂2,7), 1.84 (br m, 4H, CH₂3,6), 1.59 (br m, 4H, CH₂4,5), 1.45 (s, 6H, 2CH₃). ¹³C-NMR (50 MHz, CDCl₃, δ): 155.3, 154.9, 149.4, 139.2, 129.9, 129.4, 125.8, 121.1, 119.7, 118.4, 110.5, 105.1, 49.6 (2C), 47.0, 27.9 (2C), 27.5 (2C), 27.3 (2C). HRMS (ESI⁺): m/z calcd for C₂₁H₂₅NBr: 370.1165 [M+H]⁺; found 370.1166.

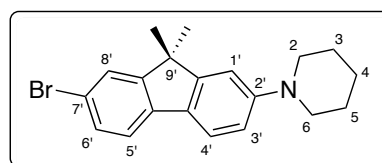


1-(7-bromo-9,9-dimethyl-9H-fluoren-2-yl)piperidine

(120): Reaction performed on 1 gram scale (2.84 mmol).

Eluent for flash chromatography (PE/EA = gradient up to 95:5, R_f = 0.6) providing **120** as a yellow solid (625 mg, 1.76 mmol, 62 %).

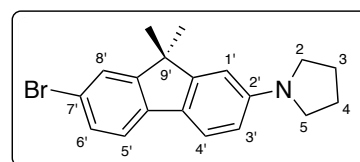
¹H-NMR (200 MHz, CDCl₃, δ): 7.55 (d, ³ J =8.0 Hz, 1H, H4'), 7.49 (d, ⁴ J =2.0 Hz, 1H, H8'), 7.42 (d, ³ J =8.0 Hz, 1H, H5'), 7.39 (dd, ³ J =8.0 Hz, ⁴ J =2.0 Hz, 1H, H6'), 7.00 (br s, 1H, H1'), 6.94 (dd, ³ J =8.0 Hz, ⁴ J =2.0 Hz, 1H, H3'), 3.23 (t, ³ J =6.0 Hz, 4H, CH₂2,6), 1.77 (br m, 4H, CH₂3,5), 1.62 (br m, 2H, CH₂4), 1.45 (s, 6H, 2CH₃). ¹³C-NMR (50 MHz, CDCl₃, δ): 155.3, 154.7, 152.6, 138.7, 130.0, 129.6, 125.9, 120.7, 120.4, 119.3, 115.5, 110.8, 51.1 (2C), 47.1, 27.3 (2C), 26.0 (2C), 24.4. HRMS (ESI⁺): m/z calcd for C₂₀H₂₃NBr: 356.1008 [M+H]⁺; found 356.1008.



1-(7-bromo-9,9-dimethyl-9H-fluoren-2-yl)pyrrolidine

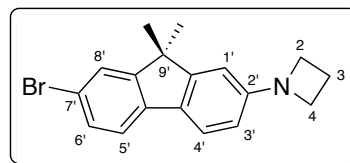
(121): Eluent for flash chromatography (PE/Et₂O = gradient up to 97:3, R_f = 0.32) providing **121** as a yellow solid (79 mg, 0.23 mmol, 83 %).

¹H-NMR (200 MHz, CDCl₃, δ): 7.41 (d, ³ J =8.0 Hz, 1H, H4'), 7.36 (br d, ⁴ J =2.0 Hz, 1H, H8'), 7.27 (m, 2H, H5',6'), 6.45 (br s, 1H, H1'), 6.42 (dd, ³ J =8.0 Hz, ⁴ J =2.0 Hz, 1H, H3'), 3.24 (t, ³ J =7.0 Hz, 4H, CH₂2,5), 1.91 (m, 4H, CH₂3,4), 1.34 (s, 6H, 2CH₃). ¹³C-NMR (50 MHz, CDCl₃, δ): 155.2, 154.9, 148.2, 139.3, 129.9 (2C), 125.8, 121.1, 119.7, 118.3, 110.9, 105.5, 48.0 (2C), 47.0, 27.5 (2C), 25.6 (2C). HRMS (ESI⁺): m/z calcd for C₁₉H₂₁NBr: 342.0852 [M+H]⁺; found 342.0852.



1-(7-bromo-9,9-dimethyl-9H-fluoren-2-yl)azetidine (122):

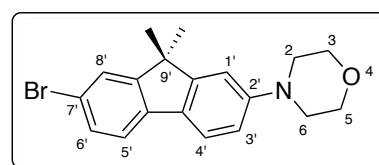
Eluent for flash chromatography (PE/Et₂O = gradient up to 98:2, *R_f* = 0.18) providing **122** as a yellow solid (45 mg, 0.14 mmol, 50 %). ¹H-NMR (200 MHz, CDCl₃, δ): 7.43 (d, ³*J*=8.0 Hz, 1H, H_{4'}),



7.39 (br s, 1H, H_{8'}), 7.33-7.27 (m, 2H, H_{5',6'}), 6.37 (br d, ⁴*J*=2.0 Hz, 1H, H_{1'}), 6.33 (dd, ³*J*=8.0 Hz, ⁴*J*=2.0 Hz, 1H, H_{3'}), 3.87 (t, ³*J*=7.0 Hz, 4H, CH₂2,4), 2.32 (q, ³*J*=7.0 Hz, 2H, CH₂3), 1.35 (s, 6H, 2CH₃). ¹³C-NMR (50 MHz, CDCl₃, δ): 155.0 (2C), 152.4, 139.1, 130.0 (2C), 125.9, 120.8, 120.0, 118.9, 110.4, 105.3, 52.7 (2C), 47.0, 27.4 (2C), 17.0. HRMS (ESI⁺): *m/z* calcd for C₁₈H₁₉NBr: 328.0695 [M+H]⁺; found 328.0696.

4-(7-bromo-9,9-dimethyl-9H-fluoren-2-yl)morpholine (123):

Eluent for flash chromatography (PE/EA = gradient up to 95:5, *R_f* = 0.15) providing **123** as a yellow solid (71 mg, 0.20 mmol, 72 %). ¹H-NMR (200 MHz, CDCl₃, δ): 7.40-7.31

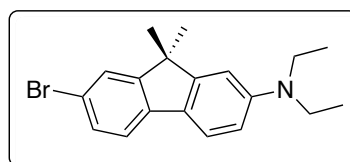


(m, 3H), 7.21 (dd, ³*J*=8.0 Hz, ⁴*J*=1.5 Hz, 1H), 6.77 (d, ⁴*J*=2.0 Hz, 1H), 6.69 (dd, ³*J*=8.0 Hz, ⁴*J*=2.0 Hz, 1H), 3.71 (t, ³*J*=5.0 Hz, 4H), 3.05 (t, ³*J*=5.0 Hz, 4H), 1.26 (s, 6H). ¹³C-NMR (50 MHz, CDCl₃, δ): 155.4, 154.9, 151.6, 138.4, 130.6, 130.1, 126.0, 120.9, 120.6, 119.7, 114.8, 110.1, 67.0 (2C), 49.8 (2C), 47.2, 27.4 (2C). HRMS (ESI⁺): *m/z* calcd for C₁₉H₂₁NOBr: 358.0801 [M+H]⁺; found 358.0804.

7-bromo-*N,N*-diethyl-9,9-dimethyl-9H-fluoren-2-amine (124):

(124):^[60] Reaction performed on 1 gram scale (2.84 mmol).

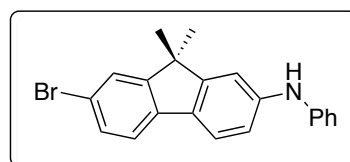
Eluent for flash chromatography (PE/Et₂O = gradient up to 98:2, *R_f* = 0.35) providing **124** as a yellow solid (606 mg, 1.76 mmol,



62 %). ¹H-NMR (200 MHz, CDCl₃, δ): 7.54-7.40 (m, 4H), 6.69-6.65 (m, 2H), 3.43 (q, ³*J*=7.0 Hz, 4H), 1.45 (s, 6H), 1.22 (t, ³*J*=7.0 Hz, 6H). ¹³C-NMR (50 MHz, CDCl₃, δ): 155.3, 154.9, 148.1, 139.1, 129.9, 125.8, 121.2, 119.8, 118.4, 111.0, 105.7, 47.0, 44.9 (2C), 27.5 (2C), 12.7 (2C). GC-MS (*m/z*): 343.1 [M]⁺.

7-bromo-9,9-dimethyl-*N*-phenyl-9H-fluoren-2-amine (125):

Reaction performed on 1 gram scale (2.84 mmol). Eluent for flash chromatography (PE/DCM = gradient up to 9:1, *R_f* = 0.13) providing **125** as a yellow solid (848 mg, 2.33 mmol, 82 %). ¹H-

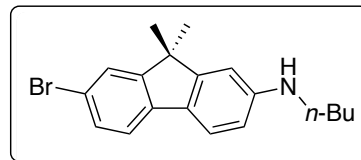


NMR (200 MHz, CDCl₃, δ): 7.62-7.41 (m, 4H), 7.37-7.22 (m, 2H), 7.16-6.95 (m, 5H), 1.47 (s, 6H). ¹³C-NMR (50 MHz, CDCl₃, δ): 155.3, 155.1, 143.1 (2C), 138.4, 131.4, 130.1, 129.5 (2C), 126.0,

121.3, 121.1, 120.5, 119.7, 118.0 (2C), 116.9, 112.0, 47.1, 27.2 (2C). HRMS (ESI⁺): *m/z* calcd for C₂₁H₁₉NBr: 364.0695 [M+H]⁺; found 364.0698.

7-bromo-*N*-butyl-9,9-dimethyl-9*H*-fluoren-2-amine (126):

Eluent for flash chromatography (PE/Et₂O = gradient up to 99:1, *R_f* = 0.11) providing **126** as a yellow solid (64 mg, 0.18 mol, 67 %). ¹H-NMR (200 MHz, CDCl₃, δ): 7.56-7.27 (m, 4H),



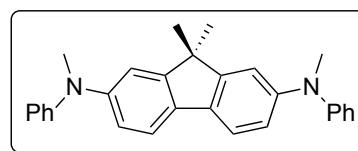
6.71-6.56 (m, 2H), 3.18 (t, ³*J*=7.0 Hz, 2H), 1.66 (q, ³*J*=7.0 Hz, 2H), 1.52-1.26 (m, 2H), 1.43 (s, 6H), 0.98 (t, ³*J*=7.0 Hz, 2H). ¹³C-NMR (50 MHz, CDCl₃, δ): 155.3, 154.9, 148.7, 140.0, 139.1, 130.0, 125.9, 121.2, 119.9, 118.8, 112.0, 106.9, 47.0, 44.2, 31.8, 27.4 (2C), 20.5, 14.1. GC-MS (*m/z*): 343.1 [M]⁺.

General Procedure (GP-B): Pd(OAc)₂ (8 mol%), *t*-BuONa (2.2 eq.), and JohnPhos (24 mol%) were added to a previously-dried reaction tube containing a magnetic bar. The tube was purged with argon for 3 cycles using Schlenk technique. The mixture was dissolved in toluene (0.1 M) and stirred for 15 min at rt under argon. Then, the dibromo aryl reagent (1 eq.) was added and followed by 15 mins further stirred for 15 mins (at rt or 100 °C for better activation). Finally, the amine (liquid or dissolved in toluene) (2.2 eq.) was added, and the reaction mixture was irradiated in the microwave oven at 300 W/ 180 °C for 1 h (or classically heated at 100 °C in an oil bath overnight for thermal activation). The reaction was monitored by TLC and GCMS until complete conversion. The resulting mixture was cooled down to room temperature, diluted by CH₂Cl₂, and filtered over a pad of Celite®. The volatiles were removed under reduced pressure, and the residue was purified by silica gel column chromatography to give the desired product.

Following GP-B, 116 and 130-133 series of products were prepared on scale (0.28 mmol).

***N*²,*N*⁷,9,9-tetramethyl-*N*²,*N*⁷-diphenyl-9*H*-fluorene-2,7-**

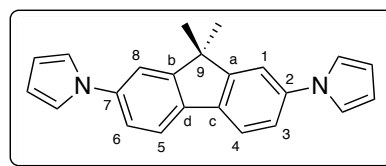
diamine (116): Eluent for flash chromatography (PE/Et₂O = gradient up to 98:2, *R_f* = 0.25) providing **116** as a yellow solid (101 mg, 0.25 mmol, 89 %). ¹H-NMR (200 MHz, CDCl₃, δ): 7.49



(d, ³*J*=8.0 Hz, 2H), 7.22 (t, ³*J*=8.0 Hz, 4H), 7.08 (br s, 2H), 6.99-6.95 (m, 6H), 6.90-6.83 (m, 2H), 3.32 (s, 6H), 1.37 (s, 6H). ¹³C-NMR (50 MHz, CDCl₃, δ): 155.0 (2C), 149.4 (2C), 147.8 (2C), 133.5 (2C), 129.3 (4C), 120.8 (2C), 120.4 (2C), 120.1 (2C), 119.1 (4C), 116.2 (2C), 47.0, 40.8 (2C), 27.4 (2C). HRMS (ESI⁺): *m/z* calcd for C₂₉H₂₉N₂: 405.2325 [M+H]⁺; found 405.2321.

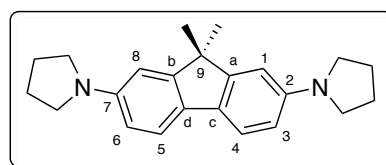
1,1'-(9,9-dimethyl-9H-fluorene-2,7-diyl)bis(1H-pyrrole)

(130): Eluent for flash chromatography (PE/Et₂O = gradient up to 98:2, *R_f* = 0.26) providing **130** as a yellow solid (70 mg, 0.22 mmol, 78 %). ¹H-NMR (200 MHz, CDCl₃, δ): 7.73 (d, ³*J*=8.0 Hz, 2H, H4,5), 7.45 (d, ⁴*J*=2.0 Hz, 2H, H1,8), 7.39 (dd, ³*J*=8.0 Hz, ⁴*J*=2.0 Hz, 2H, H3,6), 7.16 (t, ³*J*=2.0 Hz, 4H, NCHpyr), 6.39 (t, ³*J*=2.0 Hz, 4H, CHpyr), 1.55 (s, 6H, 2CH₃). ¹³C-NMR (50 MHz, CDCl₃, δ): 155.3 (2C, Ca,b), 140.3 (2C, C2,7), 136.3 (2C, Cc,d), 120.9 (2C, C4,5), 120.1 (2C, C3,6), 119.8 (4C, N(CHpyr)), 115.5 (2C, C1,8), 110.5 (4C, CHpyr), 47.4 (C9), 27.3 (2CH₃). HRMS (ESI⁺): *m/z* calcd for C₂₃H₂₁N₂: 325.1699 [M+H]⁺; found 325.1700.



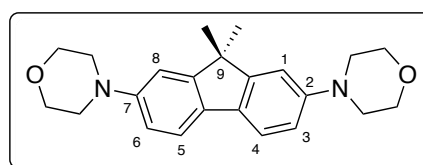
1,1'-(9,9-dimethyl-9H-fluorene-2,7-diyl)dipyrrolidine

(131): Eluent for flash chromatography (PE/EA = gradient up to 98:2, *R_f* = 0.38) providing **131** as a yellow solid (55 mg, 0.16 mmol, 59 %). ¹H-NMR (200 MHz, TFA-*d*¹, δ): 8.02 (d, ³*J*=8.5 Hz, 2H, H4,5), 7.88 (d, ⁴*J*=2.0 Hz, 2H, H1,8), 7.58 (dd, ³*J*=8.5 Hz, ⁴*J*=2.0 Hz, 2H, H3,6), 4.26 (br t, ³*J*=5.0 Hz, 4H, N(CH₂)₂), 3.79 (br t, ³*J*=5.0 Hz, 4H, N(CH₂)₂), 2.51 (m, 8H, 2N(CH₂CH₂)₂), 1.58 (s, 6H, 2CH₃). ¹³C-NMR (50 MHz, TFA-*d*¹, δ): 159.5 (2C, Ca,b), 142.3 (2C, Cc,d), 141.8 (2C, C2,7), 124.9 (2C, C4,5), 122.2 (2C, C3,6), 117.5 (2C, C1,8), 62.6 (4C, N(CH₂)), 50.5 (C9), 27.4 (2CH₃), 25.7 (4C, N(CH₂CH₂)). HRMS (ESI⁺): *m/z* calcd for C₂₃H₂₉N₂: 333.2321 [M+H]⁺; found 333.2325.



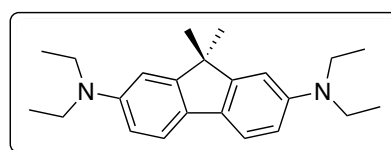
4,4'-(9,9-dimethyl-9H-fluorene-2,7-diyl)dimorpholine

(132): Eluent for flash chromatography (PE/EA= gradient up to 9:1, *R_f* = 0.16) providing **132** as a yellow solid (74 mg, 0.20 mmol, 73 %). ¹H-NMR (200 MHz, CDCl₃, δ): 7.52 (d, ³*J*=8.0 Hz, 2H, H4,5), 6.97 (d, ⁴*J*=2.0 Hz, 2H, H1,8), 6.87 (dd, ³*J*=8.0 Hz, ⁴*J*=2.0 Hz, 2H, H3,6), 3.90 (t, ³*J*=5.0 Hz, 8H, 2O(CH₂)₂), 3.21 (t, ³*J*=5.0 Hz, 8H, 2N(CH₂)₂), 1.45 (s, 6H, 2CH₃). ¹³C-NMR (50 MHz, CDCl₃, δ): 154.7 (2C), 150.5 (2C), 132.2 (2C), 119.8 (2C), 114.8 (2C), 110.7 (2C), 67.2 (4C), 50.3 (4C), 47.0, 27.8 (2C). HRMS (ESI⁺): *m/z* calcd for C₂₃H₂₉O₂N₂: 365.2224 [M+H]⁺; found 365.2226.



*N*²,*N*²,*N*⁷,*N*⁷-tetraethyl-9,9-dimethyl-9H-fluorene-2,7-

diamine (133): Eluent for flash chromatography (PE/EA = gradient up to 98:2, *R_f* = 0.34) providing **133** as a yellow solid (57 mg, 0.61 mmol, 61 %). ¹H-NMR (500 MHz, TFA-*d*¹,



δ): 8.14 (d, $^3J=8.0$ Hz, 2H, H4,5), 7.70 (s, 2H, H1,8), 7.58 (br d, $^3J=8.0$ Hz, 2H, H3,6), 3.92 (m, 4H, 2CH₂), 3.81 (m, 4H, 2CH₂), 1.66 (s, 6H, 2CH₃), 1.34 (t, 12H, $^3J=8.0$ Hz, (CH₂CH₃)₄). ¹³C-NMR (125 MHz, TFA-*d*¹, δ): 159.9 (2C), 142.6 (2C), 138.5 (2C), 125.6 (2C), 123.5 (2C), 118.6 (2C), 58.2 (2C), 50.6, 27.9 (2C), 11.4 (2C). GC-MS (*m/z*): 336.3 [M]⁺. HRMS (ESI⁺): *m/z* calcd for C₂₃H₃₃N₂: 337.2638 [M+H]⁺; found 337.2639.

General Procedure (GP-C):

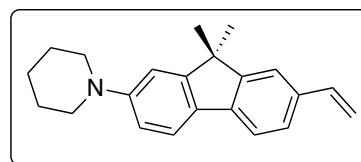
Sequential: General procedure **GP-A** was carried out, the mono-aminated bromoaromatic product was isolated. The pure product was further subjected to **GP-A** using another nucleophile (amine for a second Buchwald-Hartwig coupling or tributylvinyl tin for subsequent Stille coupling).

Sequential one-pot: Pd(OAc)₂ (4 mol%), *t*-BuONa (1.1 eq.), and BINAP (12 mol%) were added to a previously-dried reaction tube containing a magnetic bar. The tube was purged with argon for 3 cycles using Schlenk technique. The mixture was dissolved in toluene (0.1 M) and stirred for 15 min at rt under argon. Then, the dibromo aryl reagent (1 eq.) was added followed by 15 min further stirring (at rt or 100 °C for better activation). Finally, the amine (liquid or dissolved in toluene) (1.1 eq.) was added, and the reaction mixture was heated at 100 °C in an oil bath. The reaction was monitored by TLC and GCMS until *bis*-aminated product started to appear (between 12-16 h). Then, another loading of the catalytic system (4 mol% [Pd]/ 12 mol% L/ 1.1 eq. *t*-BuONa) was re-added followed by excess of second nucleophile (2 eq.). The final mixture was stirred at 100 °C overnight and monitored by TLC and GCMS until complete conversion. The reaction was cooled down to room temperature, diluted by CH₂Cl₂, and filtered over a pad of Celite®. The volatiles were removed under reduced pressure, and the residue was purified by silica gel column chromatography to give the desired product.

Following GP-C, 134-137 and 139-141 series of products were prepared on 100 mg scale (0.28 mmol).

1-(9,9-dimethyl-7-vinyl-9H-fluoren-2-yl)piperidine (134):

Eluent for flash chromatography (PE/EA = gradient up to 95:5, *R_f* = 0.71) providing **134** as a yellow solid (52 mg, 0.17 mmol, 62 %). ¹H-NMR (200 MHz, CDCl₃, δ): 7.59 (d, $^3J=8.0$ Hz, 1H),

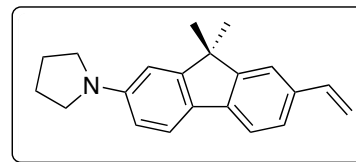


7.57 (d, $^3J=8.0$ Hz, 1H), 7.47 (br s, 1H), 7.36 (dd, $^3J=8.0$ Hz, $^4J=1.5$ Hz, 1H), 7.04 (d, $^4J=2.0$ Hz, 1H), 6.94 (dd, $^3J=8.0$ Hz, $^4J=2.0$ Hz, 1H), 6.82 (dd, $^3J_{trans}=17.5$ Hz, $^3J_{cis}=11.0$ Hz, 1H), 5.80 (d, $^3J_{trans}=17.5$ Hz, 1H), 5.24 (d, $^3J_{cis}=11.0$ Hz, 1H), 3.25 (t, $^3J=5.5$ Hz, 4H), 1.78 (br m, 4H), 1.65 (br m, 2H), 1.50

(s, 6H). $^{13}\text{C-NMR}$ (50 MHz, CDCl_3 , δ): 155.4, 153.6, 152.4, 139.6, 137.5, 135.3, 130.6, 125.7, 120.7, 120.1, 119.1, 115.5, 112.4, 111.1, 51.3 (2C), 46.8, 27.6 (2C), 26.1 (2C), 24.4. HRMS (ESI⁺): m/z calcd for $\text{C}_{22}\text{H}_{26}\text{N}$: 304.2061 [M+H]⁺; found 304.2060.

1-(9,9-dimethyl-7-vinyl-9H-fluoren-2-yl)pyrrolidine

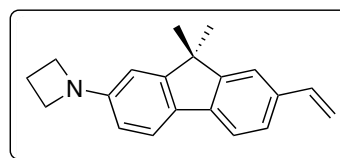
(135): Eluent for flash chromatography (PE/EA = gradient up to 95:5, R_f = 0.7) providing **135** as a yellow solid (43 mg, 0.15 mmol, 54 %). $^1\text{H-NMR}$ (200 MHz, CDCl_3 , δ): 7.54 (m, 2H), 7.43



(br s, 1H), 7.33 (dd, $^3J=8.0$ Hz, $^4J=1.5$ Hz, 1H), 6.78 (dd, $^3J_{trans}=17.0$ Hz, $^3J_{cis}=11.0$ Hz, 1H), 6.60 (d, $^4J=2.0$ Hz, 1H), 6.56 (dd, $^3J=8.0$ Hz, $^4J=2.0$ Hz, 1H), 5.75 (d, $^3J_{trans}=17.0$ Hz, 1H), 5.20 (d, $^3J_{cis}=11.0$ Hz, 1H), 3.38 (t, $^3J=6.5$ Hz, 4H), 2.04 (m, 4H), 1.48 (s, 6H). $^{13}\text{C-NMR}$ (50 MHz, CDCl_3 , δ): 156.0, 153.1, 148.1, 140.3, 137.8, 134.5, 126.9, 125.7, 121.1, 119.9, 118.4, 112.0, 110.8, 105.6, 48.1 (2C), 46.7, 27.7 (2C), 25.7 (2C). HRMS (ESI⁺): m/z calcd for $\text{C}_{21}\text{H}_{24}\text{N}$: 290.1903 [M+H]⁺; found 290.1903.

1-(9,9-dimethyl-7-vinyl-9H-fluoren-2-yl)azetidine **(136)**:

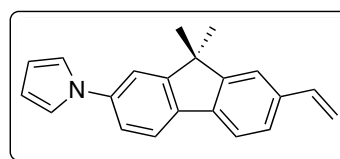
yellow solid (35 mg, 0.13 mmol, 46 %). $^1\text{H-NMR}$ (200 MHz, CDCl_3 , δ): 7.58 (d, $^3J=8.0$ Hz, 1H), 7.51 (d, $^3J=8.0$ Hz, 1H), 7.42 (br s, 1H), 7.33 (dd, $^3J=8.0$ Hz, $^4J=1.5$ Hz, 1H), 6.78 (dd, $^3J_{trans}=17.5$



Hz, $^3J_{cis}=11.0$ Hz, 1H), 6.47 (d, $^4J=2.0$ Hz, 1H), 6.42 (dd, $^3J=8.0$ Hz, $^4J=2.0$ Hz, 1H), 5.75 (d, $^3J_{trans}=17.5$ Hz, 1H), 5.20 (d, $^3J_{cis}=11.0$ Hz, 1H), 3.95 (t, $^3J=5.5$ Hz, 4H), 2.40 (quint, $^3J=5.5$ Hz, 2H), 1.46 (s, 6H). GC-MS (m/z): 275.1 [M]⁺.

1-(9,9-dimethyl-7-vinyl-9H-fluoren-2-yl)-1H-pyrrole **(137)**:

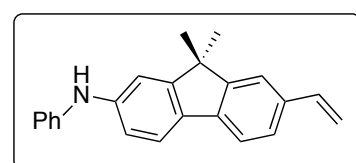
yellow solid (60 mg, 0.21 mmol, 76 %). $^1\text{H-NMR}$ (200 MHz, CDCl_3 , δ): 7.74 (d, $^3J=8.0$ Hz, 1H), 7.68 (d, $^3J=8.0$ Hz, 1H), 7.52 (s, 1H), 7.45-7.36 (m, 3H), 7.17 (t, $J=2.0$ Hz, 2H), 6.83 (dd, $^3J_{trans}=17.0$ Hz,



$^3J_{cis}=11.0$ Hz, 1H), 6.40 (t, $J=2.0$ Hz, 2H), 5.84 (d, $^3J_{trans}=17.0$ Hz, 1H), 5.30 (d, $^3J_{cis}=11.0$ Hz, 1H), 1.54 (s, 6H). $^{13}\text{C-NMR}$ (50 MHz, CDCl_3 , δ): 155.6, 154.1, 140.3, 138.4, 137.2, 136.9, 136.8, 125.9, 121.0, 120.4, 120.1, 119.9, 119.8 (2C), 115.5, 113.5, 110.5 (2C), 47.0, 27.5 (2C). HRMS (ESI⁺): m/z calcd for $\text{C}_{21}\text{H}_{20}\text{N}$: 286.1591 [M+H]⁺; found 286.1590.

9,9-dimethyl-N-phenyl-7-vinyl-9H-fluoren-2-amine **(139)**:

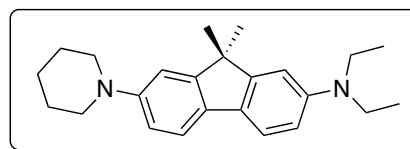
Eluent for flash chromatography (PE/DCM = gradient up to 9:1, R_f = 0.28) providing **139** as a yellow solid (60 mg, 0.19 mmol,



69 %). ¹H-NMR (200 MHz, CDCl₃, δ): 7.48 (d, ³J=8.0 Hz, 2H), 7.36 (s, 1H), 7.29-7.13 (m, 3H), 7.06-6.92 (m, 4H), 6.90-6.62 (m, 2H), 5.73 (br s, 1H, NH), 5.69 (d, ³J_{trans}=17.0 Hz, 1H), 5.15 (d, ³J_{cis}=11.0 Hz, 1H), 1.38 (s, 6H). ¹³C-NMR (50 MHz, CDCl₃, δ): 155.8, 153.6, 143.4, 142.7, 139.3, 137.4, 135.7, 132.4, 129.6 (2C), 125.8, 121.1, 121.0, 120.2, 119.2, 117.8 (2C), 117.0, 112.8, 112.4, 46.8, 27.4 (2C). HRMS (ESI⁺): *m/z* calcd for C₂₃H₂₂N: 312.1747 [M+H]⁺; found 312.1747.

***N,N*-diethyl-9,9-dimethyl-7-(piperidin-1-yl)-9H-**

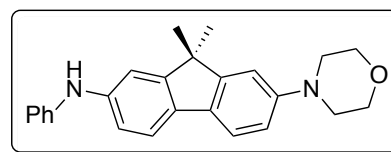
fluoren-2-amine (140): Eluent for flash chromatography (PE/Et₂O = 99:1, *R_f* = 0.12) providing **140** as a yellow solid (41 mg, 0.12 mmol, 43 %). ¹H-NMR (200 MHz, TFA-*d*, δ):



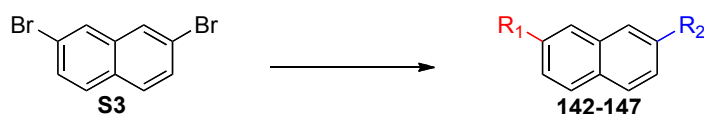
8.05-7.98 (m, 2H), 7.68-7.46 (m, 4H), 3.99-3.77 (m, 4H), 3.75-3.61 (m, 4H), 2.25-2.04 (m, 4H), 1.55 (s, 6H), 1.28-1.25 (m, 8H). ¹³C-NMR (125 MHz, TFA-*d*, δ): 159.9, 159.4, 143.7, 142.6, 142.2, 138.3, 125.4, 125.2, 123.3, 122.1, 118.4, 117.2, 61.2 (2C), 57.7 (2C), 50.4, 27.3 (2C), 25.9 (2C), 22.9, 11.4 (2C). HRMS (ESI⁺): *m/z* calcd for C₂₄H₃₃N₂: 349.2638 [M+H]⁺; found 349.2638.

9,9-dimethyl-7-morpholino-*N*-phenyl-9H-fluoren-2-

amine (141): Eluent for flash chromatography (PE/EA = gradient up to 9:1, *R_f* = 0.22) providing **141** as a yellow solid (62 mg, 0.18 mmol, 60 %). ¹H-NMR (200 MHz, CDCl₃, δ): 7.49



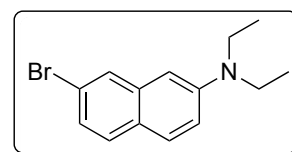
(d, ³J=8.0 Hz, 1H), 7.47 (d, ³J=8.0 Hz, 1H), 7.28-6.82 (m, 9H), 3.87 (t, ³J=5.0 Hz, 4H), 3.18 (t, ³J=5.0 Hz, 4H), 1.41 (s, 6H). ¹³C-NMR (50 MHz, CDCl₃, δ): 155.0, 154.7, 150.6, 143.9, 141.5, 133.2, 132.1, 129.5 (2C), 120.6, 120.0, 119.9, 117.6, 117.3 (2C), 114.8, 113.1, 110.7, 67.2 (2C), 50.2 (2C), 47.0, 27.6 (2C). HRMS (ESI⁺): *m/z* calcd for C₂₅H₂₇ON₂: 371.2118 [M+H]⁺; found 371.2120.



Scheme 2. 2,7-Naphthalene was prepared on (100 mg scale, 0.35 mmol of **S3**).

7-bromo-*N,N*-diethylnaphthalen-2-amine (142): Following **GP-A**.

Eluent for flash chromatography (PE/Et₂O = gradient up to 98:2, *R_f* = 0.49) providing **142** as a yellow solid (70 mg, 0.25 mmol, 72 %). ¹H-NMR (200 MHz, CDCl₃, δ): 7.76 (br s, 1H), 7.64 (d, ³J=9.0 Hz, 1H), 7.50

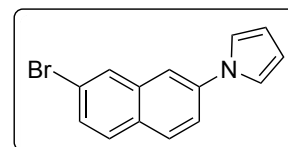


(d, ³J=8.5 Hz, 1H), 7.19 (dd, ³J=8.5 Hz, ⁴J=2.0 Hz, 1H), 7.08 (dd, ³J=9.0 ⁴J=2.5 Hz, 1H), 6.73 (d, ⁴J=2.0 Hz, 1H), 3.45 (q, ³J=7.0 Hz, 4H), 1.22 (t, ³J=7.0 Hz, 6H). ¹³C-NMR (50 MHz, CDCl₃, δ): 146.5,

136.8, 129.2, 129.0, 127.8, 124.7, 124.6, 120.4, 116.1, 104.2, 44.7 (2C), 12.8 (2C). HRMS (ESI⁺): m/z calcd for C₁₄H₁₇NBr: 278.0539 [M+H]⁺; found 278.0542.

1-(7-bromonaphthalen-2-yl)-1H-pyrrole (143): Following **GP-A**.

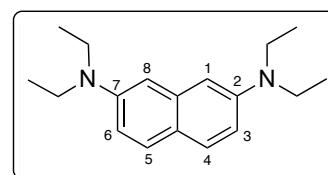
Eluent for flash chromatography (PE/Et₂O = gradient up to 98:2, R_f = 0.54) providing **143** as a yellow solid (79 mg, 0.29 mmol, 83 %). ¹H-NMR (200 MHz, CDCl₃, δ): 7.87 (br s, 1H), 7.74 (d, ³ J =9.0 Hz, 1H), 7.58



(d, ³ J =9.0 Hz, 1H), 7.56 (s, 1H), 7.47 (dd, ³ J =8.5 Hz, ⁴ J =2.0 Hz, 1H), 7.42 (dd, ³ J =8.5 Hz, ⁴ J =2.0 Hz, 1H), 7.10 (t, J =2.0 Hz, 2H), 6.32 (t, J =2.0 Hz, 2H). ¹³C-NMR (50 MHz, CDCl₃, δ): 139.1, 135.1, 129.8, 129.7 (2C), 129.5, 129.0, 121.3, 120.5, 119.5 (2C), 116.3, 111.1 (2C). HRMS (ESI⁺): m/z calcd for C₁₄H₁₁NBr: 272.0069 [M+H]⁺; found 272.0070.

N²,N²,N⁷,N⁷-tetraethylnaphthalene-2,7-diamine (144):

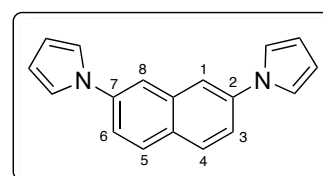
Following **GP-B**. Eluent for flash chromatography (PE/EA = gradient up to 95:5, R_f = 0.29) providing **144** as a yellow solid (62 mg, 0.23 mmol, 65 %). ¹H-NMR (200 MHz, TFA-*d*¹, δ): 8.30 (d,



³ J =9.0 Hz, 2H, H_{4,5}), 8.20 (s, 2H, H_{1,8}), 7.73 (d, ³ J =9.0 Hz, 2H, H_{3,6}), 3.85 (q, ³ J =6.5 Hz, 8H, 4CH₂), 1.23 (t, ³ J =6.5 Hz, 12H, 4CH₃). ¹³C-NMR (50 MHz, TFA-*d*¹, δ): 137.8 (2C), 136.5, 134.9 (2C), 134.8, 125.3 (2C), 121.5 (2C), 57.4 (4C), 11.3 (4C). HRMS (ESI⁺): m/z calcd for C₁₈H₂₇N₂: 271.2169 [M+H]⁺; found 271.2170.

2,7-di(1H-pyrrol-1-yl)naphthalene (145): Following **GP-B**.

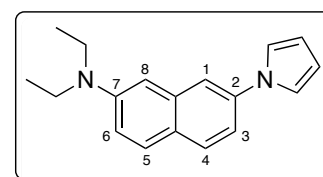
Eluent for flash chromatography (PE/EA = gradient up to 95:5, R_f = 0.5) providing **145** as a yellow solid (73 mg, 0.28 mmol, 81 %). ¹H-NMR (200 MHz, CDCl₃, δ): 7.81 (d, ³ J =9.0 Hz, 2H, H_{4,5}), 7.68



(br s, 2H, H_{1,8}), 7.47 (dd, ³ J =9.0 Hz, ⁴ J =2.0 Hz, 2H, H_{3,6}), 7.15 (t, J =2.0 Hz, 4H, NCH_{pyr}), 6.33 (t, J =2.0 Hz, 4H, CH_{pyr}). ¹³C-NMR (50 MHz, CDCl₃, δ): 139.3 (2C), 134.6, 129.6 (2C), 129.4, 119.9 (2C), 119.6 (4C), 117.0 (2C), 111.0 (4C). GC-MS (m/z): 258.1 [M]⁺.

N,N-diethyl-7-(1H-pyrrol-1-yl)naphthalen-2-amine (146):

Following **GP-C**. Eluent for flash chromatography (PE/EA = gradient up to 95:5, R_f = 0.51) providing **146** as a yellow solid (49 mg, 0.19 mmol, 53 %). ¹H-NMR (200 MHz, CDCl₃, δ): 7.70 (d, ³ J =8.5

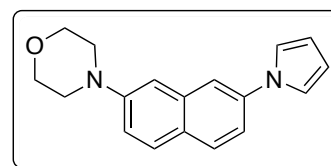


Hz, 1H), 7.68 (d, ³ J =8.5 Hz, 1H), 7.55 (d, ⁴ J =2.0 Hz, 1H), 7.26-7.15 (m, 3H), 7.05 (dd, ³ J =8.5 Hz, ⁴ J =2.0 Hz, 1H), 6.84 (d, ³ J =2.0 Hz, 1H), 7.13 (br s, 1H), 6.37 (t, ³ J =7.0 Hz, 2H), 3.47 (q, ³ J =5.0 Hz,

4H), 1.23 (t, $^3J=7.0$ Hz, 4H). HRMS (ESI⁺): m/z calcd for C₁₈H₂₁N₂: 265.1699 [M+H]⁺; found 265.1700.

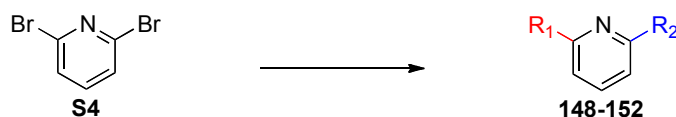
4-(7-(1H-pyrrol-1-yl)naphthalen-2-yl)morpholine (147):

Following **GP-C**. Eluent for flash chromatography (PE/EA = gradient up to 95:5, $R_f=0.13$) providing **147** as a yellow solid (62 mg, 0.22 mmol, 64 %).



¹H-NMR (200 MHz, CDCl₃, δ): 7.79 (d, $^3J=8.5$

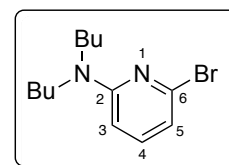
Hz, 1H), 7.76 (d, $^3J=8.5$ Hz, 1H), 7.66 (d, $^4J=2.0$ Hz, 1H), 7.41 (dd, $^3J=8.5$ Hz, $^4J=2.0$ Hz, 1H), 7.26 (m, 1H), 7.23 (t, $^3J=2.0$ Hz, 2H), 7.13 (br s, 1H), 6.41 (t, $^3J=2.0$ Hz, 2H), 3.94 (t, $^3J=5.0$ Hz, 4H), 3.30 (t, $^3J=5.0$ Hz, 4H). ¹³C-NMR (50 MHz, CDCl₃, δ): 150.1, 138.9, 135.2, 129.2, 128.8, 126.6, 119.7 (2C), 118.5, 117.8, 116.5, 110.6 (2C), 109.7, 67.0 (2C), 49.6 (2C). HRMS (ESI⁺): m/z calcd for C₁₈H₁₉ON₂: 279.1492 [M+H]⁺; found 279.1494.



Scheme 3. 1,5-Pyridine series was prepared on (100 mg scale, 0.39 mmol of **S4**).

6-bromo-N,N-dibutylpyridin-2-amine (148):^[288] Following **GP-A**.

Eluent for flash chromatography (CyHex, $R_f = 0.21$) providing **148** as a yellow solid (98 mg, 0.34 mmol, 88 %).

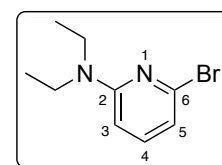


¹H-NMR (200 MHz, CDCl₃, δ): 7.18

(t, $^3J=8.0$ Hz, 1H, H₄), 6.58 (d, $^3J=8.0$ Hz, 1H, H₅), 6.29 (d, $^3J=8.0$ Hz, 1H, H₃), 3.39 (t, $^3J=7.5$ Hz, 4H, N(CH₂)₂), 1.55 (quint, $^3J=7.5$ Hz, 4H, N(CH₂CH₂)₂), 1.43-1.25 (m, 4H, (CH₃CH₂)₂), 0.95 (t, $^3J=7.0$ Hz, 6H, 2CH₃). ¹³C-NMR (50 MHz, CDCl₃, δ): 156.8, 140.4, 139.0, 113.5, 103.7, 48.4 (2C), 29.7 (2C), 20.3 (2C), 14.1 (2C). GC-MS (m/z): 286.1 [M+2]⁺.

6-bromo-N,N-diethylpyridin-2-amine (149):^[289] Following **GP-A**.

Eluent for flash chromatography (PE/DCM = gradient up to 9:1, $R_f = 0.5$) providing **149** as a yellow solid (84 mg, 0.36 mmol, 94 %).



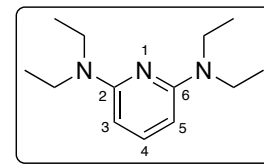
¹H-NMR (200 MHz, CDCl₃, δ): 7.10 (t, $^3J=8.0$ Hz, 1H, H₄), 6.50 (d, $^3J=8.0$ Hz, H₅), 6.23 (d, $^3J=8.0$ Hz, 1H,

H₃), 3.36 (q, $^3J=7.0$ Hz, 4H, 2CH₂), 1.06 (t, $^3J=7.0$ Hz, 6H, 2CH₃). ¹³C-NMR (50 MHz, CDCl₃, δ): 157.5, 140.4, 139.1, 113.6, 103.6, 42.5 (2C), 12.8 (2C). GC-MS (m/z): 230.1 [M+2]⁺.

***N*²,*N*²,*N*⁶,*N*⁶-tetraethylpyridine-2,6-diamine (150):**^[290] Following

GP-B. Eluent for flash chromatography (PE/Et₂O = gradient up to 98:2, *R*_f = 0.67) providing **150** as a yellow solid (69 mg, 0.31 mmol, 80 %).

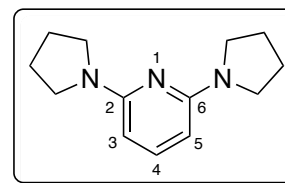
¹H-NMR (200 MHz, CDCl₃, δ): 7.23 (t, ³*J* = 8.0 Hz, 1H, H4), 5.72 (d, ³*J* = 8.0 Hz, 2H, H3,5), 3.47 (q, ³*J* = 7.0 Hz, 8H, 4CH₂), 1.16 (t, ³*J* = 7.0 Hz, 12H, 4CH₃). ¹³C-NMR (50 MHz, CDCl₃, δ): 156.8 (2C, C2,6), 138.4 (C4), 91.9 (2C, C3,5), 42.5 (4C, NCH₂), 13.4 (4C, 4CH₃). GC-MS (*m/z*): 222.2 [M]⁺.



2,6-di(pyrrolidin-1-yl)pyridine (151):^[127] Following **GP-B.** Eluent

for flash chromatography (PE/Et₂O = gradient up to 95/5, *R*_f = 0.47) providing **151** as a yellow solid (70 mg, 0.32 mmol, 83 %).

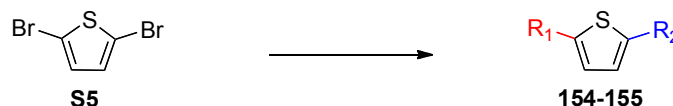
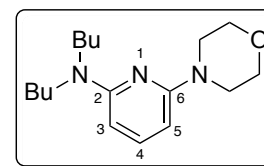
¹H-NMR (200 MHz, CDCl₃, δ): 7.25 (t, ³*J* = 8.0 Hz, 1H, H4), 5.64 (d, ³*J* = 8.0 Hz, 2H, H3,5), 3.43 (t, ³*J* = 6.5 Hz, 8H, 2N(CH₂)₂), 1.95 (q, ³*J* = 6.5 Hz, 8H, 2N(CH₂CH₂)₂). ¹³C-NMR (50 MHz, CDCl₃, δ): 157.0 (2C, C2,6), 138.1 (C4), 93.1 (2C, C3,5), 46.5 (4C, NCH₂), 25.7 (4C, CH₂). GC-MS (*m/z*): 217.2 [M]⁺.



***N,N*-dibutyl-6-morpholinopyridin-2-amine (152):** Following **GP-C.**

Eluent for flash chromatography (PE/Et₂O = gradient up to 9:1, *R*_f = 0.48) providing **152** as a yellow solid (108 mg, 0.27 mmol, 71 %).

¹H-NMR (200 MHz, CDCl₃, δ): 7.28 (t, ³*J* = 8.0 Hz, 1H, H4), 5.86 (d, ³*J* = 8.0 Hz, 2H, H3), 5.84 (d, ³*J* = 8.0 Hz, 2H, H5), 3.81 (t, ³*J* = 5.0 Hz, 4H, (CH₂)₂O), 3.44 (t, ³*J* = 5.0 Hz, 4H, (CH₂)₂N_{morph}), 3.38 (t, ³*J* = 7.5 Hz, 4H, N(CH₂)₂), 1.57 (quint, ³*J* = 7.5 Hz, 4H, N(CH₂CH₂)₂), 1.33 (m, 4H, (CH₃CH₂)₂), 0.94 (t, ³*J* = 7.5 Hz, 6H, 2CH₃). ¹³C-NMR (50 MHz, CDCl₃, δ): 158.7, 156.9, 138.7, 95.4, 92.9, 67.0 (2C), 48.7 (2C), 45.8 (2C), 30.1 (2C), 20.5 (2C), 14.2 (2C). HRMS (ESI⁺): *m/z* calcd for C₁₇H₃₀ON₃: 292.2383 [M+H]⁺; found 292.2384.

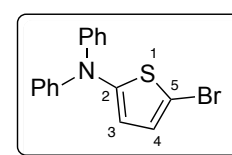


Scheme 4. Thiophenes were prepared on (100 mg scale, 0.41 mmol)

5-bromo-*N,N*-diphenylthiophen-2-amine (154): Following **GP-A.** Eluent

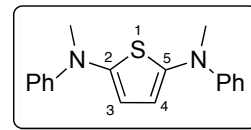
for flash chromatography (PE/Et₂O = gradient up to 99:1, *R*_f = 0.55) providing **154** as a yellow solid (72 mg, 0.22 mmol, 54 %).

¹H-NMR (200 MHz, CDCl₃, δ): 7.40-7.33 (m, 5H), 7.23-7.01 (m, 7H). ¹³C-NMR (50 MHz,



CDCl₃, δ): 146.5, 129.4, 129.3, 123.6, 123.0, 121.9, 108.8. GC-MS (*m/z*): 330.2 [M+2]⁺.

***N*²,*N*⁵-dimethyl-*N*²,*N*⁵-diphenylthiophene-2,5-diamine (155):**



Following **GP-B. 155** as a yellow solid (50 mg, 0.17 mmol, 42 %). ¹H-NMR (200 MHz, CDCl₃, δ): 7.20 (dd, ³*J*=7.5 Hz, ⁴*J*=2.0 Hz, 2H, Hphenyl), 6.95-6.82 (m, 8H, Hphenyl), 6.62 & 6.61 (d each, ⁴*J*=1.5 Hz, 2H, Hthiophene), 3.31 (s, 6H, 2CH₃). ¹³C-NMR (50 MHz, CDCl₃, δ): 153.7 (C2, C5), 149.4 (2C-*i*-Ph), 129.1 (4C-*m*-Ph), 125.9, 120.0 (C-*p*-Ph), 119.6 (C-*p*-Ph), 118.8, 116.4, 42.1 (2CH₃). GC-MS (*m/z*): 294.1 [M+2]⁺.

7-(benzo[*c*][1,2,5]thiadiazol-5-yl)-9,9-dimethyl-*N*-phenyl-9*H*-fluoren-2-amine (159):

This procedure requires the preparation of two reactions in two previously-dried tubes.

First tube: Pd(OAc)₂ (3 mg, 0.011 mmol, 4 mol%), *t*-BuONa (30 mg, 0.32 mmol, 1.1 eq.), and BINAP (21 mg, 0.034 mmol, 12 mol%) were added to a previously-dried reaction tube containing a magnetic bar. The tube was purged with argon for 3 cycles using Schlenk technique. The mixture was dissolved in 3 mL of toluene (0.1 M) and stirred for 15 min at rt under argon. Then, dibromofluorene **44** (100 mg, 0.287 mmol, 1.0 eq.) was added followed by 15 min further stirring at 100 °C. Finally, aniline (30 mg, 0.32 mmol, 1.1 eq.) was added, and the reaction mixture was heated at 100 °C in an oil bath. The reaction was monitored by TLC and GCMS until *bis*-aminated product started to appear (14 h).

Second tube: Pd(OAc)₂ (4 mg, 0.017 mmol, 4 mol% relative to 1.5 eq. of 5-bromo-2,1,3-benzothiadiazole), *t*-BuONa (45 mg, 0.47 mmol, 1.1 eq.), and BINAP (32 mg, 0.051 mmol, 12 mol%) were added to a previously-dried reaction tube containing a magnetic bar. The tube was purged with argon for 3 cycles using Schlenk technique. The mixture was dissolved in 4 mL of toluene (0.1 M) and stirred for 15 min at rt under argon. Then, 5-bromo-2,1,3-benzothiadiazole (92 mg, 0.43 mmol, 1.5 eq.) was added followed by 15 min further stirring at 100 °C. Finally, bis(tributyltin) (249 mg, 0.43 mmol, 1.5 eq.) was added, and the reaction mixture was heated at 100 °C in an oil bath for 4 h.

Note: this second reaction tube was prepared around 10 h after the beginning of the first reaction.

Then, another loading of the catalytic system (4 mol% [Pd]/ 12 mol% L/ 1.1 eq. *t*-BuONa) was re-added to the first reaction tube followed by the content of the second tube (2 eq.). The final mixture was stirred at 100 °C overnight. The reaction was cooled down to room temperature, quenched with NaOH (1N) and stirred for additional 30 min. The organic layer was extracted with DCM (2x) and the combined extracts were washed with water (3x), dried over magnesium sulfate, and evaporated under reduced pressure. The crude product was purified by flash

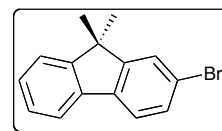
chromatography on silica gel eluted with CyHex/EA (4/1, v/v) to provide compound **159** (61 mg, 51 %) as a bright yellow solid. Purification by RP-HPLC provided an analytical sample for photophysical characterization; (apparatus: Waters™ 600 Controller with Waters™ 996 Photodiode Array Detector and Jasco LC-Net II / ADC, semi-preparative column: Clarity® 5µ Oligo-RP column 250 x 10 mm Phenomenex®, flow rate 2.5 mL/min, using the following gradient system: 25 % A –(5min)→ 5 % A / 95 % B –(25 min)→ 100 % B –(10 min) with A= 0.25 CH₃CN: 0.75 MilliQ® water and B= CH₃CN. ¹H-NMR (500 MHz, CD₂Cl₂, δ): 8.24 (d, ⁴J=1.0 Hz, 1H), 8.07 (d, ³J=8.0 Hz, 1H), 8.01 (dd, ³J=8.0 Hz, ⁴J=1.0 Hz, 1H), 7.78 (d, ⁴J=1.0 Hz, 1H), 7.76 (d, ³J=8.0 Hz, 1H), 7.31 (t, ³J=7.5 Hz, 2H), 7.22 (d, ⁴J=1.5 Hz, 1H), 7.15 (dd, ³J=7.5 Hz, ⁴J=1.0 Hz, 2H), 7.08 (dd, ³J=8.0 Hz, ⁴J=1.5 Hz, 1H), 6.96 (t, ³J=7.5 Hz, 1H), 1.54 (s, 6H). ¹³C-NMR (126 MHz, CD₂Cl₂, δ): 156.3, 156.1, 154.7, 154.6, 143.7, 143.5, 143.3, 140.2, 137.6, 131.9, 130.7, 129.8, 127.0, 122.0, 121.7, 121.6, 121.5, 119.9, 118.3, 118.3, 117.0, 112.2, 47.4, 27.5. HRMS (ESI⁺): *m/z* calcd for C₂₇H₂₂N₃S: 420.1529 [M+H]⁺; found 420.1530.

X. Chapter 3 synthetic procedures

General Procedure (GP-D): 7-amino-9,9-dimethyl-9*H*-fluorene-2-carbaldehyde (1 eq.), malononitrile (2 eq.), and basic aluminum oxide (4 eq.) were stirred in toluene (0.2 M) overnight at 70 °C. After cooling down to room temperature, the reaction mixture solution was filtered and the volatiles were reduced in vacuo. The crude was purified by silica gel column chromatography to provide the desired product as a bright red solid.^[113]

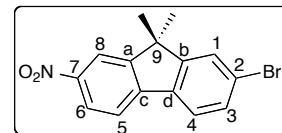
General Procedure (GP-E): Same as **GP-A** on 7-bromo-9,9-dimethyl-9*H*-fluorene-2-carbaldehyde **169**. Excess of amine and the catalytic system can be added e.g. 5-10 mol % Pd, 15-30 mol % L, 1.4 eq. Base, 2 eq. amine to ensure highest possible yields with challenging amines since there is no risk of deamination or selectivity issues with this monobromo starting material.

2-Bromo-9,9-dimethylfluorene (34). **33** (9.00 g, 36.7 mmol, 1 eq.) was dissolved in 65 mL of DMSO at 60 °C. Potassium iodide (610 mg, 3.7 mmol, 0.1 eq.) and iodomethane (11.8 g, 82.6 mmol, 2.25 eq.) were then added; finally, powdered potassium hydroxide (146.8 mmol, 8.3 g, 4 eq.) was slowly added. The reaction was stirred at room temperature overnight. Then, the mixture was poured into 500 mL of water, a light yellow precipitate was formed. The solid was filtered, washed with water, and dried under vacuum. The light yellow solid was purified by crystallization from methanol to give product **34** (9.35 g, 93 %) as white crystals. ¹H-NMR (200 MHz, CDCl₃, δ): 7.72-7.68 (m, 1H),



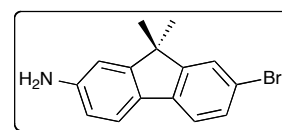
7.61-7.58 (m, 2H), 7.50-7.40 (m, 2H), 7.37-7.33 (m, 2H), 1.49 (s, 6H). ¹³C-NMR (50 MHz, CDCl₃, δ): 155.8, 153.3, 138.3, 138.3, 130.2, 127.8, 127.3, 126.3, 122.8, 121.5, 121.1, 120.2, 47.2, 27.1 (2C). GC-MS (*m/z*): 274.2 [M+2]⁺.

2-Bromo-9,9-dimethyl-7-nitrofluorene (35). 34 (5.00 g, 18.3 mmol)



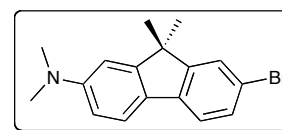
was dissolved in 100 mL of glacial acetic acid. To the formed solution, 15 mL of fuming nitric acid were added drop-wise (~10 min) at 0 °C upon vigorous stirring. After addition was completed, reaction mixture was further stirred at rt. Yellow-green residue appeared in 30 min. The reaction was monitored by TLC (solvent EA/PE=1/9, *R_f*≈0.6). After appearance of the spot of dinitroproduct (~100 min, *R_f*≈0.25), the mixture was poured into 600 mL of water. Formed residue was filtered off, washed with water, and recrystallized from 200 mL acetonitrile to give compound **35** (4.25 g, 73 %) as yellow needle crystals. ¹H-NMR (200 MHz, CDCl₃, δ): 8.28 (s, 1H, H8), 8.26 (dd, ³*J*=7.0 Hz ⁴*J*=2.0 Hz, 1H, H6), 7.79 (br d, ³*J*=7.0 Hz, 1H, H5), 7.66 (d, ³*J*=8.0 Hz, 1H, H4), 7.63 (d, ⁴*J*=1.5 Hz, 1H, H1), 7.53 (dd, ³*J*=8.0 Hz ⁴*J*=1.5 Hz, 1H, H3), 1.53 (s, 6H, 2CH₃). ¹³C-NMR (50 MHz, CDCl₃, δ): 157.1 (Cb), 154.4 (Ca), 147.5 (C7), 144.7 (Cc), 135.9 (Cd), 131.0 (C3), 126.7 (C1), 123.8 (C2), 123.7 (C6), 122.9 (C4), 120.4 (C5), 118.5 (C8), 47.7 (C9), 26.8 (2C, 2CH₃). GC-MS (*m/z*): 319.2 [M+2]⁺.

7-Bromo-9,9-dimethylfluorenyl-2-amine (36). A mixture of **35** (2.00 g, 6.23 mmol, 1 eq.), iron powder (1.00 g, 18.7 mmol, 3 eq.), and NH₄Cl (740 mg, 12.46 mmol, 2 eq.) was refluxed in aqueous ethanol



(90 mL of alcohol and 25 mL of water) at 85 °C for 2 h under inert atmosphere. The completion of the reaction was monitored by TLC (solvent Tol/DCM=9/1, *R_f*=0.26). The mixture was treated with sat. aq. NaHCO₃ and filtered through filter paper. The resulting transparent solution was concentrated under vacuum in order to remove ethanol. Formed residue was filtered off to yield compound **4** (1.31g, 72 %) as transparent plates. The crude product was batched directly in the next step without further purification. ¹H-NMR (200 MHz, CDCl₃, δ): 7.53-7.37 (m, 4H), 6.73 (d, ⁴*J*=2.0 Hz, 1H), 6.65 (dd, ³*J*=8.0 Hz ⁴*J*=2.0 Hz, 1H), 1.43 (s, 6H). ¹³C-NMR (50 MHz, CDCl₃, δ): 155.3, 154.9, 146.5, 138.7, 129.9, 129.1, 125.9, 121.1, 120.1, 119.1, 114.2, 109.4, 46.9, 27.2 (2C). GC-MS (*m/z*): 289.1 [M+2]⁺.

7-bromo-*N,N*,9,9-tetramethyl-9*H*-fluoren-2-amine (160). To the stirred mixture of **36** (750 mg, 2.60 mmol, 1 eq.) and paraformaldehyde (390 mg, 13.0 mmol, 5 eq.) in glacial acetic acid (10 mL) at 0 °C, NaBH₃CN (492 mg, 7.80 mmol, 3 eq.) was added in small

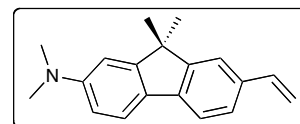


portions. The mixture was allowed to warm up to room temperature and stirred overnight before being poured into cold water (150 mL). Formed solution was extracted with ethyl acetate

(3*30 mL). Combined organic layer was washed with sat. aq. NaHCO₃ solution and dried with magnesium sulfate. Organic solvent was removed under reduced pressure and the obtained residue was purified by crystallization from ethanol to give the product **160** (720 mg, 87 %) as white crystals. Eluent (Tol/DCM = 9:1, *R_f* = 0.71). ¹H-NMR (200 MHz, CDCl₃, δ): 7.56 (d, ³*J* = 8.0 Hz, 1H), 7.49 (d, ⁴*J* = 1.0 Hz, 1H), 7.43-7.37 (m, 2H), 6.76 (s, 1H), 6.74 (dd, ³*J* = 8.0 Hz ⁴*J* = 2.0 Hz, 1H), 3.04 (s, 6H), 1.43 (s, 6H). ¹³C-NMR (50 MHz, CDCl₃, δ): 155.1, 155.1, 150.6, 138.9, 130.0, 127.6, 125.9, 120.9, 120.1, 118.9, 111.9, 106.8, 47.1, 41.2 (2C), 27.5 (2C). GC-MS (*m/z*): 265.2 [M+2]⁺.

***N,N*,9,9-tetramethyl-7-vinyl-9*H*-fluoren-2-amine (161/I-6).** 160

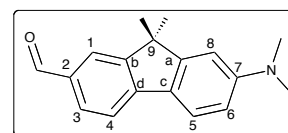
(100 mg, 0.32 mmol, 1 eq.) and Pd(PPh₃)₄ (19 mg, 0.016 mmol, 5 mol %)



were purged under argon and dissolved in dry toluene (2 mL). Then, tributylvinyltin (107 μL, 0.32 mmol, 1 eq.) was added and the mixture was heated to 80 °C overnight. The crude was quenched by NaOH (1 N) and stirred for additional 30 mins, then extracted with toluene. The organic extract was washed with water (3x), dried by magnesium sulfate, and evaporated under reduced pressure. Residue was purified by column chromatography. Eluent (DCM/CyHex = 1:1, *R_f* = 0.37) to provide compound **I-6** (66 mg, 80 %) as a brown solid. ¹H-NMR (200 MHz, CDCl₃, δ): 7.59-7.51 (m, 2H), 7.43 (s, 1H), 7.35 (d, ⁴*J* = 2.0 Hz, 1H), 6.86-6.70 (m, 3H), 5.75 (d, ³*J_{trans}* = 20.0 Hz, 1H), 5.20 (d, ³*J_{cis}* = 10.0 Hz, 1H), 3.04 (s, 6H), 1.48 (s, 6H). ¹³C-NMR (50 MHz, CDCl₃, δ): 155.7, 153.3, 150.7, 140.0, 137.6, 134.9, 128.1, 125.7, 120.9, 119.9, 118.7, 112.2, 111.7, 106.7, 46.8, 41.1 (2C), 27.7 (2C). HRMS (ESI⁺): *m/z* calcd for C₁₉H₂₂N: 264.1747 [M+H]⁺; found 264.1746.

7-dimethylamino)-9,9-dimethyl-9*H*-fluorene-2-carbaldehyde

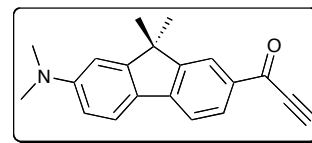
(162/PP1). 160 (1.00 g, 3.16 mmol, 1 eq.) was dissolved in dry THF (15 mL). To the resulted clear yellow solution, *n*BuLi (1.52 mL of 2.5M



solution in Hexane, 1.2 eq.) was added dropwise at -78 °C under inert atmosphere. Reaction mixture was stirred for 1h before a yellow precipitate was formed. Then, DMF (0.49 mL, 6.32 mmol, 2 eq.) was added dropwise and the formed solution was stirred for additional 2 h at -78 °C. The reaction was allowed to warm up to room temperature and stirred for 1 h, quenched with 1 M aqueous HCl and extracted with EA (2x). Organic layer was dried over MgSO₄ and evaporated in vacuum. The residue was purified by column chromatography. Eluent (EA/CyHex = 1:9, *R_f* = 0.47) to produce compound **PP1** (588 mg, 70 %) as a yellow powder. ¹H-NMR (200 MHz, CDCl₃, δ): 10.03 (s, 1H, CHO), 7.95 (br s, 1H, H1), 7.82 (dd, ³*J* = 7.5 Hz ⁴*J* = 1.0 Hz, 1H, H3), 7.68 (d, ³*J* = 7.5 Hz, 1H, H4), 7.66 (d, ³*J* = 8.0 Hz, 1H, H5), 6.78 (br s, 1H, H8), 6.75 (dd, ³*J* = 8.0 Hz ⁴*J* = 1.0 Hz, 1H, H6), 3.09 (s, 6H, N(CH₃)₂), 1.54 (s, 6H, 2CH₃). ¹³C-NMR (50 MHz, CDCl₃, δ): 192.0 (C=O), 157.1 (Ca), 153.4 (Cb), 151.6 (C7), 146.8 (Cd), 133.7 (C2), 131.2 (C3), 126.1 (Cc), 122.5 (C1),

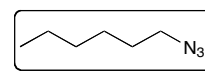
122.2 (C5), 118.4 (C4), 111.8 (C6), 105.8 (C8), 46.7 (C9), 40.6 (2C, N(CH₃)₂), 27.3 (2C, 2CH₃). GC-MS (*m/z*): 265 [M⁺].

1-(7-(dimethylamino)-9,9-dimethyl-9H-fluoren-2-yl)prop-2-yn-1-one (163/PP2). Ethynylmagnesium bromide (3.16 mL, 0.5 M in THF, 1.58 mmol, 1.4 eq.) was added dropwise to a solution of



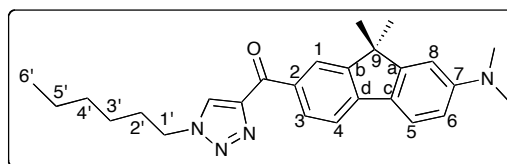
carbaldehyde 162 (300 mg, 1.13 mmol, 1 eq.) in THF (2.5 mL) at 0 °C. The mixture was stirred at the same temperature until completion of the reaction monitored by TLC (2h). Then, a saturated solution of aq. NH₄Cl (3 mL) was added and the aqueous phase was extracted with EA (3x5 mL). The combined extracts were dried (magnesium sulfate) and evaporated to yield the corresponding propargyl alcohol. The crude propargyl alcohol was batched to the next step without further purification. To a stirred suspension of MnO₂ (0.5 g, 15 eq.) in DCE (8 mL), was added dropwise a solution of the residue in DCE (3 mL). The mixture was stirred for 1 h at 0 °C, filtered through a pad of Celite®, dried over MgSO₄, and concentrated in vacuo to yield the pure ketone **PP2** (320 mg, 98 %, two steps). *R_f*= 0.55, solvent (PE/EA = 6:1). ¹H-NMR (200 MHz, CDCl₃, δ): 8.18-8.13 (m, 2H), 7.68-7.61 (m, 2H), 6.76-6.73 (br d, 2H), 3.41 (s, 1H), 3.08 (s, 6H), 1.50 (s, 6H). ¹³C-NMR (50 MHz, CDCl₃, δ): 177.0, 157.4, 153.1, 151.7, 147.0, 133.4, 130.9, 126.1, 123.0, 122.4, 118.2, 111.7, 105.9, 81.0, 80.1, 46.8, 40.7 (2C), 27.3 (2C). HRMS (ESI⁺): *m/z* calcd for C₂₀H₂₀ON: 290.1539 [M+H]⁺; found 290.1539.

1-azidohexane (S5). To a solution of sodium azide (1.73 g, 26.6 mmol, 1.1 eq.) in DMSO (53 mL), was added 1-bromohexane (4.00 g, 24.2 mmol, 1 eq.)



and the resulting solution was stirred overnight at rt. The conversion was monitored by ¹³C-NMR until completion (20 h). The mixture was poured into 100 mL of water and extracted with diethyl ether (2x30 mL). The combined organic layer was dried over MgSO₄ and concentrated at reduced pressure to get a yellow liquid, which was further purified by distillation to afford the title product **S5** as colorless oil (2.28 g, 74 %). ¹H-NMR (200 MHz, CDCl₃, δ): 3.18 (t, ³J=7.0 Hz, 2H), 1.52 (q, ³J=7.0 Hz, 2H), 1.36–1.09 (m, 6H), 0.82 (t, ³J=7.0 Hz, 3H). ¹³C-NMR (50 MHz, CDCl₃, δ): 51.3, 31.2, 28.6, 26.2, 22.3, 13.9.

(7-(dimethylamino)-9,9-dimethyl-9H-fluoren-2-yl)(1-hexyl-1H-1,2,3-triazol-4-yl)methanone (164/PP3). To a stirred solution of *n*-hexyl azide

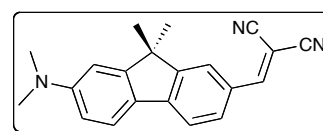


S5 (30 mg, 0.23 mmol, 1.1 eq.) in DCE (1 mL) at 0 °C under argon, was added dropwise a solution of **163** (60 mg, 0.21 mmol, 1 eq.) in DCE (1 mL). Then, DIEA (0.18 mL, 1.4 mmol, 5 eq.), CuI (78 mg, 0.41 mmol, 2 eq.), and AcOH (12 μL, 0.1 mmol, 1 eq.) were sequentially added. The reaction mixture was stirred for 3 h at rt, filtered over

a pad of Decalite®, and washed with DCM. The volatiles were reduced in *vacuo* and the resulting crude was purified by flash chromatography on silica gel eluted with (CyHex/EA = 94:6, R_f = 0.15) to provide **PP3** (30 mg, 70 %) as a yellow powder. $^1\text{H-NMR}$ (200 MHz, CDCl_3 , δ): 8.55 (dd, $^3J=8.0$ $^4J=1.5$ Hz, 1H, H3), 8.52 (d, $^4J=1.5$ Hz, 1H, H1), 8.25 (s, 1H, H_{triazole}), 7.67 (d, $^3J=8.0$ Hz, 2H, H4,5), 6.77 (s, 1H, H8), 6.75 (d, $^3J=8.0$ Hz, 1H, H6), 4.45 (t, $^3J=7.0$ Hz, 2H, H1'), 3.07 (s, 6H, $\text{N}(\text{CH}_3)_2$), 1.98 (m, 2H, H2'), 1.53 (s, 6H, 2 CH_3), 1.36-1.26 (m, 6H, H3',4',5'), 0.90 (t, $^3J=7.0$ Hz, 3H, H6'). $^{13}\text{C-NMR}$ (50 MHz, CDCl_3 , δ): 185.3 (C=O), 157.2 (Ca), 152.9 (Cb), 151.5 (C7), 148.9 (C=CH), 145.6 (Cd), 133.5 (C2), 131.3 (C3), 128.1 (C=CH), 126.9 (Cc), 124.5 (C1), 122.2 (C5), 118.1 (C4), 111.7 (C6), 106.2 (C8), 50.7 (C1'), 47.0 (C9), 40.9 (2C, $\text{N}(\text{CH}_3)_2$), 31.2 (C4'), 30.3 (C2'), 27.5 (2C, 2 CH_3), 26.2 (C3'), 22.5 (C5'), 14.1 (C6'). HRMS (ESI⁺): m/z calcd for $\text{C}_{26}\text{H}_{33}\text{N}_4\text{O}$: 417.2649 [M+H]⁺; found 417.2649.

2-((7-(dimethylamino)-9,9-dimethyl-9H-fluoren-2-

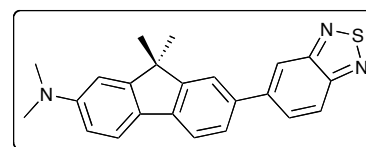
yl)methylene)malononitrile (**165/PP4**). Starting material: **160**, following **GP-D**. Eluent for flash chromatography (CyHex/EA = 9:1,



R_f = 0.2) providing **PP4** as red solid (85 %). $^1\text{H-NMR}$ (200 MHz, CDCl_3 , δ): 7.91 (s, 1H), 7.77 (dd, $^3J=8.0$ Hz $^4J=1.5$ Hz, 1H), 7.72 (s, 1H), 7.67-7.60 (m, 2H), 6.76-6.71 (m, 2H), 3.10 (s, 6H), 1.49 (s, 6H). $^{13}\text{C-NMR}$ (50 MHz, CDCl_3 , δ): 159.8, 157.8, 153.9, 152.2, 147.8, 132.3, 127.9, 125.8, 124.2, 122.8, 119.1, 115.1, 114.1, 111.8, 105.7, 77.7, 47.0, 40.7 (2C), 27.3 (2C). HRMS (ESI⁺): m/z calcd for $\text{C}_{21}\text{H}_{20}\text{N}_3$: 314.1652 [M+H]⁺; found 314.1652.

7-(benzo[*c*][1,2,5]thiadiazol-5-yl)-*N,N*,9,9-tetramethyl-9H-

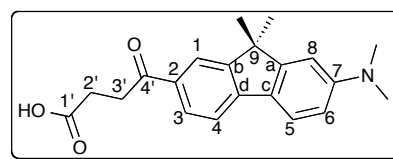
fluoren-2-amine (**166/PP5**). To a stirred solution of **160** (100 mg, 0.32 mmol, 1 eq.) and $\text{Pd}(\text{PPh}_3)_4$ (37 mg, 0.032 mmol,



10 mol%) in toluene (2 mL) under argon, was added dropwise bis(tributyltin) (210 μL , 0.41 mmol, 1 eq.) and the mixture was heated at 100 °C for 3 h. Then, additional $\text{Pd}(\text{PPh}_3)_4$ (37 mg, 0.032 mmol, 10 mol %) and 5-bromo-2,1,3-benzothiadiazole (137 mg, 0.64, 2 eq.) were sequentially added. The reaction mixture was heated at 100 °C overnight. The resulting solution was quenched with NaOH (1N) and stirred for additional 30 min. The organic layer was extracted with DCM (2x) and the combined extracts were washed with water (3x), dried over magnesium sulfate, and evaporated under reduced pressure. The crude was purified by flash chromatography on silica gel eluted with (CyHex/EA = 4:1, R_f = 0.55) to provide compound **PP5** (97 mg, 82 %) as a bright yellow solid. $^1\text{H-NMR}$ (200 MHz, CDCl_3 , δ): 8.22 (d, $^4J=1.0$ Hz, 1H), 8.07 (dd, $^3J=8.5$ Hz $^4J=1.0$ Hz, 1H), 7.98 (dd, $^3J=9.0$ Hz $^4J=1.5$ Hz, 1H), 7.72-7.62 (m, 4H), 6.80 (d, $^4J=2.0$ Hz, 1H), 6.76 (dd, $^3J=8.5$ Hz $^4J=2.0$ Hz, 1H), 3.06 (s, 6H), 1.54 (s, 6H). $^{13}\text{C-NMR}$ (50 MHz, CDCl_3 , δ): 155.9, 155.8, 154.3, 153.97, 151.0, 143.3, 140.6, 136.4, 130.7, 127.4, 126.7,

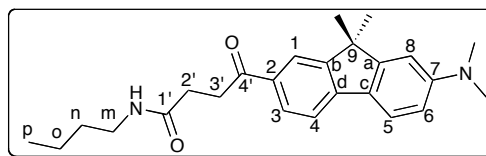
121.5, 121.4, 121.3, 119.2, 118.0, 111.7, 106.5, 47.1, 41.1 (2C), 27.7 (2C). HRMS (ESI⁺): *m/z* calcd for C₂₃H₂₂N₃S: 372.1529 [M+H]⁺; found 372.1532.

4-(7-(dimethylamino)-9,9-dimethyl-9H-fluoren-2-yl)-4-oxobutanoic acid (167).



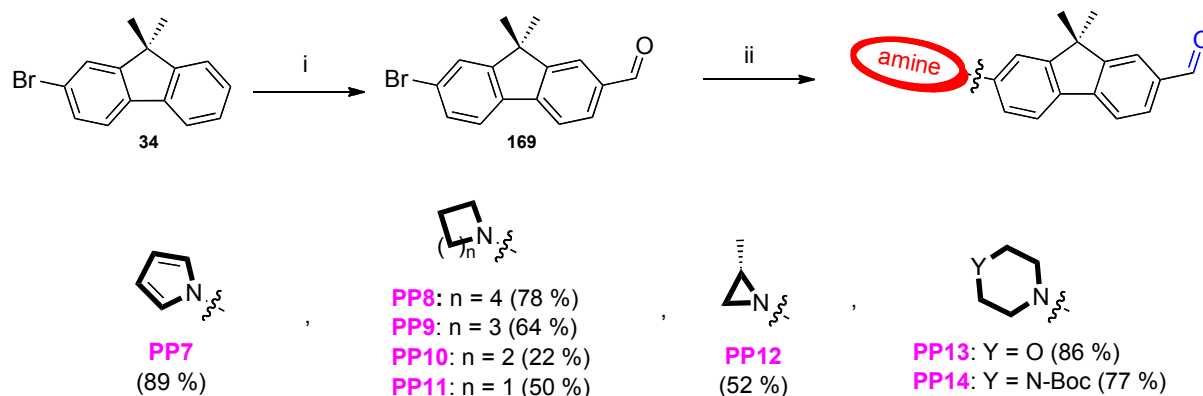
To a stirred solution of **160** (0.8 g, 2.5 mmol, 1 eq.) in THF (12 mL) under argon, were sequentially added preactivated magnesium turnings (120 mg, 5.0 mmol, 2 eq.) and 3 drops of BrCH₂CH₂Br. The reaction was initiated by heating to 50 °C. Once Grignard reagent started to form, the mixture was stirred at room temperature for 1 h. Then, the resulting solution was transferred dropwise, via a cannula over 30 min, to a solution of succinic anhydride (505 mg, 5.0 mmol, 2 eq.) in dry THF (12 mL) at -10 °C under argon. The reaction mixture was stirred for 2 h at 0 °C, and warmed up gradually to rt, before quenching by aq. HCl (1M) solution. The organic layer was extracted with chloroform (2x), dried over magnesium sulfate, filtered and concentrated under reduced pressure. The crude was purified by flash chromatography on silica gel eluted with DCM/MeOH (100/0 → 95/5, v/v) to provide the title compound **167** (510 mg, 60 %) as a yellow powder. *R_f* = 0.43 (DCM/MeOH = 98/2); ¹H NMR (200 MHz, MeOD-*d*⁴, δ): 7.85 (br s, 1H, H1), 7.76 (dd, ³*J*=8.0 Hz ⁴*J*=1.0 Hz, 1H, H3), 7.69 (d, ³*J*=8.0 Hz, 1H, H5), 7.60 (d, ³*J*=8.0 Hz, 1H, H4), 7.47 (br s, 1H, H8), 7.23 (dd, ³*J*=8.0 Hz ⁴*J*=2.0 Hz, 1H, H6), 3.10 (t, ³*J*=6.0 Hz, 2H, H3'), 3.04 (s, 6H, N(CH₃)₂), 2.45 (t, ³*J*=6.0 Hz, 2H, H2') 1.25 (s, 6H, 2CH₃). ¹H NMR (200 MHz, DMSO-*d*⁶, δ): 8.03 (d, ⁴*J*=1.0 Hz, 1H, H1), 7.92 (dd, ³*J*=8.0 Hz ⁴*J*=1.0 Hz, 1H, H3), 7.72 (d, ³*J*=8.0 Hz, 1H, H5), 7.70 (d, ³*J*=8.0 Hz, 1H, H4), 6.91 (d, ⁴*J*=2.0 Hz, 1H, H8), 6.74 (dd, ³*J*=8.0 Hz ⁴*J*=2.0 Hz, 1H, H6), 3.27 (t, ³*J*=6.0 Hz, 2H, H3'), 3.00 (s, 6H, N(CH₃)₂), 2.58 (t, ³*J*=6.0 Hz, 2H, H2') 1.44 (s, 6H, 2CH₃). ¹³C-NMR (50 MHz, MeOD-*d*⁴, δ): 200.1, 176.2, 158.4, 155.3, 145.6, 143.7, 138.4, 137.3, 129.0, 123.7, 123.3, 121.4, 119.5, 114.9, 46.2 (2C), 34.5, 29.8 (2C), 29.0, 27.0. ¹³C-NMR (50 MHz, DMSO-*d*⁶, δ): 197.7, 174.0, 156.5, 152.6, 151.2, 144.5, 133.4, 127.9, 125.7, 122.0, 121.8, 118.2, 111.6, 106.3, 46.4 (2C), 33.0, 28.0, 27.7, 27.0 (2C). MS (ESI⁺, MeOH): *m/z*: 338,17 [M+H]⁺.

***N*-butyl-4-(7-(dimethylamino)-9,9-dimethyl-9H-fluoren-2-yl)-4-oxobutanamide (168/PP6).**



167 (50 mg, 0.15 mmol, 1 eq.), DIC (26 μL, 0.16 mmol, 1.1 eq.), HOBT (25 mg, 0.16 mmol, 1.1 eq.), and Et₃N (23 μL, 0.16 mmol, 1.1 eq.) were solubilized in 2 mL dry THF and stirred for 30 mins. *n*BuNH₂ (23 μL, 0.22 mmol, 1.5 eq.) was then added and the reaction was stirred overnight. The crude was washed by NaHCO₃ (aq.) and extracted with DCM. The organic layer was washed by water, dried with magnesium sulfate, and reduced under pressure. Purification was done by FC eluent

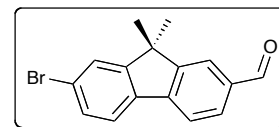
(DCM/MeOH = 99:1) to afford compound **PP6** (42 mg, 72 %) as a yellow solid. ¹H NMR (200 MHz, CDCl₃, δ): 7.98 (s, 1H, H₁), 7.95 (dd, ³J=8.5 Hz ⁴J=1.0 Hz, 1H, H₃), 7.63 (d, ³J=8.5 Hz, 1H, H₅), 7.59 (d, ³J=8.0 Hz, 1H, H₄), 6.76 (s, 1H, H₈), 6.74 (dd, ³J=8.5 Hz ⁴J=2.0 Hz, 1H, H₆), 3.41 (t, ³J=6.5 Hz, 2H, H_{3'}), 3.25 (m, 2H, H_m), 3.06 (s, 6H, N(CH₃)₂), 2.63 (t, ³J=6.5 Hz, 2H, H_{2'}), 1.48 (s, 6H, 2CH₃), 1.43-1.25 (m, 4H, H_{n,o}), 0.91 (t, ³J=7.0 Hz, 3H, H_p). ¹³C-NMR (50 MHz, CDCl₃, δ): 198.9, 172.5, 157.0, 153.1, 151.4, 145.4, 133.5, 128.3, 126.7, 122.1 (2C), 118.3, 111.7, 106.2, 47.0, 41.0 (2C), 39.5, 34.4, 31.8, 30.8, 27.4 (2C), 20.2, 13.9. MS (ESI⁺, MeOH): *m/z*: 415,2 [M+Na]⁺.



Scheme 5. Synthesis of **169** and **170-177** series (on 100 mg scale) of products corresponding to **PP7-14** respectively.

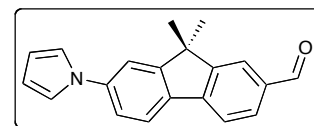
7-bromo-9,9-dimethylfluorene-2-carbaldehyde (**169**).

Following **GP-E**. To a stirred solution of **34** (2.50 g, 9.2 mmol, 1 eq.) and ZrCl₄ (3.20 g, 13.8 mmol, 1.5 eq.) [or AlCl₃] in DCM (30 mL) at 0 °C under argon, was added dropwise Cl₂CHOCH₃ (1.25 mL, 3.8 mmol, 1.5 eq.). The reaction mixture was stirred for 1 h at 0 °C then warmed up to rt and poured into ice-water bath (15 mL). The reaction is followed by TLC/GCMS to avoid diformylation. The organic layer was extracted with CHCl₃ (2x), and the combined extracts were washed with water and saturated aq. NaHCO₃ solution, dried over MgSO₄, and concentrated in vacuo. The crude was purified by flash chromatography on silica gel eluted with (CyHex/DCM = 4:1, *R_f* = 0.16) to afford the product **169** (2.10 g, 77 %) as a bright yellow solid. It is worth noting that AlCl₃ provides the same product but with minority of other isomers, difficult to remove upon purification. ¹H-NMR (200 MHz, CDCl₃, δ): 10.06 (s, 1H), 7.96 (d, ⁴J=1.0 Hz, 1H), 7.88 (br d, ³J=8.0 Hz, 1H), 7.84 (s, 1H), 7.68-7.61 (m, 2H), 7.52 (dd, ³J=8.0 Hz ⁴J=2.0 Hz, 1H), 1.52 (s, 6H). ¹³C-NMR (50 MHz, CDCl₃, δ): 192.1, 157.0, 154.1, 144.6, 136.8, 135.9, 130.8, 130.7, 126.6, 123.2 (2C), 122.7, 120.5, 47.4, 26.9 (2C). GC-MS (*m/z*): 302.1 [M⁺].



9,9-dimethyl-7-(1H-pyrrol-1-yl)-9H-fluorene-2-carbaldehyde

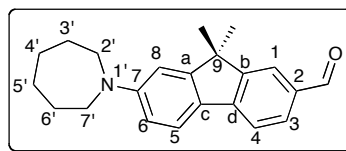
(**170/PP7**). Following **GP-E**. Yellow solid, Eluent (Hex/EA = 94:6, *R_f*



= 0.23), yield=(89 %, MW; 81%: thermal). ¹H-NMR (200 MHz, CDCl₃, δ): 10.06 (s, 1H), 7.89 (s, 1H), 7.91-7.81 (m, 3H), 7.84 (d, ⁴J=1.5 Hz, 1H), 7.42 (dd, ³J=8.0 Hz ⁴J=2.0 Hz, 1H), 7.17 (t, ³J=2.0 Hz, 2H), 6.40 (t, ³J=2.0 Hz, 2H), 1.56 (s, 6H). ¹³C-NMR (50 MHz, CDCl₃, δ): 192.2, 156.8, 154.4, 145.0, 141.6, 135.5, 135.1, 130.9, 123.1, 122.4, 120.3, 120.1, 119.6 (2C), 115.3, 110.9 (2C), 47.3, 27.1 (2C). HRMS (ESI⁺): *m/z* calcd for C₂₀H₁₈NO: 288.1383 [M+H]⁺; found 288.1383.

7-(azepan-1-yl)-9,9-dimethyl-9H-fluorene-2-carbaldehyde

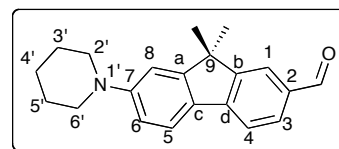
(171/PP8). Following GP-E. Yellow solid, Eluent (PE/EA = 98:2, *R_f* = 0.38), yield=(78 %: MW, 70 %: thermal). ¹H-NMR (500 MHz, CDCl₃, δ): 9.97 (s, 1H, CHO), 7.87 (d, ⁴J=1.5 Hz, 1H, H1), 7.77 (dd,



³J=7.5 Hz ⁴J=1.5 Hz, 1H, H3), 7.63 (d, ³J=7.5 Hz, 1H, H4), 7.61 (br d, ³J=7.0 Hz, 1H, H5), 6.72 (br s, 1H, H8), 6.71 (dd, ³J=7.0 Hz ⁴J=2.5 Hz, 1H, H6), 3.55 (t, ³J=6.0 Hz, 4H, CH₂2',7'), 1.84 (br m, 4H, CH₂3',6'), 1.59 (br m, 4H, CH₂4',5'), 1.49 (s, 6H, 2CH₃). ¹³C-NMR (125 MHz, CDCl₃, δ): 192.2, 157.5, 153.4, 150.5, 147.1, 133.6, 131.4, 125.4, 122.6, 122.5, 118.3, 110.9, 105.0, 49.7 (2C), 46.8, 27.8 (2C), 27.4 (2C), 27.3 (2C). HRMS (ESI⁺): *m/z* calcd for C₂₂H₂₆ON: 320.2009 [M+H]⁺; found 320.2010.

9,9-dimethyl-7-(piperidin-1-yl)-9H-fluorene-2-carbaldehyde

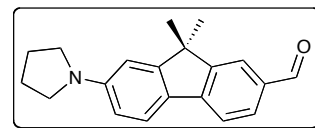
(172/PP9). Following GP-E. Yellow solid, Eluent (PE/EA = 98:2, *R_f* = 0.31), yield=64 % (MW). ¹H-NMR (200 MHz, CDCl₃, δ): 10.00



(s, 1H, CHO), 7.90 (d, ⁴J=1.0 Hz, 1H, H1), 7.80 (dd, ³J=8.0 Hz ⁴J=1.0 Hz, 1H, H3), 7.69 (d, ³J=8.0 Hz, 1H, H4), 7.65 (d, ³J=8.0 Hz, 1H, H5), 6.99 (d, ⁴J=2.5 Hz, 1H, H8), 6.93 (dd, ³J=8.0 Hz ⁴J=2.5 Hz, 1H, H6), 3.29 (t, ³J=6.0 Hz, 4H, CH₂2',6'), 1.73 (br m, 4H, CH₂3',5'), 1.62 (br m, 2H, CH₂4'), 1.49 (s, 6H, 2CH₃). ¹³C-NMR (50 MHz, CDCl₃, δ): 192.3 (C=O), 156.8 (Ca), 153.9 (Cb), 153.4 (C7), 146.5 (Cd), 134.2 (C2), 131.2 (C3), 128.6 (Cc), 122.7 (C1), 122.1 (C5), 119.0 (C4), 115.4 (C6), 110.1 (C8), 50.6 (2C, C2',6'), 46.9 (C9), 27.3 (2CH₃), 25.9 (2C, C3',5'), 24.4 (C4'). HRMS (ESI⁺): *m/z* calcd for C₂₁H₂₄ON: 306.1852 [M+H]⁺; found 306.1853.

9,9-dimethyl-7-(pyrrolidin-1-yl)-9H-fluorene-2-carbaldehyde

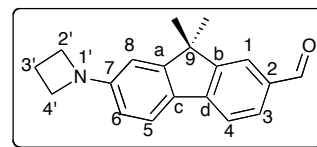
(173/PP10). Following GP-E. Yellow solid, Eluent (PE/EA = 98:2, *R_f* = 0.25), yield=22 % (MW). ¹H-NMR (200 MHz, CD₂Cl₂, δ): 9.94 (s,



1H), 7.85 (d, ⁴J=1.0 Hz, 1H), 7.77 (dd, ³J=8.0 Hz ⁴J=1.0 Hz, 1H), 7.67-7.61 (m, 2H), 6.60-6.55 (m, 2H), 3.38 (t, ³J=6.0 Hz, 4H), 2.04 (br q, 4H), 1.47 (s, 6H). HRMS (ESI⁺): *m/z* calcd for C₂₀H₂₂ON: 292.1696 [M+H]⁺; found 292.1695. Product was obtained with full conversion on GC-MS, but was sufficiently unstable during purification.

7-(azetidin-1-yl)-9,9-dimethyl-9H-fluorene-2-carbaldehyde

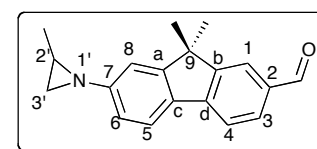
(174/PP11). Following GP-E. Yellow solid, Eluent (PE/EA = 98:2, R_f = 0.21), yield=50 % (MW). The amine is azetidine hydrochloride.



It was stirred with toluene and the base for 30 mins. This can explain the low yield of the coupling. $^1\text{H-NMR}$ (500 MHz, CDCl_3 , δ): 9.98 (s, 1H, CHO), 7.88 (d, 4J =1.0 Hz, 1H, H1), 7.78 (dd, 3J =8.0 Hz 4J =1.0 Hz, 1H, H3), 7.66 (d, 3J =8.0 Hz, 1H, H4), 7.62 (d, 3J =8.0 Hz, 1H, H5), 6.45 (d, 4J =2.0 Hz, 1H, H8), 6.42 (dd, 3J =8.0 Hz 4J =2.0 Hz, 1H, H6), 3.99 (t, 3J =7.5 Hz, 4H, CH_2 2',4'), 2.41 (q, 3J =7.5 Hz, 2H, CH_2 3'), 1.48 (s, 6H, 2 CH_3). $^{13}\text{C-NMR}$ (125 MHz, CDCl_3 , δ): 192.2 (C=O), 157.2 (Ca), 153.4 (Cb), 153.2 (C7), 146.9 (Cd), 133.9 (C2), 131.3 (C3), 127.1 (Cc), 122.6 (C1), 122.2 (C5), 118.6 (C4), 110.5 (C6), 104.9 (C8), 52.4 (2C, C2',4'), 46.8 (C9), 27.3 (2 CH_3), 16.9 (C3'). HRMS (ESI⁺): m/z calcd for $\text{C}_{19}\text{H}_{20}\text{ON}$: 278.1539 [M+H]⁺; found 278.1540.

(S)-9,9-dimethyl-7-(2-methylaziridin-1-yl)-9H-fluorene-2-

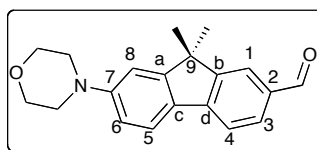
carbaldehyde (175/PP12). Following GP-E. Yellow solid, Eluent (PE/EA = 98:2, R_f = 0.11), yield=(52 %: thermal, 43 %: MW). $^1\text{H-NMR}$ (200 MHz, CDCl_3 , δ): 10.01 (s, 1H, CHO), 7.91 (d, 4J =1.5 Hz, 1H, H1),



7.81 (dd, 3J =8.0 Hz 4J =1.0 Hz, 1H, H3), 7.73 (d, 3J =8.0 Hz, 1H, H4), 7.64 (d, 3J =8.0 Hz, 1H, H5), 7.05 (d, 4J =2.0 Hz, 1H, H8), 6.99 (dd, 3J =8.0 Hz 4J =2.0 Hz, 1H, H6), 2.31-2.24 (m, 1H, H2'), 2.17 (d, 3J =6.0 Hz, 1H, H3'), 2.11 (d, 3J =3.5 Hz, 1H, H3'), 1.49 (s, 6H, 2 CH_3), 1.44 and 1.41 (2s, 3H, CH_3 aziridine). $^{13}\text{C-NMR}$ (50 MHz, CDCl_3 , δ): 192.3, 156.5, 156.3, 154.1, 145.9, 134.8, 132.1, 131.0, 122.9, 121.9, 120.3, 119.5, 115.2, 46.9, 35.6, 35.3, 27.1 (2C), 18.5. HRMS (ESI⁺): m/z calcd for $\text{C}_{19}\text{H}_{20}\text{ON}$: 278.1539 [M+H]⁺; found 278.1541.

9,9-dimethyl-7-morpholino-9H-fluorene-2-carbaldehyde

(176/PP13). Following GP-E. Yellow solid, Eluent (CyHex/EA = 9:1, R_f = 0.1), yield=86 % (MW). $^1\text{H-NMR}$ (200 MHz, CDCl_3 , δ):



10.01 (s, 1H, CHO), 7.91 (d, 4J =2.0 Hz, 1H, H1), 7.82 (dd, 3J =8.0 Hz 4J =1.0 Hz, 1H, H3), 7.72 (d, 3J =8.0 Hz, 1H, H4), 7.68 (d, 3J =8.0 Hz, 1H, H5), 6.98 (d, 4J =2.5 Hz, 1H, H8), 6.92 (dd, 3J =8.0 Hz 4J =2.5 Hz, 1H, H6), 3.91 (t, 3J =4.5 Hz, 4H, $(\text{CH}_2)_2\text{O}$), 3.28 (t, 4H, $(\text{CH}_2)_2\text{N}$), 1.50 (s, 6H, 2 CH_3). $^{13}\text{C-NMR}$ (50 MHz, CDCl_3 , δ): 192.2 (C=O), 156.9 (Ca), 153.9 (Cb), 152.6 (C7), 146.1 (Cd), 134.5 (C2), 131.1 (C3), 129.7 (Cc), 122.8 (C1), 122.3 (C5), 119.2 (C4), 114.8 (C6), 109.6 (C8), 67.0 (2C, $(\text{CH}_2)_2\text{O}$), 49.4 (2C, $(\text{CH}_2)_2\text{N}$), 47.0 (C9), 27.3 (2 CH_3). HRMS (ESI⁺): m/z calcd for $\text{C}_{20}\text{H}_{22}\text{O}_2\text{N}$: 308.1645 [M+H]⁺; found 308.1645.

tert-butyl-4-(7-formyl-9,9-dimethyl-9H-fluoren-2-

yl)piperazine-1-carboxylate (177/PP14). Following GP-E.

Yellow solid, Eluent (PE/EA = 8:2, R_f = 0.38), yield=77 % (MW).

$^1\text{H-NMR}$ (200 MHz, CDCl_3 , δ): 10.01 (s, 1H, CHO), 7.91 (br s, 1H,

H1), 7.81 (dd, $^3J=7.5$ Hz $^4J=1.0$ Hz, 1H, H3), 7.71 (d, $^3J=7.5$ Hz, 1H, H4), 7.07 (d, $^3J=8.5$ Hz, 1H, H5),

6.98 (d, $^4J=2.0$ Hz, 1H, H8), 6.94 (dd, $^3J=8.5$ Hz $^4J=2.0$ Hz, 1H, H6), 3.63 (t, $^3J=5.0$ Hz, 4H, $\text{CH}_2\text{2}',6'$),

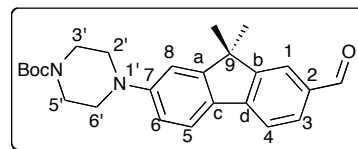
3.26 (t, $^3J=5.0$ Hz, 4H, $\text{CH}_2\text{3}',5'$), 1.49 (s, 15H, 5 CH_3). $^{13}\text{C-NMR}$ (50 MHz, CDCl_3 , δ): 192.2 (C=O),

156.9 (Ca), 154.8 (COO), 153.9 (Cb), 152.5 (C7), 146.1 (Cd), 134.52(C2), 131.1 (C3), 129.9 (Cc),

122.8 (C1), 122.2 (C5), 119.3 (C4), 115.6 (C6), 110.4 (C8), 80.2 (CMe₃), 49.4 (2C, C3',5'), 47.0

(C9), 44.0 (2C, C2',6'), 28.6 (3C, 3 CH_3Boc), 27.6 (2C, 2 CH_3). HRMS (ESI⁺): m/z calcd for

$\text{C}_{25}\text{H}_{31}\text{O}_3\text{N}_2$: 407.2329 [M+H]⁺; found 407.2331.



2-((9,9-dimethyl-7-(piperidin-1-yl)-9H-fluoren-2-

yl)methylene)malononitrile (178/PP15). Following GP-D.

Red solid, Eluent (CyHex/EA = 9:1, R_f = 0.28, yield=87 %. $^1\text{H-}$

NMR (200 MHz, CDCl_3 , δ): 7.98 (d, $^4J=1.5$ Hz, 1H, H1), 7.80 (dd,

$^3J=8.0$ Hz $^4J=1.5$ Hz, 1H, H3), 7.73 (s, 1H, CH=C), 7.55 (d, $^3J=8.0$ Hz, 2H, H4,5), 6.96 (s, 1H, H8),

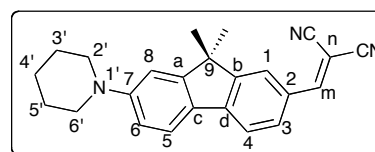
6.94 (dd, $^3J=8.0$ Hz $^4J=2.0$ Hz, 1H, H6), 3.33 (t, $^3J=5.0$ Hz, 4H, H2',6'), 1.72 (m, 6H, H3',4',5'), 1.48

(s, 6H, 2 CH_3). $^{13}\text{C-NMR}$ (50 MHz, CDCl_3 , δ): 159.9 (Cm), 157.4 (Ca), 154.2 (Cb), 153.8 (C7), 147.3

(Cd), 132.1 (C3), 128.3 (C2), 127.8 (Cc), 124.3 (C1), 122.6 (C5), 119.5 (C4), 115.2 (C6), 115.0

(CN), 113.9 (CN), 109.4 (C8), 78.3 (Cn), 50.1 (2C, C2',6'), 47.1 (C9), 27.2 (2C, 2 CH_3), 25.8 (2C,

C3',5'), 24.4 (C4'). HRMS (ESI⁺): m/z calcd for $\text{C}_{24}\text{H}_{24}\text{N}_3$: 354.1965 [M+H]⁺; found 354.1965.



2-((9,9-dimethyl-7-morpholino-9H-fluoren-2-

yl)methylene)malononitrile (179/PP16). Following GP-D.

Red solid, Eluent (CyHex/EA = 9:1, R_f = 0.3, yield=72 %. $^1\text{H-}$

NMR (200 MHz, CDCl_3 , δ): 7.99 (br s, 1H, H1), 7.80 (dd, $^3J=8.0$

Hz $^4J=1.5$ Hz, 1H, H3), 7.75 (s, 1H, CH=C), 7.68 (d, $^3J=8.0$ Hz, 2H, H4,5), 6.96 (s, 1H, H8), 6.94 (dd,

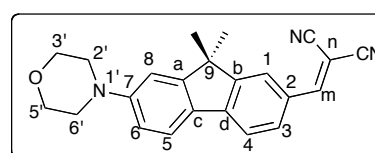
$^3J=8.0$ Hz $^4J=2.0$ Hz, 1H, H6), 3.90 (t, $^3J=5.0$ Hz, 4H, H3',5'), 3.31 (t, $^3J=5.0$ Hz, 4H, H2',6'), 1.49 (s,

6H, 2 CH_3). $^{13}\text{C-NMR}$ (50 MHz, CDCl_3 , δ): 159.9 (Cm), 157.3 (Ca), 154.2 (Cb), 153.0 (C7), 146.9

(Cd), 131.9 (C3), 129.0 (C2), 128.6 (Cc), 124.4 (C1), 122.7 (C5), 119.7 (C4), 114.8 (C6), 113.8 (2C,

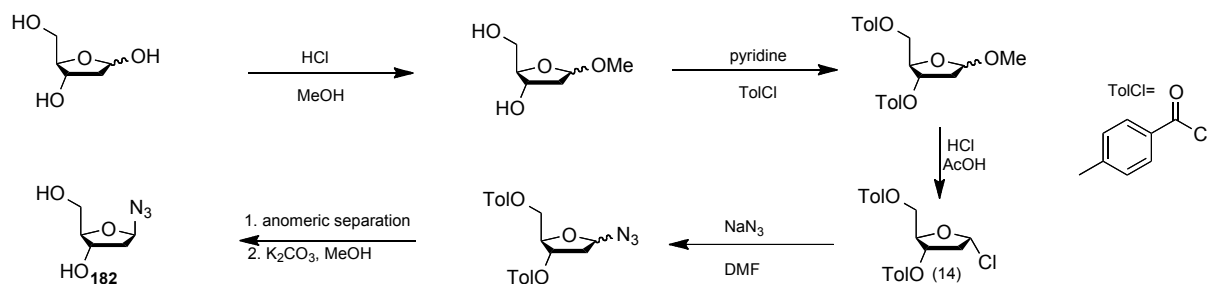
2CN), 109.1 (C8), 78.9 (Cn), 66.9 (2C, C3',5'), 48.9 (2C, C2',6'), 47.1 (C9), 27.2 (2C, 2 CH_3). HRMS

(ESI⁺): m/z calcd for $\text{C}_{23}\text{H}_{22}\text{ON}_3$: 356.1757 [M+H]⁺; found 356.1760.



XI. Chapter 4 synthetic procedures

General procedure (GP-F) used for the synthesis of (165-167/F1-3): The propioloxy fluorene 163 (1 eq.) and clickable anchor/sugar (1.2 eq.) were dissolved in a mixture DMF/water (3/1). $\text{CuSO}_4 \cdot 5\text{H}_2\text{O}$ (0.5 eq.) and sodium ascorbate (0.7 eq.) were dissolved in an eppendorf with water and the solution was mixed until the mixture turned yellow/orange. The content of the eppendorf was then transferred into the reaction vial and stirred at room temperature for 1 h. The volatiles were then removed under vacuum and the crude product was purified by gel filtration chromatography.



Scheme 6. Synthesis of the “clickable” sugar **182**

The azido sugar was prepared with slight modifications from published procedures, and the final product was characterized herein in the text. ^[166,269,270]

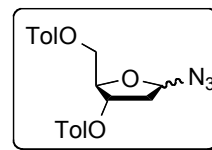
To a solution of 5.0 g (37.3 mmol) of 2-deoxy-D-ribose in MeOH (60 mL) was added methanolic hydrogen chloride. The reaction mixture was stirred at room temperature for **25** minutes and neutralized by adding solid sodium bicarbonate (2.0 g). After filtration, the methanol was removed under reduced pressure.

The mixture was re-dissolved in pyridine (30 mL), cooled to 0 °C and p-toluoyl chloride (11 mL, 80 mmol) was added dropwise, and stirred at room temperature overnight. The reaction mixture was diluted with cold water (80 mL) and extracted 3 times with CH_2Cl_2 . The combined organic layers were washed twice with saturated aqueous solution of NaHCO_3 , once with 2N HCl solution and once with water, dried on MgSO_4 , and evaporated.

To the resulting colored sirup (13.0 g) dissolved in acetic acid (20 mL) was slowly added a saturated solution of HCl in acetic acid at 0 °C and stirred 1 h after the formation of yellowish precipitate (3 h in total). 50 mL of cyclohexane was added and the solid was filtered off, washed

with cold dry ether, dried in a vacuum dessicator; yield 8.4 g (58%).

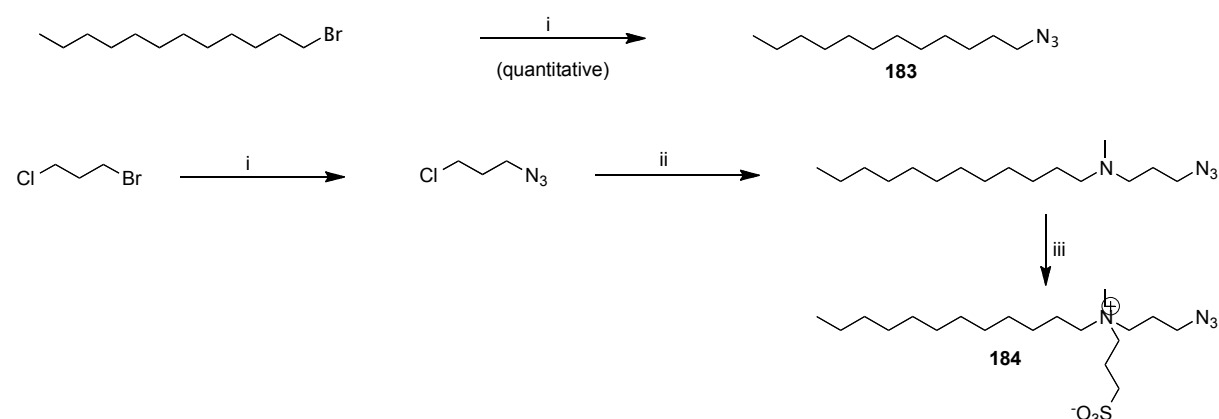
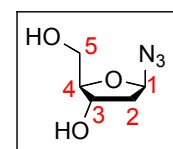
NaN₃ (1.17 g, 18.0 mmol) was added to a mixture of α and β -chlorosugar 4 (4.5 g, 11.6 mmol) in dry DMF (150 mL), stirred at RT for 4 h in an inert atmosphere. After completion of the reaction, EtOAc (100 mL) was added to the mixture to form a uniform organic layer. The organic layer was washed with water, brine, and dried (over anhydrous MgSO₄). Evaporation under reduced pressure afforded the crude product mixture. The β sugar was eluted as the first fraction. Yield: 2.47 g (55%); R_f= 0.55 (diethyl ether/hexanes=3:7). ¹H NMR (200 MHz, CDCl₃): 7.97 (d, 2H, J=8.1 Hz), 7.89 (d, 2H, J= 8.2 Hz), 7.24–7.21 (m, 4 H), 5.70 (t, 1H, J=5.2 Hz), 5.56 (td, 1H, J=5.5, 2.4 Hz), 4.59–4.50 (m, 3H), 2.42–2.39 ppm (m, 8H); HRMS: calcd for C₂₁H₂₁N₃NaO₅ [M+Na]⁺: 418.1379; found: 418.1376.



Dry MeOH (100 mL) followed by potassium carbonate (0.82 g, 15.16 mmol) were added to a dry round-bottom flask loaded with toluoyl -protected (2.18 g, 4.8 mmol). The reaction mixture was stirred under inert atmosphere at RT for 24 h and monitored by TLC. The residue was loaded on a silica gel column, and the desired product was isolated when eluted with 5% MeOH in diethyl ether. Yield: 0.62 g (81%); R_f=0.60 (methanol/diethyl ether=5:95)

(2R,3S,5R)-5-azido-2-(hydroxymethyl)tetrahydrofuran-3-ol (182).

¹H NMR (200 MHz, Acetone-*d*₆, δ): 5.44 (dd, ³J = 4.0, 5.5 Hz, 1H, H₁), 4.33 (q, ³J = 5.0 Hz, 1H, H₃), 3.89 (q, ³J = 5.0 Hz, 1H, H₄), 3.60 (m, 2H, H₅), 2.03 (m, 2H, H₂). ¹³C-NMR (50 MHz, Acetone-*d*₆, δ): 92.7, 88.8, 72.0, 63.7, 41.7.

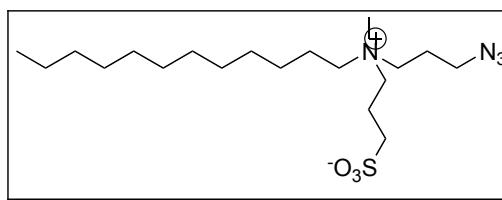


Scheme 7. Synthesis of the clickable anchors 183-184. . i) NaN₃, DMF, 25 °C, 20 h (86 %), ii) N-methyldodecylamine, CH₃CN, 80 °C, 6 h (38 %), iii) 1,3-propanesultone, K₂CO₃, CH₃CN, 90 °C, 12 h (61 %).

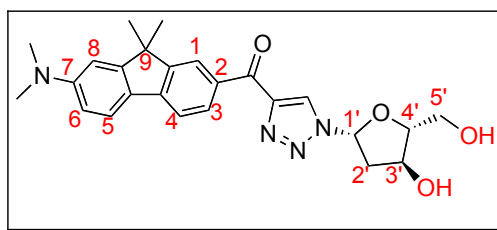
azidopropyl)(dodecyl)(methyl)ammonio)propane-1-sulfonate (184). Published

procedure^[166]

1-azido-3-chloropropane (0.602 g, 5.016 mmol, 1 eq) and dodecyl(methyl)amine (1.000 g, 5.016 mmol, 1 eq) were dissolved in 15 mL of CH₃CN. The



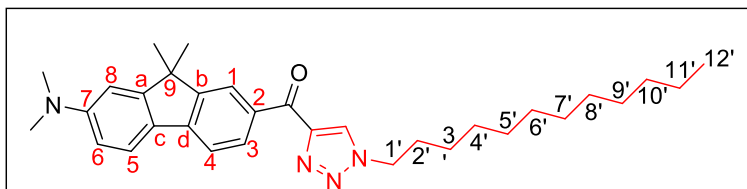
solution was then heated at 80°C in a sealed flask (to avoid evaporation) for 6h. The solvent was removed with the help of a rotary evaporator and the crude product was purified by column chromatography with CH₂Cl₂/MeOH (5 to 10 % of MeOH) as eluent. A yellowish oil was obtained, yield 38%. ¹H NMR (400 MHz, Chloroform-*d*) δ 3.28 (t, *J* = 6.8 Hz, 2H), 2.38 (t, *J* = 7.2 Hz, 2H), 2.33 – 2.24 (m, 2H), 2.17 (s, 3H), 1.71 (p, *J* = 6.9 Hz, 2H), 1.41 (q, *J* = 7.5, 7.0 Hz, 2H), 1.20 (d, *J* = 7.8 Hz, 18H), 0.86 – 0.75 (m, 3H). ¹³C NMR (101 MHz, CDCl₃) δ 57.9, 54.6, 49.6, 42.2, 31.9, 29.7, 29.6, 29.6, 29.5, 29.34, 27.51, 27.30, 26.80, 22.68, 14.09. HRMS (ES⁺) Calc. for C₁₆H₃₅N₄ [M+H]⁺ 283.2856, found 283.2852. Then, the intermediate (500 mg, 1.770 mmol, 1eq) was dissolved in ACN (15 mL), and 1,3-propanesultone (1.100 g, 8.851 mmol, 5 eq) was added to the mixture. The reaction was then heated to reflux for 12h. The white solid that formed was filtered off and washed several times with ACN and dried. A white powder was obtained, yield 61%. ¹H NMR (400 MHz, Methanol-*d*⁴) δ 3.46 – 3.36 (m, 4H), 3.31 – 3.24 (m, 2H), 2.96 (s, 3H), 2.77 (t, *J* = 6.7 Hz, 2H), 2.13 – 2.00 (m, 2H), 1.97 – 1.86 (m, 2H), 1.75 – 1.60 (m, 2H), 1.36 – 1.13 (m, 18H), 0.80 (t, *J* = 6.8 Hz, 2H). ¹³C NMR (101 MHz, CDCl₃) δ 61.9, 61.4, 59.0, 48.7, 48.1, 47.6, 31.9, 29.6, 29.5, 29.4, 29.3, 29.2, 26.4, 22.7, 22.3, 22.3, 19.1, 14.1. HRMS (ES⁺) Calc. for C₁₉H₄₁N₄O₃S. [M+H]⁺ 405.2894, found 405.2899.



(7-(dimethylamino)-9,9-dimethyl-9H-fluoren-2-yl)(1-((2R,4S,5R)-4-hydroxy-5-hydroxymethyl)tetrahydrofuran-2-yl)-1H-1,2,3-triazol-4-yl)methanone (165/F1).

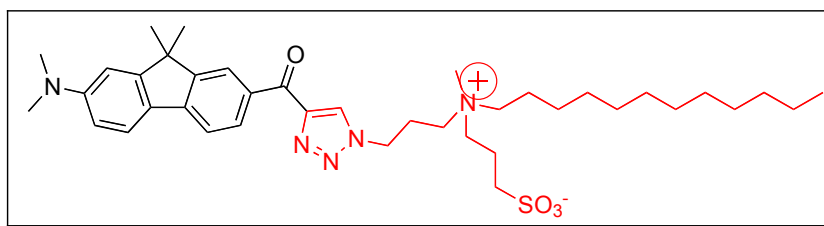
Substrates: Fluorene 163 and azidosugar 182 (40 mg, 0.14 mmol, 1 eq.). The crude was purified by flash chromatography on silica gel (Eluent DCM/Ac=7/3, *R_f*=0.40) to provide **F1** (50 mg, 80 %) as bright yellow solid ¹H-NMR (200 MHz, C₅D₅N, δ): 9.48 (s, 1H, H_{triazole}), 8.86 (br s, 1H, H1), 8.82 (br d, ³*J*=8.0 Hz, 1H, H3), 7.83 (d, ³*J*=8.0 Hz, 1H, H4), 7.81 (d, ³*J*=8.5 Hz, 2H, H4,5), 6.99 (t, ³*J*=6.5 Hz, 1H, H1'), 6.90 (d, ⁴*J*=2.0 Hz, 1H, H8), 6.77 (dd, ³*J*=8.5 Hz ⁴*J*=2.0 Hz, 1H, H6), 5.22 (m, 1H, H3'), 4.62 (m, 1H, H4'), 4.17 (m, 2H, H5'), 3.17-2.85 (m, 2H, H2'), 2.87 (s, 6H, N(CH₃)₂), 1.50 (s,

6H, 2CH₃). ¹³C-NMR (50 MHz, C₅D₅N, δ): 185.1 (C=O), 157.4 (Ca), 153.2 (Cb), 152.1 (C7), 149.0 (C=CH), 145.8 (Cd), 134.3 (C2), 131.4 (C3), 128.3 (C=CH), 126.6 (Cc), 125.0 (C1), 122.6 (C5), 118.4 (C4), 112.1 (C6), 106.4 (C8), 90.1 (C4'), 90.0 (C1'), 71.1 (C3'), 62.2 (C5'), 47.1 (C9), 42.1 (2C, N(CH₃)₂), 40.3 (C2'), 27.3 (2C, 2CH₃).



(7-(dimethylamino)-9,9-dimethyl-9H-fluoren-2-yl)(1-dodecyl-1H-1,2,3-triazol-4-

yl)methanone (186/F2): Substrate: Fluorene 163 and dodecyl azide 183 (10 mg, 0.035 mmol, 1 eq.). The crude was purified by flash chromatography on silica gel (Eluent CyHex/EA=9/1, *R_f*=0.14) to provide **F2** (13 mg, 75 %) as bright yellow solid. ¹H-NMR (200 MHz, CDCl₃, δ): 8.54 (dd, ³*J*=8.0 ⁴*J*=1.5 Hz, 1H, H3), 8.44 (d, ⁴*J*=1.5 Hz, 1H, H1), 8.24 (s, 1H, H_{triazole}), 7.67 (d, ³*J*=8.0 Hz, 2H, H4,5), 6.76 (s, 1H, H8), 6.74 (d, ³*J*=8.0 Hz, 1H, H6), 4.45 (t, ³*J*=7.0 Hz, 2H, H1'), 3.07 (s, 6H, N(CH₃)₂), 1.98 (m, 2H, H2'), 1.52 (s, 6H, 2CH₃ 9,9), 1.35-1.25 (m, 18H, H3'-11'), 0.87 (t, ³*J*=7.0 Hz, 3H, H12'). ¹³C-NMR (50 MHz, CDCl₃, δ): 185.5 (C=O), 157.5 (Ca), 152.9 (Cb), 151.2 (C7), 148.8 (C=CH), 145.7 (Cd), 133.8 (C2), 131.6 (C3), 128.1 (C=CH), 126.8 (Cc), 124.5 (C1), 122.2 (C5), 118.1 (C4), 111.7 (C6), 106.1 (C8), 50.8 (C1'), 47.0 (C9), 40.9 (2C, N(CH₃)₂), 32.0 (C10'), 30.3 (C2'), 29.7-29.1 (6C, C4'-10'), 27.5 (2C, 2CH₃), 26.6 (C3'), 22.8 (C11'), 14.3 (C12'). HRMS (ESI⁺): *m/z* calcd for C₃₂H₄₅ON₄: 501.3588 [M+H]⁺; found 501.3588.



3-((3-(4-(7-(dimethylamino)-9,9-dimethyl-9H-fluorene-2-carbonyl)-1H-1,2,3-triazol-1-

yl)propyl)(methyl)(tridecyl)ammonio)propane-1-sulfonate (187/F3): Substrate: Fluorene 163 (10 mg, 0.035 mmol, 1 eq.) and the zwitterion 184. The crude was purified by flash chromatography on silica gel (Eluent DCM/MeOH=9/1, *R_f*=0.15) to provide **F3** (15 mg, 61 %) as bright yellow solid. **F3** was further purified by HPLC to remove silica. It was analyzed (0.5 mL/min) and purified (2.5 mL/min) by RP HPLC (HPLC apparatus: WatersTM 600 Controller with WatersTM 996 Photodiode Array Detector and Jasco LC-Net II / ADC apparatus. Column:

semi-preparative, Clarity® 5u Oligo-RP column 250 x 10 mm Phenomenex®). The following gradient system was used: 25 % A -(5min)→ 5 % A / 95 % B -(25 min)→ 100 % B -(10 min) with A= 0.25 CH₃CN: 0.75 MilliQ® water and B= CH₃CN. ¹H-NMR (500 MHz, CD₃OD-*d*⁴, δ): 8.71 (s, 1H), 8.33 (s, 1H), 8.31 (dd, ³J=8.0 ⁴J=1.5 Hz, 1H), 7.71 (d, ³J=8.0 Hz, 1H), 7.69 (d, ³J=8.5 Hz, 1H), 6.87 (d, ⁴J=2.0 Hz, 1H), 6.80 (dd, ³J=8.5 ⁴J=2.0 Hz, 1H), 4.67 (t, ³J=6.5 Hz, 2H), 3.54 (m, 2H), 3.45 (m, 2H), 3.07 (s, 3H), 3.05 (s, 6H), 2.88 (t, ³J=6.5 Hz, 2H), 2.51 (m, 2H), 2.17 (m, 2H), 1.61 (m, 2H), 1.50 (s, 6H), 1.33-1.23 (m, 22H), 0.87 (t, ³J=6.5 Hz, 3H). HRMS (ESI⁺): *m/z* calcd for C₃₉H₆₀O₄N₅S: 694.4361 [M+H]⁺; found 694.4361.

XII. Chapter 5 synthetic procedures

General procedure (GP-G) of metal-halogen exchange reaction used for the synthesis of (195 and S20): The bromofluorene (1 eq.) was dissolved in dry THF (0.2 M). To the resulted clear yellow solution, *n*BuLi (2.5M solution in Hexane, 1.2 eq.) was added dropwise at -78 °C under inert atmosphere. Reaction mixture was stirred for 1h before a yellow precipitate was formed. Then, DMF (2-3 eq.) was added dropwise and the formed solution was stirred for additional 2 h at -78 °C. The reaction was allowed to warm up to room temperature and stirred for 1 h, quenched with 1 M aqueous HCl and extracted with EA (2x). Organic layer was dried over MgSO₄ and evaporated in vacuum. The residue was purified by column chromatography.

General procedure (GP-H) to synthesize the clickable fluorenes (196 and 203). Ethynylmagnesium bromide (0.5 M in THF, 1.4 eq.) was added dropwise to a solution of the carbaldehyde (1 eq.) in THF (2.5 mL) at 0 °C. The mixture was stirred at the same temperature until completion of the reaction monitored by TLC (1-2h). Then, a saturated solution of aq. NH₄Cl was added and the aqueous phase was extracted with EA. The combined extracts were dried (magnesium sulfate) and evaporated to yield the corresponding propargyl alcohol. The crude propargyl alcohol was purified by flash chromatography. N.B. It is better to batch to next step without purification.

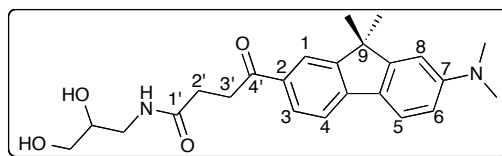
General procedure (GP-I) of click protocol with β -toluoyl-protected deoxyribose for the synthesis of (S13 and S15). To a stirred solution of S7 (1.1 eq.) in DCE (2.5 M) at 0 °C under argon, was added dropwise a 2.5 M solution of propioloyl fluorene push-pull (1 eq.) in DCE (4 mL). Then, DIEA (5 eq.), CuI (2 eq.), and AcOH (1 eq.) were sequentially added. The reaction mixture was stirred for 3 h at rt, filtered over a pad of Decalite[®], and washed with DCM. The volatiles were reduced *in vacuo* and the resulting crude was purified by flash chromatography on silica gel.

General procedure (GP-J) of toluoyl deprotection for the synthesis of (165, 197, and S21). The clicked intermediate (1 eq.) is dissolved in Dry MeOH (0.1 M) followed by addition of potassium carbonate (3.2 eq.) and stirring under inert atmosphere at rt for 24 h until completion of the reaction monitored by TLC. The residue was loaded on a silica gel column and purified by chromatography.

General procedure (GP-K) of DMTr protection for the synthesis of (S14, S16, and S23). To a stirred solution of the clicked deprotected deoxyribose sugar (1 eq.) in a mixture of dry DMF (0.25 M) and DIEA (5 eq.) previously cooled down to 0 °C, was added DMTrCl (1.15 eq) under argon. The reaction mixture was stirred at rt overnight and monitored by TLC. A subsequent addition of DIEA (5 eq.) and DMTrCl (1.15 eq.) was re-added if the reaction was not complete. The volatiles were evaporated and the residue was purified by flash chromatography on silica gel.

General procedure (GP-L) for the synthesis of the final phosphoramidite (FM2-4). To a stirred solution of the DMTr-protected intermediate (1eq., previously dried azeotropically by coevaporation with dry toluene) in DCM (0.1 M) under argon and cooled down at 0 °C, were sequentially added DIEA (5 eq.) and 2-cyanoethyl-*N,N*-diisopropylchlorophosphoramidite (2 eq). The reaction mixture was stirred at rt for 1-3 h and monitored by TLC until starting material was completely transformed into the diastereomers. The volatiles were removed *in vacuo* and the residue was purified by fast flash chromatography on silica gel.

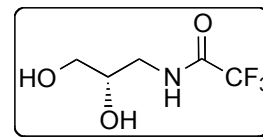
***N*-(2,3-dihydroxypropyl)-4-(7-(dimethylamino)-9,9-dimethyl-9*H*-fluoren-2-yl)-4-oxobutanamide (190).** 167 (200 mg, 0.59 mmol, 1 eq.), DIC (114 μL, 0.71 mmol, 1.2 eq.), HOBT (111 mg, 0.71 mmol, 1.2



eq.), and Et₃N (252 μL, 1.78 mmol, 3 eq.) were solubilized in 6 mL dry DMF under argon and stirred for 30 mins at 0 °C. Aminopropanediol 189 (110 mg, 1.19 mmol, 2 eq.) was then added and the reaction was stirred overnight at rt. The crude was washed by NaHCO₃ (aq.) and extracted with DCM. The organic layer was washed by water, dried with magnesium sulfate, and reduced under pressure. Purification was done by FC. Eluent (DCM/MeOH = 98: 2, *R_f* = 0.29) to afford compound **190** (185 mg, 73 %) as a yellow solid. ¹H NMR (200 MHz, MeOD-*d*⁴, δ): 8.0 (s, 1H, H1), 7.96 (dd, ³*J*=8.5 Hz ⁴*J*=2.0 Hz, 1H, H3), 7.54 (d, ³*J*=8.5 Hz, 1H, H4,5), 6.80 (s, 1H, H8), 6.71 (d, ³*J*=8.5, 1H, H6), 3.78-3.67 (m, 1H, CHOH), 3.53-3.50 (m, 2H, CH₂OH), 3.33-3.17 (m, 4H, CH₂NH₂ and H3'), 3.03 (s, 6H, N(CH₃)₂), 2.64 (t, ³*J*=6.5 Hz, 2H, H2') 1.47 (s, 6H, 2CH₃). ¹³C NMR (50 MHz, MeOD-*d*⁴, δ): 200.4, 175.8, 158.0, 154.3, 152.8, 146.7, 134.8, 129.2, 128.1, 122.9 (2C), 119.2, 113.3, 107.6, 72.1, 65.0, 43.4, 41.2 (2C), 34.8, 30.9, 30.7, 27.6 (2C). HRMS (ESI⁺): *m/z* calcd for C₂₄H₃₁O₄N₂: 411.2278 [M+H]⁺; found 411.2277.

3-Trifluoroacetamido-1,2-propanediol (191). 3-Amino-1,2-

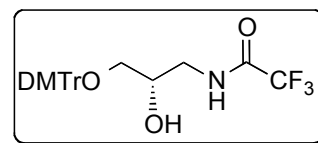
propanediol 189 (1.36 g, 15 mmol, 1 eq) was dissolved in methyl trifluoroacetate (15 ml, 150 mmol, 10 eq.) by sonication and stirred



overnight at rt. The reaction mixture was evaporated and dried by coevaporation with toluene (3*40 mL) to give the title product **191** (2.73 g, 98%) as a colorless oil: ¹H-NMR (200 MHz, CDCl₃, δ): 6.82 (br.s, 1H, NH), 3.92 (m, 1H, CHOH), 3.73 (m, 1H, CH₂H_bOH), 3.62 (m, 1H, CH₂H_bNH), 3.57 (m, 1H, CH₂H_bOH), 3.42 (m, 1H, CH₂H_bNH).

3-Trifluoroacetamido-1-(4,4'-dimethoxytriphenyl-methyl)-2-

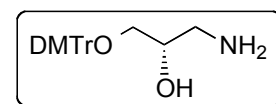
propanediol (192). 4,4-Dimethoxytrityl chloride (2.04 g, 2.9 mmol, 1.2 eq) was added to propanediol 191(0.9 g, 2.4 mmol, 1 eq)



solution in 6 mL of dry pyridine. The mixture was agitated overnight at rt. Solvents were removed by evaporation, and the residue was dissolved in 25 ml of EA, washed with saturated sodium hydrocarbonate solution, dried over MgSO₄, and evaporated to dryness. The product was isolated by flash chromatography. Eluent (DCM/MeOH = 99: 1 in the presence of 0.1% Et₃N) providing the **192** as pale yellow oil (0.98 g, 76 %). ¹H-NMR (200 MHz, CDCl₃, δ): 8.52 (br. s, 1H, NH), 7.43-6.81 (m, 13H, arom.), 3.92 (m, 1H, CHOH), 3.79 (s, 6H, 2CH₃), 3.61 (m, 1H, CH₂H_bNH), 3.31 (m, 1H, CH₂H_bNH), 3.25 (dd, 1H, J = 7.5, 9.5 Hz, CH₂H_bODMTr), 3.15 (dd, 1H, J = 7.5, 9.5 Hz, CH₂H_bODMTr).

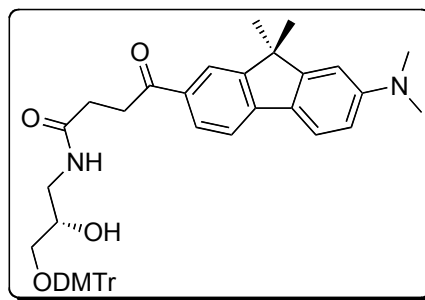
1-Amino-3-O-(4,4'-dimethoxytrityl)-2,3-propane- diol (193). 192

(0.9g, 1 eq) was dissolved in 45 mL of 6 M ethanolic ammonia solution and stirred overnight. The crude was evaporated and purified by a



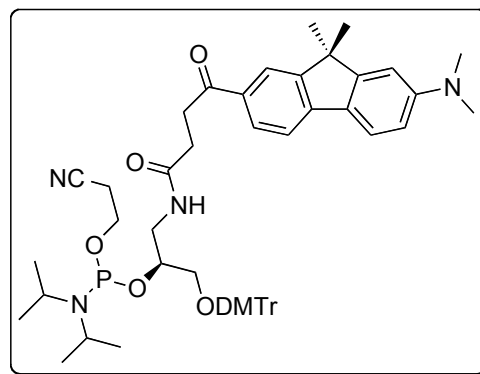
column chromatography. Eluent (DCM/MeOH = 99: 1 in the presence of 0.1% Et₃N) giving the desired compound **193** as pale yellow oil (0.51 g, 61 %). Note: the product degrades on silica and DMTr is cleaved very quickly. The product can be taken to next step without purification. ¹H-NMR (500 MHz, CDCl₃, δ): 7.44 (br. d, ³J=8.5 Hz, 2H, arom.), 7.31 (dd, ³J=8.5, ⁴J=1.0 Hz, 4H, arom.), 7.27 (t, ³J=7.5 Hz, 2H, arom.), 7.19 (t, ³J=7.5 Hz, 1H, arom.), 6.84 (d, ³J=8.5, 2H, arom.), 3.76 (s, 6H, 2CH₃), 3.31 (m, 1H, CHOH), 3.17 (m, 1H, CH₂H_bNH), 3.03 (m, 1H, CH₂H_bNH), 3.83 (m, 1H, CH₂H_bODMTr), 2.63 (m, 1H, CH₂H_bODMTr). ¹³C NMR (125 MHz, CDCl₃, δ): 158.7, 144.5, 135.5, 130.0, 128.0, 127.0, 113.3, 113.0, 86.63, 69.0, 65.0, 55.2. MS (ESI⁺, MeOH): C₂₄H₂₇NO₄. m/z: 416,2 [M+Na]⁺.

(S)-N-(3-(bis(4-methoxyphenyl)(phenyl)methoxy)-2-hydroxypropyl)-4-(7-(dimethylamino)-9,9-dimethyl-9H-fluoren-2-yl)-4-oxobutanamide (194): 167 (200 mg, 0.59 mmol, 1 eq.), DIC (114 μ L, 0.71 mmol, 1.2 eq.), HBTU (311 mg, 0.72 mmol, 1.2 eq.), and Et₃N (252 μ L, 1.78 mmol, 3 eq.) were solubilized in 6 mL dry DMF under argon and stirred for 30 mins at 0 °C. Protected sugar 193



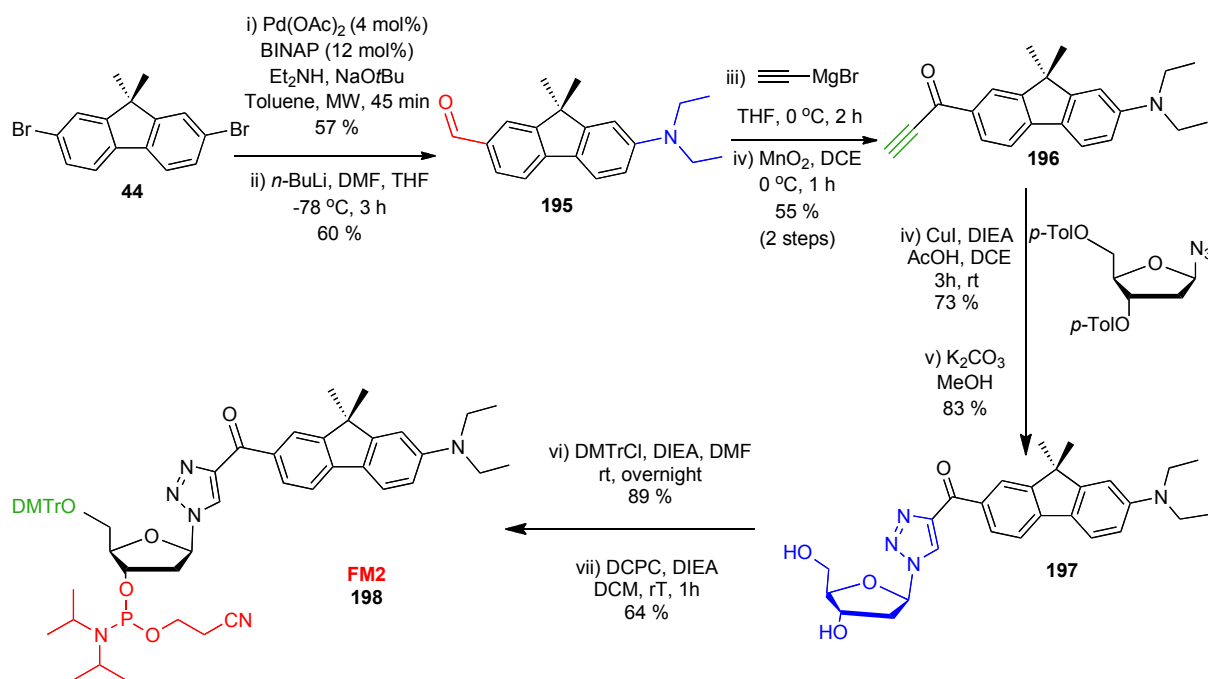
(110 mg, 1.19 mmol, 2 eq.) was then added and the reaction was stirred overnight at rt. The crude was washed by NaHCO₃ (aq.) and extracted with DCM. The organic layer was washed by water, dried with magnesium sulfate, and reduced under pressure. Purification was done by FC. Eluent (DCM/MeOH = 98: 2, R_f = 0.4) to afford compound **194** (312 mg, 71 %) as a yellow solid. ¹H-NMR (200 MHz, CDCl₃, δ): 7.91 (s, 1H), 7.87 (d, ³J=8.0 Hz, 1H), 7.58 (d, ³J=8.0 Hz, 1H), 7.54 (d, ³J=8.0 Hz, 1H), 7.36 (d, ³J=8.0 Hz, 1H), 7.34 (s, 1H), 7.27-7.08 (m, 9H), 6.76 (d, ³J=8.0 Hz, 4H), 3.83 (m, 1H), 3.71 (s, 6H), 3.51 (m, 1H), 3.42-3.20 (m, 3H), 3.12 (m, 2H), 3.0 (s, 6H), 2.53 (m, 2H), 1.41 (s, 6H). ¹³C NMR (50 MHz, CDCl₃, δ): 198.6, 173.8, 158.6 (2C), 157.0, 153.0, 151.5, 145.5, 144.8, 138.0, 136.0, 135.9, 130.1 (4C), 129.3, 129.1 (2C), 128.3 (2C), 128.2, 128.0, 125.4 (2C), 122.1, 118.2, 113.3, 111.7, 106.1, 86.3, 70.4, 65.0, 55.3 (2C), 46.9, 42.2, 40.9(2C), 34.1, 30.5, 27.4 (2C). MS (ESI⁺, MeOH): C₄₅H₄₈N₂O₆, m/z : 713,2 [M+H]⁺.

(S)-1-(bis(4-methoxyphenyl)(phenyl)methoxy)-3-(4-(7-(dimethylamino)-9,9-dimethyl-9H-fluoren-2-yl)-4-oxobutanamido)propan-2-yl (2-cyanoethyl) diisopropylphosphoramidite (188/FM1). Following GP-L on substrate 194.



Yellow solid, Eluent (Tol/Ac = 85:5, R_f = 0.5, 0.58), yield=30 %. ¹H-NMR (200 MHz, CDCl₃, δ): 7.98 (s, 1H), 7.84 (d, ³J=8.0 Hz, 1H), 7.64 (d, ³J=8.0 Hz, 1H),

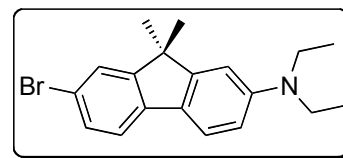
7.60 (d, ³J=8.0 Hz, 1H), 7.46 (d, ³J=8.0 Hz, 1H), 7.45 (s, 1H), 7.36-7.21 (m, 9H), 6.86-6.71 (m, 4H), 4.13-4.02 (m, 2H), 3.78 (s, 6H), 3.69-3.15 (m, 7H), 3.05 (s, 6H), 2.7-2.45 (m, 2H), 1.43 (s, 6H), 1.26-1.11 (m, 12 H). The higher integration by 3 protons in the DMTr region (7.36-6.71) corresponds to initiation of deprotection of the extremely sensitive DMTr in this type of compounds. ³¹P-NMR (CD₃CN, 81 MHz, δ): 149.0, 148.8. MS (ESI⁺, MeOH): C₅₄H₆₅N₄O₇P, m/z : 913,5 [M+H]⁺.



Scheme 8. Synthesis of **FM2**

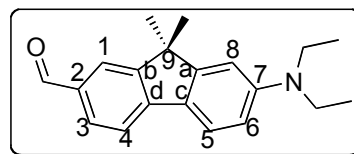
7-bromo-*N,N*-diethyl-9,9-dimethyl-9*H*-fluorene-2-amine

(S12): Following **GP-A** on substrate 44. Eluent for flash chromatography (PE/Et₂O = 98/2, *R_f* = 0.35) providing the amine intermediate **S12** as a yellow solid (57 %). ¹H-NMR (200 MHz, CDCl₃, δ): 7.54-7.40 (m, 4H), 6.69-6.65 (m, 2H), 3.43 (q, ³J=7.0 Hz, 4H), 1.45 (s, 6H), 1.22 (t, ³J=7.0 Hz, 6H). ¹³C-NMR (50 MHz, CDCl₃, δ): 155.3, 154.9, 148.1, 139.1, 129.9, 129.4, 125.8, 121.2, 119.8, 118.4, 111.0, 105.7, 47.0, 44.9 (2C), 27.5 (2C), 12.7 (2C). GC-MS (*m/z*): 343.1 [M]⁺.



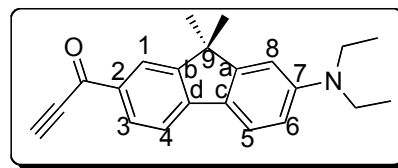
7-(diethylamino)-9,9-dimethyl-9*H*-fluorene-2-carbaldehyde

(195). Following **GP-G** on S12 as starting material. Eluent for flash chromatography (CyHex/EA = 95:5, *R_f* = 0.28) providing the title compound **195** as a yellow solid (60 %). ¹H-NMR (500 MHz, CDCl₃, δ): 9.97 (s, 1H, CHO), 7.87 (d, ⁴J=1.5 Hz, 1H, H1), 7.77 (dd, ³J=7.5 Hz ⁴J=1.5 Hz, 1H, H3), 7.63 (d, ³J=7.5 Hz, 1H, H4), 7.61 (br d, ³J=8.0 Hz, 1H, H5), 6.70 (br s, 1H, H8), 6.69 (dd, ³J=8.0 Hz ⁴J=2.0 Hz, 1H, H6), 3.45 (q, ³J=7.0 Hz, 4H, N(CH₂CH₃)₂), 1.49 (s, 6H, 2CH₃ 9,9), 1.23 (t, ³J=7.0 Hz, 6H, N(CH₂CH₃)₂). ¹³C-NMR (125 MHz, CDCl₃, δ): 192.20 (C=O), 157.51 (Ca), 153.39 (Cb), 149.20 (C7), 147.07 (Cd), 133.61 (C2), 131.41 (C3), 125.41 (Cc), 122.63 (C1), 122.53 (C5), 118.29 (C4), 111.08 (C6), 105.28 (C8), 46.78 (C9), 44.87 (2C, N(CH₂CH₃)₂), 27.40 (2CH₃), 12.75 (2C, N(CH₂CH₃)₂). GC-MS (*m/z*): 293.2 [M]⁺.



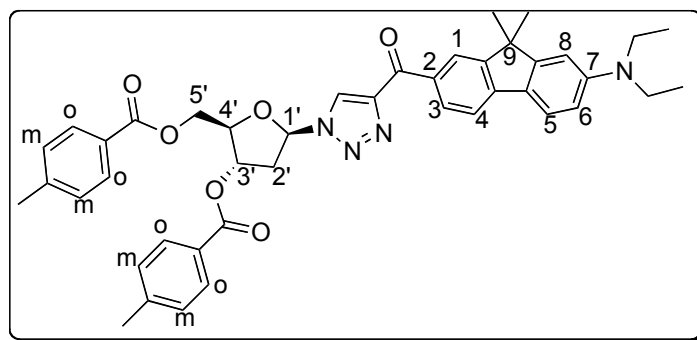
1-(7-(diethylamino)-9,9-dimethyl-9H-fluoren-2-yl)prop-

2-yn-1-one (196). Following **GP-H** on 195 (700 mg, 2.39 mmol) as starting material. Eluent for flash chromatography (CyHex/EA = 9:1, R_f = 0.24) providing the clickable push-pull

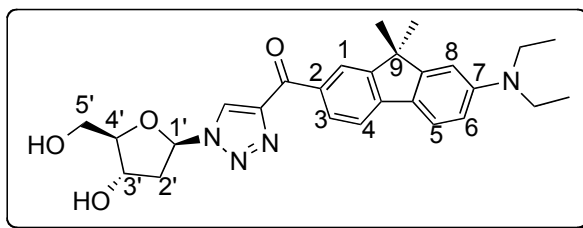


196 as a yellow solid (700 mg, 55 %). $^1\text{H-NMR}$ (500 MHz, CDCl_3 , δ): 8.14 (dd, $^3J=8.0$ Hz $^4J=1.5$ Hz, 1H, H3), 8.12 (s, 1H, H1), 7.62 (d, $^3J=8.5$ Hz, 1H, H4), 7.59 (d, $^3J=8.0$ Hz, 1H, H5), 6.70 (s, 1H, H8), 6.68 (dd, $^3J=8.5$ Hz $^4J=2.0$ Hz, 1H, H6), 3.45 (q, $^3J=7.0$ Hz, 4H, $\text{N}(\text{CH}_2\text{CH}_3)_2$), 3.40 (s, 1H, $\text{C}\equiv\text{CH}$) 1.49 (s, 6H, 2 CH_3), 1.23 (t, $^3J=7.0$ Hz, 6H, $\text{N}(\text{CH}_2\text{CH}_3)_2$). $^{13}\text{C-NMR}$ (125 MHz, CDCl_3 , δ): 177.1 (C=O), 157.7 (Ca), 153.0 (Cb), 149.3 (C7), 147.2 (Cd), 133.3 (C2), 131.1 (C3), 125.3 (Cc), 123.0 (C1), 122.8 (C5), 117.9 (C4), 111.1 (C6), 105.2 (C8), 81.1 ($\text{C}\equiv\text{CH}$), 79.9 ($\text{C}\equiv\text{CH}$), 46.8 (C9), 44.9 (2C, $\text{N}(\text{CH}_2\text{CH}_3)_2$), 27.4 (2 CH_3), 12.7 (2C, $\text{N}(\text{CH}_2\text{CH}_3)_2$). GC-MS (m/z): 317.2 [M] $^+$.

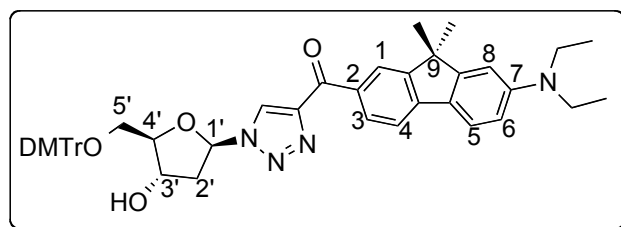
This type of Micheal acceptor compounds is very reactive and cannot be stored for long time.



(2R,3S,5R)-5-(4-(7-(diethylamino)-9,9-dimethyl-9H-fluorene-2-carbonyl)-1H-1,2,3-triazol-1-yl)-2-(((4-methylbenzoyl)oxy)methyl)tetrahydrofuran-3-yl 4-methylbenzoate (S13). Following **GP-I** on 196 (230 mg, 0.73 mmol) as starting material. Eluent for flash chromatography (CyHex/EA = 8:2, R_f = 0.33) providing **S13** as a brown solid (390 mg, 73 %). $^1\text{H-NMR}$ (200 MHz, CDCl_3 , δ): 8.46 (s, 1H, $\text{H}_{\text{triazole}}$), 8.45 (dd, $^3J=8.0$ Hz $^4J=1.5$ Hz, 1H, H3), 8.39 (d, $^3J=8.0$ Hz, 1H, H1), 7.96 (d, $^3J=8.0$ Hz, 2H, H_{otol}), 7.84 (d, $^3J=8.0$ Hz, 2H, H_{otol}), 7.64 (d, $^3J=8.0$ Hz, 1H, H4), 7.62 (d, $^3J=8.0$ Hz, 1H, H5), 7.28 (d, $^3J=8.0$ Hz, 2H, H_{mtol}), 7.17 (d, $^3J=8.0$ Hz, 2H, H_{mtol}), 6.71 (s, 1H, H8), 6.69 (dd, $^3J=8.0$ Hz $^4J=1.5$ Hz, 1H, H6), 6.56 (t, $^3J=6.0$ Hz, 1H, H1'), 5.82 (m, 1H, H3'), 4.71 (m, 1H, H4'), 4.64 (m, 2H, H5'), 3.46 (q, $^3J=7.0$ Hz, 4H, $\text{N}(\text{CH}_2\text{CH}_3)_2$), 3.28 (m, 1H, H2'a), 2.94 (m, 1H, H2'b), 2.44 (s, 3H, CH_3tol), 2.31 (s, 3H, CH_3tol), 1.52 (s, 6H, 2 CH_3), 1.24 (t, $^3J=7.0$ Hz, 6H, $\text{N}(\text{CH}_2\text{CH}_3)_2$). $^{13}\text{C-NMR}$ (50 MHz, CDCl_3 , δ): 184.8, 166.3 (2C), 166.0 (2C), 157.5, 152.7, 149.0, 145.5, 144.7, 144.3, 133.0, 131.3, 130.0 (2C), 129.8 (2C), 129.5 (2C), 129.4 (2C), 127.3, 126.6, 126.5, 124.4, 122.5, 117.8, 111.0, 105.4, 89.3, 84.1, 74.8, 63.9, 47.0, 44.9 (2C), 38.6, 27.5 (2C), 21.9, 21.8, 12.8 (2C).

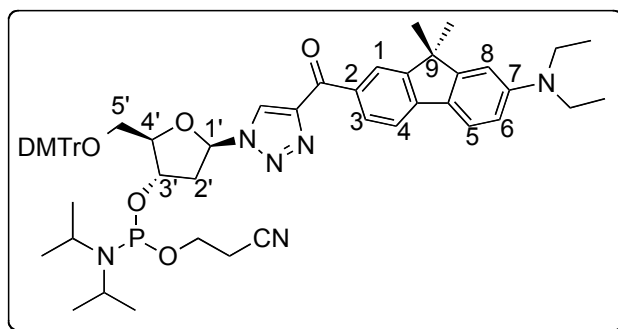


(7-(diethylamino)-9,9-dimethyl-9H-fluoren-2-yl)(1-((2R,4S,5R)-4-hydroxy-5-(1-((2R,4S,5R)-hydroxymethyl)tetrahydrofuran-2-yl)-1H-1,2,3-triazol-4-yl)methanone (197). Following GP-J on S13 (390 mg, 0.55 mmol) as starting material. Eluent for flash chromatography (DCM/Ac = 8:2, R_f = 0.3) providing **197** as a bright yellow solid (205 mg, 79 %). $^1\text{H-NMR}$ (200 MHz, $\text{C}_5\text{D}_5\text{N}$, δ): 9.49 (s, 1H, $\text{H}_{\text{triazole}}$), 8.87 (br s, 1H, H1), 8.83 (br d, 3J =8.0 Hz, 1H, H3), 7.81 (d, 3J =8.0 Hz, 2H, H4,5), 6.99 (t, 3J =6.0 Hz, 1H, H1'), 6.90 (br s, 1H, H8), 6.75 (dd, 3J =8.0 Hz 4J =2.0 Hz, 1H, H6), 5.22 (m, 1H, H3'), 4.62 (m, 1H, H4'), 4.17 (m, 2H, H5'), 3.30 (q, 3J =7.0 Hz, 4H, $\text{N}(\text{CH}_2\text{CH}_3)_2$), 3.30-2.20 (m, 2H, H2'), 1.50 (s, 6H, 2 CH_3), 1.07 (t, 3J =7.0 Hz, 6H, $\text{N}(\text{CH}_2\text{CH}_3)_2$). $^{13}\text{C-NMR}$ (50 MHz, $\text{C}_5\text{D}_5\text{N}$, δ): 184.6 (C=O), 157.2 (Ca), 152.2 (Cb), 149.3 (C7), 148.5 (C=C), 145.5 (Cd), 133.6 (C2), 131.0 (C3), 127.8 (C=CH), 125.3 (Cc), 124.5 (C1), 122.9 (C5), 117.6 (C4), 111.0 (C6), 105.2 (C8), 89.6 (C4'), 89.5 (C1'), 70.6 (C3'), 61.6 (C5'), 46.5 (C9), 44.2 (2C, $\text{N}(\text{CH}_2\text{CH}_3)_2$), 41.6 (C2'), 26.8 (2C, 2 CH_3), 12.1 (2C, $\text{N}(\text{CH}_2\text{CH}_3)_2$). HRMS (ESI⁺): m/z calcd for $\text{C}_{27}\text{H}_{33}\text{O}_4\text{N}_4$: 477.2496 [M+H]⁺; found 477.2491.

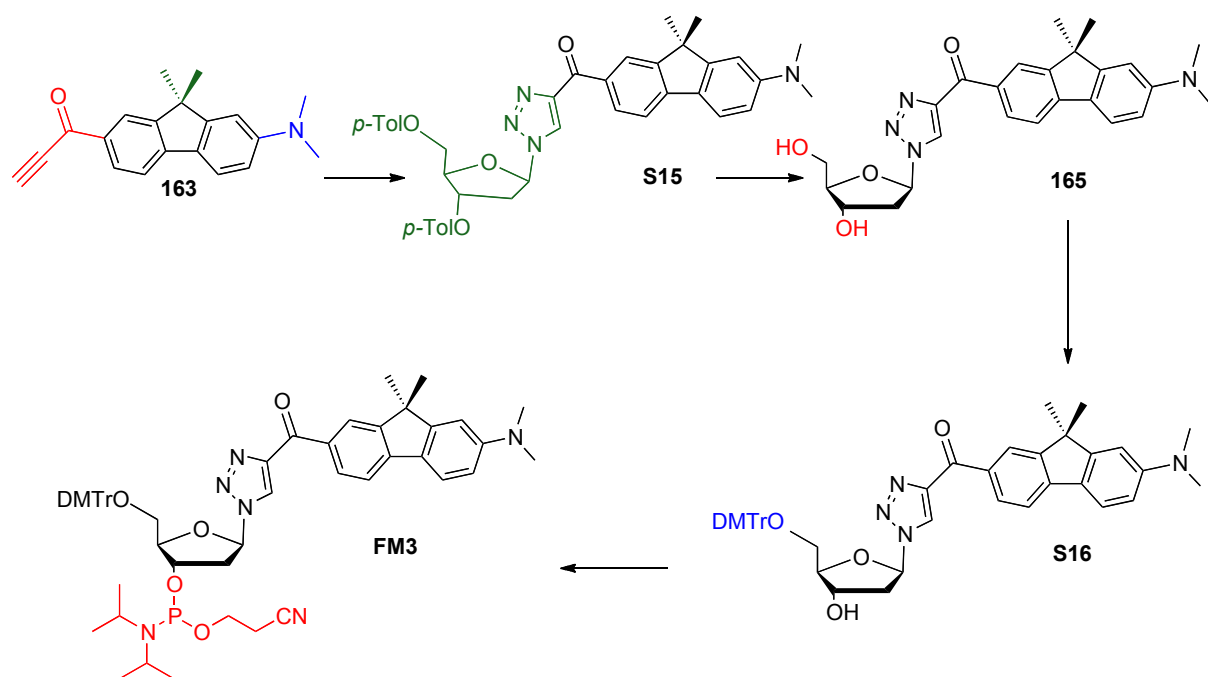


(7-(diethylamino)-9,9-dimethyl-9H-fluoren-2-yl)(1-((2R,4S,5R)-5-((bis(4-methoxyphenyl)(phenyl)methoxy)methyl)-4-hydroxytetrahydrofuran-2-yl)-1H-1,2,3-triazol-4-yl)methanone (S14). Following GP-K on 197 (140 mg, 0.29 mmol) as starting material. Eluent for flash chromatography (Tol/Ac = 8:2, in presence of 1% Et_3N , R_f = 0.5) providing **S14** as a bright yellow solid (215 mg, 89 %). $^1\text{H-NMR}$ (200 MHz, CD_2Cl_2 , δ): 8.40 (s, 1H, $\text{H}_{\text{triazole}}$), 8.39 (br s, 1H, H1), 8.34 (dd, 3J =8.0 4J =2.0 Hz, 1H, H3), 7.61 (2d, 3J =8.0 Hz, 2H, H4,5), 7.40-7.14 (m, 9H, H-DMTr), 6.79 (d, 3J =8.0, 4H, H-DMTr), 6.72 (br s, 1H, H8), 6.69 (dd, 3J =8.0 Hz 4J =2.0 Hz, 1H, H6), 6.42 (t, 3J =6.0 Hz, 1H, H1'), 4.68 (m, 1H, H3'), 4.17 (m, 1H, H4'), 3.71 (s, 6H, (O- CH_3)₂), 3.44 (m, 4H, $\text{N}(\text{CH}_2\text{CH}_3)_2$), 3.29 (m, 2H, H5'), 2.94 (m, 1H, H2'), 2.62 (m, 1H, H2'), 1.49 (s, 6H, 2 CH_3 9,9), 1.22 (t, 3J =7.0 Hz, 6H, $\text{N}(\text{CH}_2\text{CH}_3)_2$). (+ Et_3N) $^{13}\text{C-NMR}$ (50 MHz, $\text{C}_5\text{D}_5\text{N}$, δ): 185.1

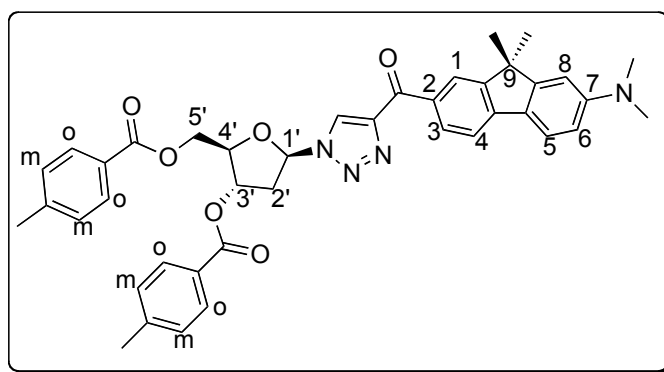
(C=O), 159.03 (2C, C_p-PhOMe), 157.7 (Ca), 153.1 (Cb), 149.4 (C7), 148.7 (C=CH), 146.0 and 145.1 (Cd and C_i-Ph), 136.1 (C_i-PhOMe), 136.0 (C_i-PhOMe), 133.6 (C2), 131.3 (C3), 130.3 (4C, C_o-PhOMe), 128.4 (2C, C_m-Ph), 128.3 (2C, C_o-Ph), 127.5 (C_p-Ph), 127.2 (C=CH), 125.7 (Cc), 124.5 (C1), 122.7 (C5), 117.9 (C4), 113.7 (4C, C_m-PhOMe), 111.2 (C6), 105.6 (C8), 89.3 (C4'), 87.2 (5'-O-C_{IV}), 86.9 (C1'), 72.1 (C3'), 66.1 (C5'), 55.5 (2C, O-CH₃), 47.1 (C9), 45.1 (2C, N(CH₂CH₃)₂), 41.0 (C2'), 27.5 (2C, 2CH₃), 12.7 (2C, N(CH₂CH₃)₂). HRMS (ESI⁺): *m/z* calcd for C₄₈H₅₀O₆N₄Na: 801.3623 [M+Na]⁺; found 801.3623.



((2*R*,3*S*,5*R*)-2-((bis(4-methoxyphenyl)(phenyl)methoxy)methyl)-5-(4-(7-(diethylamino)-9,9-dimethyl-9*H*-fluorene-2-carbonyl)-1*H*-1,2,3-triazol-1-yl)tetrahydrofuran-3-yl)(2-cyanoethyl)diisopropylphosphoramidite (198/FM2). Following **GP-L** on S14 (200 mg, 0.26 mmol) as starting material. Eluent for flash chromatography (Tol/EA = 9:1, in presence of 1% Et₃N, *R_f* = 0.3) providing **FM2** as a bright yellow solid (160 mg, 64 %). ¹H-NMR (200 MHz, CD₂Cl₂, δ): 8.43 (d, ⁴*J* = 2.0 Hz, 1H, H1), 8.38 (dd, ³*J* = 8.0 Hz, ⁴*J* = 2.0 Hz, 1H, H3), 8.32 (s, 1H, H_{triazole}), 7.63 (d, ³*J* = 8.0 Hz, 1H, H4), 7.59 (d, ³*J* = 8.0 Hz, 1H, H5), 7.40-7.14 (m, 9H, H-DMTr), 6.79 (d, ³*J* = 8.0, 4H, H-DMTr), 6.73 (s, 1H, H8), 6.71 (dd, ³*J* = 8.0 Hz, ⁴*J* = 2.0 Hz, 1H, H6), 6.46 (t, ³*J* = 6.0 Hz, 1H, H1'), 4.76 (m, 1H, H3'), 4.34 (m, 1H, H4'), 3.91-3.54 (m, 4H, POCH₂ and N(CH₂CH₃)₂), 3.72 (s, 6H, (O-CH₃)₂), 3.47 (q, ³*J* = 7.0 Hz, 4H, N(CH₂CH₃)₂), 3.29 (m, 2H, H5'), 2.94 (m, 1H, H2'), 2.79 (m, 1H, H2'), 2.64 (t, ³*J* = 6.0 Hz, 1H, CH₂CN), 2.48 (t, ³*J* = 6.0 Hz, 1H, CH₂CN), 1.50 (s, 6H, 2CH₃), 1.26 (m, 18H, N(CH₂CH₃)₂ and N(CH₂CH₃)₂). ³¹P-NMR (CD₃CN, 81 MHz, δ): 149.0, 148.8. HRMS (ESI⁺): *m/z* calcd for C₅₇H₆₈O₇N₆P: 979.4882 [M+H]⁺; found 979.4882.



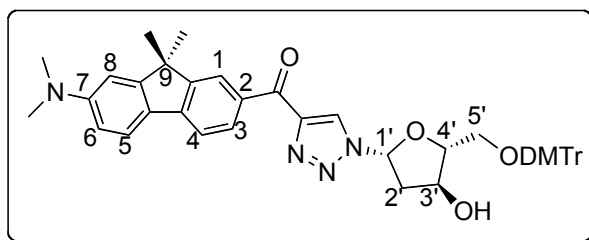
Scheme 9. Synthesis of **FM3**



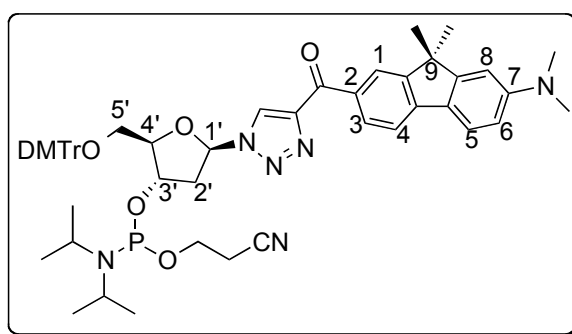
(2*R*,3*S*,5*R*)-5-(4-(7-(dimethylamino)-9,9-dimethyl-9*H*-fluorene-2-carbonyl)-1*H*-1,2,3-triazol-1-yl)-2-(((4-methylbenzoyl)oxy)methyl)tetrahydrofuran-3-yl 4-methylbenzoate (S15**)**. Following **GP-I** on **163** (260 mg, 0.90 mmol) as starting material. Eluent for flash chromatography (CyHex/EA = 8:2, R_f = 0.2) providing **S15** as a bright yellow solid (430 mg, 77 %). $^1\text{H-NMR}$ (200 MHz, CDCl_3 , δ): 8.48 (s, 1H, $\text{H}_{\text{triazole}}$), 8.46 (dd, $^3J=8.0$ Hz $^4J=1.5$ Hz, 1H, H3), 8.42 (br s, 1H, H1), 7.96 (d, $^3J=8.0$ Hz, 2H, $\text{H}_{\text{o,tol}}$), 7.85 (d, $^3J=8.0$ Hz, 2H, $\text{H}_{\text{o,tol}}$), 7.68 (d, $^3J=8.5$ Hz, 1H, H5), 7.63 (d, $^3J=8.0$ Hz, 1H, H4), 7.27 (d, $^3J=8.0$ Hz, 2H, $\text{H}_{\text{m,tol}}$), 7.17 (d, $^3J=8.0$ Hz, 2H, $\text{H}_{\text{m,tol}}$), 6.78 (s, 1H, H8), 6.75 (br d, $^3J=8.5$ Hz, 1H, H6), 6.56 (t, $^3J=6.0$ Hz, 1H, H1'), 5.83 (m, 1H, H3'), 4.71 (m, 1H, H4'), 4.65 (m, 2H, H5'), 3.29 (m, 1H, H2'a), 3.07 (s, 6H, $\text{N}(\text{CH}_3)_2$), 2.94 (m, 1H, H2'b), 2.43 (s, 3H, CH_3tol), 2.31 (s, 3H, CH_3tol), 1.53 (s, 6H, 2 CH_3). $^{13}\text{C-NMR}$ (50 MHz, CDCl_3 , δ): 184.8, 166.2 (2C), 165.9 (2C), 157.2, 152.9, 148.9, 145.5, 144.6, 144.2, 133.4, 131.2, 129.9 (2C), 129.8 (2C),

129.4 (2C), 129.3 (2C), 127.3, 126.6, 126.4, 124.5, 122.2, 118.1, 111.8, 106.2, 89.2, 84.1, 74.8, 63.8, 47.0, 40.9 (2C), 38.5, 27.4 (2C), 21.8, 21.7. HRMS (ESI⁺): *m/z* calcd for C₄₁H₄₁O₆N₄: 685.3021 [M+H]⁺; found 685.3021.

Deprotection of S15 by GP-J protocol provides compound 165/F1 (yield=79 %), which was characterized in the compounds of chapter 4

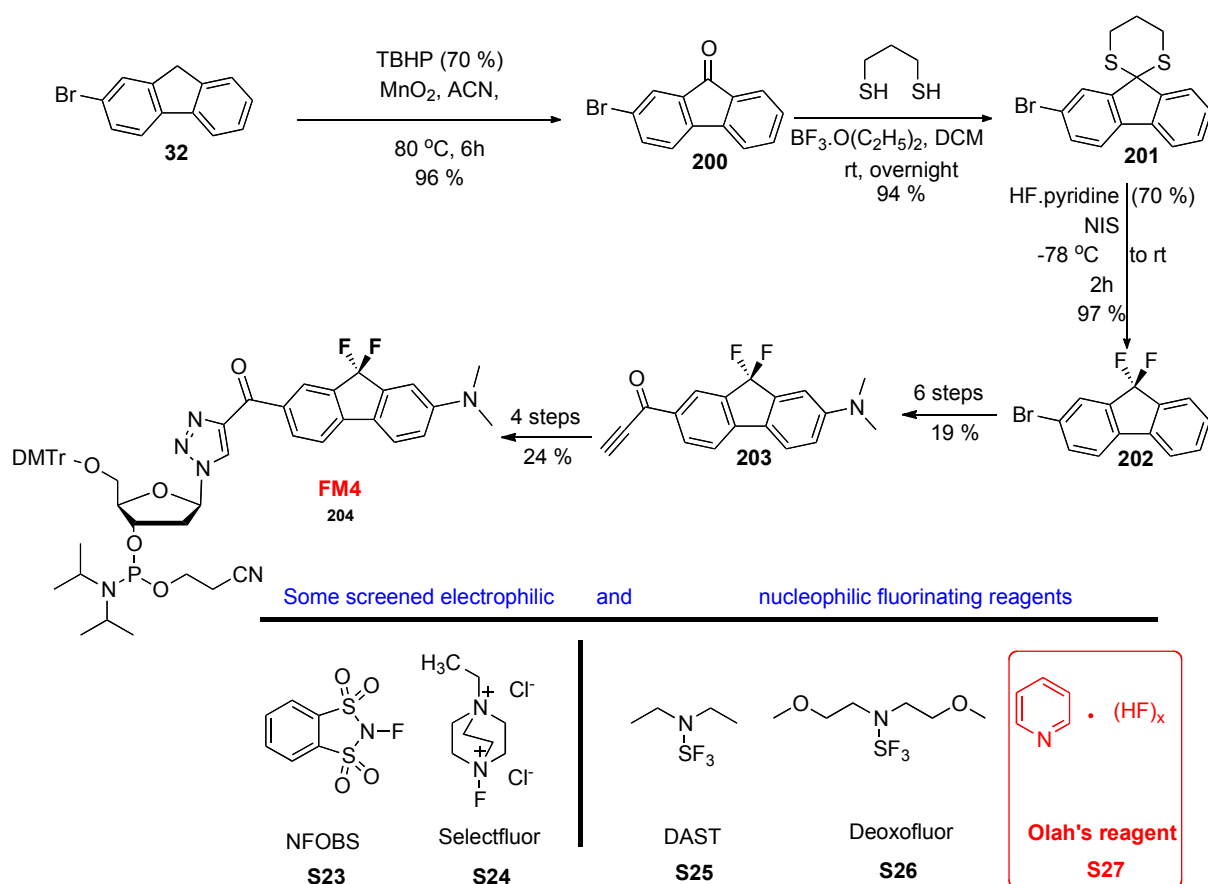


(7-(dimethylamino)-9,9-dimethyl-9H-fluorene-2-yl)(1-((2R,4S,5R)-5-ethyl-4-hydroxytetrahydrofuran-2-yl)-1H-1,2,3-triazol-4-yl) (S16). Following GP-K on 197 (185 mg, 0.41 mmol) as starting material. Eluent for flash chromatography (CyHex/EA = 7:3, in presence of 1% Et₃N, *R_f*= 0.19) providing **S16** as a bright yellow solid (210 mg, 68 %). ¹H-NMR (200 MHz, CD₃CN, δ): 8.12 (s, 1H, H_{triazole}), 7.85 (s, 1H, H1), 8.83 (d, ³*J*=8.0 Hz, 1H, H3), 7.57 (d, ³*J*=8.5 Hz, 1H, H5), 7.55 (d, ³*J*=8.0 Hz, 1H, H4), 7.27-7.09 (m, 9H, H-DMTr), 6.78 (s, 1H, H8), 6.75 (br d, ³*J*=8.5 Hz, 1H, H6), 6.67 (d, ³*J*=8.0, 4H, H-DMTr), 6.32 (t, ³*J*=6.0 Hz, 1H, H1'), 4.53 (m, 1H, H3'), 4.00 (m, 1H, H4'), 3.57 (s, 6H, (O-CH₃)₂), 3.29 (m, 1H, H2'a), 2.85 (s, 6H, N(CH₃)₂), 2.94 (m, 1H, H2'b), 2.43 (s, 3H, OCH₃), 2.31 (s, 3H, OCH₃), 1.53 (s, 6H, 2CH₃). ¹³C-NMR (50 MHz, CDCl₃, δ): 185.1, 158.5 (2C), 157.0, 152.8, 151.5, 148.1, 145.4, 144.57, 136.8, 135.7, 133.5, 130.9, 130.1 (2C), 130.02 (2C), 128.1 (2C), 127.9 (2C), 127.0, 126.9, 125.5, 124.1, 122.1, 117.9, 113.2 (4C), 111.2, 106.0, 89.3, 87.1, 86.4, 71.6, 63.9, 55.2, 46.9, 40.8 (2C), 27.4 (2C). HRMS (ESI⁺): *m/z* calcd for C₄₁H₄₁O₆N₄: 685.3021 [M+H]⁺; found 685.3021.



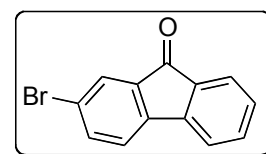
2-cyanoethyl((2R,3S,5R)-5-(4-(7-(dimethylamino)-9,9-dimethyl-9H-fluorene-2-carbonyl)-1H-1,2,3-triazol-1-yl)-2-((3-methoxyphenyl)(4-methoxyphenyl)(phenyl)methoxy)methyl)tetrahydrofuran-3-yl) diisopropylphosphoramidite (199/FM3). Following GP-L on S16 (115 mg, 0.15 mmol) as

starting material. Eluent for flash chromatography (Tol/Ac = 8:2, in presence of 1% Et₃N) providing **FM2** as a bright yellow solid (171 mg, 59 %). ¹H-NMR (200 MHz, CD₂Cl₂, δ): 8.44 (d, ⁴J=2.0 Hz, 1H, H1), 8.40 (dd, ³J=8.0 ⁴J=2.0 Hz, 1H, H3), 8.34 (s, 1H, H_{triazole}), 7.67 (d, ³J=8.0 Hz, 1H, H4), 7.62 (d, ³J=8.0 Hz, 1H, H5), 7.48-7.15 (m, 9H, H-DMTr), 6.85-6.73 (d, ³J=8.0, 4H, H-DMTr), 6.85-6.73 (m, 6H, H6,8 and 4H-DMTr), 6.46 (t, ³J=6.0 Hz, 1H, H1'), 4.80-4.64 (m, 1H, H3'), 4.37-4.07 (m, 1H, H4'), 3.83-3.55 (m, 2H, POCH₂), 3.72 (s, 6H, (O-CH₃)₂), 3.49-3.42 (m, 1H, NCH), 3.27 (m, 2H, H5'), 3.23-3.18 (m, 1H, NCH), 3.06 (s, 6H, N(CH₃)₂), 2.94-2.72 (m, 2H, H2'), 2.64 and 2.51 (2t, ³J=6.0 Hz, 2H, CH₂CN), 1.51 (s, 6H, 2CH₃), 1.28-1.10 (m, 12H, N(CH₂CH₃)₂). ³¹P-NMR (CD₃CN, 81 MHz, δ): 149.1, 149.0. HRMS (ESI⁺): *m/z* calcd for C₅₅H₆₃O₇N₆NaP: 973.4395 [M+Na]⁺; found 973.4388.



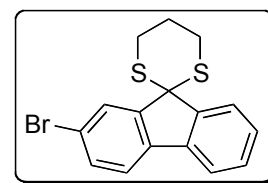
Scheme 10. Synthesis of **FM4** and screened fluorinating reagents^[279]

2-bromo-9H-fluoren-9-one (200). To a solution of 2-bromofluorene **32** (1 g, 4.1 mmol, 1 eq.) dissolved in 12 ml of ACN, MnO₂ (180 mg, 2.06 mmol, 0.5 eq.) then *tert*-butyl hydroperoxide TBHP (1.8 ml, 10 % solution, 3 eq.) were added consecutively at rt. The resulting suspension was refluxed at 80 °C



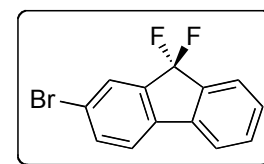
for 6 hrs, after which it was cooled down to rt, diluted by EA and filtered over a pad of Celite®. EA solution was washed with water, dried over MgSO₄, filtered and reduced under vacuum to afford compound **200** (1.02 g, 96 %) as a bright yellow solid; $R_f = 0.29$ (DCM/MeOH = 98/2); $R_f = 0.74$ (Tol/Et₂O = 99/1). ¹H-NMR (200 MHz, CDCl₃, δ): 7.65 (d, ⁴J=1.5 Hz, 1H), 7.56 (d, ³J=7.5 Hz, 1H), 7.51 (dd, ³J=7.5 Hz ⁴J=2Hz, 1H), 7.41 (m, 2H), 7.30 (d, ³J=7.5 Hz, 1H), 7.22 (m, 1H). ¹³C-NMR (50 MHz, CDCl₃, δ): 192.3, 143.6, 142.9, 137.1, 135.7, 135.0, 134.0, 129.4, 127.4, 124.5, 122.9, 121.7, 120.5. GC-MS (m/z): 257.9 [M]⁺.

2-bromospiro[fluorene-9,2'-[1,3]dithiane] (201). Compound 200 (900 mg, 3.49 mmol, 1 eq.), boron trifluoride-etherate (0.43 ml, 3.49 mmol, 1 eq.), 1,3-propanedithiol (756 mg, 7.0 mmol, 2 eq.) and DCM (35 ml) were placed in a round-bottom flask and allowed to react overnight.



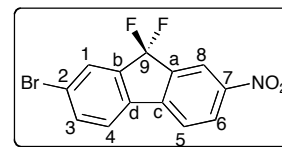
Then, the mixture was washed by NaOH (1N, 75 ml) and brine (75 ml), dried over magnesium sulfate and concentrated *in vacuo* to afford the product **201** (1.2 g, 98%) as white solid; $R_f = 0.88$ (Tol/Et₂O = 99/1). ¹H-NMR (200 MHz, CDCl₃, δ): 8.05 (m, 1H), 7.90 (m, 1H), 7.70 (m, 1H), 7.58 (m, 2H), 7.41 (m, 2H), 3.28 (m, 4H), 2.35 (m, 2H). ¹³C-NMR (50 MHz, CDCl₃, δ): 151.9, 149.1, 137.2, 137.0, 131.9, 129.2, 128.5, 127.4, 124.5, 121.8, 121.6, 120.5, 52.5, 27.8, 24.3. GC-MS (m/z): 347.9 [M]⁺.

2-bromo-9,9-difluoro-9H-fluorene (202): To a solution of NIS (3.3 g, 8.56 mmol, 3 eq.) in 25 ml of DCM, HF.pyridine (1.5 ml of 70 % solution, 27.6 mmol, 10 eq.) was added at -78 °C. Then, a solution of compound **201** (950 mg, 2.76 mmol, 1 eq.) in 15 ml DCM was added drop-wise. The



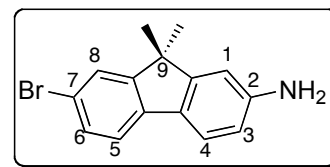
reaction was stirred 1 hr at -78 °C, then 1 hr at rt. When conversion was complete by GC, the mixture was diluted by 15 ml of DCM and filtered over basic alumina. The solution was concentrated to one third, then washed by 10 ml of sodium sulfite, 10 ml of potassium carbonate, dried over magnesium sulfate, filtered and concentrated *in vacuo* to afford compound **202** (741 mg, 97 %) as yellow solid taken to next step without further purification. ¹H-NMR (200 MHz, CDCl₃, δ): 7.75 (d, ⁴J=1.5 Hz, 1H), 7.64-7.57 (m, 2H), 7.52 (dd, ⁴J=1.5 Hz ³J=7.5 Hz, 1H), 7.48-7.32 (m, 3H). ¹³C-NMR (50 MHz, CDCl₃, δ): 139.8 (t, $J_{FC}=24.5$ Hz), 138.5 (m, 2C), 137.5 (t, $J_{FC}=24.5$ Hz), 135.1, 132.4, 129.2, 127.3, 124.0, 122.6 (t, $J_{FC}=24.2$ Hz), 122.4, 121.8, 120.6. ¹⁹F-NMR (188 MHz, CDCl₃, δ): -111.29. GC-MS (m/z): 280.0 [M]⁺.

2-bromo-9,9-difluoro-7-nitro-9H-fluorene (S17). Compound 202 (400 mg, 1.43 mmol) was dissolved in 8 ml of glacial acetic acid. To the formed solution, 6.7 ml of fuming nitric acid was added dropwise (~10 min) at 0°C upon vigorous stirring. After addition was completed,



reaction mixture was further stirred at rt until complete conversion was achieved by GC/TLC (~3 hrs). The mixture was poured into 75 mL of water. Formed residue was filtered off, washed with water and recrystallized from acetonitrile to yield the pure nitro **S17** intermediate (464 mg, 93 %) as yellow needle crystals. ¹H-NMR (200 MHz, CDCl₃, δ): 8.45 (d, ⁴J=2.0 Hz, 1H, H8), 8.39 (dd, ⁴J=2.0 Hz ³J=8.0 Hz, 1H, H6), 7.83 (d, ⁴J=1.5 Hz, 1H, H1), 7.70 (d, ³J=8.0 Hz, 2H, H4,5), 7.54 (d, ³J=8.0 Hz, 1H, H3). ¹³C-NMR (50 MHz, CDCl₃, δ): 148.5 (C7), 144.6 (t, *J*_{FC}=5.0 Hz, Cc), 140.6 (t, *J*_{FC}=25.0 Hz, Cb), 138.9 (t, *J*_{FC}=25.0 Hz, Ca), 136.4 (t, *J*_{FC}=5.0 Hz, Cd), 135.9 (C4), 128.3 (C6), 128.1 (C1), 127.4 (m, C9), 125.1 (C2), 123.2 (C3), 121.1 (C5), 119.8 (C8). ¹⁹F-NMR (188 MHz, CDCl₃, δ): -111.63. GC-MS (*m/z*): 324.9 [M]⁺.

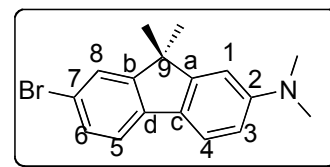
7-bromo-9,9-difluoro-9H-fluoren-2-amine (S18). A mixture of nitro intermediate (250 mg, 0.77 mmol, 1 eq.), iron powder (129 mg, 2.31 mmol, 3 eq.), and NH₄Cl (82 mg, 1.54 mmol, 2 eq.) was refluxed in aqueous ethanol (15 ml of alcohol and 5 ml of water) at



85 °C for 4 h under inert atmosphere. After complete transformation of the initial compound, the reaction mixture was treated with 10 ml of aqueous saturated sodium bicarbonate and filtered through paper filter. Transparent solution was concentrated in vacuum in order to remove organic solvent. Formed residue was filtered off, washed by water, then subjected to Flash chromatography (Toluene/1 % Et₃N) leading to pure amino product S18 (205 mg, 91 %) as bright yellow solid. ¹H-NMR (200 MHz, CDCl₃, δ): 7.55 (d, ⁴J=1.5 Hz, 1H, H8), 7.38 (dd, ³J=8.5 Hz ⁴J=1.5 Hz, 1H, H6), 7.15 (d, ³J=8.5 Hz, 1H, H4), 7.10 (d, ³J=8.5 Hz, 1H, H5), 6.78 (d, ⁴J=2.0 Hz, 1H, H1), 6.57 (dd, ³J=8.5 Hz ⁴J=2.0 Hz, 1H, H3), 3.79 (br s, 2H, NH₂). ¹³C-NMR (50 MHz, CDCl₃, δ): 147.9, 139.5 (m), 139.2 (m), 138.7 (m), 134.9, 128.4 (t, *J*_{FC}=5.0 Hz), 126.9, 122.6 (m), 121.7, 120.5, 120.1, 117.7, 110.4. ¹⁹F-NMR (188 MHz, CDCl₃, δ): -110.23. GC-MS (*m/z*): 295.0 [M]⁺.

7-bromo-9,9-difluoro-*N,N*-dimethyl-9H-fluoren-2-amine

(S19). To the stirred mixture of 7-Bromo-9,9-dimethylfluorenyl-2-amine (180 mg, 0.61 mmol, 1 eq.) and paraformaldehyde (125 mg, 6.10 mmol, 10 eq.) in 99 % glacial acetic acid (3 ml) at 0 °C,



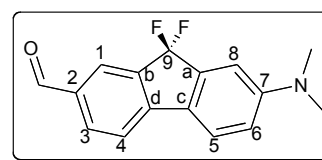
NaCNBH₃ (192 mg, 3.05 mmol, 5 eq.) was added in small portions. The mixture was left to warm up to room temperature and stirred overnight, and then poured into cold water (5 mL). Formed

solution was extracted with ethyl acetate (3*5 mL). Combined organic layer was washed with saturated aqueous solution of NaHCO₃ and dried with magnesium sulfate. Organic solvent was removed under reduced pressure and the obtained residue was purified by flash chromatography on silica gel. Eluent (PE/Et₂O = 98:2, *R_f*= 0.19) to obtain pure dimethylamino product (118 mg, 60 %) as yellow solid. ¹H-NMR (200 MHz, CDCl₃, δ): 7.56 (d, ⁴*J*=1.5 Hz, 1H, H8), 7.39 (br d, ³*J*=8.0 Hz, 1H, H6), 7.25 (d, ³*J*=8.5 Hz, 1H, H4), 7.14 (d, ³*J*=8.0 Hz, 1H, H5), 6.85 (d, ⁴*J*=1.5 Hz, 1H, H1), 6.61 (dd, ³*J*=8.5 Hz ⁴*J*=1.5 Hz, 1H, H3), 2.93 (s, 6H, N(CH₃)₂). ¹³C-NMR (50 MHz, CDCl₃, δ): 151.3 (C2), 139.7 (t, *J_{FC}*=5.0 Hz, Cd), 139.2 (m, *J_{FC}*=5.0 Hz, Ca), 138.6 (m, *J_{FC}*=5.0 Hz, Cb), 134.9 (C6), 126.9 (C8), 125.9 (t, *J_{FC}*=5.0 Hz, Cc), 122.9 (t, *J_{FC}*=243 Hz, C9), 121.5 (C4), 120.3 (C5), 119.6 (C7), 114.7 (C3), 107.4 (C1), 40.5 (2C, N(CH₃)₂). ¹⁹F-NMR (188 MHz, CDCl₃, δ): -109.48. GC-MS (*m/z*): 323.0 [M]⁺.

The reactions above were scaled up to prepare more starting materials.

7-(dimethylamino)-9,9-difluoro-9H-fluorene-2-carbaldehyde

(S20). Following GP-G on S19 starting material. **Yield = 49 %**. ¹H-NMR (200 MHz, CDCl₃, δ): 9.94 (s, 1H, CHO), 8.01 (d, ⁴*J*=1.5 Hz, 1H, H1), 7.89 (br d, ³*J*=8.0 Hz, 1H, H3), 7.48 (d, ³*J*=8.0 Hz, 1H, H4), 7.44



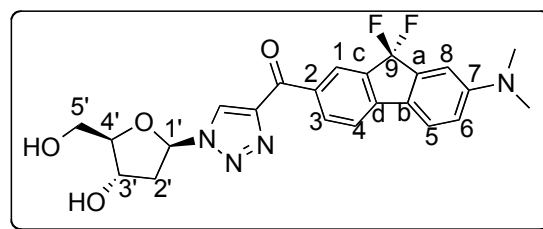
(d, ³*J*=8.5 Hz, 1H, H5), 6.95 (d, ⁴*J*=2.0 Hz, 1H, H8), 6.72 (dd, ³*J*=8.0 Hz ⁴*J*=2.0 Hz, 1H, H6), 3.06 (s, 6H, N(CH₃)₂). ¹³C-NMR (50 MHz, CDCl₃, δ): 190.9 (C=O), 152.2 (C7), 147.0 (t, *J_{FC}*=5.0 Hz, Cd), 140.8 (t, *J_{FC}*=25.0 Hz, Ca), 138.2 (t, *J_{FC}*=25.0 Hz, Cb), 135.0 (C3), 134.8 (C2), 125.2 (t, *J_{FC}*=25.0 Hz, Cc), 124.4 (C1), 122.7 (C5), 122.6 (C9), 119.1 (C4), 114.7 (C6), 107.33 (C8), 40.6 (N(CH₃)₂). ¹⁹F-NMR (188 MHz, CDCl₃, δ): -110.38. HRMS (ESI⁺): *m/z* calcd for C₁₆H₁₄ONF₂: 274.1038 [M+H]⁺; found 274.1038.

HRMS (ESI⁺): *m/z* calcd for C₁₆H₁₄ONF₂: 274.1038 [M+H]⁺; found 274.1038.

1-(7-(dimethylamino)-9,9-difluoro-9H-fluoren-2-yl)prop-2-yn-1-one (203). Following GP-H on S20 as starting material (1.2 g, 4.0 mmol), which was clicked to the azido sugar without purification. This product degrades extremely fast.

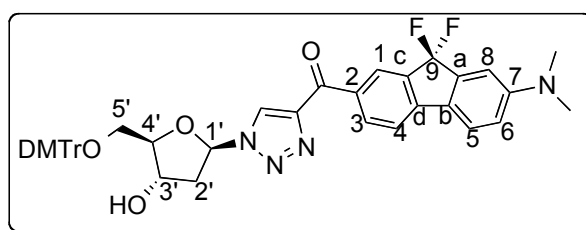
(7-(dimethylamino)-9,9-difluoro-9H-fluoren-2-yl)(1-((2R,4S,5R)-4-hydroxy-5-(hydroxymethyl)tetrahydrofuran-2-yl)-1H-1,2,3-triazol-4-yl)methanone (S21)

Following GP-I for clicking the substrate and batching directly into deprotection GP-J protocol. Yield=39 % over two steps. ¹H-NMR (200 MHz, C₅D₅N,



δ): 9.50 (s, 1H, H_{triazole}), 9.09 (br s, 1H, H1), 8.75 (br d, ³J=8.0 Hz, 1H, H3), 7.60 (d, ³J=8.0 Hz, 2H, H4,5), 7.20 (d, 1H, ⁴J=2.0 Hz, H8), 6.99 (t, ³J=6.0 Hz, 1H, H1'), 6.73 (dd, ³J=8.0 Hz ⁴J=2.0 Hz, 1H, H6), 5.23 (m, 1H, H3'), 4.63 (m, 1H, H4'), 4.20 (m, 2H, H5'), 3.20-2.78 (m, 2H, H2'), 2.86 (s, 6H, N(CH₃)₂), 1.57 (s, 6H, 2CH₃). ¹³C-NMR (50 MHz, C₅D₅N, δ): 183.6 (C=O), 152.0 (C7), 148.2 (C=CH), 145.6 (t, J_{FC}=5.0 Hz, Cd), 140.5 (t, J_{FC}=25.0 Hz, Ca), 137.3 (t, J_{FC}=25.0 Hz, Cb), 135.6 and 135.2 (C2), 135.1 (C3), 128.3 (C=CH), 125.7 (C1), 125.6 (m, C9), 125.2 (t, J_{FC}=5.0 Hz, Cc), 122.9 (C5), 118.9 (C4), 114.9 (C6), 107.2 (C8), 89.8 (2C, C1',4'), 70.8 (C3'), 61.9 (C5'), 41.8 (C2'), 39.7 (2C, N(CH₃)₂).

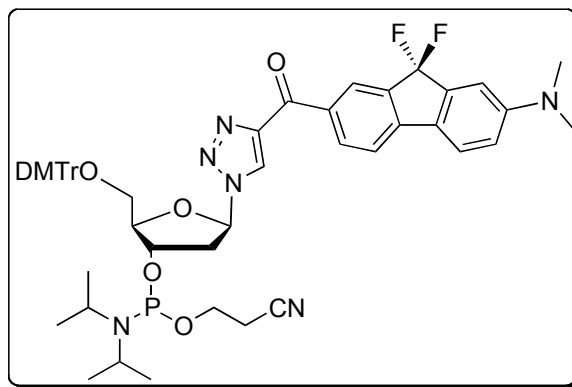
HRMS (ESI⁺): *m/z* calcd for C₂₃H₂₂O₄N₄F₂Na: 479.1501 [M+Na]⁺; found 479.1498.



(1-((2R,4S,5R)-5-((bis(4-methoxyphenyl)(phenyl)methoxy)methyl)-4-

hydroxytetrahydrofuran-2-yl)-1H-1,2,3-triazol-4-yl)(7-(dimethylamino)-9,9-difluoro-9H-

fluoren-2-yl)methanone (S22). Following **GP-K** on S12 (150 mg, 0.22 mmol) as starting material. Eluent for flash chromatography (Tol/Ac = 7:3, *R_f* = 0.25) providing the title compound **S22** as a yellow solid (149 mg, 71 %). ¹H-NMR (200 MHz, CD₂Cl₂, δ): 8.56 (br s, 1H, H1), 8.51 (br d, ³J=8.0, 1H, H3), 8.46 (s, 1H, H_{triazole}), 7.51 (2d, ³J=8.0 Hz, 2H, H4,5), 7.40-7.16 (m, 9H, H-DMTr), 6.01 (d, ⁴J=2.0 Hz, 1H, H8), 6.80 (d, ³J=8.0, 5H, H-DMTr and H6), 6.43 (t, ³J=6.0 Hz, 1H, H1'), 4.67 (m, 1H, H3'), 4.21 (m, 1H, H4'), 3.73 (s, 6H, (O-CH₃)₂), 3.29 (m, 2H, H5'), 3.07 (s, 6H, N(CH₃)₂), 2.94 (m, 1H, H2'), 2.66 (m, 1H, H2'). ¹³C-NMR (50 MHz, CD₂Cl₂, δ): 183.9, 162.8, 159.0 (2C), 152.5, 148.3, 145.9, 145.1, 141.17, 140.9 (t, J_{FC}=5.0 Hz) 137.6 (t, J_{FC}=25.0 Hz), 136.1, 136.0 (2C), 135.0, 130.4 (2C), 130.3 (2C), 128.4 (2C), 128.3 (2C), 127.8, 127.2, 125.7, 125.5 (t, J_{FC}=5.0 Hz), 123.4, 122.9, 118.9, 115.0, 113.5 (4C), 107.4, 89.5, 87.3, 86.8, 72.0, 64.0, 55.5 (2C), 41.1, 40.7 (2C). HRMS (ESI⁺): *m/z* calcd for C₄₄H₄₀O₆N₄F₂Na: 781.2806 [M+Na]⁺; found 781.2808.

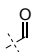
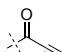
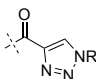
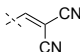
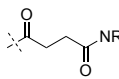


(2*R*,3*S*,5*R*)-2-((bis(4-methoxyphenyl)(phenyl)methoxy)methyl)-5-(4-(7-(dimethylamino)-9,9-difluoro-9*H*-fluorene-2-carbonyl)-1*H*-1,2,3-triazol-1-yl)tetrahydrofuran-3-yl (2-cyanoethyl) diisopropylphosphoramidite (FM4). Following GP-L on S22 (100 mg, 0.09 mmol) as starting material. Eluent for flash chromatography (Tol/Ac = 8:2, R_f = 0.35) providing phosphoramidite **FM4** as a yellow solid (105 mg, 88 %). $^1\text{H-NMR}$ (200 MHz, CD_2Cl_2 , δ): 8.57 (s, 1H,), 8.52-8.44 (m, 2H), 7.53-7.48 (m, 2H), 7.40-7.14 (m, 9H), 7.01 (d, 4J =2.0 Hz, 1H), 6.82-6.78 (m, 5H,)), 6.46 (t, 3J =6.0 Hz), 4.80-4.72 (m, 1H), 4.37-4.09 (m, 1H), 3.8-3.41 (m, 9H), 3.32-3.27 (m, 2H), 3.07-2.67 (m, 9H), 2.64 and 2.48 (2t, 3J =6.0 Hz), 1.28-1.10 (m, 12H). $^{19}\text{F-NMR}$ (188 MHz, CDCl_3 , δ): -110.73. $^{31}\text{P-NMR}$ (CD_3CN , 81 MHz, δ): 149.1. HRMS (ESI⁺): m/z calcd for $\text{C}_{53}\text{H}_{57}\text{O}_7\text{N}_6\text{F}_2\text{NaP}$: 981.3893 [$\text{M}+\text{Na}$]⁺; found 981.3887.

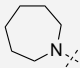
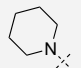
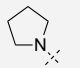
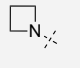
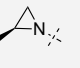
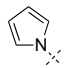
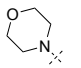
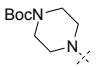
XIII. Supplementary characterization of chapter 3

XIII.1 Transition Dipole Moment of push-pull dyes (in Debye):

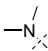
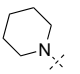
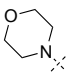
Varied-acceptor / fixed donor (NMe₂):

PP1	PP2	PP3	PP4	PP6
				
12,9	12,9	13,5	14,1	12,6

Varied-ring size amine / fixed acceptor (formyl):

PP8	PP9	PP10	PP11	PP12	PP7	PP13	PP14
							
13,3	12,1	13,7	13,3	11,4	13,4	13,1	12,1

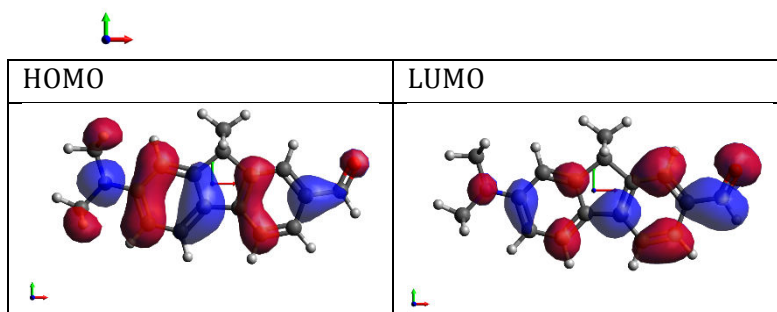
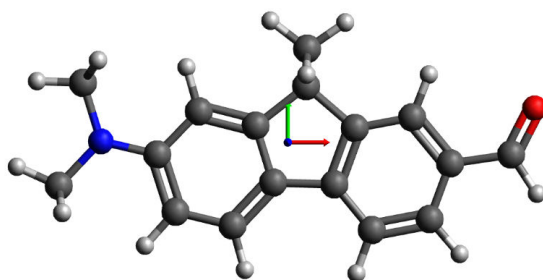
Optimized push-pull dyes (fixed acceptor methylenemalonitrile):

PP4	PP15	PP16
		
14,1	14,4	14,9

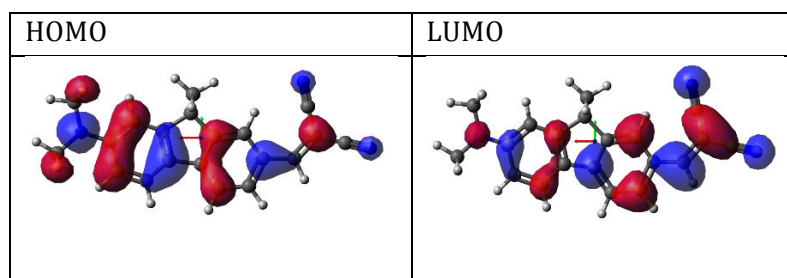
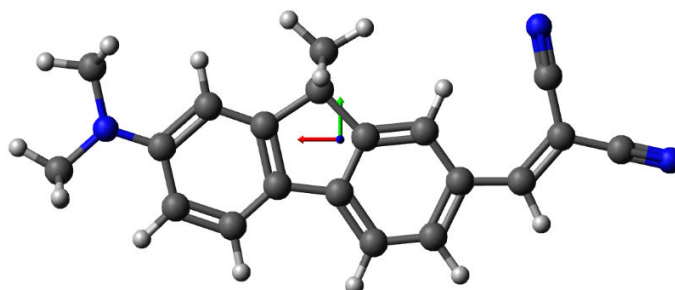
XIII.2 DFT and TDDFT calculations.

All calculations were carried out using the Gaussian03 program. Geometry optimizations of molecules were performed at the B3LYP/6-31+G(d,p) level for all atoms without any symmetry restriction. The first singlet excited states were obtained using time-dependent DFT calculations for isolated molecules starting from optimized geometries at the mPW1PW91/6-31+G(d,p) level of theory. The effects of solvents were taken into account by using the polarisable continuum model (PCM).^[252]

DFT optimized geometries, HOMO, LUMO, experimental versus theoretical wavelength values, oscillator strengths and x,y,z coordinates. Some compounds are shown here.

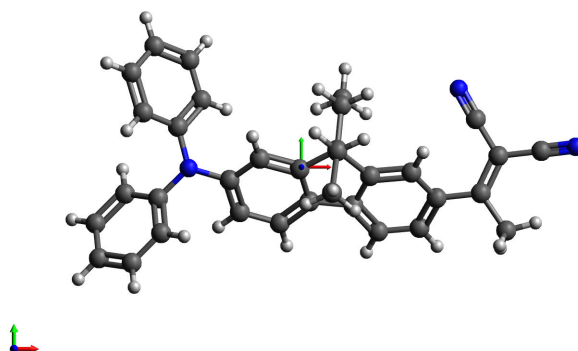
PP1 (d=10.30)

Solvent	λ_{\max} exp (nm)	λ_{\max} calc. (nm)	f: oscillator strength	Dx	Dy	Dz
CH ₃ CN	384	404	0.8266	-3.3174	0.0449	0.0009
CHCl ₃	391	402	0.8556	-3.3659	-0.0494	0.0014
Toluene	387	395	0.8681	-3.3594	-0.0507	0.0001

PP4 (d=10.34)

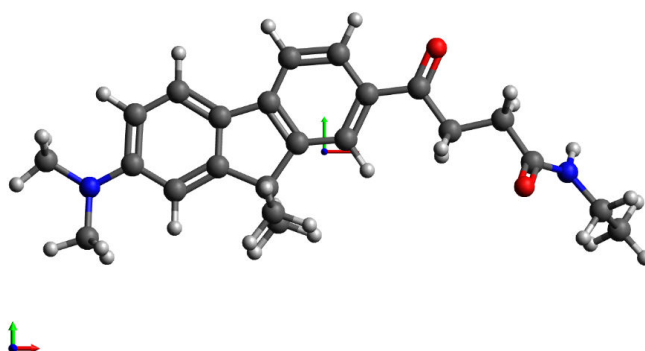
Solvent	λ_{\max} exp (nm)	λ_{\max} calc. (nm)	f: oscillator strength	Dx	Dy	Dz
CH ₃ CN	488	510	1.0792	-4.2528	-0.1655	-0.0013
CHCl ₃	486	505	1.0950	-4.2634	-0.1877	-0.0011
Toluene	474	497	1.0955	-4.2279	-0.2048	-0.0010

Control compound: contrôle (d=9.37)



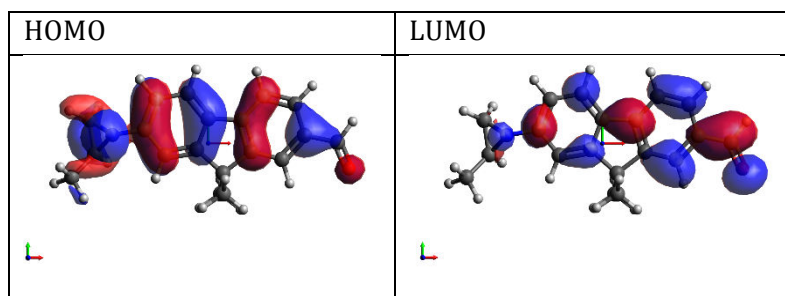
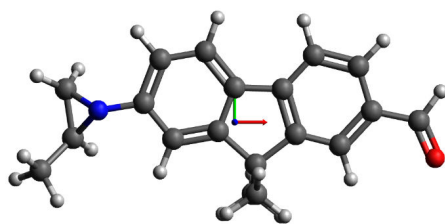
E S0-S1 (nm)	Osc. strength	HOMO	LUMO	Dx ; Dy ; Dz
491 (Exp 488)	0.4900			2.8146 0.0414 -0.0109

PP6 (d=10.64)

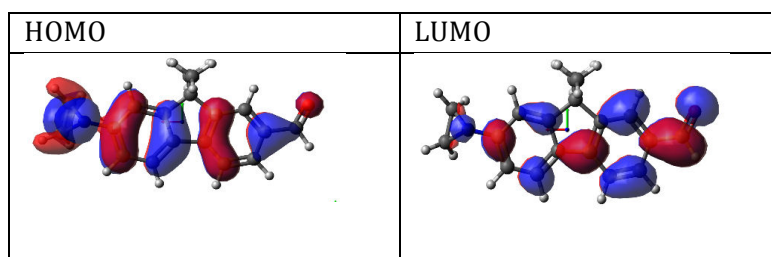
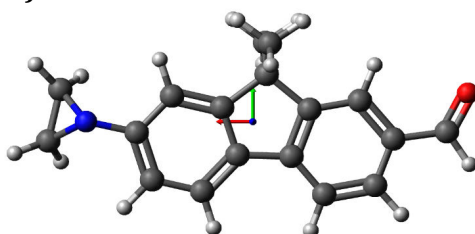


HOMO	LUMO

Solvent	λ_{\max} exp (nm)	λ_{\max} calc. (nm)	f: oscillator strength	Dx	Dy	Dz
CH ₃ CN	399	368	0.83	-3.2061	-0.8058	-0.0555
CHCl ₃	381	401	0.8211	-3.1968	-0.7700	-0.0675
Toluene	374	391	0.8601	-3.2292	-0.7963	-0.0518

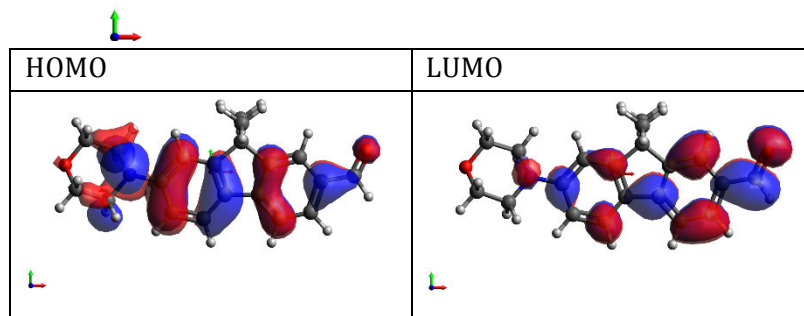
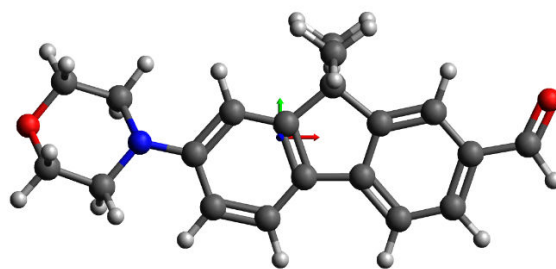
PP12 (d=10.35)

Solvent	λ_{\max} exp (nm)	λ_{\max} calc. (nm)	f: oscillator strength	Dx	Dy	Dz
CH ₃ CN	351	368	0.8373	-3.1836	0.0535	-0.0569
CHCl ₃	352	366	0.8687	-3.2343	0.0547	-0.0543
Toluene	352	363	0.8844	-3.2481	0.0529	-0.0505

Contole- aziridine (d=10.35)

Solvent	λ_{\max} calc. (nm)	f: oscillator strength	Dx	Dy	Dz
CH ₃ CN	371	0.8542	3.2206	-0.2149	-0.0492
CHCl ₃	369	0.8846	3.2684	-0.2219	-0.0459
Toluene	365	0.8995	3.2804	-0.2223	-0.0415

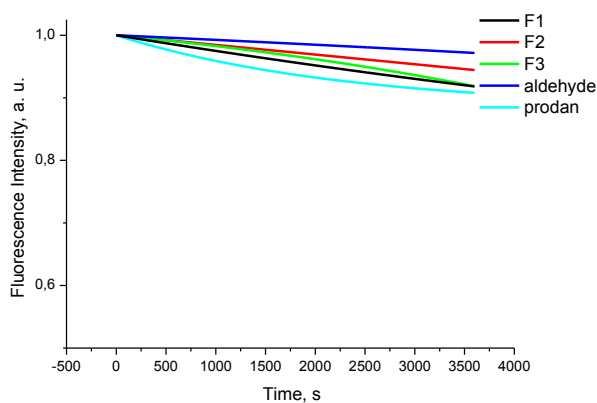
PP14 (d=10.36)



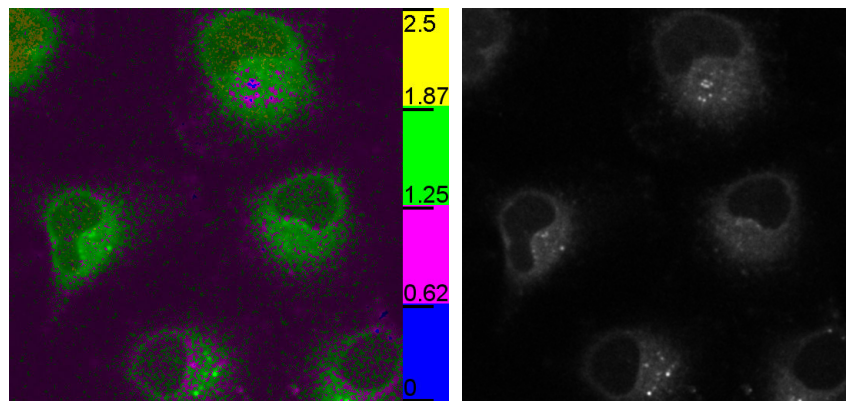
Solvent	λ_{\max} exp (nm)	λ_{\max} calc. (nm)	f: oscillator strength	Dx	Dy	Dz
CH ₃ CN	365	390	0.8240	-3.2485	-0.1510	-0.0308
CHCl ₃	368	386	0.8593	-3.3017	-0.1599	-0.0431
Toluene	365	381	0.8746	-3.3068	-0.1636	-0.0459

XIV. Supplementary characterization of chapter 4

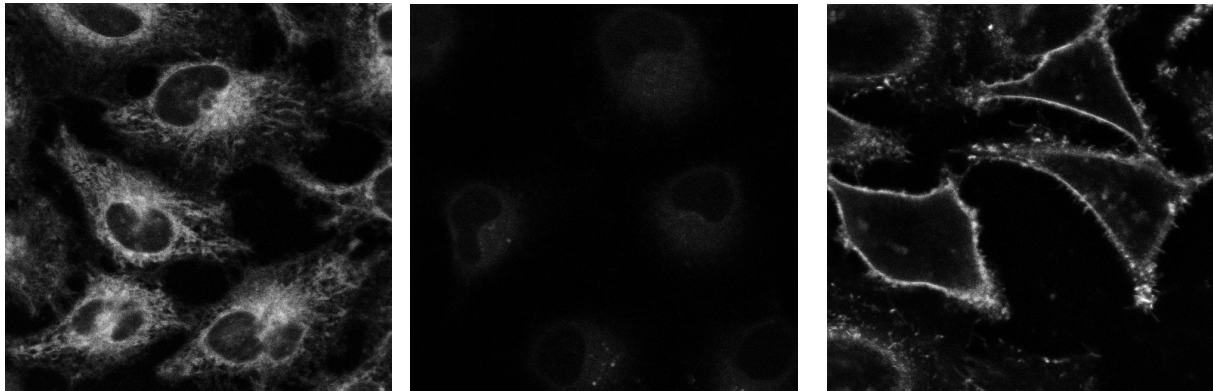
XIV.1 Photodegradation decay curves of F1-3 as a function of time in ethanol



XIV.2 Ratio images for F2 probe in cells



XIV.3 Comparison of the intensity of dyes; F1, F2, and F3 respectively.





XV. Supplementary characterization of chapter 5

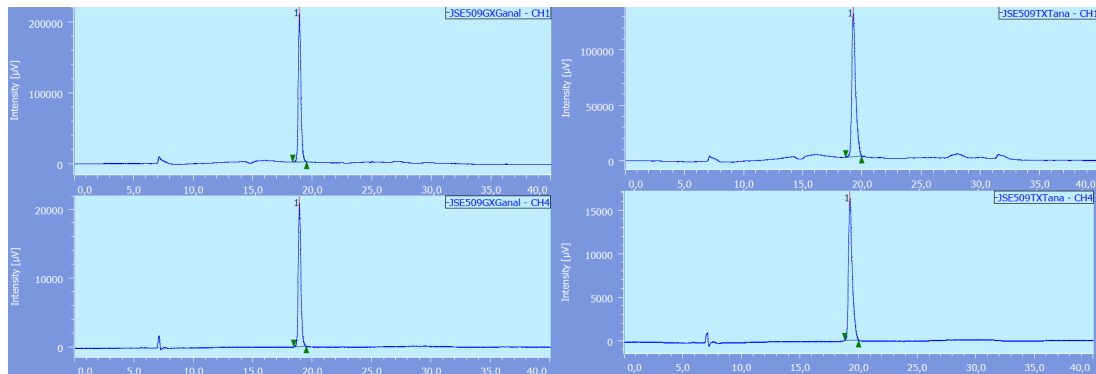
XV.1 Photophysical characterization of Dye 190

Solvent ^[a]					
Water	λ_{Abs} (nm)	360	DCM	λ_{Abs} (nm)	372
	λ_{Em} (nm)	607		λ_{Em} (nm)	507
	$\Delta\lambda_{\text{SS}}$ (nm)	247		$\Delta\lambda_{\text{SS}}$ (nm)	135
	Φ (%)	10		Φ (%)	58
Methanol	λ_{Abs} (nm)	373	DCE	λ_{Abs} (nm)	373
	λ_{Em} (nm)	573		λ_{Em} (nm)	512
	$\Delta\lambda_{\text{SS}}$ (nm)	200		$\Delta\lambda_{\text{SS}}$ (nm)	139
	Φ (%)	36		Φ (%)	59
Ethanol	λ_{Abs} (nm)	374	CHCl_3	λ_{Abs} (nm)	376
	λ_{Em} (nm)	560		λ_{Em} (nm)	506
	$\Delta\lambda_{\text{SS}}$ (nm)	186		$\Delta\lambda_{\text{SS}}$ (nm)	130
	Φ (%)	42		Φ (%)	73
Acetonitrile	λ_{Abs} (nm)	368	EA	λ_{Abs} (nm)	367
	λ_{Em} (nm)	528		λ_{Em} (nm)	491
	$\Delta\lambda_{\text{SS}}$ (nm)	160		$\Delta\lambda_{\text{SS}}$ (nm)	124
	Φ (%)	82		Φ (%)	68
DMF	λ_{Abs} (nm)	374	Dioxane	λ_{Abs} (nm)	368
	λ_{Em} (nm)	514		λ_{Em} (nm)	461
	$\Delta\lambda_{\text{SS}}$ (nm)	140		$\Delta\lambda_{\text{SS}}$ (nm)	93
	Φ (%)	63		Φ (%)	80
Acetone	λ_{Abs} (nm)	369	Toluene	λ_{Abs} (nm)	373
	λ_{Em} (nm)	514		λ_{Em} (nm)	465
	$\Delta\lambda_{\text{SS}}$ (nm)	145		$\Delta\lambda_{\text{SS}}$ (nm)	92
	Φ (%)	51		Φ (%)	74

[a] as table 3.

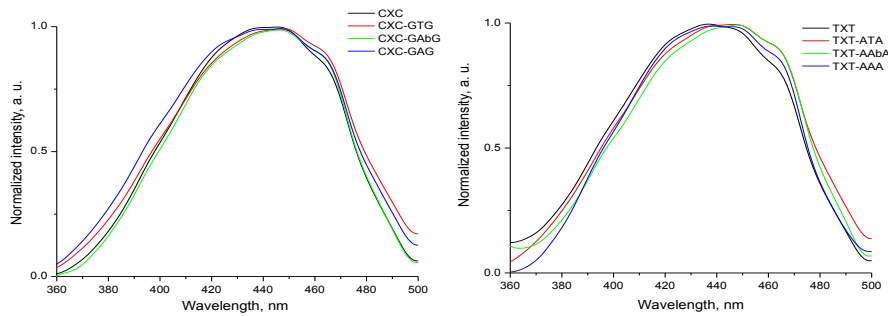
XV.2 HPLC profile:

GXG (left) and TXT (right) single strand ODN (255 nm up – 390 nm down); X-label is FM2.



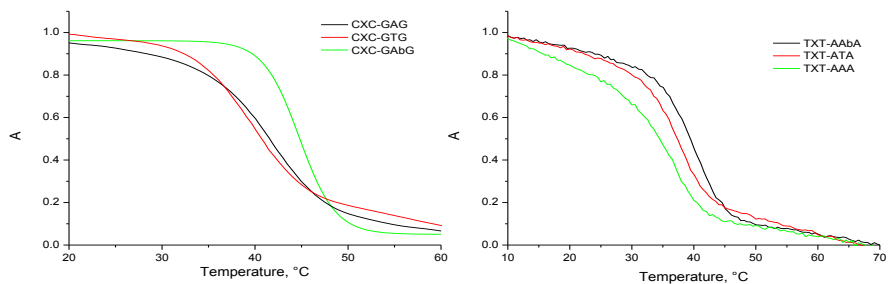
XV.3 Excitation spectra

CXC (left) and TXT (right) investigations, X label is FM4.



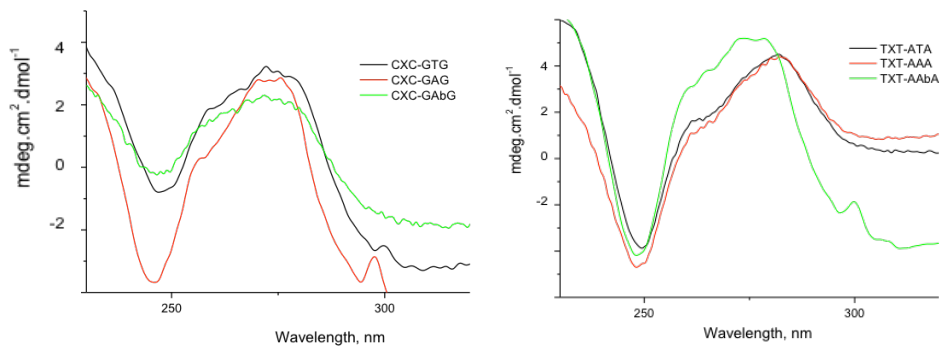
XV.4 Melting temperature curves

CXC (left) and TXT (right) duplexes, X label is FM4.

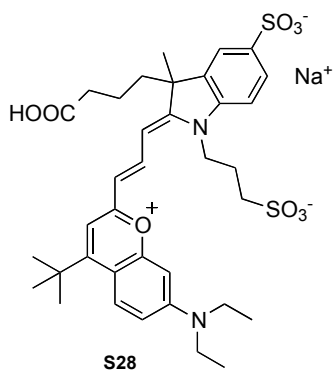


XV.5 CD spectra

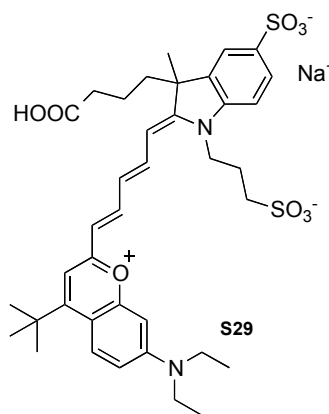
CXC (left) and TXT (right) duplexes



XV.6 Acceptor Dyes used in FRET



Dy681
 Abs: 691 nm / Em: 708 nm
 Abs Coef.: 140.000 M⁻¹cm⁻¹
 Ethanol



Dy781
 Abs: 783 nm / Em: 800 nm
 Abs Coef.: 170.000 M⁻¹cm⁻¹
 Ethanol

References

- [1] A. P. Demchenko, *Introduction to Fluorescence Sensing*, Springer, New York, 2nd edn, **2015**.
- [2] B. Valeur, M. N. Berberan-Santos, *Molecular Fluorescence: Principles and Applications*, Wiley-VCH, Weinheim, 2nd edn, **2012**.
- [3] J. R. Lakowicz, *Principles of Fluorescence Spectroscopy*, Springer, New York, 3rd edn, **2006**.
- [4] S. E. Braslavsky, Glossary of Terms Used in Photochemistry, 3rd edition (IUPAC Recommendations 2006). *Pure Appl. Chem.* **2007**, 79(3), 293.
- [5] D. Dziuba, Synthèse de nouvelles sondes de fluorescence bicolores pour le marquage des acides nucléiques et l'étude des interactions protéines-acides nucléiques, Université Nice Sophia Antipolis SFA, 2011.
- [6] Michael Seery. <https://photochemistry.wordpress.com/2009/08/24/light-absorption-and-fate-of-excited-state/>
- [7] J. Franck, E. G. Dymond, *Trans. Faraday Soc.* **1926**, 21, 536.
- [8] H. Kobayashi, M. Ogawa, R. Alford, P. L. Choyke, Y. Urano, *Chem. Rev.* **2010**, 110, 2620.
- [9] N. P. F. Barthes, Epigénétique et méthylation de l'ADN: Développement d'outils pour la compréhension du mécanisme de méthylation de l'ADN impliquant UHRF1, Université Nice Sophia Antipolis SFA, 2011.
- [10] A. Jabłoński, *Nature*. **1933**, 131, 839.
- [11] M. Kasha, *Discuss. Faraday Soc.* **1950**, 9, 14.
- [12] G. Weber, F. W. J. Teale, *Trans. Faraday Soc.* **1957**, 53, 646.
- [13] S.-H. Kim, E.-M. Lee, in *Encyclopedia of Color Science and Technology*, Springer, Berlin, Heidelberg, **2014**, pp. 1-7.
- [14] J. Liu, Z. Cao, Y. Lu, *Chem. Rev.* **2009**, 109, 1948.
- [15] M. Zimmer, *Chem. Rev.* **2002**, 102, 759.
- [16] K. Maxwell, G. N. Johnson, *J. Exp. Bot.* **2000**, 51, 659.
- [17] M. C. Morris, M. C. Morris, *Fluorescence-Based Biosensors: From Concepts to Applications*, Elsevier, 1st edn, **2013**.
- [18] R. Heim, A. B. Cubitt, R. Y. Tsien, *Nature* **1995**, 373, 663.
- [19] X. Shu, A. Royant, M. Z. Lin, T. A. Aguilera, V. Lev-Ram, P. A. Steinbach, R. Y. Tsien, *Science* **2009**, 324, 804.
- [20] A. P. Demchenko, *Methods Appl. Fluoresc.* **2013**, 1, 022001.
- [21] W. E. Moerner, *J. Phys. Chem. B* **2002**, 106, 910.
- [22] W. E. Moerner, D. P. Fromm, *Rev. Sci. Instrum.* **2003**, 74, 3597.
- [23] T. Aotake, H. Tanimoto, H. Hotta, D. Kuzuhara, T. Okujima, H. Uno, H. Yamada, *Chem. Commun.* **2013**, 49, 3661.
- [24] H. Zhu, F. D. Lewis, *Bioconjugate Chem.* **2007**, 18, 1213.
- [25] G. K. Bains, S. H. Kim, E. J. Sorin, V. Narayanaswami, *Biochemistry* **2012**, 51, 6207.
- [26] M. S. T. Gonçalves, *Chem. Rev.* **2009**, 109, 190.
- [27] L. Song, E. J. Hennink, I. T. Young, H. J. Tanke, *Biophysj* **1995**, 68, 2588.
- [28] J. E. Berlier, A. Rothe, G. Buller, J. Bradford, D. R. Gray, B. J. Filanoski, W. G. Telford, S. Yue, J. Liu, C.-Y. Cheung, et al., *J. Histochem. Cytochem.* **2003**, 51, 1699.
- [29] O. V. Przhonska, S. Webster, L. A. Padilha, H. Hu, A. D. Kachkovski, D. J. Hagan, E. W. Van Stryland, in *Advanced Fluorescence Reporters in Chemistry and Biology I*, Springer Berlin Heidelberg, Berlin, Heidelberg, **2010**, pp. 105.
- [30] G. S. Loving, M. Sainlos, B. Imperiali, *Trends in Biotechnology* **2010**, 28, 73.
- [31] C. Reichardt, *Chem. Rev.* **1994**, 94, 2319.
- [32] D. M. Owen, *Methods in Membrane Lipids*, Springer, New York, 2nd edn, **2015**.
- [33] J. Yin, Y. Hu, J. Yoon, *Chem. Soc. Rev.* **2015**, 44, 4619.
- [34] M. A. Haidekker, E. A. Theodorakis, *Org. Biomol. Chem.* **2007**, 5, 1669.

- [35] H. M. Kim, B. H. Jeong, J.-Y. Hyon, M. J. An, M. S. Seo, J. H. Hong, K. J. Lee, C. H. Kim, T. Joo, S.-C. Hong, et al., *J. Am. Chem. Soc.* **2008**, *130*, 4246.
- [36] S. J. Cartwright, *Homeopathy* **2016**, *105*, 55.
- [37] A. Marini, A. Muñoz-Losa, A. Biancardi, B. Mennucci, *J. Phys. Chem. B* **2010**, *114*, 17128.
- [38] P. F. Gordon, P. Gregory, *Organic Chemistry in Colour*, Springer-Verlag Berlin Heidelberg, **1987**.
- [39] N. P. F. Barthes, I. A. Karpenko, D. Dziuba, M. Spadafora, J. Auffret, A. P. Demchenko, Y. Mély, R. Benhida, B. Y. Michel, A. Burger, *RSC Adv.* **2015**, *5*, 33536.
- [40] D. Dziuba, I. A. Karpenko, N. P. F. Barthes, B. Y. Michel, A. S. Klymchenko, R. Benhida, A. P. Demchenko, Y. Mély, A. Burger, *Chem. Eur. J.* **2014**, *20*, 1998.
- [41] D. Dziuba, V. Y. Postupalenko, M. Spadafora, A. S. Klymchenko, V. Guérineau, Y. Mély, R. Benhida, A. Burger, *J. Am. Chem. Soc.* **2012**, *134*, 10209.
- [42] N. P. F. Barthes, K. Gavvala, D. Dziuba, D. Bonhomme, I. A. Karpenko, A. S. Dabert-Gay, D. Debayle, A. P. Demchenko, R. Benhida, B. X. T. Y. Michel, et al., *J. Mater. Chem. C* **2016**, *1*.
- [43] A. A. Kuznetsova, N. A. Kuznetsov, Y. N. Vorobjev, N. P. F. Barthes, B. Y. Michel, A. Burger, O. S. Fedorova, *PLoS ONE* **2014**, *9*, e100007.
- [44] P. Greenspan, E. P. Mayer, S. D. Fowler, *J. Cell Biol.* **1985**, *100*, 965.
- [45] J. D. Dattelbaum, *Protein Science* **2005**, *14*, 284.
- [46] S. S. Lehrer, Y. Ishii, *Biochemistry* **1988**, *27*, 5899.
- [47] G. Weber, F. J. Farris, *Biochemistry* **1979**, *18*, 3075.
- [48] Z. Lu, S. J. Lord, H. Wang, W. E. Moerner, R. J. Twieg, *J. Org. Chem.* **2006**, *71*, 9651.
- [49] T. Soujanya, R. W. Fessenden, *J. Phys. Chem.* **1996**, *100*, 3507.
- [50] G. F. Mes, B. De Jong, H. J. Van Ramesdonk, J. W. Verhoeven, J. M. Warman, M. P. De Haas, et al. *J. Am. Chem. Soc.* **1984**, *106*, 6524.
- [51] R. J. Clarke, D. J. Kane, *Biochim. Biophys. Acta* **1997**, *1323*, 223.
- [52] F. Bureš, *RSC Adv.* **2014**, *4*, 58826.
- [53] C. Duan, F. Huang, Y. Cao, *J. Mater. Chem.* **2012**, *22*, 10416.
- [54] I. V. Kurdyukova, A. A. Ishchenko, *Russ. Chem. Rev.* **2012**, *81*, 258.
- [55] A. V. Kulinich, N. A. Derevyanko, A. A. Ishchenko, S. L. Bondarev, V. N. Knyukshto, *J. Photochem. Photobiol. A* **2008**, *200*, 106.
- [56] J. F. Lovell, T. W. B. Liu, J. Chen, G. Zheng, *Chem. Rev.* **2010**, *110*, 2839.
- [57] I. Cohanoschi, K. D. Belfield, F. E. Hernández, *Chem. Phys. Lett.* **2005**, *406*, 462.
- [58] F. E. Hernández, K. D. Belfield, I. Cohanoschi, M. Balu, K. J. Schafer, *Appl Opt* **2004**, *43*, 5394.
- [59] K. D. Belfield, A. R. Morales, J. M. Hales, D. J. Hagan, E. W. Van Stryland, V. M. Chapela, J. Percino, *Chem. Mater.* **2004**, *16*, 2267.
- [60] O. A. Kucherak, P. Didier, Y. Mély, A. S. Klymchenko, *J. Phys. Chem. Lett.* **2010**, *1*, 616.
- [61] J.-Z. Cheng, C.-C. Lin, P.-T. Chou, A. Chaskar, K.-T. Wong, *Tetrahedron* **2011**, *67*, 734.
- [62] C. L. Chiang, M. F. Wu, D. C. Dai, Y. S. Wen, J. K. Wang, C. T. Chen, *Adv. Funct. Mater.* **2005**, *15*, 231.
- [63] H.-F. Huang, S.-H. Xu, Y.-B. He, C.-C. Zhu, H.-L. Fan, X.-H. Zhou, X.-C. Gao, Y.-F. Dai, *Dyes and Pigments* **2013**, *96*, 705.
- [64] T.-C. Lin, Y.-H. Lee, C.-Y. Liu, B.-R. Huang, M.-Y. Tsai, Y.-J. Huang, J.-H. Lin, Y.-K. Shen, C.-Y. Wu, *Chem. Eur. J.* **2012**, *19*, 749.
- [65] R. Abbel, A. P. H. J. Schenning, E. W. Meijer, *J. Polym. Sci. A Polym. Chem.* **2009**, *47*, 4215–4233.
- [66] I. Fischer, A. P. H. J. Schenning, *Nanoparticles Based on Π -Conjugated Polymers and Oligomers for Optoelectronic, Imaging, and Sensing Applications: the Illustrative Example of Fluorene-Based Polymers and Oligomers*, Wiley-VCH Verlag GmbH & Co. KGaA, Weinheim, Germany, **2013**.
- [67] M. Leclerc, *J. Polym. Sci. A Polym. Chem.* **2001**, *39*, 2867.
- [68] S. Yao, K. D. Belfield, *Eur. J. Org. Chem.* **2012**, *2012*, 3199.

-
- [69] M. A. Oar, J. M. Serin, W. R. Dichtel, J. M. J. Fréchet, T. Y. Ohulchanskyy, P. N. Prasad, *Chem. Mater.* **2005**, *17*, 2267.
- [70] R. R. Birge, B. M. Pierce, *Int. J. Quantum Chem.* **1986**, *29*, 639.
- [71] P. So, C. Y. Dong, B. R. Masters, *Annu. Rev. Biomed. Eng.* **2000**, *2*, 399.
- [72] M. E. Dickinson, E. Simbuerger, B. Zimmermann, C. W. Waters, S. E. Fraser, *J. Biomed. Opt.* **2003**, *8*, 329.
- [73] J. Trägårdh, G. Robb, R. Amor, W. B. Amos, J. Dempster, G. Mcconnell, *J. Microsc.* **2015**, *259*, 210.
- [74] S. Yao, H.-Y. Ahn, X. Wang, J. Fu, E. W. Van Stryland, D. J. Hagan, K. D. Belfield, *J. Org. Chem.* **2010**, *75*, 3965.
- [75] C. Le Droumaguet, O. Mongin, M. H. V. Werts, M. Blanchard-Desce, *Chem. Commun.* **2005**, 2802.
- [76] Y. Hong, J. W. Y. Lam, B. Z. Tang, *Chem. Commun.* **2009**, 4332.
- [77] J. Wu, P. Wang, J. Ge, W. Liu, H. Zhang, *Chem. Soc. Rev.* **2011**, *40*, 3483.
- [78] Z. Chen, J. Zhang, M. Song, J. Yin, G.-A. Yu, S. H. Liu, *Chem. Commun.* **2014**, 1.
- [79] A. Szałpa, S. Kula, U. Błaszkiwicz, M. Grucela, E. Schab-Balcerzak, M. Filapek, *Dyes and Pigments* **2016**, *129*, 80.
- [80] F. L. Minn, J. P. Pinion, N. Filipescu, *J. Phys. Chem.* **1971**, *75*, 1794.
- [81] J. I. Lee, V. Y. Lee, R. D. Miller, *ETRI Journal* **2002**, *24*, 409.
- [82] S. Dufresne, L. Callaghan, W. G. Skene, *J. Phys. Chem. B* **2009**, *113*, 1554.
- [83] P. J. Homnick, P. M. Lahti, *Phys. Chem. Chem. Phys.* **2012**, *14*, 11961.
- [84] M. J. Kim, Y. Seo, G. T. Hwang, *RSC Adv.* **2014**, *4*, 12012.
- [85] S. Sasaki, Y. Niko, A. S. Klymchenko, G.-I. Konishi, *Tetrahedron* **2014**, *70*, 7551.
- [86] Z. Wang, G. Zheng, P. Lu, *Org. Lett.* **2005**, *7*, 3669.
- [87] B. Hu, P. Lu, Y. Wang, *New J. Chem.* **2013**, *37*, 1645.
- [88] R. Pudzich, T. Fuhrmann-Lieker, J. Salbeck, in *Emissive Materials Nanomaterials*, Springer Berlin Heidelberg, Berlin, Heidelberg, **2006**, pp. 83–142.
- [89] J. U. Wallace, S. H. Chen, in *Polyfluorenes*, Springer Berlin Heidelberg, Berlin, Heidelberg, **2008**, pp. 145–186.
- [90] J. J. Peterson, M. Willgert, S. Hansson, E. Malmström, K. R. Carter, *J. Polym. Sci. A Polym. Chem.* **2011**, *49*, 3004.
- [91] E. Scheler, P. Strohmriegel, *Liquid Crystals* **2007**, *34*, 667.
- [92] Y. Deng, W. Yuan, Z. Jia, G. Liu, *J. Phys. Chem. B* **2014**, *118*, 14536.
- [93] B. Liu, G. C. Bazan, *Macromol. Rapid Commun.* **2007**, *28*, 1804.
- [94] B. Liu, G. C. Bazan, *Chem. Mater.* **2004**, *16*, 4467.
- [95] S. Wang, G. C. Bazan, *Chem. Commun.* **2004**, 2508.
- [96] G. C. Bazan, S. Wang, *Organic Semiconductors in Sensor Applications* **2008**, *1*, 1.
- [97] S. Wang, B. Liu, B. S. Gaylord, G. C. Bazan, *Adv. Funct. Mater.* **2003**, *13*, 463.
- [98] Q. Zhao, S. Liu, W. Huang, *Polyfluorenes*, Wiley-VCH Verlag GmbH & Co. KGaA, Weinheim, Germany, **2010**.
- [99] X.-D. Zhuang, Y. Chen, B.-X. Li, D.-G. Ma, B. Zhang, Y. Li, *Chem. Mater.* **2010**, *22*, 4455.
- [100] J. Ritchie, J. A. Crayston, J. P. J. Markham, I. D. W. Samuel, *J. Mater. Chem.* **2006**, *16*, 1651.
- [101] H. E. Cingil, I. M. Storm, Y. Yorulmaz, *J. Am. Chem. Soc.* **2015**, *137*, 9800.
- [102] K. Rathore, C. S. Lim, Y. Lee, B. R. Cho, *Org. Biomol. Chem.* **2014**, *12*, 3406.
- [103] B. A. Reinhardt, L. L. Brott, S. J. Clarson, *Chem. Mater.* **1998**, *10*, 1863.
- [104] T. C. Lin, Y. H. Lee, C. L. Hu, Y. K. Li, Y. J. Huang, *Eur. J. Org. Chem.* **2012**, *2012*, 1737.
- [105] X. Dong, J. H. Han, C. H. Heo, H. M. Kim, Z. Liu, B. R. Cho, *Anal. Chem.* **2012**, *84*, 8110.
- [106] A. Frazer, A. R. Morales, A. W. Woodward, P. Tongwa, T. Timofeeva, K. D. Belfield, *J. Fluoresc.* **2013**, *24*, 239.
- [107] C. Mallet, M. Le Borgne, M. Starck, W. G. Skene, *Polym. Chem.* **2013**, *4*, 250.
- [108] J. O. Link, J. G. Taylor, L. Xu, M. Mitchell, H. Guo, H. Liu, D. Kato, T. Kirschberg, J. Sun, N.

-
- Squires, et al., *J. Med. Chem.* **2014**, *57*, 2033.
- [109] X. Yue, Z. Armijo, K. King, M. V. Bondar, A. R. Morales, A. Frazer, I. A. Mikhailov, O. V. Przhonska, K. D. Belfield, *ACS Appl. Mater. Interfaces* **2015**, *7*, 2833.
- [110] K. D. Belfield, M. V. Bondar, A. R. Morales, O. Yavuz, O. V. Przhonska, *J. Phys. Org. Chem.* **2003**, *16*, 194.
- [111] K. D. Belfield, A. R. Morales, B.-S. Kang, J. M. Hales, D. J. Hagan, E. W. Van Stryland, V. M. Chapela, J. Percino, *Chem. Mater.* **2004**, *16*, 4634.
- [112] K. D. Belfield, M. V. Bondar, F. E. Hernández, A. E. Masunov, I. A. Mikhailov, A. R. Morales, O. V. Przhonska, S. Yao, *J. Phys. Chem. C* **2009**, *113*, 4706.
- [113] A. R. Morales, A. Frazer, A. W. Woodward, H.-Y. Ahn-White, A. Fonari, P. Tongwa, T. Timofeeva, K. D. Belfield, *J. Org. Chem.* **2013**, *78*, 1014.
- [114] K. Ogawa, *App. Sci.* **2014**, *4*, 1.
- [115] S.-Y. Ku, L.-C. Chi, W.-Y. Hung, S.-W. Yang, T.-C. Tsai, K.-T. Wong, Y.-H. Chen, C.-I. Wu, *J. Mater. Chem.* **2009**, *19*, 773.
- [116] Y. Lin, Y. Chen, T.-L. Ye, Z.-K. Chen, Y.-F. Dai, D.-G. Ma, *J. Photochem. Photobiol. A* **2012**, *230*, 55.
- [117] C.-H. Chen, Y.-C. Hsu, H.-H. Chou, K. R. J. Thomas, J. T. Lin, C.-P. Hsu, *Chem. Eur. J.* **2010**, *16*, 3184.
- [118] K. Lim, C. Kim, J. Song, T. Yu, W. Lim, K. Song, P. Wang, N. Zu, J. Ko, *J. Phys. Chem. C* **2011**, *115*, 22640.
- [119] H. Zhang, J. Fan, H. Dong, S. Zhang, W. Xu, J. Wang, P. Gao, X. Peng, *J. Mater. Chem. B* **2013**, *1*, 5450.
- [120] J. K. Sørensen, J. Fock, A. H. Pedersen, A. B. Petersen, K. Jennum, K. Bechgaard, K. Kilså, V. Geskin, J. Cornil, T. Bjørnholm, et al., *J. Org. Chem.* **2011**, *76*, 245.
- [121] Q. Lu, J. Zhao, S. Xue, P. Yin, Y. Zhang, S. Yao, *Analyst* **2015**, *140*, 1155.
- [122] J. Louie, J. F. Hartwig, *Tetrahedron Lett.* **1995**, *36*, 3609.
- [123] A. S. Guram, R. A. Rennels, S. L. Buchwald, *Angew. Chem. Int. Ed.* **1995**, *34*, 1348.
- [124] D. S. Surry, S. L. Buchwald, *Angew. Chem. Int. Ed.* **2008**, *47*, 6338.
- [125] J. F. Hartwig, *Acc. Chem. Res.* **2008**, *41*, 1534.
- [126] A. Chartoire, X. Frogneux, S. P. Nolan, *Adv. Synth. Cat.* **2012**, *354*, 1897.
- [127] R. N. Prabhu, R. Ramesh, *Tetrahedron Lett.* **2013**, *54*, 1120.
- [128] D. S. Surry, S. L. Buchwald, *Chem. Sci.* **2011**, *2*, 27.
- [129] L. Y. Chiang, P. A. Padmawar, T. Canteenwala, L.-S. Tan, G. S. He, R. Kannan, R. Vaia, T.-C. Lin, Q. Zheng, P. N. Prasad, *Chem. Commun.* **2002**, 1854.
- [130] W. H. Nguyen, C. D. Bailie, J. Burschka, T. Moehl, M. Grätzel, M. D. McGehee, A. Sellinger, *Chem. Mater.* **2013**, *25*, 1519.
- [131] M. R. Schrimpf, K. B. Sippy, C. A. Briggs, D. J. Anderson, T. Li, J. Ji, J. M. Frost, C. S. Surowy, W. H. Bunnelle, M. Gopalakrishnan, et al., *Bioorg. Med. Chem. Lett.* **2012**, *22*, 1633-.
- [132] G. Saroja, Z. Pingzhu, N. P. Ernsting, J. Liebscher, *J. Org. Chem.* **2004**, *69*, 987.
- [133] J. A. Smith, R. K. Jones, G. W. Booker, S. M. Pyke, *J. Org. Chem.* **2008**, *73*, 8880.
- [134] Z. Wang, B. Wang, J. Wu, *J. Comb. Chem.* **2007**, *9*, 811.
- [135] T. H. M. Jonckers, B. U. W. Maes, G. L. F. Lemièrre, R. Dommissie, *Tetrahedron* **2001**, *57*, 7027.
- [136] G. Malleshm, C. Swetha, S. Niveditha, M. E. Mohanty, N. J. Babu, A. Kumar, K. Bhanuprakash, V. J. Rao, *J. Mater. Chem. C* **2015**, *3*, 1208-1224.
- [137] I. Smari, L. Zhao, K. Yuan, H. Ben Ammar, H. Doucet, *Catal. Sci. Tech.* **2014**, *4*, 3723.
- [138] I. P. Beletskaya, A. G. Bessmertnykh, A. D. Averin, F. Denat, R. Guillard, *Eur. J. Org. Chem.* **2005**, *2005*, 281.
- [139] A. D. Averin, E. R. Ranyuk, N. V. Lukashev, I. P. Beletskaya, *Chem. Eur. J.* **2005**, *11*, 7030.
- [140] I. P. Beletskaya, A. D. Averin, A. G. Bessmertnykh, F. Denat, R. Guillard, *Russ J Org Chem* **2010**, *46*, 947.
- [141] J. Liu, C. Liu, W. He, *Curr. Org. Chem.* **2013**, *17*, 564.

- [142] Y. Yang, Q. Zhao, W. Feng, F. Li, *Chem. Rev.* **2013**, *113*, 192.
- [143] L. Yuan, W. Lin, K. Zheng, S. Zhu, *Acc. Chem. Res.* **2013**, *46*, 1462.
- [144] J. C. Owicki, *J. Biomol. Screening* **2000**, *5*, 297.
- [145] D. M. Owen, A. Magenau, D. Williamson, K. Gaus, *Bioessays* **2012**, *34*, 739.
- [146] K. Simons, E. Ikonen, *Nature* **1997**, *387*, 569.
- [147] G. Vereb, J. Szöllosi, J. Matkó, P. Nagy, T. Farkas, L. Vigh, L. Mátyus, T. A. Waldmann, S. Damjanovich, *Proc. Natl. Acad. Sci. U.S.A.* **2003**, *100*, 8053.
- [148] D. A. Brown, E. London, *J. Membr. Biol.* **1998**, *164*, 103.
- [149] L. J. Pike, *J. Lipid Res.* **2006**, *47*, 1597.
- [150] K. Jacobson, O. G. Mouritsen, R. G. W. Anderson, *Nat. Cell Biol.* **2007**, *9*, 7.
- [151] A. S. Klymchenko, R. Kreder, *Chemistry & Biology* **2014**, *21*, 97.
- [152] A. P. Demchenko, Y. Mély, G. Duportail, A. S. Klymchenko, *Biophys. J.* **2009**, *96*, 3461.
- [153] Y. Niko, P. Didier, Y. Mély, G.-I. Konishi, A. S. Klymchenko, *Sci. Rep.* **2015**, *1*.
- [154] R. G. Hanshaw, B. D. Smith, *Bioorg. & Med. Chem.* **2005**, *13*, 5035.
- [155] B. Fadeel, D. Xue, *Crit. Rev. Biochem. Mol. Biol.* **2009**, *44*, 264.
- [156] G. Koopman, C. P. Reutelingsperger, G. A. Kuijten, R. M. Keehnen, S. T. Pals, M. H. van Oers, *Blood* **1994**, *84*, 1415.
- [157] B. Schutte, R. Nuydens, H. Geerts, F. Ramaekers, *J. Neurosci. Meth.* **1998**, *86*, 63.
- [158] C. Smith, R. Mehta, D. F. Gibson, Z. Levashova, F. G. Blankenberg, J. F. Tait, *Bioconjugate Chem.* **2010**, *21*, 1554.
- [159] V. V. Shynkar, Y. Mély, G. Duportail, E. Piémont, A. S. Klymchenko, A. P. Demchenko, *J. Phys. Chem. A* **2003**, *107*, 9522.
- [160] B. Mesmin, F. R. Maxfield, *BBA - Mol. Cell Biol. L.* **2009**, *1791*, 636.
- [161] E. Ikonen, *Nat. Rev. Mol. Cell. Biol.* **2008**, *9*, 125.
- [162] G. Bains, A. B. Patel, V. Narayanaswami, *Molecules* **2011**, *16*, 7909.
- [163] B. R. Lentz, *Chem. Phys. Lipids* **1989**, *50*, 171.
- [164] R. Šachl, I. Boldyrev, L. B. Å. Johansson, *Phys. Chem. Chem. Phys.* **2010**, *12*, 6027.
- [165] G. Gimpl, K. Gehrig-Burger, *Biosci Rep* **2007**, *27*, 335.
- [166] M. Collot, R. Kreder, A. L. Tatarets, L. D. Patsenker, Y. Mély, A. S. Klymchenko, *Chem. Commun.* **2015**, *51*, 17136.
- [167] R. Garzon, G. Marcucci, C. M. Croce, *Nature Rev. Drug Discovery* **2010**, *9*, 775.
- [168] C. R. Calladine, H. R. Drew, B. F. Luisi, A. A. Travers, *Understanding DNA*, Elsevier, **2004**.
- [169] J. Kyrp, I. Kejnovská, D. Renciuik, M. Vorlícková, *Nucleic Acids Res.* **2009**, *37*, 1713.
- [170] P. Belmont, J. F. Constant, M. Demeunynck, *Chem. Soc. Rev.* **2001**, *30*, 70.
- [171] S. H. Weisbrod, A. Marx, *Chem. Commun.* **2008**, 5675.
- [172] C. B. Reese, *Org. Biomol. Chem.* **2005**, *3*, 3851.
- [173] N. D. Sinha, J. Biernat, H. Köster, *Tetrahedron Lett.* **1983**, *24*, 5843.
- [174] S. Roy, M. Caruthers, *Molecules* **2013**, *18*, 14268.
- [175] T. Abramova, *Molecules* **2013**, *18*, 1063–1075.
- [176] A. B. Sierzchala, D. J. Dellinger, J. R. Betley, T. K. Wyrzykiewicz, C. M. Yamada, M. H. Caruthers, *J. Am. Chem. Soc.* **2003**, *125*, 13427.
- [177] G. Hayashi, A. Okamoto, *Chemical record (New York, N.Y.)* **2013**, *13*, 209.
- [178] A. Okamoto, *Chem. Soc. Rev.* **2011**, *40*, 5815.
- [179] A. Okamoto, K. Tainaka, T. Unzai, I. Saito, *Tetrahedron* **2007**, *63*, 3465.
- [180] H. Gudnason, M. Dufva, D. D. Bang, A. Wolff, *Nucleic Acids Res.* **2007**, *35*, 127.
- [181] J. Sumranjit, S. Chung, *Molecules* **2013**, *18*, 10425.
- [182] P. Y. Kwok, X. Chen, *Curr. Issues Mol. Biol.* **2003**, *5*, 43.
- [183] J. Kapuscinski, *Biotech Histochem* **1995**, *70*, 220.
- [184] M. C. Vega, M. Coll, C. Alemán, *Eur. J. Biochem.* **1996**, *239*, 376.
- [185] X. Peng, T. Wu, J. Fan, J. Wang, S. Zhang, F. Song, S. Sun, *Angew. Chem. Int. Ed.* **2011**, *50*, 4180.
- [186] J. N. Wilson, E. T. Kool, *Org. Biomol. Chem.* **2006**, *4*, 4265.

- [187] R. W. Sinkeldam, N. J. Greco, Y. Tor, *Chem. Rev.* **2010**, *110*, 2579.
- [188] M. J. Davies, A. Shah, I. J. Bruce, *Chem. Soc. Rev.* **2000**, *29*, 97.
- [189] F. Wojciechowski, C. J. Leumann, *Chem. Soc. Rev.* **2011**, *40*, 5669.
- [190] M. L. Capobianco, M. Naldi, M. Zambianchi, G. Barbarella, *Tetrahedron Lett.* **2005**, *46*, 8181.
- [191] K. Tram, D. Twohig, H. Yan, *Nucleosides Nucleotides Nucleic Acids* **2011**, *30*, 1.
- [192] P. Grünefeld, C. Richert, *J. Org. Chem.* **2004**, *69*, 7543.
- [193] R. X.-F. Ren, N. C. Chaudhuri, P. L. Paris, S. Rumney, E. T. Kool, *J. Am. Chem. Soc.* **1996**, *118*, 7671.
- [194] C. Strässler, N. E. Davis, E. T. Kool, *Helvetica Chimica Acta* **1999**, *82*, 2160.
- [195] A. Okamoto, K. Tainaka, Y. Fujiwara, *J. Org. Chem.* **2006**, *71*, 3592.
- [196] L. M. Wilhelmsson, *Quart. Rev. Biophys.* **2010**, *43*, 159.
- [197] N. B. Gaied, *Nucleic Acids Res.* **2005**, *33*, 1031.
- [198] N. J. Greco, Y. Tor, *Tetrahedron* **2007**, *63*, 3515.
- [199] H. Liu, J. Gao, S. R. Lynch, Y. D. Saito, L. Maynard, E. T. Kool, *Science* **2003**, *302*, 868.
- [200] R. Huber, N. Amann, H.-A. Wagenknecht, *J. Org. Chem.* **2004**, *69*, 744.
- [201] A. V. Azhayev, M. L. Antopolsky, *Tetrahedron* **2001**, *57*, 4977.
- [202] A. Okamoto, Y. Saito, I. Saito, *J. Photochem. and Photobiol. C* **2005**, *6*, 108.
- [203] Y. Saito, A. Suzuki, Y. Okada, Y. Yamasaka, N. Nemoto, I. Saito, *Chem. Commun.* **2013**, *49*, 5684.
- [204] B. H. Kim, *Nucleic Acids Symp. Ser.* **2005**, *49*, 13.
- [205] Y. J. Seo, J. H. Ryu, B. H. Kim, *Org. Lett.* **2005**, *7*, 4931.
- [206] C. Massif, S. Dautrey, A. Haefele, R. Ziessel, P.-Y. Renard, A. Romieu, *Org. Biomol. Chem.* **2012**, *10*, 4330.
- [207] N. Minakawa, Y. Ono, A. Matsuda, *J. Am. Chem. Soc.* **2003**, *125*, 11545.
- [208] T. Pesnot, L. M. Tedaldi, P. G. Jambrina, E. Rosta, G. K. Wagner, *Org. Biomol. Chem.* **2013**, *11*, 6357.
- [209] A. H. El-Sagheer, T. Brown, *Chem. Soc. Rev.* **2010**, *39*, 1388.
- [210] C. Beyer, H.-A. Wagenknecht, *Chem. Commun.* **2010**, *46*, 2230.
- [211] J. B. Crumpton, W. L. Santos, *Chem. Commun.* **2012**, *48*, 2018.
- [212] K. Tanabe, Y. Ando, S.-I. Nishimoto, *Tetrahedron Lett.* **2011**, *52*, 7135.
- [213] L. T. C. França, E. Carrilho, T. B. L. Kist, *Quart. Rev. Biophys.* **2002**, *35*, 1.
- [214] L. D. Lavis, R. T. Raines, *ACS Chem. Biol.* **2008**, *3*, 142.
- [215] S. Kim, A. Misra, *Annu. Rev. Biomed. Eng.* **2007**, *9*, 289.
- [216] D. Dodd, R. Hudson, *MROC* **2009**, *6*, 378.
- [217] J. W. Lee, M. Jung, G. R. Rosania, Y.-T. Chang, *Chem. Commun.* **2003**, 1852.
- [218] P. S. Nagle, C. McKeever, F. Rodriguez, B. Nguyen, W. D. Wilson, I. Rozas, *J. Med. Chem.* **2014**, *57*, 7663.
- [219] G. T. Hwang, Y. J. Seo, B. H. Kim, *J. Am. Chem. Soc.* **2004**, *126*, 6528.
- [220] J. H. Ryu, Y. J. Seo, G. T. Hwang, J. Y. Lee, B. H. Kim, *Tetrahedron* **2007**, *63*, 3538.
- [221] J. Guo, T. Wang, R. Yang, *Mol. BioSyst.* **2012**, *8*, 2347.
- [222] J. Guo, L. Han, X. Bao, Z. Du, T. Wang, R. Yang, *J. Phys. Chem. C* **2014**, *118*, 9368.
- [223] E. Ergen, M. Weber, J. Jacob, A. Herrmann, K. Müllen, *Chem. Eur. J.* **2006**, *12*, 3707.
- [224] D. Dziuba, P. Pospíšil, J. Matyášovský, J. Brynda, D. Nachtigallová, L. Rulíšek, R. Pohl, M. Hof, M. Hocek, *Chem. Sci.* **2016**, *00*, 1–11.
- [225] R. J. Fitzmaurice, Z. C. Etheridge, E. Jumel, D. N. Woolfson, S. Caddick, *Chem. Commun.* **2006**, 4814.
- [226] A. Basso, *Diversity Oriented Synthesis* **2014**, *1*, 1.
- [227] J. F. Hartwig, *Pure Appl. Chem.* **1999**, *71*, 1417.
- [228] Y. Sunesson, E. Limé, S. O. Nilsson Lill, R. E. Meadows, P.-O. Norrby, *J. Org. Chem.* **2014**, *79*, 11961.
- [229] F. Barrios-Landeros, J. F. Hartwig, *J. Am. Chem. Soc.* **2005**, *127*, 6944.
- [230] S. Shekhar, P. Ryberg, J. F. Hartwig, J. S. Mathew, D. G. Blackmond, E. R. Strieter, S. L.

- Buchwald, *J. Am. Chem. Soc.* **2006**, *128*, 3584.
- [231] I. J. S. Fairlamb, *Org. Biomol. Chem.* **2008**, *6*, 3645.
- [232] J. P. Wolfe, S. L. Buchwald, *J. Org. Chem.* **2000**, *65*, 1144.
- [233] F. Ma, X. Xie, L. Zhang, Z. Peng, L. Ding, L. Fu, Z. Zhang, *J. Org. Chem.* **2012**, *77*, 5279.
- [234] S. Breitler, N. J. Oldenhuis, B. P. Fors, S. L. Buchwald, *Org. Lett.* **2011**, *13*, 3262.
- [235] I. P. Beletskaya, A. G. Bessmertnykh, R. Guilard, *Tetrahedron Lett.* **1999**, *40*, 6393.
- [236] S. Shekhar, P. Ryberg, J. F. Hartwig, *Org. Lett.* **2006**, *8*, 851.
- [237] W. Yu, Y. Mei, Y. Kang, Z. Hua, Z. Jin, *Org. Lett.* **2004**, *6*, 3217.
- [238] K. Nomura, N. Yamamoto, R. Ito, M. Fujiki, Y. Geerts, *Macromolecules* **2008**, *41*, 4245.
- [239] Y. Wang, J. Zhou, X. Wang, X. Zheng, Z. Lu, W. Zhang, Y. Chen, Y. Huang, X. Pu, J. Yu, *Dyes and Pigments* **2014**, *100*, 87.
- [240] J. Muzart, *J. Mol. Catal. A* **2009**, *308*, 15.
- [241] G. Mignani, F. Leising, R. Meyrueix, H. Samson, *Tetrahedron Lett.* **1990**, *31*, 4743.
- [242] B. Strehmel, A. M. Sarker, H. Detert, *ChemPhysChem* **2003**, *4*, 249.
- [243] T. Peng, D. Yang, *Org. Lett.* **2010**, *12*, 496.
- [244] L. Wu, K. Burgess, *J. Org. Chem.* **2008**, *73*, 8711.
- [245] C. A. G. N. Montalbetti, V. Falque, *Tetrahedron* **2005**, *61*, 10827.
- [246] S. M. Ormson, R. G. Brown, F. Vollmer, W. Rettig, *J. Photochem. Photobiol. A* **1994**, *81*, 65.
- [247] W. H. Melhuish, *J. Phys. Chem.* **1961**, *65*, 229.
- [248] M. Shimizu, K. Mochida, M. Katoh, T. Hiyama, *J. Phys. Chem. C* **2010**, *114*, 10004.
- [249] A. Baheti, P. Singh, K. R. J. Thomas, *Dyes and Pigments* **2011**, *88*, 195.
- [250] E. Lippert, *Zeitschrift für Naturforschung A* **1955**, *10*, DOI 10.1515/zna-1955-0707.
- [251] N. Mataga, Y. Kaifu, M. Koizumi, *Bull. Chem. Soc. Jpn.* **1956**, *29*, 465.
- [252] For DFT-TDDFT calculation: Gaussian03, Revision C.02, M. J. Frisch, G. W. Trucks, H. B. Schlegel, G. E. Scuseria, M. A. Robb, J. R. Cheeseman, V. G. Zakrzewski, J. A. J. Montgomery, R. E. Stratmann, J. C. Burant, S. Dapprich, J. M. Millam, A. D. Daniels, K. N. Kudin, M. C. Strain, O. Farkas, J. Tomasi, V. Barone, M. Cossi, R. Cammi, B. Mennucci, C. Pomelli, C. Adamo, S. Clifford, J. Ochterski, G. A. Petersson, P. Y. Ayala, Q. Cui, K. Morokuma, D. K. Malick, A. D. Rabuck, K. Raghavachari, J. B. Foresman, J. Cioslowski, J. V. Ortiz, A. G. Baboul, B. B. Stefanov, G. Liu, A. Liashenko, P. Piskorz, I. Komaromi, R. Gomperts, R. L. Martin, D. J. Fox, T. Keith, M. A. Al-Laham, C. Y. Peng, A. Nanayakkara, C. Gonzalez, M. Challacombe, P. M. W. Gill, B. Johnson, W. Chen, M. W. Wong, J. L. Andres, C. Gonzalez, M. Head-Gordon, E. S. Replogle, J. A. Pople, Gaussian, Inc., Wallingford CT, 2004.
- [253] J. B. Grimm, B. P. English, J. Chen, J. P. Slaughter, Z. Zhang, A. Revyakin, R. Patel, J. J. Macklin, D. Normanno, R. H. Singer, et al., *Nature Methods* **2015**, *1*.
- [254] A. T. Krueger, B. Imperiali, *ChemBioChem* **2013**, *14*, 788.
- [255] R. A. Moore, J. Lee, G. W. Robinson, *J. Phys. Chem.* **1985**, *89*, 3648–3654.
- [256] a) R. R. Gupta, M. Kumar, V. Gupta, in *Heterocyclic Chemistry*, Springer, Berlin, Heidelberg, **1998**, pp. 275–355; b) O. C. Dermer, G. E. Ham, in *Ethyleneimine and Other Aziridines. Chemistry and Applications*, Academic Press, New York, **1969**, pp. 592; c) D. Tanner, C. Birgersson, *Tet. Lett.* **1991**, *32*, 2533; d) A. de Meijere, *Angew. Chem. Int. Ed. Engl.* **1979**, *18*, 809.
- [257] T. Ohwada, H. Hirao, A. Ogawa, *J. Org. Chem.* **2004**, *69*, 7486.
- [258] F. Liu, W. Du, Q. Liang, Y. Wang, J. Zhang, J. Zhao, S. Zhu, *Tetrahedron* **2010**, *66*, 5467.
- [259] B. Lu, J. Zhang, J. Li, J. Yao, M. Wang, Y. Zou, S. Zhu, *Tetrahedron* **2012**, *68*, 8924.
- [260] J.-C. Kuhlmann, P. de Bruyn, R. K. M. Bouwer, A. Meetsma, P. W. M. Blom, J. C. Hummelen, *Chem. Commun.* **2010**, *46*, 7232.
- [261] Y. Niko, S. Kawauchi, G.-I. Konishi, *Chem. Eur. J.* **2013**, *19*, 9760.
- [262] For DFT-TDDFT calculation: Gaussian03, Revision C.02, M. J. Frisch, G. W. Trucks, H. B. Schlegel, G. E. Scuseria, M. A. Robb, J. R. Cheeseman, V. G. Zakrzewski, J. A. J. Montgomery, R. E. Stratmann, J. C. Burant, S. Dapprich, J. M. Millam, A. D. Daniels, K. N.

- Kudin, M. C. Strain, O. Farkas, J. Tomasi, V. Barone, M. Cossi, R. Cammi, B. Mennucci, C. Pomelli, C. Adamo, S. Clifford, J. Ochterski, G. A. Petersson, P. Y. Ayala, Q. Cui, K. Morokuma, D. K. Malick, A. D. Rabuck, K. Raghavachari, J. B. Foresman, J. Cioslowski, J. V. Ortiz, A. G. Baboul, B. B. Stefanov, G. Liu, A. Liashenko, P. Piskorz, I. Komaromi, R. Gomperts, R. L. Martin, D. J. Fox, T. Keith, M. A. Al-Laham, C. Y. Peng, A. Nanayakkara, C. Gonzalez, M. Challacombe, P. M. W. Gill, B. Johnson, W. Chen, M. W. Wong, J. L. Andres, C. Gonzalez, M. Head-Gordon, E. S. Replogle, J. A. Pople, Gaussian, Inc., Wallingford CT, 2004.
- [263] D. W. Silverstein, N. Govind, H. J. J. van Dam, L. Jensen, *J. Chem. Theory Comput.* **2013**, *9*, 5490.
- [264] H. C. Ishikawa-Ankerhold, R. Ankerhold, G. P. C. Drummen, *Molecules* **2012**, *17*, 4047.
- [265] O. A. Kucherak, S. Oncul, Z. Darwich, D. A. Yushchenko, Y. Arntz, P. Didier, Y. Mély, A. S. Klymchenko, *J. Am. Chem. Soc.* **2010**, *132*, 4907–.
- [266] T. Parasassi, E. Gratton, W. M. Yu, P. Wilson, M. Levi, *Biophys. J.* **1997**, *72*, 2413.
- [267] H. M. Kim, H.-J. Choo, S.-Y. Jung, Y.-G. Ko, W.-H. Park, S.-J. Jeon, C. H. Kim, T. Joo, B. R. Cho, *ChemBioChem* **2007**, *8*, 553.
- [268] L. A. Bagatolli, *Biochimica et Biophysica Acta (BBA) - Biomembranes* **2006**, *1758*, 1541.
- [269] V. Rolland, M. Kotera, J. Lhomme, *Synth. Commun.* **1997**, *27*, 3505.
- [270] A. Maity, J.-S. Choi, T. S. Teets, N. Deligonul, A. J. Berdis, T. G. Gray, *Chem. Eur. J.* **2013**, *19*, 15924.
- [271] Q. Zheng, M. F. Juette, S. Jockusch, M. R. Wasserman, Z. Zhou, R. B. Altman, S. C. Blanchard, *Chem. Soc. Rev.* **2014**, *43*, 1044.
- [272] C. Rentero, A. Magenau, A. Abu-Siniyeh, D. M. Owen, K. Gaus, *Nat Protoc* **2011**, *7*, 24–35.
- [273] O. Golfetto, E. Hinde, E. Gratton, *Biophys. J.* **2013**, *104*, 1238.
- [274] C. Holzhauser, S. Berndl, F. Menacher, M. Breunig, A. Göpferich, H.-A. Wagenknecht, *Eur. J. Org. Chem.* **2010**, *2010*, 1239.
- [275] F. Menacher, M. Rubner, S. Berndl, H.-A. Wagenknecht, *J. Org. Chem.* **2008**, *73*, 4263.
- [276] T. Ehrenschwender, H.-A. Wagenknecht, *J. Org. Chem.* **2011**, *76*, 2301.
- [277] C. Holzhauser, H.-A. Wagenknecht, *Angew. Chem. Int. Ed.* **2011**, *50*, 7268.
- [278] a) G. Vesnaver, C. N. Chang, M. Eisenberg, A. P. Grollman, K. J. Breslauer, *Proc. Natl. Acad. Sci. U.S.A.* **1989**, *86*, 3614; b) J. Barbaric, C. Wanninger-Weiß, H.-A. Wagenknecht, *Eur. J. Org. Chem.* **2009**, *2009*, 364.
- [279] a) G. S. Lal, G. P. Pez, R. G. Syvret, *Chem. Rev.* **1996**, *96*, 1737–1756; b) R. P. Singh, J. M. Shreeve, *Synthesis* **2002**, *2002*, 2561–2578; c) S. Kyasa, P. H. Dussault, *Org. Lett.* **2014**, *16*, 5235–5237.
- [280] U. C. Yoon, P. S. Mariano, *Acc. Chem. Res.* **1992**, *25*, 233.
- [281] a) G. Lamm, G. R. Pack, *Proc. Natl. Acad. Sc. USA* **1990**, pp. 9033–9036; b) S. Hanlon, L. Wong, G. R. Pack, *Biophys. J.* **1997**, *72*, 291.
- [282] U. Asseline, M. Delarue, G. Lancelot, F. Toulmé, F.; N. T. Thuong, T. Montenay-Garestier, C. Hélène, *Proc. Natl. Acad. Sc. USA*.
- [283] a) J. L. Mergny, L. Lacroix, *Oligonucleotides* **2003**, *13*, 515; b) J. B. Kenneth, L. Michael, G. K. A. Johnson, *Methods in Enzymology*, **1995**, *259*, 221–242.
- [284] W. L. F. Armarego, C. L. L. Chai, Purification of Laboratory Chemicals; Butterworth-Heinemann: Oxford, 7th ed. **2013**.
- [285] W. C. Still, M. Kahn, A. Mitra, *J. Org. Chem.* **1978**, *43*, 2923.
- [286] G. R. Fulmer, A. J. M. Miller, N. H. Sherden, H. E. Gottlieb, A. Nudelman, B. M. Stoltz, J. E. Bercaw, K. I. Goldberg, *Organometallics* **2010**, *29*, 2176.
- [287] M. J. Hope, M. B. Bally, G. Webb, P. R. Cullis, *Biochim. Biophys. Acta* **1985**, *812*, 55.
- [288] J. L. Bolliger, M. Oberholzer, C. M. Frech, *Adv. Synth. Catal.* **2011**, *353*, 945.
- [289] P. K. Agarwal, M. Saifuddin, B. Kundu, *Tetrahedron* **2010**, *66*, 862.
- [290] M. Subat, B. König, *Synthesis* **2001**, *2001*, 1818.

Abstract: Extensive research focuses on finding straightforward synthesis and prospective probes for biological applications. Push-pull dyes are of particular interest for various uses as biosensors for membranes and nucleic acids. These dyes are highly responsive to changes of their environments. Specifically, push-pull fluorenes exhibit low cytotoxicity and high photostability, but are not yet reported in the two mentioned applications. Furthermore, their synthesis is highly demanding. In this context, our work presents: 1) Step-economic and concise approaches to access challenging aminoaromatics *via* optimized air-stable Pd catalytic systems involving selective *mono/di*-amination and sequential one-pot synthesis, 2) Synthesis of a fluorene library varying the acceptor and the donor groups, 3) Structure-photophysics relationships, 4) Synthesis of three advanced dyes and concluding the first plasma membrane-specific fluorene probe that can be a powerful tool for studying the structure and biophysical dynamics of membranes. The optimal dye surpasses the features of commonly used probes showing: red-shifted absorption matching the 405 nm diode laser, higher brightness decreasing the dye concentration for staining by ~10-15 folds, high photostability, comparably strong sensitivity to liquid domains of cell membrane, and 5) Synthesis of 4 fluorene-labeled phosphoramidites and their site-specific ODN incorporations evidencing high sensitivity to protic media and pH. Labeled sequences exhibited a far-red emission with modest quantum yields in line with their strong charge transfer character. In DNA duplexes, the dye efficiently base-discriminated opposite cytidine and thymidine. A preliminary application of the DNA fluorescent marker involved testing it as a mega-Stokes shift donor in an emissive FRET pair in combination with Dy681 acceptor. The FRET demonstrated a ratiometric turn-on in NIR region with a shift of 300 nm.

Key words: fluorene, push-pull dye, palladium, CuAAC, biosensor, membrane, lipids, nucleic acids

Résumé: Le développement de nouvelles voies synthétiques permettant l'accès à des sondes à applications biologiques connaît un intérêt accru. Les travaux de cette thèse s'inscrivent dans ce cadre. Ils portent particulièrement sur les colorants « Push-pull » qui se caractérisent par leur sensibilité aux changements de leur environnement, leur faible cytotoxicité et leur photostabilité élevée. En outre, la synthèse de ces fluorènes est très exigeante. Nos travaux ont abouti à : 1) Des approches synthétiques concises pour accéder à des composés aromatiques aminés difficiles à synthétiser, celles-ci *via* des systèmes Pallado-catalysés optimisés impliquant une amination sélective et une synthèse séquentielle en « one pot », 2) La synthèse d'une bibliothèque vaste de fluorènes avec la diversification des groupements accepteur et donneur. 3) Des relations structure- propriétés photophysiques. 4) La synthèse de trois colorants avancés engendrant la première sonde de fluorènes spécifique aux membranes : un outil puissant pour étudier la structure et les dynamiques biophysiques de ces membranes. Le colorant optimal surpasse les caractéristiques des sondes couramment utilisées montrant: une absorption décalée vers le rouge attendant 405 nm en diode laser, une luminosité plus élevée diminuant la concentration du colorant pour la coloration de ~ 10-15 fois, une haute photo-stabilité, une forte sensibilité aux domaines liquides des membranes des cellules. 5) La Synthèse de 4 phosphoramidites marqués et leurs incorporations dans les oligonucléotides attestant une grande sensibilité aux milieux protiques et au pH. En duplex d'ADN, le colorant est efficace pour la différenciation des bases opposées. Une application du marqueur d'ADN fluorescent l'a testé comme un donneur pour le déplacement de Stokes dans une paire de FRET émissive en combinaison avec l'accepteur Dy681. Le FRET a démontré une augmentation ratiométrique dans la région proche infrarouge avec un décalage de 300 nm.

Mots clés: fluorène, push-pull colorant, palladium, CuAAC, biocapteurs, membranes, lipides, acides nucléiques